

# Medicine and food homology: Emerging tool and methodology for separation and analysis of the bioactive factors

**Edited by**

Haining Zhuang, Irena Choma, Wenyi Kang  
and Yisheng Chen

**Published in**

Frontiers in Nutrition



## FRONTIERS EBOOK COPYRIGHT STATEMENT

The copyright in the text of individual articles in this ebook is the property of their respective authors or their respective institutions or funders. The copyright in graphics and images within each article may be subject to copyright of other parties. In both cases this is subject to a license granted to Frontiers.

The compilation of articles constituting this ebook is the property of Frontiers.

Each article within this ebook, and the ebook itself, are published under the most recent version of the Creative Commons CC-BY licence. The version current at the date of publication of this ebook is CC-BY 4.0. If the CC-BY licence is updated, the licence granted by Frontiers is automatically updated to the new version.

When exercising any right under the CC-BY licence, Frontiers must be attributed as the original publisher of the article or ebook, as applicable.

Authors have the responsibility of ensuring that any graphics or other materials which are the property of others may be included in the CC-BY licence, but this should be checked before relying on the CC-BY licence to reproduce those materials. Any copyright notices relating to those materials must be complied with.

Copyright and source acknowledgement notices may not be removed and must be displayed in any copy, derivative work or partial copy which includes the elements in question.

All copyright, and all rights therein, are protected by national and international copyright laws. The above represents a summary only. For further information please read Frontiers' Conditions for Website Use and Copyright Statement, and the applicable CC-BY licence.

ISSN 1664-8714  
ISBN 978-2-8325-3793-0  
DOI 10.3389/978-2-8325-3793-0

## About Frontiers

Frontiers is more than just an open access publisher of scholarly articles: it is a pioneering approach to the world of academia, radically improving the way scholarly research is managed. The grand vision of Frontiers is a world where all people have an equal opportunity to seek, share and generate knowledge. Frontiers provides immediate and permanent online open access to all its publications, but this alone is not enough to realize our grand goals.

## Frontiers journal series

The Frontiers journal series is a multi-tier and interdisciplinary set of open-access, online journals, promising a paradigm shift from the current review, selection and dissemination processes in academic publishing. All Frontiers journals are driven by researchers for researchers; therefore, they constitute a service to the scholarly community. At the same time, the *Frontiers journal series* operates on a revolutionary invention, the tiered publishing system, initially addressing specific communities of scholars, and gradually climbing up to broader public understanding, thus serving the interests of the lay society, too.

## Dedication to quality

Each Frontiers article is a landmark of the highest quality, thanks to genuinely collaborative interactions between authors and review editors, who include some of the world's best academicians. Research must be certified by peers before entering a stream of knowledge that may eventually reach the public - and shape society; therefore, Frontiers only applies the most rigorous and unbiased reviews. Frontiers revolutionizes research publishing by freely delivering the most outstanding research, evaluated with no bias from both the academic and social point of view. By applying the most advanced information technologies, Frontiers is catapulting scholarly publishing into a new generation.

## What are Frontiers Research Topics?

Frontiers Research Topics are very popular trademarks of the *Frontiers journals series*: they are collections of at least ten articles, all centered on a particular subject. With their unique mix of varied contributions from Original Research to Review Articles, Frontiers Research Topics unify the most influential researchers, the latest key findings and historical advances in a hot research area.

Find out more on how to host your own Frontiers Research Topic or contribute to one as an author by contacting the Frontiers editorial office: [frontiersin.org/about/contact](https://frontiersin.org/about/contact)



# Medicine and food homology: Emerging tool and methodology for separation and analysis of the bioactive factors

## Topic editors

Haining Zhuang — Shanghai Urban Construction Vocational College, China

Irena Choma — Marie Curie-Skłodowska University, Poland

Wenyi Kang — Henan University, China

Yisheng Chen — Shanxi Agricultural University, China

## Citation

Zhuang, H., Choma, I., Kang, W., Chen, Y., eds. (2023). *Medicine and food homology: Emerging tool and methodology for separation and analysis of the bioactive factors*. Lausanne: Frontiers Media SA. doi: 10.3389/978-2-8325-3793-0

# Table of contents

- 04 **Editorial: Medicine and food homology: emerging tool and methodology for separation and analysis of the bioactive factors**  
Yisheng Chen, Wenyi Kang, Irena M. Choma and Haining Zhuang
- 06 **Evaluation of pharmacological activities and active components in *Tremella aurantialba* by instrumental and virtual analyses**  
Yonghuan Yan, Mengtian Wang, Xiaoruo Gan, Xu Wang, Chenghao Fu, Yuemin Li, Ning Chen, Pin Lv and Yan Zhang
- 22 **Isolation, purification, and structural elucidation of *Stropharia rugosoannulata* polysaccharides with hypolipidemic effect**  
Yinlu Gao, Gulijiannaiti Abuduaini, Chenhe Yang, Shanshan Zhang, Yanrong Zhang, Hongxiu Fan, Xu Teng, Chenligen Bao, Hongcheng Liu, Dawei Wang and Tingting Liu
- 36 **Effect of total glycosides of *Cistanche deserticola* on the energy metabolism of human HepG2 cells**  
Duo Feng, Shi-qi Zhou, Ya-xi Zhou, Yong-jun Jiang, Qiao-di Sun, Wei Song, Qian-qian Cui, Wen-jie Yan and Jing Wang
- 46 **Screening of heat stress-regulating active fractions in mung beans**  
Yuchao Feng, Xia Fan, Dengcheng Suo, Shu Zhang, Yantao Ma, Haoyu Wang, Xin Guan, Hongzhi Yang and Changyuan Wang
- 61 **Oligosaccharides isolated from *Rehmannia glutinosa* protect LPS-induced intestinal inflammation and barrier injury in mice**  
Xiao Li, Rong Gui, Xuefang Wang, Erjuan Ning, Lixian Zhang, Yi Fan, Ling Chen, Liqin Yu, Jie Zhu, Zhining Li, Lei Wei, Wei Wang, Zihong Li, Yue Wei and Xuebing Wang
- 75 **Analysis of the active ingredients and health applications of cistanche**  
Shiqi Zhou, Duo Feng, Yaxi Zhou, Hao Duan, Yongjun Jiang and Wenjie Yan
- 94 **Simultaneous determination of nine phenolic compounds in imitation wild *Dendrobium officinale* samples using ultrahigh-performance liquid chromatography–tandem mass spectrometry**  
Yingsu Mu, Li Cheng, Xiaojian Gong, Jiangxiong Ma, Shiyu Zhang, Yinghua Mu, Kang Liang, Xin Zhou and Chao Zhao
- 104 **Rapid identification of  $\alpha$ -glucosidase inhibitors from *Poria* using spectrum-effect, component knock-out, and molecular docking technique**  
Changyang Ma, Jie Lu, Mengjie Ren, Qiuyi Wang, Changqin Li, Xuefeng Xi and Zhenhua Liu
- 119 **Bioactive profiles of edible vegetable oils determined using 10D hyphenated comprehensive high-performance thin-layer chromatography (HPTLCxHPTLC) with on-surface metabolism (nanoGIT) and planar bioassays**  
Isabel Müller, Alexander Gulde and Gertrud E. Morlock



## OPEN ACCESS

## EDITED AND REVIEWED BY

Michael Rychlik,  
Technical University of Munich, Germany

## \*CORRESPONDENCE

Yisheng Chen  
✉ chenisheng@sxau.edu.cn

RECEIVED 04 September 2023

ACCEPTED 03 October 2023

PUBLISHED 11 October 2023

## CITATION

Chen Y, Kang W, Choma IM and Zhuang H (2023) Editorial: Medicine and food homology: emerging tool and methodology for separation and analysis of the bioactive factors. *Front. Nutr.* 10:1288237. doi: 10.3389/fnut.2023.1288237

## COPYRIGHT

© 2023 Chen, Kang, Choma and Zhuang. This is an open-access article distributed under the terms of the [Creative Commons Attribution License \(CC BY\)](#). The use, distribution or reproduction in other forums is permitted, provided the original author(s) and the copyright owner(s) are credited and that the original publication in this journal is cited, in accordance with accepted academic practice. No use, distribution or reproduction is permitted which does not comply with these terms.

# Editorial: Medicine and food homology: emerging tool and methodology for separation and analysis of the bioactive factors

Yisheng Chen<sup>1\*</sup>, Wenyi Kang<sup>2</sup>, Irena M. Choma<sup>3</sup> and Haining Zhuang<sup>4</sup>

<sup>1</sup>College of Food Science and Engineering, Shanxi Agricultural University, Taiyuan, China, <sup>2</sup>National R&D Center for Edible Fungus Processing Technology, Henan University, Zhengzhou, China, <sup>3</sup>Department of Chromatography, Institute of Chemical Sciences, Faculty of Chemistry, Marie Curie-Skłodowska University, Lublin, Poland, <sup>4</sup>School of Food and Tourism, Shanghai Urban Construction Vocational College, Shanghai, China

## KEYWORDS

medicine and food homology, bioactive factor, separation, functional value, analytical tool

## Editorial on the Research Topic

Medicine and food homology: emerging tool and methodology for separation and analysis of the bioactive factors

This Research Topic was dedicated to introducing emerging tool and methodology tailored for dealing with separation, identification, authentication, and elucidation of bioactive factors in Medicine and Food Homology (MFH) materials and products, in a direct and cost-efficient way. From the manuscripts submitted to the editorial team, a total of eight original research article and one review article focusing on this theme were eventually selected for publication.

With the increasing awareness of healthy life and scientific nutrition, the conception of MFH attracted marked attention around the world. MFH refers to edible materials that can be both employed as food and medicines. As matter of fact, there is no absolute boundary between each other. As the critical intersection of food and medicine, MFH materials are not only rich in nutrition, but also able to maintain people health, prevent, and cure diseases. With a long-standing history around the world, the revival and popularity of MFH conform to today's public trends of returning to a natural and healthy life. More importantly, MFH materials are a treasure resource of bioactive factors for current health-beneficial food and pharmaceuticals. Instead of consuming them in the form of raw material, future direction of MFH research is to unambiguously identify the compound responsible for the bioactivity, precisely isolate these bioactive factors and apply them into value-added usage, making them into more widely accepted functional foods and therapeutic drugs.

Therefore, further excavation and better understanding of these bioactive factors would be greatly helpful for sparkling innovative ideas of MFH materials processing. Nevertheless, the MFH material, as a whole, is a rather sophisticated bio-mixture, containing large array of phytochemicals. Besides, functional value of the MFH materials is highly influenced by

many factors. More specifically, the real efficacy component may be flooded by the huge number of co-existed phytochemicals. Moreover, conventional analytical approaches are not able to directly and accurately establish the relationship between chemical structures and observed bioactivity. All these difficulties pose serious challenges to the precise separation, identification, authentication, and elucidation of bioactive factors in MFH materials. As a key to solve these bottlenecks, powerful tool and methodology are urgently needed.

The research targets of the nine articles presented in this Research Topic covered a large array of MFH samples, including *Rehmannia glutinosa*, *Dendrobium officinale*, Cistanche, Mung Beans, *Rugosoannulata*, Poria, and *Tremella aurantialba*, vegetable oil. The individual bioactive factor, such as unsaturated fatty acid, polyphenol, oligosaccharide, and peptide, mainly responsible for the observed bioactivity in these MFH was individually separated and evaluated, chemically, biologically, and pharmacologically. A couple of state-of-the-art analytical tools and methodologies were highlighted in these articles.

Generally, the importance of ultra-high-performance liquid chromatography (UHPLC) was acknowledged in the separation of MFH, enabling simultaneous separation of hundreds of chemicals in MFH. On this basis, structural elucidation of the obtained separation result can be easily realized with the aid of advanced mass spectrometers, which is greatly helpful for the targeted and un-targeted analysis of MFH. Remarkably, a series of specialized software and online-database was introduced and exemplarily studied in this Research Topic. In combination with advanced separation devices, these powerful tools opened a new horizon for precisely matching the bioactivity of compounds with targeted biomacromolecules. For instance, Yan et al. attempted to employ network pharmacological analysis for unveiling the pharmacological mechanism of *Tremella aurantialba*, in which compounds with potential therapeutic effect for nervous system, immune system, endocrine system, neoplasm system, as well as cardiovascular system diseases were virtually identified. Guided by the similar principle, spectrum-effect, component knock-out, and molecular docking technique were used by Ma et al. for the analysis of Poria, unambiguously confirm that eight individual compounds, i.e., poricoic acid B, dehydrotumulosic acid, poricoic acid A, polyporenic acid C, 3-epidehydrotumulosic acid, dehydropachymic acid, 3-O-acetyl-16 $\alpha$ -hydroxytrametenolic acid, and pachymic acid, were mainly responsible for inhibitory activity against  $\alpha$ -glucosidase. These studies could be good examples showing how to establish the relationship between the observed bioactivity and the related compound in MFH.

Apart from column chromatographic tools like HPLC/GC utilized in the articles within this Research Topic, the editorial team was very enthusiastic to introduce the innovative application of instrumentalized planar chromatography (the so called high performance thin-layer chromatography, HPTLC) as a flexible and versatile tool for MFH analysis. Apart from being able to perform 2-dimensional chromatographic separation, HPTLC was more importantly used by Müller et al. as an all-in-one platform efficiently combining on-surface metabolization and multi-bioassays for profiling the real health function of vegetable oils. Particularly, this analytical tool can be performed without elaborate sample preparation or fractionation to ensure sample integrity. Thus, no sample part was lost, and the whole sample was studied on a single surface regarding all aspects. This made the methodology as well as technology miniaturized, lean, all-in-one, and very sustainable for screening bioactivity of MFH. This study may be a good evidence that instrumentalized planar chromatography is still an essential tool for MFH analysis.

All in all, the nine articles worth being read.

## Author contributions

YC: Conceptualization, Data curation, Funding acquisition, Writing—original draft, Writing—review and editing. WK: Writing—review and editing. IC: Writing—review and editing. HZ: Writing—review and editing.

## Conflict of interest

The authors declare that the research was conducted in the absence of any commercial or financial relationships that could be construed as a potential conflict of interest.

## Publisher's note

All claims expressed in this article are solely those of the authors and do not necessarily represent those of their affiliated organizations, or those of the publisher, the editors and the reviewers. Any product that may be evaluated in this article, or claim that may be made by its manufacturer, is not guaranteed or endorsed by the publisher.



## OPEN ACCESS

## EDITED BY

Yisheng Chen,  
Shanxi Agricultural University, China

## REVIEWED BY

Lanzhou Li,  
Jilin Agricultural University, China  
Leilei Chen,  
Shandong Academy of Agricultural  
Sciences, China

## \*CORRESPONDENCE

Pin Lv  
lvpin@hebmu.edu.cn  
Yan Zhang  
snowwinglv@126.com

## SPECIALTY SECTION

This article was submitted to  
Food Chemistry,  
a section of the journal  
Frontiers in Nutrition

RECEIVED 29 October 2022

ACCEPTED 21 November 2022

PUBLISHED 07 December 2022

## CITATION

Yan Y, Wang M, Gan X, Wang X, Fu C,  
Li Y, Chen N, Lv P and Zhang Y (2022)  
Evaluation of pharmacological  
activities and active components  
in *Tremella aurantialba* by  
instrumental and virtual analyses.  
*Front. Nutr.* 9:1083581.  
doi: 10.3389/fnut.2022.1083581

## COPYRIGHT

© 2022 Yan, Wang, Gan, Wang, Fu, Li,  
Chen, Lv and Zhang. This is an  
open-access article distributed under  
the terms of the [Creative Commons  
Attribution License \(CC BY\)](#). The use,  
distribution or reproduction in other  
forums is permitted, provided the  
original author(s) and the copyright  
owner(s) are credited and that the  
original publication in this journal is  
cited, in accordance with accepted  
academic practice. No use, distribution  
or reproduction is permitted which  
does not comply with these terms.

# Evaluation of pharmacological activities and active components in *Tremella aurantialba* by instrumental and virtual analyses

Yonghuan Yan<sup>1,2</sup>, Mengtian Wang<sup>1,2</sup>, Xiaoruo Gan<sup>3</sup>,  
Xu Wang<sup>2,3</sup>, Chenghao Fu<sup>3</sup>, Yuemin Li<sup>3</sup>, Ning Chen<sup>3</sup>, Pin Lv<sup>3\*</sup>  
and Yan Zhang<sup>1,2\*</sup>

<sup>1</sup>Hebei Key Laboratory of Forensic Medicine, School of Forensic Medicine, Hebei Medical University, Shijiazhuang, China, <sup>2</sup>Hebei Food Inspection and Research Institute, Hebei Food Safety Key Laboratory, Key Laboratory of Special Food Supervision Technology for State Market Regulation, Hebei Engineering Research Center for Special Food Safety and Health, Shijiazhuang, China, <sup>3</sup>Key Laboratory of Neural and Vascular Biology of Ministry of Education, Department of Cell Biology, Cardiovascular Medical Science Center, Hebei Medical University, Shijiazhuang, China

As a kind of medicinal and edible homologous fungus, there is a lack of data on the medicinal value of *Tremella aurantialba*. In this study, ultra-performance liquid chromatography-quadrupole-time of flight-mass spectrometry (UPLC-Q-TOF/MS) was used to screen the chemical components in *T. aurantialba*. Then, network pharmacology was used to reveal the potential biological activities, active compounds, and therapeutic targets of *T. aurantialba*. Finally, the potential binding sites of the active compounds of *T. aurantialba* and key targets were studied by molecular docking. Results showed that 135 chemical components in *T. aurantialba*, especially linoleic acid, and linolenic acid have significant biological activities in neuroprotective, anticancer, immune, hypoglycemic, and cardiovascular aspects. The existence of these bioactive natural products in *T. aurantialba* is consistent with the traditional use of *T. aurantialba*. Moreover, the five diseases have comorbidity molecular mechanisms and therapeutic targets. The molecular docking showed that linolenic acid, adenosine, and vitamin D2 had higher binding energy with RXRA, MAPK1, and JUN, respectively. This study is the first to systematically identify chemical components in *T. aurantialba* and successfully predict its bioactivity, key active compounds, and drug targets, providing a reliable novel strategy for future research on the bioactivity development and utilization of *T. aurantialba*.

## KEYWORDS

*Tremella aurantialba*, component analysis, active compounds, drug targets, biological activity, virtual screening



## Introduction

*Tremella aurantialba* is a well-known medicinal and edible plant belonging to *fungi*, *Basidiomycota*, *Basidiomycotina*, *Tremellales*, *Naemateliaceae*, *Naematelia* Fr (1). It is widely distributed in Asia and Europe, North and America and Oceania; and can now be found all over the world due to artificial planting. *Tremella aurantialba* is rich in a variety of nutrients such as polysaccharide, dietary fiber, protein and other nutrients, and has great health value. As a high-quality precious medicinal and edible fungi, pharmacological effects of *Tremella aurantialba* have long been mentioned in TCM books. According to the “Compendium of Materia Medica” of the Ming Dynasty, *Tremella aurantialba* traditionally served to treat multiple diseases, especially moistening the lung and relieving cough, protecting the liver and tonifying the kidney. It is mentioned in Famous Doctor Bie Lu that *Tremella aurantialba* also has the effects of nourishing Qi and prolonging life, invigorating brain and dispersing cold. Xizang Common Chinese Herbal Medicine also records the effects of *Tremella aurantialba* on asthenia tuberculosis cough, hemoptysis, tuberculosis, asthma, hypertension and chronic bronchitis in the elderly. In Asian and European countries, *Tremella aurantialba* has been used as an edible food source and traditional medicine for millenary. The identification of functional components of edible fungi and the exploration of their functions have become the new hot spots and new trend in recent years (2–5). However, there are few modern studies on the compositions and activities of *Tremella aurantialba*, which limit the development and utilization of *Tremella aurantialba*.

Phytochemical profile analysis is a key step in the development and utilization of plant resources and quality safety assurance. So far, research on the composition of *Tremella aurantialba* has mainly involved the nutritional composition (6, 7), polysaccharides (8, 9), volatile components (6, 10) on the fruiting body, mycelium and fermentation broth, while several literatures reported the small-molecule chemical composition of *Tremella aurantialba*. Li isolated and purified 19 monomer compounds from petroleum ether, ethyl acetate and butyl alcohol extracts of the fruiting body of *Tremella aurantialba* by means of atmospheric pressure or vacuum silica gel column chromatography, thin layer chromatography, recrystallization and Sephadex LH-20 gel column chromatography, and finally 13 monomer compounds were identified for the first time through their physical and chemical properties and various spectral data. Among them, 3 $\beta$ -hydroxyl-24 $\alpha$ -lanoster-31-O- $\alpha$ -D-glucose-8, 24-dien is a new compound (11). However, the above studies adopted the traditional mode of “separation, enrichment, purification and identification” of monomer compounds, ignoring the overall analysis of the chemical profile of *Tremella aurantialba*, which was not conducive to the comprehensive excavation of the active components of *Tremella aurantialba*.

More importantly, the various therapeutic effects of *Tremella aurantialba* mentioned in Chinese medicine books

have rarely been confirmed by modern pharmacological studies. Several studies have reported the biological activities of the crude extracts or related products of *Tremella aurantialba* *in vivo* or *in vitro*. Liu et al. found that the crude lipids extract of *Tremella aurantialba* could promote the penetration of Evans blue through the blood-brain barrier (12). Du et al. found that the chloroform extract of *Tremella aurantialba* fruiting body has a good inhibitory effect on neoplasm cells L210 and SW620 (13). In addition, due to the high content of polysaccharides in *Tremella aurantialba*, more modern studies have emphasized the bioactivities of *Tremella aurantialba* polysaccharide, including enhancing immunity (14), anti-oxidation (9, 15) and so on. However, these studies on the evaluation of the biological activity of *Tremella aurantialba* were not comprehensive, and they only briefly evaluated the role of *Tremella aurantialba* or its main component polysaccharide in some diseases or some of its active functions. Furthermore, the mechanism of *Tremella aurantialba* in the prevention and treatment of diseases is still unclear.

So far, many studies have shown diverse health effects of fungi due to the presence of a variety of bioactive compounds (16–19). These compounds tend to be biologically multiple-functional. However, due to the unclear chemical profile of *Tremella aurantialba*, the biological activities of *Tremella aurantialba* cannot be further excavated at present. Thus, to better apply *Tremella aurantialba* resources, it is urgent to comprehensively analyze the chemical components and biological activities of *Tremella aurantialba*. The main purpose of this study here was to systematically evaluate the chemical composition and bioactivity of *Tremella aurantialba* using UPLC-Q/TOF MS system combined with network pharmacology that have never been systematically investigated. The key active components in *Tremella aurantialba* and their pharmacodynamic targets were also revealed. Whether the component binds to the target were validated by molecular docking. Moreover, the comorbidity mechanisms and potential therapeutic targets of five diseases were explored. In this direction, the research aims to provide some knowledge on the chemical composition and bioactivities of *Tremella aurantialba* from the health point of view, which will help to verify its clinical application and the further development of *Tremella aurantialba* resources.

## Materials and methods

### Chemicals and reagents

Liquid chromatography-mass spectrometry (LC-MS) grade methanol, acetonitrile, ammonium formate and formic acid were purchased from Sigma-Aldrich (St. Louis, MO, USA). Deionized water (18.3 M $\Omega$ ) was generated by a Milli-Q water purification system (Millipore Ltd., Bedford, MA, USA). *Tremella aurantialba* were collected from Yunnan Bacteria Horizon Biotechnology Co., Ltd.

## Samples preparation

*Tremella aurantialba* samples was frozen dried under vacuum condition and crushed into powder through a 100-mesh screen. Then the samples were kept at  $-80^{\circ}\text{C}$  for further use. The extraction procedure and conditions were performed as following: 1.0 g of freeze drying *Tremella aurantialba* powder was weighted and placed in 50 mL centrifuge tube, and then the sample was extracted with 20 mL methanol-water (7: 3, V/V) (Darmstadt, Germany). After vortexing for 1 min and sonicating at room temperature for 30 min, the mixture was centrifuged at 10 000 r/min at  $4^{\circ}\text{C}$  for 5 min. 1 mL supernatant was filtered with a  $0.22\ \mu\text{m}$  nylon membrane before UPLC-Q-TOF/MS analysis.

## Instrumentation

A LC-30AD UPLC system (Shimadzu Corporation, Kyoto, Japan) was used for the chromatographic separation of the samples. Compounds separation was performed on a Waters ACQUITY UPLC HSS T3 column ( $100\ \text{mm} \times 2.1\ \text{mm}$ ,  $1.8\ \mu\text{m}$ ) using a gradient elution consist of 0.01% formic acid + 2 mmol/L ammonium formate (A) and acetonitrile + 0.01% formic acid + 2 mmol/L ammonium formate (B). The gradient program was: 5–12% B at 0–5 min, 12–55% B at 5–7 min, 55–65% B at 7–10 min, 65–98% B at 10–20 min, 98% B at 20–25 min, 98–5% B at 25–25.1 min and 5% B at 25.1–28 min. The flow rate was 0.3 mL/min, the column temperature was maintained at  $40^{\circ}\text{C}$ . The sample injection volume was  $2\ \mu\text{L}$ .

The QTOF MS analysis, controlled by the Sciex OS software (version 1.5.0, Sciex, USA), was performed on a hybrid quadrupole time-of-flight tandem mass spectrometer Q-TOF/MS with an electrospray ionization (ESI) source (Triple TOF<sup>TM</sup> 5600 + MS system, AB Sciex Corporation., Foster City, CA, USA). The ionization of compounds was in the positive or negative mode. Information dependent acquisition method was used for acquiring spectra data with a scan range from 100 to 1000  $m/z$ . Other optimized MS parameters were set as follows: ion spray voltage 5500 V in positive ion mode and 4500 V in negative ion mode; the ion source gas1, 50 psi; the ion source gas 250 psi; the curtain gas, 35 psi; ion source temperature,  $500^{\circ}\text{C}$ ; declustering potential, 80 V; collision energy, 60 V.

## Network pharmacology analysis

### Target prediction of *Tremella aurantialba*

First, the active components of *Tremella aurantialba* were screened by SwissADME platform<sup>1</sup> and literatures. At

SwissADME platform, gastrointestinal absorption, one of the pharmacokinetic parameters, was set as “HIGH” as the condition for drug absorption and active compounds with good oral bioavailability were screened. At SwissADME platform, the screening criteria for bioavailability are lipophilicity: XLOGP3 between  $-0.7$  and  $+5.0$ , size: MW between 150 and 500 g/mol, polarity: TPSA between 20 and  $130\ \text{\AA}^2$ , solubility: log S not higher than 6, saturation: fraction of carbons in the  $\text{sp}^3$  hybridization not less than 0.25, and flexibility: no more than 9 rotatable bonds. Besides, the drug-likeness is also considered. For cosmeceutical parameters (Lipinski, Ghose, Veber, Egan, Muegge), two or more of them with “YES” can be regarded as active components. At the same, the components with significant pharmacological activity reported in the literature are also considered as active ingredients. Secondly, Swiss Target Prediction platform<sup>2</sup> was applied to predict the possible targets. Swiss Target Prediction selected the targets whose probability is  $>0.12$  in the prediction results for further analysis. At the same time, experimentally verified targets information was downloaded from NPASS<sup>3</sup> and the entries related to the active components of *Tremella aurantialba* were extracted. Finally, target information was integrated and accumulated to obtain the possible targets of *Tremella aurantialba* active components.

### Prediction for targets of five diseases

Data for all-associated disease targets were acquired from six databases, including the National Center for Biotechnology Information database (NCBI<sup>4</sup>), the Online Mendelian Inheritance in Man Database (OMIM<sup>5</sup>), the GeneCards database,<sup>6</sup> the Therapeutic Target Database (TTD<sup>7</sup>), the Comparative Toxicogenomics Database (CTD<sup>8</sup>), a database of gene-disease associations (DisGNet<sup>9</sup>), using “Nervous system disease,” “Immune System Diseases,” “Endocrine System Diseases,” “Neoplasms,” “Cardiovascular Diseases” and their synonyms and descendants in the CTD Database as the keywords, respectively. The above targets were converted and queried into the UniProt ID format with “Homo sapiens” as the qualifying condition in the UniProt database.<sup>10</sup> Finally, the gene library of all was established by eliminating repeated targets.

<sup>2</sup> <http://www.swisstargetprediction.ch/>

<sup>3</sup> <https://bidd.group/NPASS/index.php>

<sup>4</sup> <https://www.ncbi.nlm.nih.gov/>

<sup>5</sup> <https://www.omim.org/>

<sup>6</sup> <https://www.genecards.org/>

<sup>7</sup> <http://db.idrblab.net/ttd>

<sup>8</sup> <https://ctdbase.org/>

<sup>9</sup> <https://www.disgenet.org/>

<sup>10</sup> <https://www.uniprot.org/>

<sup>1</sup> <http://swissADME.ch/index.php>

## Intersection between active compounds and disease targets

The intersection targets between the disease genes and the predicted *Tremella aurantialba* targets were obtained and the National Genomics Data Center website<sup>11</sup> was used to construct a Venn diagram for visualization.

## Protein-protein interaction network construction

The intersection targets above were imported into the STRING database<sup>12</sup> for protein interaction network analysis. The screening condition of the species was set to “Homo sapiens” and the minimum required interaction score was “highest confidence (0.9)”. Input protein-protein interaction (PPI) information into Cytoscape 3.7.1<sup>13</sup> for visualization and constructs network of potential key targets.

## Topological and cluster analyses of the protein-protein interaction network

The CytoHubba plugin in Cytoscape was used to identify hub genes. Three critical topological parameters were chosen for screening the core composite targets based on the PPI network: degree (D), betweenness (B) and closeness (C). Values for the three parameters indicated the significance as well as the impact of relevant nodes in the entire network. The top 10 nodes were set as the core targets and the hub gene was obtained through the intersection of the top 10 core targets obtained by different algorithms. The MCODE plug-in in Cytoscape was used to screen PPI network modules using various cut-offs: degree = 2, k-core = 2, node score = 0.2, and max depth = 100.

## Gene ontology and kyoto encyclopedia of genes and genomes enrichment analyses

The intersection targets above were subjected to the Gene Ontology (GO) biological process analysis and the Kyoto Encyclopedia of Genes and Genomes (KEGG) enrichment analyses using the DAVID database,<sup>14</sup> with FDR < 0.05 and  $P < 0.05$  as cut-off values. R version 3.4.1 was used to visualize the results.

## Construction of active compound-target network

After obtaining the intersection genes, reverse screening the active components in *Tremella aurantialba*. For visualization, potential active components and matching intersection targets were imported into Cytoscape 3.7.1 software and a network of compound-target network was built. Each component of targets is represented by nodes and the relationship between

the components, diseases and the targets are represented by connecting lines.

## Verification of the compound-target interactions

The crystal structures of the targets and the chemical structures of the composition were obtained from the PDB<sup>15</sup> and the PubChem.<sup>16</sup> Molecular docking was performed using the AutoDock software. The water molecules and atoms were removed from the target receptors and then the affinities were obtained. Finally, the binding sites of composition and targets were visualized by the PyMOL software.

## Results and discussion

### Targeted and untargeted analysis of chemical components in *Tremella aurantialba*

In this study, targeted and untargeted analysis strategies combined with UPLC-Q/TOF MS were firstly used for the qualitative screening of chemical components in *Tremella aurantialba* and the chromatography condition was optimized to obtained higher peak capacity, shorter retention and better resolution of components in *Tremella aurantialba*. Subsequently, a total of 135 chemical components were rapidly identified by comparing with TCM MS/MS database, online Chemspider database or inferred through mass spectrometry fragment ion analysis and literature data, including 22 organic acids, 20 amino acids and their derivatives, 12 fatty acids, 13 saccharides, 8 nucleosides, 6 vitamins, 7 alkaloids, 8 esters, 4 amides, 3 terpenoids, 2 phenols, 2 ethers, 1 alcohol, 1 ketone and 26 other classes (Table 1). Among these components, fatty acids, organic acids and saccharides were the major components of *Tremella aurantialba*. In addition, the species of amino acids in *Tremella aurantialba* are abundant. The total ion chromatograms of *Tremella aurantialba* are shown in Supplementary Figure 1. By comparing with the available credible standards and literatures, and cross-checking with some available spectral databases, TCM, Metlin and Chemspider, the components of *Tremella aurantialba* were identified and characterized. It could be summarized as follows and some specific compounds were taken as examples.

### Identification of fatty acids

A total of 12 fatty acids mainly originated from *Tremella aurantialba*, including linoleic acid, oleic acid, palmitic acid,

<sup>11</sup> <https://ngdc.cncb.ac.cn/bit/venn>

<sup>12</sup> <http://string-db.org>

<sup>13</sup> <https://www.cytoscape.org/>

<sup>14</sup> <https://david.ncifcrf.gov/>

<sup>15</sup> <https://www.rcsb.org>

<sup>16</sup> <https://pubchem.ncbi.nlm.nih.gov/>

TABLE 1 Identification of components in *Tremella aurantialba* by UPLC-Q/TOF MS.

No.	Compounds	Formulas	Adducts	Precursor ions <i>m/z</i>	Peak area	Retention time/min.	Compound types
1	Linoleic acid	C <sub>18</sub> H <sub>32</sub> O <sub>2</sub>	[M-H] <sup>-</sup>	279.2341	6.00E + 07	19.92	Fatty acids
2	Oleic acid	C <sub>18</sub> H <sub>34</sub> O <sub>2</sub>	[M-H] <sup>-</sup>	281.2496	4.31E + 07	20.64	Fatty acids
3	Palmitic acid	C <sub>16</sub> H <sub>32</sub> O <sub>2</sub>	[M-H] <sup>-</sup>	255.2335	9.15E + 06	20.35	Fatty acids
4	Hydroperoxy-octadecadienoic acid isomer 1	C <sub>18</sub> H <sub>32</sub> O <sub>4</sub>	[M-H] <sup>-</sup>	311.2236	7.21E + 06	15.14	Fatty acids
5	Linolenic acid	C <sub>18</sub> H <sub>30</sub> O <sub>2</sub>	[M + H] <sup>+</sup>	279.2313	2.89E + 06	16.79	Fatty acids
6	Stearic acid	C <sub>18</sub> H <sub>36</sub> O <sub>2</sub>	[M-H] <sup>-</sup>	283.2648	1.75E + 06	21.49	Fatty acids
7	Palmitoleic acid	C <sub>16</sub> H <sub>30</sub> O <sub>2</sub>	[M-H] <sup>-</sup>	253.2175	8.67E + 05	19.45	Fatty acids
8	Trihydroxyoctadecenoic acid	C <sub>18</sub> H <sub>34</sub> O <sub>5</sub>	[M-H] <sup>-</sup>	329.2331	2.05E + 05	11.99	Fatty acids
9	Lignoceric acid	C <sub>24</sub> H <sub>48</sub> O <sub>2</sub>	[M-H] <sup>-</sup>	367.3576	9.00E + 04	25.42	Fatty acids
10	Arachidic acid	C <sub>20</sub> H <sub>40</sub> O <sub>2</sub>	[M-H] <sup>-</sup>	311.2956	7.39E + 04	22.58	Fatty acids
11	Behenic acid	C <sub>22</sub> H <sub>44</sub> O <sub>2</sub>	[M-H] <sup>-</sup>	339.3267	7.38E + 04	23.84	Fatty acids
12	Hydroxystearic acid	C <sub>18</sub> H <sub>35</sub> O <sub>3</sub>	[M-H] <sup>-</sup>	298.2501	6.97E + 03	8.58	Fatty acids
13	Citric acid	C <sub>6</sub> H <sub>8</sub> O <sub>7</sub>	[M-H] <sup>-</sup>	191.0197	4.83E + 06	0.98	Organic acids
14	Maleic acid	C <sub>4</sub> H <sub>6</sub> O <sub>5</sub>	[M-H] <sup>-</sup>	133.0145	1.24E + 06	0.91	Organic acids
15	Galactonic acid	C <sub>6</sub> H <sub>12</sub> O <sub>7</sub>	[M + H] <sup>+</sup>	197.0653	9.67E + 05	0.84	Organic acids
16	Phthalic acid	C <sub>8</sub> H <sub>6</sub> O <sub>4</sub>	[M + H] <sup>+</sup>	167.0334	8.55E + 05	21.16	Organic acids
17	Indoleacrylic acid	C <sub>11</sub> H <sub>9</sub> NO <sub>2</sub>	[M + H] <sup>+</sup>	188.0707	6.78E + 05	5.42	Organic acids
18	Amber Acid	C <sub>4</sub> H <sub>6</sub> O <sub>4</sub>	[M-H] <sup>-</sup>	117.0194	1.38E + 05	1.5	Organic acids
19	Hydroxymethylglutaric acid	C <sub>6</sub> H <sub>10</sub> O <sub>5</sub>	[M-H] <sup>-</sup>	161.0455	5.18E + 04	0.9	Organic acids
20	Ursolic acid	C <sub>30</sub> H <sub>48</sub> O <sub>3</sub>	[M-H] <sup>-</sup>	455.3527	5.10E + 04	22.47	Organic acids
21	3-Phenylbutyric acid	C <sub>10</sub> H <sub>12</sub> O <sub>2</sub>	[M + H] <sup>+</sup>	165.0905	4.02E + 04	7.56	Organic acids
22	Oleanolic acid	C <sub>30</sub> H <sub>48</sub> O <sub>3</sub>	[M-H] <sup>-</sup>	455.3515	3.57E + 04	22.45	Organic acids
23	D-Glucose 6-phosphate	C <sub>6</sub> H <sub>13</sub> O <sub>9</sub> P	[M + H] <sup>+</sup>	261.0363	3.40E + 04	0.85	Organic acids
24	Sinapic acid 4-O-glucoside	C <sub>17</sub> H <sub>22</sub> O <sub>10</sub>	[M-H] <sup>-</sup>	385.1149	3.24E + 04	0.87	Organic acids
25	Phenyllactic acid	C <sub>9</sub> H <sub>10</sub> O <sub>3</sub>	[M-H] <sup>-</sup>	165.0558	2.08E + 04	8.17	Organic acids
26	2-Aminoisobutyric acid	C <sub>4</sub> H <sub>9</sub> NO <sub>2</sub>	[M + H] <sup>+</sup>	104.0704	1.82E + 04	0.84	Organic acids
27	Aconitic acid	C <sub>6</sub> H <sub>6</sub> O <sub>6</sub>	[M-H] <sup>-</sup>	173.0094	1.09E + 04	0.98	Organic acids
28	Quinic acid	C <sub>7</sub> H <sub>12</sub> O <sub>6</sub>	[M-H] <sup>-</sup>	191.056	9.64E + 03	0.94	Organic acids
29	4-Hydroxybenzoic acid	C <sub>7</sub> H <sub>6</sub> O <sub>3</sub>	[M + H] <sup>+</sup>	139.0387	8.59E + 03	0.95	Organic acids
30	3-O-caffeoyl-shikimic acid	C <sub>16</sub> H <sub>16</sub> O <sub>8</sub>	[M-H] <sup>-</sup>	335.0783	8.59E + 03	1.84	Organic acids
31	cinnamic acid	C <sub>9</sub> H <sub>8</sub> O <sub>2</sub>	[M + H] <sup>+</sup>	149.0595	4.55E + 03	13.41	Organic acids
32	<i>p</i> -Anisic acid	C <sub>8</sub> H <sub>8</sub> O <sub>3</sub>	[M + H] <sup>+</sup>	153.0546	4.00E + 03	9.56	Organic acids
33	2,4-dihydroxybenzoic acid	C <sub>7</sub> H <sub>6</sub> O <sub>4</sub>	[M-H] <sup>-</sup>	153.0198	1.15E + 03	1.02	Organic acids
34	Shikimic acid	C <sub>7</sub> H <sub>10</sub> O <sub>5</sub>	[M-H] <sup>-</sup>	173.0455	1.07E + 03	0.94	Organic acids
35	L-Carnitine	C <sub>7</sub> H <sub>15</sub> NO <sub>3</sub>	[M + H] <sup>+</sup>	162.1125	3.69E + 06	0.82	Amino acids
36	L- (+)-Valinol	C <sub>5</sub> H <sub>13</sub> NO	[M + H] <sup>+</sup>	104.1072	1.91E + 06	0.82	Amino acids
37	L-Leucine	C <sub>6</sub> H <sub>13</sub> NO <sub>2</sub>	[M + H] <sup>+</sup>	132.1018	1.27E + 06	1.7	Amino acids
38	L-aspartic acid	C <sub>4</sub> H <sub>7</sub> NO <sub>4</sub>	[M + H] <sup>+</sup>	134.0448	1.34E + 05	0.85	Amino acids
39	L-Methionine	C <sub>5</sub> H <sub>11</sub> NO <sub>2</sub> S	[M + H] <sup>+</sup>	150.0578	7.39E + 04	1.18	Amino acids
40	Pipecolic acid	C <sub>6</sub> H <sub>11</sub> NO <sub>2</sub>	[M + H] <sup>+</sup>	130.0862	3.88E + 04	0.93	Amino acids
41	L-tyrosine	C <sub>9</sub> H <sub>11</sub> NO <sub>3</sub>	[M + H] <sup>+</sup>	182.0812	2.90E + 04	0.95	Amino acids
42	Histidine	C <sub>6</sub> H <sub>9</sub> N <sub>3</sub> O <sub>2</sub>	[M + H] <sup>+</sup>	156.0765	2.58E + 04	0.94	Amino acids
43	L-Alanine	C <sub>3</sub> H <sub>7</sub> NO <sub>2</sub>	[M + H] <sup>+</sup>	90.0547	2.03E + 04	5	Amino acids
44	Isoleucine	C <sub>6</sub> H <sub>13</sub> NO <sub>2</sub>	[M + H] <sup>+</sup>	132.1018	2.02E + 04	1.77	Amino acids
45	L-Aspartyl-L-phenylalanine	C <sub>13</sub> H <sub>16</sub> N <sub>2</sub> O <sub>5</sub>	[M + H] <sup>+</sup>	281.113	1.68E + 04	2.39	Amino acids
46	Phenylalanine	C <sub>9</sub> H <sub>11</sub> NO <sub>2</sub>	[M + H] <sup>+</sup>	166.0861	1.67E + 04	0.97	Amino acids
47	Arginine	C <sub>6</sub> H <sub>14</sub> N <sub>4</sub> O <sub>2</sub>	[M + H] <sup>+</sup>	175.119	1.59E + 04	0.94	Amino acids
48	L-Glutamic acid	C <sub>5</sub> H <sub>9</sub> NO <sub>4</sub>	[M + H] <sup>+</sup>	148.0604	1.55E + 04	0.93	Amino acids
49	Glutamine	C <sub>5</sub> H <sub>10</sub> N <sub>2</sub> O <sub>3</sub>	[M + H] <sup>+</sup>	145.0617	1.40E + 04	0.88	Amino acids
50	Proline	C <sub>5</sub> H <sub>9</sub> NO <sub>2</sub>	[M + H] <sup>+</sup>	116.0706	1.15E + 04	0.94	Amino acids
51	Levodopa	C <sub>9</sub> H <sub>11</sub> NO <sub>4</sub>	[M + H] <sup>+</sup>	198.076	8.80E + 03	0.96	Amino acids
52	Threonine	C <sub>4</sub> H <sub>9</sub> NO <sub>3</sub>	[M + H] <sup>+</sup>	120.0654	5.92E + 03	0.91	Amino acids
53	Valine	C <sub>5</sub> H <sub>11</sub> NO <sub>2</sub>	[M + H] <sup>+</sup>	118.0867	5.38E + 03	0.99	Amino acids
54	GABA	C <sub>4</sub> H <sub>9</sub> NO <sub>2</sub>	[M + H] <sup>+</sup>	104.0703	4.33E + 03	0.87	Amino acids

(Continued)

TABLE 1 (Continued)

No.	Compounds	Formulas	Adducts	Precursor ions <i>m/z</i>	Peak area	Retention time/min.	Compound types
55	Gluconic acid	C <sub>6</sub> H <sub>12</sub> O <sub>7</sub>	[M-H] <sup>-</sup>	195.0522	2.77E + 07	0.8	Saccharides
56	Mannitol	C <sub>6</sub> H <sub>14</sub> O <sub>6</sub>	[M-H] <sup>-</sup>	181.0719	4.40E + 06	0.82	Saccharides
57	D-Sorbitol	C <sub>6</sub> H <sub>14</sub> O <sub>6</sub>	[M-H] <sup>-</sup>	181.072	3.41E + 06	0.82	Saccharides
58	Sucrose	C <sub>12</sub> H <sub>22</sub> O <sub>11</sub>	[M-H] <sup>-</sup>	341.1091	2.85E + 06	0.85	Saccharides
59	Trehalose	C <sub>12</sub> H <sub>22</sub> O <sub>11</sub>	[M-H] <sup>-</sup>	341.1091	2.85E + 06	0.85	Saccharides
60	Xylitol	C <sub>5</sub> H <sub>12</sub> O <sub>5</sub>	[M-H] <sup>-</sup>	151.0611	5.66E + 05	0.86	Saccharides
61	D- (+) – Mannose	C <sub>6</sub> H <sub>12</sub> O <sub>6</sub>	[M-H] <sup>-</sup>	179.056	1.26E + 05	0.91	Saccharides
62	Gluconic acid	C <sub>6</sub> H <sub>10</sub> O <sub>7</sub>	[M-H] <sup>-</sup>	193.0355	7.87E + 04	0.74	Saccharides
63	Melezitose	C <sub>18</sub> H <sub>32</sub> O <sub>16</sub>	[M-H] <sup>-</sup>	503.1613	5.18E + 04	0.93	Saccharides
64	Beta-N-Acetylglucosamine	C <sub>8</sub> H <sub>15</sub> NO <sub>6</sub>	[M + H] <sup>+</sup>	222.0973	1.48E + 04	0.88	Saccharides
65	D-xylose	C <sub>5</sub> H <sub>10</sub> O <sub>5</sub>	[M-H] <sup>-</sup>	149.0459	1.12E + 04	0.9	Saccharides
66	Neoriciocitrin	C <sub>27</sub> H <sub>32</sub> O <sub>15</sub>	[M-H] <sup>-</sup>	595.1696	4.05E + 03	20.39	Saccharides
67	D- (+) – digitoxose	C <sub>6</sub> H <sub>12</sub> O <sub>4</sub>	[M-H] <sup>-</sup>	147.0665	2.50E + 03	2.38	Saccharides
68	Adenine	C <sub>5</sub> H <sub>5</sub> N <sub>5</sub>	[M + H] <sup>+</sup>	136.062	4.75E + 06	1.82	Nucleosides
69	Uridine	C <sub>9</sub> H <sub>12</sub> N <sub>2</sub> O <sub>6</sub>	[M-H] <sup>-</sup>	243.0622	6.15E + 05	1.83	Nucleosides
70	Uracil	C <sub>4</sub> H <sub>4</sub> N <sub>2</sub> O <sub>2</sub>	[M + H] <sup>+</sup>	113.0342	3.24E + 05	1.73	Nucleosides
71	Cytidine	C <sub>9</sub> H <sub>13</sub> N <sub>3</sub> O <sub>5</sub>	[M-H] <sup>-</sup>	242.0791	2.89E + 05	0.79	Nucleosides
72	Hydroxypurine	C <sub>5</sub> H <sub>4</sub> N <sub>4</sub> O	[M + H] <sup>+</sup>	137.0456	1.10E + 05	1.55	Nucleosides
73	Adenosine	C <sub>10</sub> H <sub>13</sub> N <sub>5</sub> O <sub>4</sub>	[M + H] <sup>+</sup>	268.1039	5.45E + 04	4.88	Nucleosides
74	Xanthine	C <sub>5</sub> H <sub>4</sub> N <sub>4</sub> O <sub>2</sub>	[M + H] <sup>+</sup>	153.0408	5.36E + 04	1.29	Nucleosides
75	Cytosine	C <sub>4</sub> H <sub>5</sub> N <sub>3</sub> O	[M + H] <sup>+</sup>	112.0502	6.89E + 03	0.95	Nucleosides
76	Nicotinic acid	C <sub>6</sub> H <sub>5</sub> NO <sub>2</sub>	[M + H] <sup>+</sup>	124.0393	2.57E + 06	0.91	Vitamins
77	Nicotinamide	C <sub>6</sub> H <sub>6</sub> N <sub>2</sub> O	[M + H] <sup>+</sup>	123.0554	5.42E + 05	2.66	Vitamins
78	Vitamin D2	C <sub>28</sub> H <sub>44</sub> O	[M + H] <sup>+</sup>	397.3456	2.67E + 05	24.12	Vitamins
79	Pantothenic acid	C <sub>9</sub> H <sub>17</sub> NO <sub>5</sub>	[M-H] <sup>-</sup>	218.1036	1.92E + 05	4.93	Vitamins
80	γ-Tocotrienol	C <sub>28</sub> H <sub>42</sub> O <sub>2</sub>	[M-H] <sup>-</sup>	409.3106	1.25E + 05	20.24	Vitamins
81	Vitamin C	C <sub>6</sub> H <sub>8</sub> O <sub>6</sub>	[M-H] <sup>-</sup>	175.025	9.58E + 03	0.9	Vitamins
82	Trigonelline	C <sub>7</sub> H <sub>7</sub> NO <sub>2</sub>	[M + H] <sup>+</sup>	138.0551	1.96E + 06	0.86	Alkaloids
83	Choline	C <sub>5</sub> H <sub>13</sub> NO	[M + H] <sup>+</sup>	104.1072	1.85E + 06	0.82	Alkaloids
84	Nicotine	C <sub>10</sub> H <sub>14</sub> N <sub>2</sub>	[M + H] <sup>+</sup>	163.1229	9.04E + 04	11.76	Alkaloids
85	(R, S)-anatabine	C <sub>10</sub> H <sub>12</sub> N <sub>2</sub>	[M + H] <sup>+</sup>	161.1073	8.14E + 04	14.94	Alkaloids
86	Lupinine	C <sub>10</sub> H <sub>19</sub> NO	[M + H] <sup>+</sup>	170.1536	1.16E + 04	19.59	Alkaloids
87	Arecoline	C <sub>8</sub> H <sub>13</sub> NO <sub>2</sub>	[M + H] <sup>+</sup>	156.1017	3.65E + 03	0.96	Alkaloids
88	Stachydrine	C <sub>7</sub> H <sub>13</sub> NO <sub>2</sub>	[M + H] <sup>+</sup>	144.1012	2.29E + 03	0.95	Alkaloids
89	Methyl linoleate	C <sub>19</sub> H <sub>34</sub> O <sub>2</sub>	[M + H] <sup>+</sup>	295.2629	1.24E + 06	21.29	Esters
90	C20 sphinganine	C <sub>20</sub> H <sub>43</sub> NO <sub>2</sub>	[M + H] <sup>+</sup>	330.3358	1.06E + 06	10.76	Esters
91	Phytosphingosine	C <sub>18</sub> H <sub>39</sub> NO <sub>3</sub>	[M + H] <sup>+</sup>	318.2992	8.80E + 05	9.23	Esters
92	Gluconolactone	C <sub>6</sub> H <sub>10</sub> O <sub>6</sub>	[M + H] <sup>+</sup>	179.0548	8.17E + 05	1.01	Esters
93	3-N-butyl-4, 5-dihydrophthalide	C <sub>12</sub> H <sub>16</sub> O <sub>2</sub>	[M + H] <sup>+</sup>	193.1219	8.80E + 04	9.94	Esters
94	Glycerophosphoric acid	C <sub>3</sub> H <sub>9</sub> O <sub>6</sub> P	[M-H] <sup>-</sup>	171.0065	1.73E + 04	0.77	Esters
95	2-linoleoyl-sn-glycero-3-phosphoethanolamine	C <sub>23</sub> H <sub>44</sub> NO <sub>7</sub> P	[M-H] <sup>-</sup>	476.2778	1.16E + 04	17.93	Esters
96	1-oleoyl phosphatidylethanolamine	C <sub>23</sub> H <sub>46</sub> NO <sub>7</sub> P	[M-H] <sup>-</sup>	478.2939	7.86E + 03	18.76	Esters
97	Thraustochytride-2	C <sub>43</sub> H <sub>79</sub> NO <sub>8</sub>	[M + H] <sup>+</sup>	738.5864	7.96E + 06	24.47	Amides
98	Thraustochytride-1	C <sub>42</sub> H <sub>77</sub> NO <sub>8</sub>	[M + H] <sup>+</sup>	724.5706	3.29E + 06	23.2	Amides
99	Thraustochytride A	C <sub>41</sub> H <sub>75</sub> NO <sub>8</sub>	[M + H] <sup>+</sup>	710.5548	1.18E + 06	22.24	Amides
100	Feruloylagmatine	C <sub>15</sub> H <sub>22</sub> N <sub>4</sub> O <sub>3</sub>	[M-H] <sup>-</sup>	305.1606	1.70E + 05	8.21	Amides
101	Glochidone	C <sub>30</sub> H <sub>46</sub> O	[M + H] <sup>+</sup>	423.3606	8.95E + 04	11.98	Terpenoids
102	F2 Ginsenoside	C <sub>42</sub> H <sub>72</sub> O <sub>13</sub>	[M-H] <sup>-</sup>	783.4919	5.36E + 03	17.99	Terpenoids
103	Helianthin	C <sub>20</sub> H <sub>25</sub> O <sub>6</sub>	[M-H] <sup>-</sup>	360.1563	7.72E + 02	8.18	Terpenoids
104	Dihydrocapsiate	C <sub>18</sub> H <sub>28</sub> O <sub>4</sub>	[M-H] <sup>-</sup>	307.1909	7.52E + 03	22.72	Phenols
105	Isoacteoside	C <sub>29</sub> H <sub>36</sub> O <sub>15</sub>	[M + NH <sub>4</sub> ] <sup>+</sup>	642.2412	2.63E + 02	21.17	Phenols
106	(+)-Costunolide	C <sub>15</sub> H <sub>20</sub> O <sub>2</sub>	[M + H] <sup>+</sup>	233.1538	9.34E + 04	7.33	Ethers

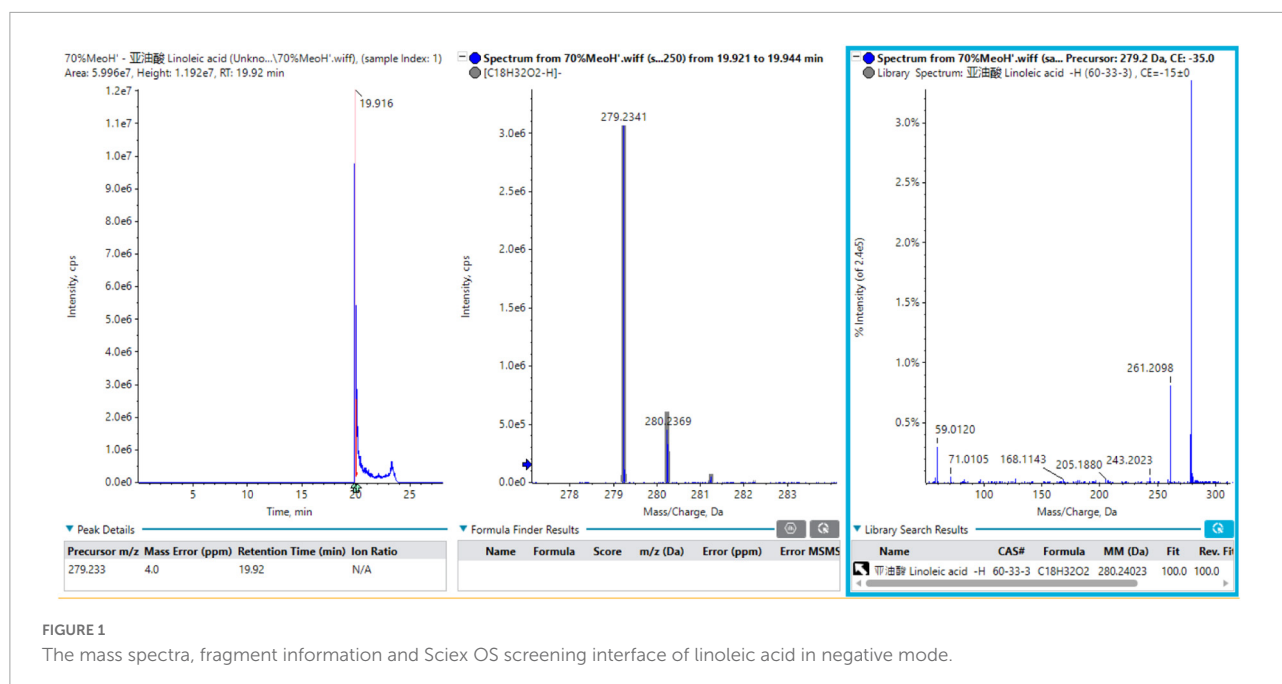
(Continued)



TABLE 1 (Continued)

No.	Compounds	Formulas	Adducts	Precursor ions <i>m/z</i>	Peak area	Retention time/min.	Compound types
107	Di-2-propenyl disulfide	C <sub>6</sub> H <sub>10</sub> S <sub>2</sub>	[M + FA-H] <sup>−</sup>	191.02	8.95E + 04	0.98	Ethers
108	N-(4-Acetylphenyl) maleimide	C <sub>12</sub> H <sub>9</sub> NO <sub>3</sub>	[M-H] <sup>−</sup>	214.0513	9.27E + 05	0.8	Ketone
109	Mycosporine serinol	C <sub>11</sub> H <sub>19</sub> NO <sub>6</sub>	[M + H] <sup>+</sup>	262.1276	2.21E + 05	0.91	Alcohols
110	Glycerophosphocholine	C <sub>8</sub> H <sub>20</sub> NO <sub>6</sub> P	[M + H] <sup>+</sup>	258.1112	1.86E + 07	0.81	Other classes
111	N1-[[2-(Diethylamino)-1,3-thiazol-5-yl] methyl]-N2, N2, 4-trimethyl-1, 2-pentanediamine	C <sub>16</sub> H <sub>32</sub> N <sub>4</sub> S	[M-H] <sup>−</sup>	311.2269	2.27E + 06	10.03	Other classes
112	Metilox	C <sub>18</sub> H <sub>28</sub> O <sub>3</sub>	[M + H] <sup>+</sup>	293.2107	2.19E + 06	8.45	Other classes
113	2-Dodecyl-N-(1, 2, 2, 6, 6-Pentamethylpiperidin-4-yl) succinimide	C <sub>26</sub> H <sub>48</sub> N <sub>2</sub> O <sub>2</sub>	[M + H] <sup>+</sup>	421.3803	1.82E + 06	17.28	Other classes
114	N-[2-((4-(Diethylamino)butyl) carbamothioyl) amino) ethyl] pentanamide	C <sub>16</sub> H <sub>34</sub> N <sub>4</sub> OS	[M-H] <sup>−</sup>	329.2376	1.57E + 06	8.24	Other classes
115	Phenylacetylene	C <sub>8</sub> H <sub>6</sub>	[M + H] <sup>+</sup>	103.0545	1.45E + 06	2.53	Other classes
116	1-(Dicyclohexylphosphino)-4-methylpiperazine	C <sub>17</sub> H <sub>33</sub> N <sub>2</sub> P	[M-H] <sup>−</sup>	295.2321	1.02E + 06	11.63	Other classes
117	Dimethyl (1-((2E)-3-[4-hydroxy-3,5-bis(2-methyl-2-propenyl)-5,6,7,8-tetrahydro-1-naphthalenyl]-2-propenoyl) cyclopentyl) phosphonate	C <sub>28</sub> H <sub>43</sub> O <sub>5</sub> P	[M-H] <sup>−</sup>	489.2779	9.71E + 05	7.7	Other classes
118	(2E)-N-Cycloheptyl-3-(4-propoxyphenyl) acrylamide	C <sub>19</sub> H <sub>27</sub> NO <sub>2</sub>	[M-H] <sup>−</sup>	300.197	6.28E + 05	7.27	Other classes
119	(E)-2-[4-(Dimethylamino)benzyl]-N-hexadecyldiazene-carbothioamide	C <sub>26</sub> H <sub>46</sub> N <sub>4</sub> S	[M-H] <sup>−</sup>	445.3378	5.38E + 05	17.56	Other classes
120	HexCer 37:2;3	C <sub>43</sub> H <sub>81</sub> NO <sub>9</sub>	[M-H] <sup>−</sup>	754.5853	5.02E + 05	23.68	Other classes
121	HexCer 36:2;3	C <sub>42</sub> H <sub>79</sub> NO <sub>9</sub>	[M-H] <sup>−</sup>	740.569	3.65E + 05	23.29	Other classes
122	Ile-Gly-Ile	C <sub>14</sub> H <sub>27</sub> N <sub>3</sub> O <sub>4</sub>	[M + H] <sup>+</sup>	302.2066	1.33E + 05	7.26	Other classes
123	Leu-Val	C <sub>11</sub> H <sub>22</sub> N <sub>2</sub> O <sub>3</sub>	[M + H] <sup>+</sup>	231.1699	1.30E + 05	4.71	Other classes
124	Thr-Leu	C <sub>10</sub> H <sub>20</sub> N <sub>2</sub> O <sub>4</sub>	[M + H] <sup>+</sup>	233.1517	8.34E + 04	7.34	Other classes
125	Thr-Val-Leu	C <sub>15</sub> H <sub>29</sub> N <sub>3</sub> O <sub>5</sub>	[M + H] <sup>+</sup>	332.217	8.21E + 04	7.26	Other classes
126	Colneleic acid isomer 1	C <sub>18</sub> H <sub>30</sub> O <sub>3</sub>	[M-H] <sup>−</sup>	293.2123	7.90E + 04	14.31	Other classes
127	Ile-Glu	C <sub>11</sub> H <sub>20</sub> N <sub>2</sub> O <sub>5</sub>	[M + H] <sup>+</sup>	261.1442	7.11E + 04	1.78	Other classes
128	AC1L1 × 1Z	C <sub>23</sub> H <sub>46</sub> N <sub>6</sub> O <sub>13</sub>	[M + H] <sup>+</sup>	637.3017	6.10E + 04	17.08	Other classes
129	NCGC00380283-0114-[5-[[4-[5-[acetyl(hydroxy) amino] pentylamino]-4-oxobutanoyl]-hydroxyamino] pentylamino]-4-oxobutanoic acid	C <sub>20</sub> H <sub>36</sub> N <sub>4</sub> O <sub>8</sub>	[M + H] <sup>+</sup>	478.2894	5.46E + 04	10.38	Other classes
130	Massbank: RP016503 Ala-Phe[(2S)-2-[[[(2S)-2-azaniumylpropanoyl] amino]-3-phenylpropanoate	C <sub>12</sub> H <sub>16</sub> N <sub>2</sub> O <sub>3</sub>	[M + H] <sup>+</sup>	237.1224	2.54E + 04	3.12	Other classes
131	11-Hydroperoxy-octadecatrienoic acid	C <sub>18</sub> H <sub>30</sub> O <sub>4</sub>	[M-H] <sup>−</sup>	309.2069	2.43E + 04	10.36	Other classes
132	Val-Gly-Val	C <sub>12</sub> H <sub>23</sub> N <sub>3</sub> O <sub>4</sub>	[M + H] <sup>+</sup>	274.1752	1.20E + 04	4.28	Other classes
133	Met-Phe	C <sub>14</sub> H <sub>20</sub> N <sub>2</sub> O <sub>3</sub> S	[M + H] <sup>+</sup>	297.126	1.04E + 04	6.7	Other classes
134	Lauryl hydrogen sulfate	C <sub>12</sub> H <sub>26</sub> O <sub>4</sub> S	[M-H] <sup>−</sup>	265.1475	3.26E + 03	15.03	Other classes
135	Fraxin	C <sub>16</sub> H <sub>18</sub> O <sub>10</sub>	[M-H] <sup>−</sup>	369.0841	2.11E + 03	0.86	Other classes

hydroperoxy-octadecadienoic acid isomer 1, linolenic acid, stearic acid, palmitoleic acid, trihydroxyoctadecenoic acid, lignoceric acid, arachidic acid, behenic acid and hydroxystearic acid. In order to better understand the MS fragmentation pattern of fatty acids from *Tremella aurantialba* constituents, we took compound 1 as an example, which showed [M-H]<sup>−</sup> ion at *m/z* 279.2341 on the TOF-MS spectrum. The molecular formula was speculated to be C<sub>18</sub>H<sub>32</sub>O<sub>2</sub> based on the analysis of its



elemental composition and fractional isotope abundance. The main fragment ions were observed at  $m/z$  261.2098 [M-H-H<sub>2</sub>O]<sup>-</sup>, 243.2023 [M-H-2H<sub>2</sub>O]<sup>-</sup>, 205.1880 [M-H-C<sub>3</sub>H<sub>6</sub>O<sub>2</sub>]<sup>-</sup> in the negative ion spectrum by the TOF-MS/MS screening. These fragments were coincided with the linoleic acid in the TCM MS/MS database and the reference substance linoleic acid. As such, compound 1 was finally identified to be linoleic acid. The mass spectra, fragment information and Sciex OS screening interface of linoleic acid in negative mode were illustrated in **Figure 1**.

For the components not in the TCM MS/MS database, analysis was conducted using the XCMS online (Metlin) database, fragmentation pathway and literature data. We took compound 3 as an example, which showed a protonated ion [M-H]<sup>-</sup> at  $m/z$  255.2335 with the molecular formula C<sub>16</sub>H<sub>32</sub>O<sub>2</sub> in the negative ionization mode. The hydrogen adducts [M-H]<sup>-</sup> were observed in negative ionization mode. Further MS/MS scan showed that they produced fragment ions at  $m/z$  237.2087, 201.8310, etc. Compound 3 was identified as palmitic acid after comparison with available MS data in the literature (20). The mass spectra and fragment information and Sciex OS screening interface were illustrated in **Supplementary Figure 2**.

## Identification of organic acids

A total of 22 organic acids mainly originated from *Tremella aurantialba*. We took compound 13 as an example. Based on the analysis of its elemental composition and fractional isotope abundance, its molecular formula was predicted to be C<sub>6</sub>H<sub>8</sub>O<sub>7</sub>. The precise molecular weight was 192.0270, and the main fragment ions were analyzed via the MS/MS screening and

observed at  $m/z$  129.0115 [M-H-H<sub>2</sub>O-CO<sub>2</sub>]<sup>-</sup>, 111.0018 [M-H-2H<sub>2</sub>O-CO<sub>2</sub>]<sup>-</sup>, 85.0241 [M-H-H<sub>2</sub>O-2CO<sub>2</sub>]<sup>-</sup> and 67.0143 [M-H-2H<sub>2</sub>O-2CO<sub>2</sub>]<sup>-</sup> in the negative ion spectrum. It was identified as citric acid by searching the database, inferred through mass spectrometry fragment ion analysis and literature data (21). The mass spectra, fragmentation pathway and Sciex OS screening interface of citric acid in negative mode are illustrated in **Supplementary Figure 3**.

## Identification of saccharides

A total of 13 saccharides mainly originated from *Tremella aurantialba*. Took compound 56 as an example, the precise molecular weight was 181.0790, and the molecular formula was speculated to be C<sub>6</sub>H<sub>14</sub>O<sub>6</sub> based on the analysis of its elemental composition and fractional isotope abundance. The main fragment ions were analyzed via the MS/MS screening and observed at  $m/z$  163.0508 [M-H-H<sub>2</sub>O]<sup>-</sup>, 119.0260 [M-H-C<sub>2</sub>H<sub>6</sub>O<sub>2</sub>]<sup>-</sup>, 101.0172 [M-H-2H<sub>2</sub>O-CO<sub>2</sub>]<sup>-</sup>, 89.0186 [M-H-C<sub>3</sub>H<sub>8</sub>O<sub>3</sub>]<sup>-</sup>, 71.0092 [M-H-C<sub>3</sub>H<sub>8</sub>O<sub>3</sub>-H<sub>2</sub>O]<sup>-</sup>, 59.0101 [M-H-C<sub>4</sub>H<sub>10</sub>O<sub>4</sub>]<sup>-</sup>. Compound 56 was identified as mannitol by comparing with TCM MS/MS database and literature data (22). The mass spectra, fragment information and Sciex OS screening interface were illustrated in **Supplementary Figure 4**.

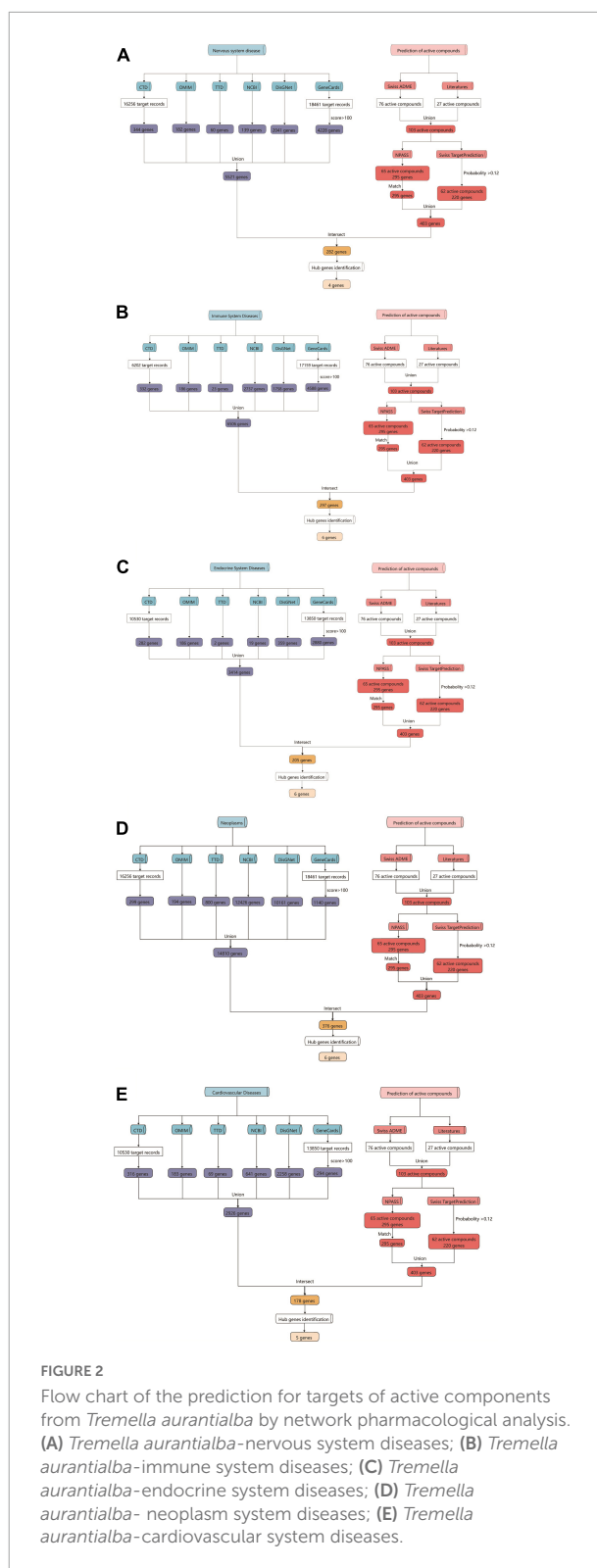
## Identification of others

In addition, other compounds have been identified from *Tremella aurantialba*, including amino acids, nucleosides and vitamins, etc. Compound 76 was selected as an example. The precise molecular weight was 124.0393, and the main fragment ions were analyzed via the MS/MS screening and observed at  $m/z$  106.0280 [M + H-H<sub>2</sub>O]<sup>+</sup>, 80.0498 [M + H-CO<sub>2</sub>]<sup>+</sup>, 53.0413

$[M + H-C_3H_3O_2]^+$  in the positive ion spectrum (23). Based on the analysis of its elemental composition and fractional isotope abundance, its molecular formula was predicted to be  $C_6H_5NO_2$ . According to the fragment information and TCM MS/MS database, the compound was identified as nicotinic acid. The secondary fragment of this substance was consistent with the secondary fragment of the reference substance in the TCM MS/MS database. The mass spectra, fragment information and Sciex OS screening interface of nicotinic acid in positive mode are illustrated in **Supplementary Figure 5**.

## Biological activities analysis of *Tremella aurantialba*

As a functional food raw material or traditional Chinese medicine formula, *Tremella aurantialba* is put into use as a whole. There are many kinds of compounds with complex systems, and the bioactivity evaluation and mechanism study of single component cannot truly reflect the overall physiological effects of *Tremella aurantialba*. Here, the potential bioactivity of *Tremella aurantialba* was also systematically predicted by enrichment analysis of the targets of active components. As shown in **Figure 2** and **Supplementary Table 1**, Swiss ADME database was used to screen the gastrointestinal absorbance and drug-like properties of the identified chemical components of *Tremella aurantialba*, and 76 active components were obtained. In addition, this study also conducted literature research on the pharmacological activities of the identified components in *Tremella aurantialba*. The results are shown in **Supplementary Table 2**. The existence of these bioactive natural products in *Tremella aurantialba* is consistent with the traditional use of *Tremella aurantialba*. Then, 27 components that do not meet the ADME screening criteria but have clear pharmacological effects are also included in the list of active components, in order to more comprehensively identify the efficacy and material basis of *Tremella aurantialba*. Swiss TargetPrediction database was used to predict the targets of 101 active components, and 62 active compounds and their corresponding gene targets were obtained. At the same time, the active components were further verified by NPASS database, and 65 active compounds and 295 corresponding protein targets were screened, and 295 gene targets were obtained after the protein targets were matched. Finally, 403 putative targets related to the active components of *Tremella aurantialba* were obtained from the two databases. In order to elucidate the biological activity of *Tremella aurantialba*, the targets of the above active compounds were introduced into DAVID Database and the related biological process and pathways of *Tremella aurantialba* were obtained (**Supplementary Table 3**). As shown in **Figure 3**, the predicted biological processes and pathways are mainly involved with nervous, immune, endocrine, neoplasm, as well



as cardiovascular diseases. The analysis results were consistent with the function of *Tremella aurantialba* and its active components reported.

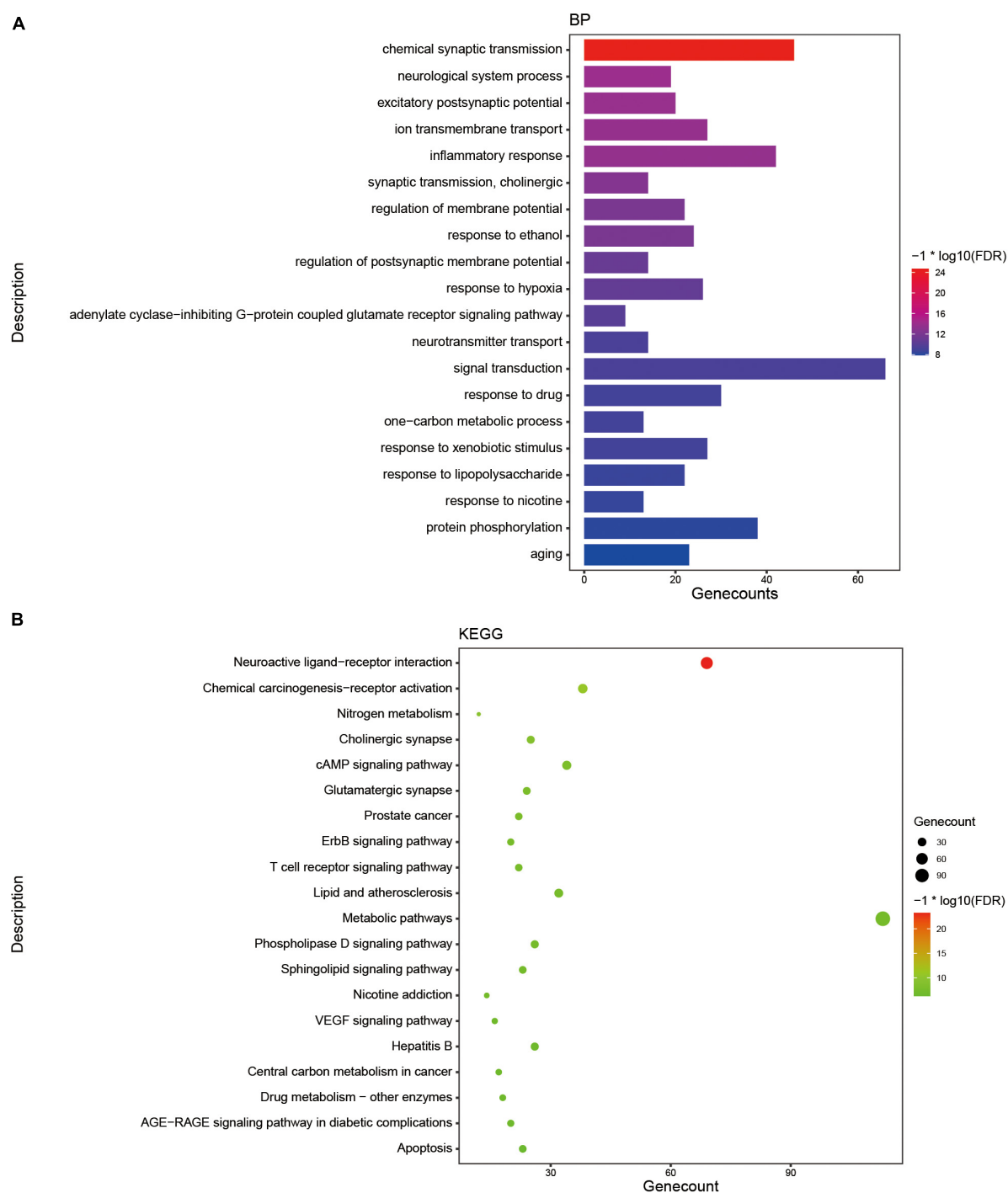


FIGURE 3

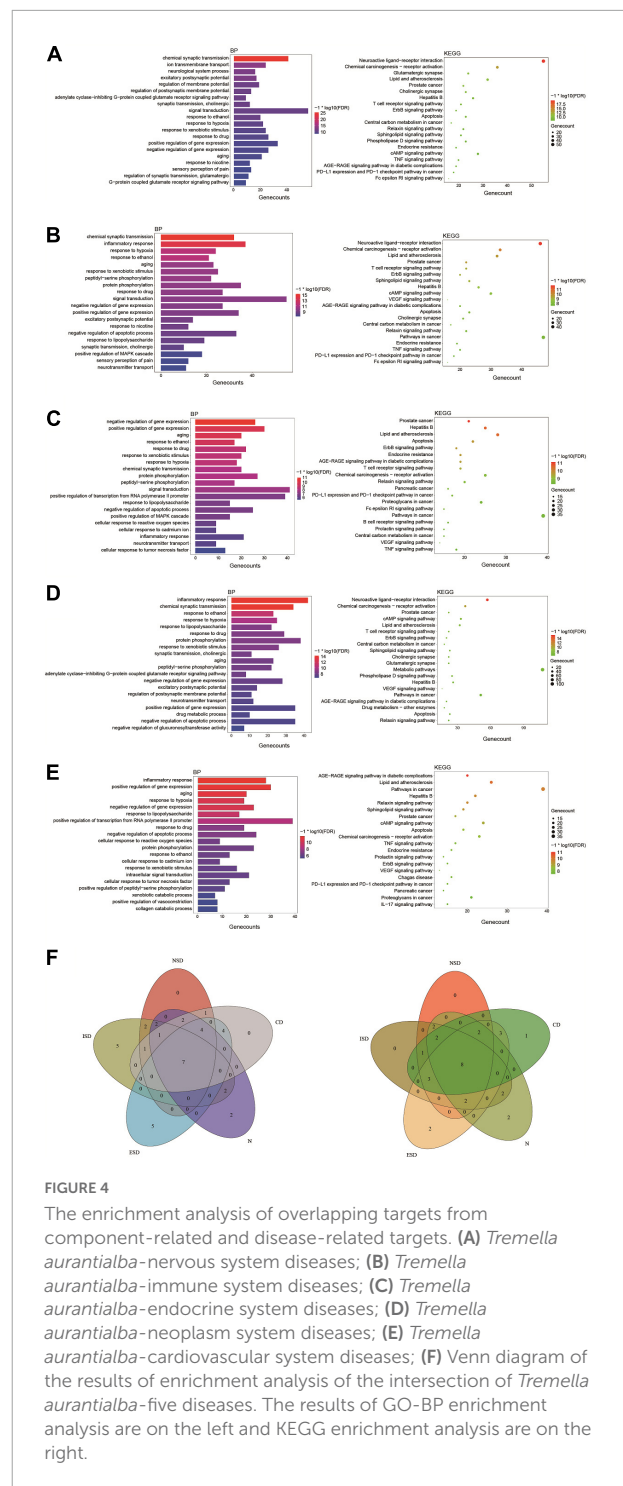
The enrichment analysis of targets of active components from *Tremella aurantialba*. (A) Histogram of GO enrichment analysis of targets. (B) Bubble chart of KEGG enrichment analysis of targets.

Based on the enrichment analysis of components targets, the related targets of five disease above were, respectively, searched from NCBI, OMIM, CTD, TTD, GeneCards and DisGNet databases. After summarizing and repeating, 5521, 6506, 3414, 14810 and 2926 candidate genes related

with nervous system, immune system, endocrine system, neoplasm and cardiovascular system were obtained, respectively (Supplementary Table 4). Then, the corresponding 282, 297, 205, 376 and 178 overlapping ones from component-related and disease-related targets were obtained with the National

Genomics Data Center website (Figure 2 and Supplementary Table 5). Finally, further enrichment analysis was adopted to analyzed overlapping targets and the detailed results were shown in Figures 4A–E and Supplementary Table 6. It was indicated that *Tremella aurantialba* had potential effect on regulating overlapping targets and multiple pathways, and so on to be a latent multi-target, multi-pathway treatment for five diseases mentioned above. Moreover, the molecular mechanisms of *Tremella aurantialba* involved in the interactions between the five diseases were identified. For instance, neuroactive ligand-receptor interactions and chemical carcinogenesis-receptor activation are the first two most important metabolic pathways in the intervention of *Tremella aurantialba* on nervous system diseases, immune system diseases and neoplasm; AGE-RAGE signaling pathway in diabetic complications and lipid and atherosclerosis are the first two most important metabolic pathways for *Tremella aurantialba* to intervene in cardiovascular system diseases; Lipid and atherosclerosis and apoptosis are the first two most important pathways of *Tremella aurantialba* in the intervention of endocrine system diseases. Besides, chemical synaptic transmission and ion transmembrane transport are the first two most important biological processes of *Tremella aurantialba* in the intervention of nervous system diseases; Chemical synaptic transmission and inflammatory response are the first two most important biological processes of *Tremella aurantialba* in the intervention of immune system diseases, neoplasm and cardiovascular system diseases; Aging and response to ethanol are the first two most important biological processes in the treatment of endocrine system diseases by *Tremella aurantialba*.

Notably, for five diseases, GO enrichment analysis showed that the targets of *Tremella aurantialba* were always closely related to 7 biological processes, including response to xenobiotic stimulus, response to ethanol, response to drug, aging, response to hypoxia, positive regulation of gene expression and negative regulation of gene expression; KEGG pathway enrichment analysis indicated that the targets of *Tremella aurantialba* were always significantly enriched in 8 pathways, including AGE-RAGE signaling pathway in diabetic complications, lipid and atherosclerosis, hepatitis B, relaxin signaling pathway, prostate cancer, apoptosis, chemical carcinogenesis-receptor activation, ErbB signaling pathway (Figure 4F). Various evidences indicated that these key biological processes and metabolic pathways play important roles in five diseases, but how to block the occurrence and progression of diseases through these biological processes and pathways is still an important problem to be solved. Thus, this study offers a potential scheme to this thorny problem. This means that *Tremella aurantialba* may simultaneously intervene in five diseases of our concern through these key biological processes and metabolic pathways. Moreover, this work also provides new ideas for the treatment of current disease-related



complications. Here, we discuss several important pathways of interest.

At present, AGE-RAGE signaling pathway in diabetic complications has been widely reported. The interaction between advanced glycation end products (AGEs) and its receptor RAGE can cause functional disorders of blood vessels



TABLE 2 The key targets for *Tremella aurantialba* on five diseases.

Diseases	Key targets	Core key targets
NSD	AKT1, JUN, ESR1, RXRA	
ISD	RELA, AKT1, RXRA, ESR1, MAPK1, JUN	
ESD	ESR1, PIK3CA, AKT1, JUN, RELA, MAPK14	AKT1, JUN, ESR1
Neu	JUN, MAPK14, RELA, ESR1, RXRA, AKT1	
CSD	AKT1, JUN, ESR1, MAPK14, RELA	

and immune cells, changes in programmed cell death signals and so on (24). Endogenous AGEs are irreversibly formed and accumulated mainly under chronic hyperglycemic, thus most studies have emphasized the important role of AGE-RAGE signaling pathway in diabetic complications, such as diabetes-related cardiovascular disease (25), malignant neoplasms (26) and neuroinflammation (27). In addition, there are few reports that AGE-RAGE signaling pathway plays an important role in five diseases unrelated to diabetes. Only AGEs are considered to be a major cardiovascular risk factors unrelated to diabetes (28). Here, this work first provides theoretical support for *Tremella aurantialba* to hinder the occurrence and development of five diabetes-related diseases by inhibiting the AGE-RAGE signaling pathway that mediates diabetes complications.

The ErbB protein family is a family of four structurally related receptor tyrosine kinases, including EGFR1/ErbB1/HER1, EGFR2/ErbB2/HER2, EGFR3/ErbB3/HER3, and EGFR4/ErbB4/HER4. These receptors can form homodimers or heterodimers with each other, and dimers are required for signaling activity. So far, there are many evidences about the importance of ErbB signaling pathway in the development of cancer, nervous system diseases and cardiovascular diseases. For example, CARF promotes colorectal cancer stemness by activating the ErbB signaling pathway (29). ErbB activity amplifies signals through the core RAS pathway, thereby promoting KRAS-driven lung neoplasm (30). Head and neck squamous carcinomas can trigger the reprogramming and transformation of ErbB family members, which up-regulates ErbB3 at the transcriptional level and promotes neoplasm cell survival and growth (31). These studies mainly emphasized the function of ErbB1/2/3 in cancer while the role of ErbB4 in cancer remains controversial. Neuregulin-1 (NRG1) is a family of EGF-like factors that activates ErbB receptors. NRG1/ErbB signaling is a key regulatory pathway in the repair processes of pathologic central and peripheral nervous system (32). Xu et al. reported that NRG1/ErbB signaling pathway is one of the main target pathways of organophosphorus-induced spinal cord injury in mice, suggesting that NRG1/ErbB signaling pathway may play a functional role in the central nervous system, but not in the peripheral nervous system (33). Xu

et al. found that tri-o-cresyl phosphate-induced hyperactivation of NRG1/ErbB signaling in Schwann cells might lead to the disturbance of neuropathy target esterase activity and degenerative pathology in spinal cord and sciatic nerve (34). Besides, vascular cells regulate cardiomyocyte survival and angiogenesis through NRG/ErbB signaling pathway, which has a protective paracrine effect on cardiac cells as well as vascular smooth muscle cells in the setting of an injury (35). Dang et al. first found that the effect of antipsychotic exposure on myocardial NRG1/ErbB signaling and activated NRG1/ErbB system in brain (36). In addition, excluding the deficiency of NRG1 signal transduction, NRG1/ErbB signaling pathway may be a promising therapeutic target for glucose intolerance, which may improve liver insulin sensitivity by inducing erBB1-ErBB3 dimerization, increasing ErbB3 phosphorylation, and thus play a hypoglycemic role. However, it has no effect on skeletal muscle insulin resistance, which is different from other studies and deserves further discussion (37). ErbB family also can induce immune cell infiltration and may influence the progression of skin melanoma through MDSC (38). In this work, the important relationship between ErbB signaling pathway and diseases of nervous system, immune system, endocrine system, neoplasm and cardiovascular system is proposed again, which is consistent with other reports. These results provide a basis for the intervention of five diseases through ErbB signaling pathway.

Relaxin (RLN) is a part of the insulin superfamily, including RLN1, RLN2 and RLN3. RLN2 acts as neuropeptides in the nervous system, as vasodilators and cardiac stimulants in the cardiovascular system, and as antifibrotic agents while the roles of RLN1 and RLN3 are unclear. Many of the effects of human gene-2 relaxin (H2 relaxin) are mediated by its homologous G protein-coupled receptor (GPCR) and relaxin family peptide receptor (RXFP1). For example, the activation of RXFP1 by rh-RLN2 can improve mast cell degranulation and neurological function by inhibiting NF- $\kappa$ B of PI3K-AKT/neoplasm necrosis factor- $\alpha$ -induced protein 3 (TNFAIP3) signaling pathway, which indicated that rh-RLN2 may be a promising therapeutic agent to reduce neuroinflammation and secondary brain injury in germinal matrix hemorrhage patients (39). RLN-2 produces endothelium- and NO-dependent relaxation of mouse mesenteric arteries by activation of RXFP1 coupled to Gi2-PI3K-eNOS pathway. Targeting vasodilatory Gi-protein-coupled RXFP1 pathways may provide promising opportunities for drug discovery in endothelial dysfunction and cardiometabolic disease (40). RLN can improve cardiac function, decrease the content of type I and type III Collagen in myocardial tissue, increase myocardial micro vessel density, and inhibit endothelial-mesenchymal transition-induced myocardial fibrosis through Notch-mediated signal transduction pathway (41). Besides, RLN can regulate a variety of cytokines and signaling pathways to treat cardiovascular

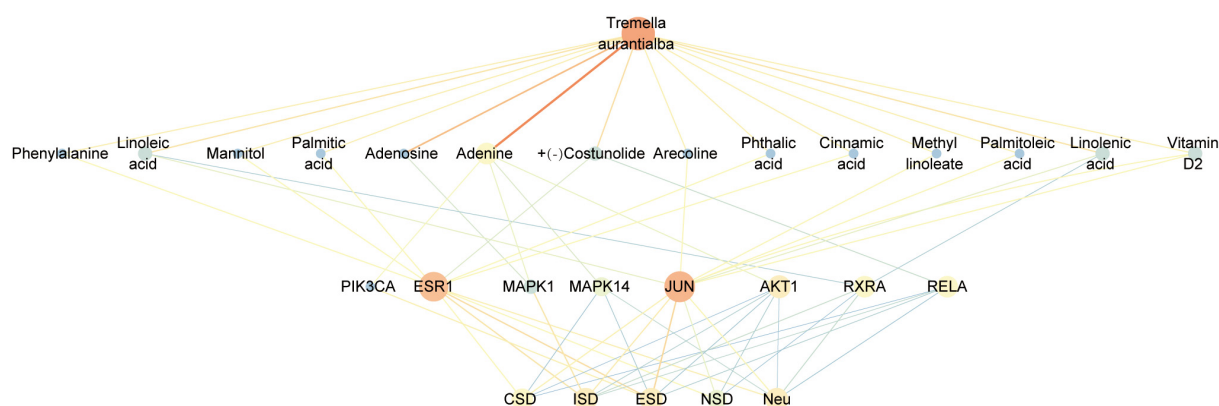


FIGURE 5

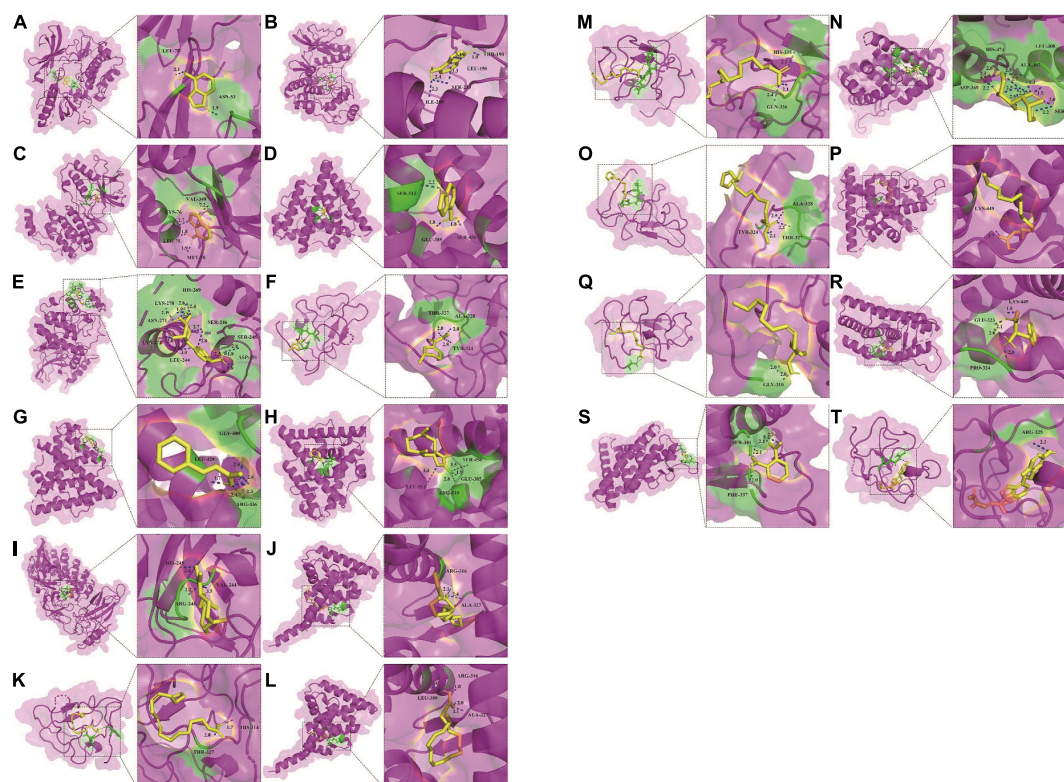
Components-targets-diseases network diagram of *Tremella aurantialba*.

FIGURE 6

Molecular docking of 14 active compounds with key targets. **(A)** Three-dimensional binding mode of adenine and AKT1 (PDB: 3O96). **(B)** Three-dimensional binding mode of adenine and MAPK1 (PDB: 6SLG). **(C)** Three-dimensional binding mode of adenine and MAPK14 (PDB: 3PG3). **(D)** Three-dimensional binding mode of adenine and PIK3CA (PDB: 4A55). **(E)** Three-dimensional binding mode of adenosine and MAPK1 (PDB: 6SLG). **(F)** Three-dimensional binding mode of arecoline and JUN (PDB: 6OSN). **(G)** Three-dimensional binding mode of cinnamic acid and ESR1 (PDB: 5ACC). **(H)** Three-dimensional binding mode of costunolide and ESR1 (PDB: 5ACC). **(I)** Three-dimensional binding mode of costunolide and RELA (PDB: 1NFI). **(J)** Three-dimensional binding mode of linoleic acid and RXRA (PDB: 6JNO). **(K)** Three-dimensional binding mode of linoleic acid and JUN (PDB: 6OSN). **(L)** Three-dimensional binding mode of linolenic acid and RXRA (PDB: 6JNO). **(M)** Three-dimensional binding mode of linolenic acid and JUN (PDB: 6OSN). **(N)** Three-dimensional binding mode of mannitol and ESR1 (PDB: 5ACC). **(O)** Three-dimensional binding mode of methyl linoleate and JUN (PDB: 6OSN). **(P)** Three-dimensional binding mode of palmitic acid and ESR1 (PDB: 5ACC). **(Q)** Three-dimensional binding mode of palmitoleic acid and JUN (PDB: 6OSN). **(R)** Three-dimensional binding mode of phenylalanine and ESR1 (PDB: 5ACC). **(S)** Three-dimensional binding mode of phthalic acid and ESR1 (PDB: 5ACC). **(T)** Three-dimensional binding mode of vitamin D2 and JUN (PDB: 6OSN).

disease and inflammation-related diseases (such as heart failure, diabetes) (42). Moreover, RLN2/RXFP1 signaling has recently been increasingly shown to mediate anti-apoptotic functions, angiogenesis and chemoresistance in cancer cells (43). RLN and its related receptor GPCR RXFP1 can form an autocrine signaling loop and promote the development and proliferation of ovarian cancer (44). RLN2/RXFP1 signaling induces cell invasion via the  $\beta$ -Catenin pathway in endometrial cancer (45). Here, the important role of the RLN signaling pathway in the five diseases is also emphasized, which makes it possible for *Tremella aurantialba* to fight disease through this pathway.

## Prediction of potential therapeutic targets

Protein-protein interaction (PPI) network was used to analyze the interactions between overlapping targets. Among the overlapped 282, 297, 205, 376 and 178 targets, a total of 598, 640, 446, 725 and 343 PPIs were obtained from STRING Database, respectively. By setting a degree value greater than 3, optimized PPI networks were further constructed using Cytoscape software (Supplementary Figure 6 and Supplementary Table 7). Further, clusters from the PPI network were screened using MCODE modules and the results were shown in Supplementary Figure 7.

Finally, the corresponding 4, 6, 6, 6 and 5 key targets for *Tremella aurantialba* on five diseases (NSD, ISD, ESD, Neu and CSD) were obtained, respectively, by CytoHubba plugin analysis and the common core targets of *Tremella aurantialba* on five diseases were also obtained, such as AKT1, JUN and ESR1 (Table 2). The importance of these three targets in five diseases has also been highlighted. Due to their versatility, these three targets have been proposed by some researchers as potential therapeutic targets for some diseases (46).

## Screening of key active components of *Tremella aurantialba*

Fourteen active components, including adenine, palmitoleic acid, arecoline, linoleic acid, linolenic acid, methyl linoleate, vitamin D2, palmitic acid, phthalic acid, (+)-costunolide, phenylalanine, cinnamic acid, mannitol, adenosine, were obtained by reverse screening based on the above key targets. They were considered key active components that have the activity of exacerbating or fighting five diseases in this study. Except adenosine, which was only selected as a key compound for immune system, the other compounds were speculated to have potential effects on all five diseases. A visual network of key active compounds, key genes and five diseases were shown in Figure 5 and Supplementary Table 8. The further molecular docking study was adopted to predict the mode of the interaction between the above hub genes and the corresponding

active compounds from *Tremella aurantialba*, based on the results of the network pharmacology analysis. Visual binding patterns showed good interaction between the receptor and ligand, especially linolenic acid and RXRA, with binding energy of  $-7.12$ , adenosine and MAPK1, with binding energy of  $-6.68$ , and vitamin D2 and JUN with binding energy of  $-6.63$ , suggesting that these compounds and targets may play a key role in the prevention and treatment of abdominal aortic aneurysms by *Tremella aurantialba* (Figure 6 and Supplementary Table 9). But the docking results were tentative, and only a speculation. Further *in vivo* and *in vitro* validation of the results is needed. In addition, according to the literature and other information, we further investigated the potential significant biological activities of these key compounds. Among them, the activities of most of the predicted compounds were consistent with those reported in the literature, and only a few compounds had different activity prediction results from those reported in the literature. For example, the fact that adenosine could also exert biological activity in other four diseases has been reported, but this study only obtained the potential of its effect on immune system diseases, which shows that the network pharmacology analysis method has certain limitations. It is not difficult to understand, because the network pharmacology analysis technology needs to be carried out on the basis of existing research, so it has a certain lag.

## Conclusion

As a famous medicinal and edible homologous fungus, the traditional pharmacological effects of *Tremella aurantialba* have been widely recorded in TCM books. However, there are few modern studies on the chemical components and pharmacological activities of *Tremella aurantialba*, which seriously hinder the development and utilization of *Tremella aurantialba*. Traditional Chinese medicine emphasizes the holistic concept and its drug use has the characteristics of multi-target and multi-function. However, for TCM with unclear chemical composition, blindly relying on the experience of ancestors will bring some safety risks to patients, and it is impossible to fully explore the pharmacological effects of *Tremella aurantialba*. In this study, UPLC-Q/TOF-MS was first used to investigate the chemical components of *Tremella aurantialba* and network pharmacological analysis was used to explore the potential pharmacological activities of *Tremella aurantialba*. Then, a total of 135 compounds were identified or tentatively characterized. Among them, the enrichment analysis of the targets of the active components of *Tremella aurantialba* suggests that *Tremella aurantialba* has potential pharmacological effects on nerve, immune, endocrine, neoplasm and cardiovascular diseases, which is consistent with the traditional Chinese medicine books and related literature reports. Next, the targets of five diseases were collected and collated, and the intersection with the

targets of *Tremella aurantialba* components was obtained. Then, the main targets, biological processes and metabolic pathways of *Tremella aurantialba* for the intervention of five diseases were also obtained. Simultaneously, fourteen active components and their key targets were first screened by reverse screening to have potential therapeutic effect for nervous system, immune system, endocrine system, neoplasm system, as well as cardiovascular system diseases. Chinese medicine components are the material basis of efficacy. By extrapolating the active components acting on the key intersection targets, we hypothesized that these components might be the important material basis for the pharmacological activities of *Tremella aurantialba* in five diseases. In this regard, we used molecular docking technology combined with literature review to verify and investigate the above predicted results. Interestingly, we also identified key comorbid mechanisms for *Tremella aurantialba* to simultaneously intervene in five diseases. In this step, three core targets, seven biological processes and eight metabolic pathways were identified. These results provide reference for the treatment of some disease complications and the exploration of potential disease treatment targets. In conclusion, this study will provide new ideas for further understanding the pharmacological activities of dominant plant resources such as *Tremella aurantialba* and exploring key functional components (groups), and provide important research strategies for the full development and utilization of dominant plant resources. Of course, the prediction results need to be further verified *in vivo* and *in vitro*.

## Data availability statement

The original contributions presented in this study are included in the article/**Supplementary material**, further inquiries can be directed to the corresponding authors.

## Author contributions

YY: conceptualization, writing—original draft, and supervision. MW: methodology, investigation, and data curation. XG: data curation. XW, YL, and NC: validation. CF: supervision and writing—review and editing. PL: investigation,

conceptualization, and funding acquisition. YZ: investigation, conceptualization, and writing—review and editing. All authors read and agreed to the published version of the manuscript.

## Funding

This work was supported by Major Public Welfare Projects in Henan Province (201300110200) and National Key Research Project of Hebei Province (20375502D).

## Acknowledgments

We are thankful to Yunnan Bacteria Horizon Biotechnology Co., Ltd. for providing *Tremella aurantialba* and Linlin Guo from AB Sciex Analytical Instrument Trading Co., for data curation.

## Conflict of interest

The authors declare that the research was conducted in the absence of any commercial or financial relationships that could be construed as a potential conflict of interest.

## Publisher's note

All claims expressed in this article are solely those of the authors and do not necessarily represent those of their affiliated organizations, or those of the publisher, the editors and the reviewers. Any product that may be evaluated in this article, or claim that may be made by its manufacturer, is not guaranteed or endorsed by the publisher.

## Supplementary material

The Supplementary Material for this article can be found online at: <https://www.frontiersin.org/articles/10.3389/fnut.2022.1083581/full#supplementary-material>

## References

1. Yang L, Li R, Cao Y, Li M, Luo X, Yang X, et al. Research on the scientific name and taxonomic status of *Tremella aurantialba*. *Edible Med Mushrooms*. (2020) 28:252–5.
2. Zhang Y, Lv P, Ma J, Chen N, Guo H, Chen Y, et al. *Antrodia cinnamomea* exerts an anti-hepatoma effect by targeting PI3K/AKT-mediated cell cycle progression *in vitro* and *in vivo*. *Acta Pharm Sin B*. (2022) 12:890–906. doi: 10.1016/j.apsb.2021.07.010
3. Subbulakshmi M, Dhanasekaran S, Abirami S, Kannan M, Palaniappan R, Venugopal D. Phylogenetic analysis and protective effects of thymol and its chromatographic fractions from a novel wild mushroom in combating oxidative stress. *Food Sci Hum Wellness*. (2021) 10:452–9. doi: 10.1016/j.fshw.2021.04.007
4. Dan A, Hu Y, Chen R, Lin X, Tian Y, Wang S. Advances in research on chemical constituents and pharmacological effects of *Paecilomyces hepiali*. *Food Sci Hum Wellness*. (2021) 10:401–7. doi: 10.1016/j.fshw.2021.04.002



5. Hou R, Liu X, Wu X, Zheng M, Fu J. Therapeutic effect of natural melanin from edible fungus *Auricularia auricula* on alcohol-induced liver damage *in vitro* and *in vivo*. *Food Sci Hum Wellness*. (2021) 10:514–22. doi: 10.1016/j.fshw.2021.04.014
6. Han X, Zhang J, Liu Y, Jia F, Liu Z, Xue B. Analysis of nutrition and volatile components of wild *Tremella aurantialba* in tibet under different drying methods. *Food Res Dev*. (2020) 41:49–55. doi: 10.12161/j.issn.1005-6521.2020.13.008
7. Li X, Deng L, Zhou Y, Zhong L, Zhao S, Lei X, et al. Nutritional components comparison between *Tremella aurantialba*, *Tremella fuciformis* and *Auricularia auricula*. *Food Res Dev*. (2021) 42:77–82. doi: 10.12161/j.issn.1005-6521.2021.16.012
8. Yuan Q, Zhang X, Ma M, Long T, Xiao C, Zhang J, et al. Immunoenhancing glucuronoxylomannan from *Tremella aurantialba* Bandoni et Zang and its low-molecular-weight fractions by radical depolymerization: properties, structures and effects on macrophages. *Carbohydr Polym*. (2020) 238:116184. doi: 10.1016/j.carbpol.2020.116184
9. Du X, Wang X, Chen Y, Tian S, Lu S. Antioxidant activity and oxidative injury rehabilitation of chemically modified polysaccharide (TAPA1) from *Tremella aurantialba*. *Macromol Res*. (2018) 26:479–83. doi: 10.1007/s13233-018-6078-0
10. Dai C, Huang X, Lv R, Zhang Z, Sun J, Aheto J. Analysis of volatile compounds of *Tremella aurantialba* fermentation via electronic nose and HS-SPME-GC-MS. *J Food Saf*. (2018) 38:e12555. doi: 10.1111/jfs.12555
11. Li Y. *Studies on chemical composition and antioxidant activity in vitro from Tremella aurantialba fruiting bodies*. Changchun: Jilin Agricultural University (2016).
12. Liu N, Li J, Guo C, Guo Y. Effect of *Tremella aurantialba* lipid extracts on the penetration of Evans blue through blood brain barrier. *Sci Technol Food Ind*. (2019) 40:62–6.
13. Du X, Zhang J, Jia W. Antitumor and immunostimulating activities of the extracts from *Tremella aurantialba* fruiting bodies *in vitro*. *Nat Prod Res Dev*. (2011) 23:351–5.
14. Yuan Q, Zhao L, Li H, Wei Z. Immunoenhancing glucuronoxylomannan from *Tremella aurantialba* Bandoni et Zang and its low-molecular-weight fractions by radical depolymerization: properties, structures and effects on macrophages. *Carbohydr Polym*. (2020) 238:116184.
15. Wang D. *Study on extraction, isolation and purification of polysaccharide from tremella aurantialba and its antioxidant activity*. Liaocheng: Liaocheng University (2018).
16. Cui L, Liu Y, Liu M, Ren M, Ahmed A, Kang W. Identification of phytochemicals from *Lentinus edodes* and *Auricularia auricula* with UPLC-Q-Exactive Orbitrap MS. *J Future Foods*. (2022) 2:253–60. doi: 10.1016/j.jfutfo.2022.06.006
17. Yin Z, Sun-Waterhouse D, Wang J, Ma C, Waterhouse G, Kang W. Polysaccharides from edible fungi *Pleurotus spp.*: advances and perspectives. *J Future Foods*. (2021) 1:128–40. doi: 10.1016/j.jfutfo.2022.01.002
18. Yin Z, Liang Z, Li C, Wang J, Ma C, Kang W. Immunomodulatory effects of polysaccharides from edible fungus: a review. *Food Sci Hum Wellness*. (2021) 10:393–400. doi: 10.1016/j.fshw.2021.04.001
19. Zhang Y, Ma A, Xi H, Chen N, Wang R, Yang C, et al. *Antrodia cinnamomea* ameliorates neointimal formation by inhibiting inflammatory cell infiltration through downregulation of adhesion molecule expression *in vitro* and *in vivo*. *Food Sci Hum Wellness*. (2021) 10:421–30. doi: 10.1016/j.fshw.2021.04.004
20. Pérez-Navarro J, Da Ros A, Masuero D, Izquierdo-Cañas P, Hermosín-Gutiérrez I, Gómez-Alonso S, et al. LC-MS/MS analysis of free fatty acid composition and other lipids in skins and seeds of *Vitis vinifera* grape cultivars. *Food Res Int*. (2019) 125:108556. doi: 10.1016/j.foodres.2019.108556
21. Aliabadi M, Karami-Osboo R, Kobarfard F, Jahani R, Nabi M, Yazdanpanah H, et al. Detection of lime juice adulteration by simultaneous determination of main organic acids using liquid chromatography-tandem mass spectrometry. *J Food Compos Anal*. (2022) 105:104223. doi: 10.1016/j.jfca.2021.104223
22. Kubica P, Kot-Wasik A, Wasik A, Namieśnik J, Landowski P. Modern approach for determination of lactulose, mannitol and sucrose in human urine using HPLC-MS/MS for the studies of intestinal and upper digestive tract permeability. *J Chromatogr B*. (2012) 907:34–40. doi: 10.1016/j.jchromb.2012.08.031
23. Caprioli G, Sagratini G, Vittori S, Torregiani E. Optimization of an extraction procedure for the simultaneous quantification of riboflavin, nicotinamide and nicotinic acid in anchovies (*Engraulis encrasicolus*) by high-performance liquid chromatography-tandem mass spectrometry. *J Food Compos Anal*. (2018) 66:23–9. doi: 10.1016/j.jfca.2017.11.004
24. Waghela B, Vaidya F, Ranjan K, Chhipa A, Tiwari B, Pathak C. AGE-RAGE synergy influences programmed cell death signaling to promote cancer. *Mol Cell Biochem*. (2021) 476:585–98. doi: 10.1007/s11010-020-03928-y
25. Burr S, Dorroh C, Stewart J Jr. Rap1a activity elevated the impact of endogenous AGEs in diabetic collagen to stimulate increased myofibroblast transition and oxidative stress. *Int J Mol Sci*. (2022) 9:4480. doi: 10.3390/ijms23094480
26. Pan S, Guan Y, Ma Y, Cui Q, Tang Z, Li J, et al. Advanced glycation end products correlate with breast cancer metastasis by activating RAGE TLR4 signaling. *BMJ Open Diabetes Res Care*. (2022) 10:e2697. doi: 10.1136/bmjdr-2021-002697
27. Yu X, Zhang D, Xiao C, Zhou Y, Li X, Wang L, et al. P-Coumaric acid reverses depression-like behavior and memory deficit via inhibiting AGE-RAGE-mediated neuroinflammation. *Cells*. (2022) 11:1594. doi: 10.3390/cells11101594
28. Kosmopoulos M, Drekolias D, Zavras P, Piperi C, Papavassiliou A. Impact of advanced glycation end products (AGEs) signaling in coronary artery disease. *Biochim Biophys Acta (BBA) Mol Basis Dis*. (2019) 1865:611–9. doi: 10.1016/j.bbdis.2019.01.006
29. Dong W, Cao Z, Pang Y, Feng T, Tian H. CARF, as an oncogene, promotes colorectal cancer stemness by activating ERBB signaling pathway. *Oncotargets Ther*. (2019) 12:9041–51. doi: 10.2147/OTT.S225733
30. Kruspig B, Monteverde T, Neidler S, Hock A, Kerr E, Nixon C, et al. The ERBB network facilitates KRAS-driven lung tumorigenesis. *Sci Transl Med*. (2018) 10:eao2565.
31. Humtsoe J, Pham E, Louie R, Chan D, Kramer R. ErbB3 upregulation by the HNSCC 3D microenvironment modulates cell survival and growth. *Oncogene*. (2016) 35:1554–64. doi: 10.1038/ncr.2015.220
32. Kataria H, Alizadeh A, Karimi-Abdolrezaee S. Neuregulin-1 ErbB network an emerging modulator of nervous system injury and repair. *Prog Neurobiol*. (2019) 180:101643. doi: 10.1016/j.pneurobio.2019.101643
33. Xu H, Sun Y, Sun Y, Wu Y, Xu M, Chen L, et al. Lapatinib alleviates TOCP-induced axonal damage in the spinal cord of mouse. *Neuropharmacology*. (2021) 189:108535. doi: 10.1016/j.neuropharm.2021.108535
34. Xu H, Wang P, Sun Y, Xu M, Zhu L, Wu Y. Activation of neuregulin 1 ErbB signaling is involved in the development of TOCP-induced delayed neuropathy. *Front Mol Neurosci*. (2018) 11:129. doi: 10.3389/fnmol.2018.00129
35. Hedhli N, Kalinowski A, Russell K. Cardiovascular effects of neuregulin-1 ErbB signaling role in vascular signaling and angiogenesis. *Curr Pharm Des*. (2014) 20:4899–905. doi: 10.2174/1381612819666131125151058
36. Dang R, Guo Y, Cai H, Yang R, Liang D, Lv C, et al. Effects of prolonged antipsychotic administration on neuregulin-1 ErbB signaling in rat prefrontal cortex and myocardium implications for the therapeutic action and cardiac adverse effect. *J Toxicol*. (2016) 41:303–9. doi: 10.2131/jts.41.303
37. Caillaud K, Boisseau N, Ennequin G, Chavanelle V, Etienne M, Li X, et al. Neuregulin 1 improves glucose tolerance in adult and old rats. *Diabetes Metab*. (2016) 42:96–104. doi: 10.1016/j.diabet.2015.08.003
38. Liu S, Geng R, Lin E, Zhao P, Chen Y. ERBB family can induce immune cell infiltration and may influence the progression of skin melanoma through MDSC. *Front Genet*. (2021) 12:602160. doi: 10.3389/fgene.2021.602160
39. Li P, Zhao G, Chen F, Ding Y, Wang T, Liu S, et al. Rh-relaxin-2 attenuates degranulation of mast cells by inhibiting NF- $\kappa$ B through PI3K-AKT TNFAIP3 pathway in an experimental germinal matrix hemorrhage rat model. *J Neuroinflammation*. (2020) 17:250. doi: 10.1186/s12974-020-01926-x
40. Lian X, Beer-Hammer S, König G, Kostenis E, Nürnberg B, Gollasch M. RXFP1 receptor activation by relaxin-2 induces vascular relaxation in mice via a G $\alpha$ i2-Protein/PI3K/ $\gamma$ /Nitric oxide-coupled pathway. *Front Physiol*. (2018) 9:1234. doi: 10.3389/fphys.2018.01234
41. Zhou X. Relaxin inhibits cardiac fibrosis and endothelial-mesenchymal transition via the Notch pathway. *Drug Des Devel Ther*. (2015) 9:4599–611. doi: 10.2147/DDDT.S85399
42. Martin B, Gabris-Weber B, Reddy R, Romero G, Chattopadhyay A, Salama G. Relaxin reverses inflammatory and immune signals in aged hearts. *PLoS One*. (2018) 13:e190935. doi: 10.1371/journal.pone.0190935
43. Rizvi S, Gores G. The two faces of relaxin in cancer: antitumor or protumor? *Hepatology*. (2021) 71:1117–9. doi: 10.1002/hep.30998
44. Burston H, Kent O, Communal L, Udaskin M, Sun R, Brown K, et al. Inhibition of relaxin autocrine signaling confers therapeutic vulnerability in ovarian cancer. *J Clin Invest*. (2021) 131:e142677. doi: 10.1172/JCI142677
45. Fue M, Miki Y, Takagi K, Hashimoto C, Yaegashi N, Suzuki T, et al. Relaxin 2 RXFP1 signaling induces cell invasion via the  $\beta$ -catenin pathway in endometrial cancer. *Int J Mol Sci*. (2018) 19:2438. doi: 10.3390/ijms19082438
46. Novoszel P, Holcman M, Stulnig G, De Sa F, Zylina V, Borek I, et al. Psoriatic skin inflammation is promoted by c-Jun/AP-1-dependent CCL2 and IL-23 expression in dendritic cells. *EMBO Mol Med*. (2021) 13:e12409. doi: 10.15252/emmm.202012409





## OPEN ACCESS

## EDITED BY

Wenyi Kang,  
Henan University, China

## REVIEWED BY

Bin Du,  
Hebei Normal University of Science  
and Technology, China  
Wenjian Yang,  
Nanjing University of Finance  
and Economics, China

## \*CORRESPONDENCE

Dawei Wang  
✉ wangdawei@jlu.edu.cn  
Tingting Liu  
✉ liutingting@jlu.edu.cn

## SPECIALTY SECTION

This article was submitted to  
Food Chemistry,  
a section of the journal  
Frontiers in Nutrition

RECEIVED 08 November 2022

ACCEPTED 30 November 2022

PUBLISHED 16 December 2022

## CITATION

Gao Y, Abuduaini G, Yang C, Zhang S,  
Zhang Y, Fan H, Teng X, Bao C, Liu H,  
Wang D and Liu T (2022) Isolation,  
purification, and structural elucidation  
of *Stropharia rugosoannulata*  
polysaccharides with hypolipidemic  
effect.  
*Front. Nutr.* 9:1092582.  
doi: 10.3389/fnut.2022.1092582

## COPYRIGHT

© 2022 Gao, Abuduaini, Yang, Zhang,  
Zhang, Fan, Teng, Bao, Liu, Wang and  
Liu. This is an open-access article  
distributed under the terms of the  
Creative Commons Attribution License  
(CC BY). The use, distribution or  
reproduction in other forums is  
permitted, provided the original  
author(s) and the copyright owner(s)  
are credited and that the original  
publication in this journal is cited, in  
accordance with accepted academic  
practice. No use, distribution or  
reproduction is permitted which does  
not comply with these terms.

# Isolation, purification, and structural elucidation of *Stropharia rugosoannulata* polysaccharides with hypolipidemic effect

Yinlu Gao<sup>1,2</sup>, Guljiannaiti Abuduaini<sup>1,3</sup>, Chenhe Yang<sup>1,4</sup>,  
Shanshan Zhang<sup>1,3</sup>, Yanrong Zhang<sup>1,3</sup>, Hongxiu Fan<sup>1,2</sup>,  
Xu Teng<sup>1,4</sup>, Chenligen Bao<sup>1,4</sup>, Hongcheng Liu<sup>1,3</sup>,  
Dawei Wang<sup>1,2\*</sup> and Tingting Liu<sup>1,2\*</sup>

<sup>1</sup>School of Food Science and Engineering, Jilin Agricultural University, Changchun, China,

<sup>2</sup>Scientific Research Base of Edible Mushroom Processing Technology Integration, Ministry of Agriculture and Rural Affairs, Changchun, China, <sup>3</sup>Engineering Research Center of Grain Deep-Processing and High-Efficiency Utilization of Jilin, Changchun, China, <sup>4</sup>Key Laboratory of Technological Innovations for Grain Deep-Processing and High-Efficiency Utilization of By-Products of Jilin, Changchun, China

*Stropharia rugosoannulata* is a widely grown edible mushroom with a high nutritional value. *S. rugosoannulata* polysaccharides is one of the most important bioactive components of *S. rugosoannulata* and has a wide range of activities. A *S. rugosoannulata* polysaccharides, named SRF-3, was derived from the *S. rugosoannulata* extraction by freeze-thaw combine with hot water extraction method, then prepared with DEAE-cellulose column and Sephacryl S-200 HR gel column, and its hypolipidemic activity was determined. The structural characteristics of SRF-3 were analyzed by infrared spectral scanning (FT-IR), ultra-high performance liquid chromatography (UHPLC), acid hydrolysis, methylation analysis, nuclear magnetic resonance (NMR), and Gas Chromatography-Mass Spectrometer (GC-MS). SRF-3 is composed of mannose, galactose, methyl galactose and fructose with ratios of 16, 12, 58 and 12, respectively. In addition, the average relative molecular mass of SRF-3 is approximately 24 kDa. The main chain of SRF-3 is mainly composed of repeating  $\alpha$ -D-1,6-Galp and  $\alpha$ -D-1,6-Me-Galp units, with branches in the O-2 position of Gal. The structure is presumed to be a mannogalactan, with a small amount of t- $\beta$ -D-Manp present as a side chain. Hypolipidemic activity assay showed that SRF-3 had good antioxidant and hypolipidemic effects *in vitro*, suggesting that SRF-3 have potential application in reducing liver fat accumulation.

## KEYWORDS

*Stropharia rugosoannulata*, polysaccharides, hypolipidemic, antioxidation, structure

## 1 Introduction

Edible fungi is a general term for large fungi that people can eat. More than 120,000 species of fungi have been described in the world, and more than 6,000 species can form large seed entities or mycorrhizal tissue, and more than 2,000 species are available for consumption (1, 2).

Mushrooms have a long history of consumption and are nutritious, tasty and high in protein, low in fat, essential amino acids, minerals, vitamins, and polysaccharides, making them a “healthy food” (3–6). In addition, mushrooms are unique in their nutritional value as they ensure the body’s need for non-saturated fatty acids and prevent the harmful effects of too much saturated fatty acids (7–9). They are also known for their ability to lower blood cholesterol and treat high blood pressure (10–13), while *Lentinula edodes*, *Flammulina velutipes*, and *Hericium erinaceus* contain substances that enhance the body’s ability to fight cancer (14–17).

Polysaccharides are water-soluble natural polymers composed of more than 10 monosaccharide units, and are one of the basic substances to maintain the normal life activities of the body. Polysaccharides are also commonly found in edible mushrooms, which are gradually being recognized as healthy food and medicine (18). Many studies have confirmed that edible mushroom polysaccharides are not only anti-aging and antioxidant (19, 20), but also have immunomodulatory and anti-tumor effects, in addition to regulating blood lipids, lowering cholesterol, protecting the liver and detoxifying the body, and preventing obesity and diabetes (19–28).

*Stropharia rugosoannulata* is native to Europe and the United States, but is now widely grown around the world and is one of the top 10 most traded species on the international edible mushroom market. It is rich in nutrients, with over 65% high quality carbohydrates, and studies in recent years have shown that in addition to its nutritional value, mushrooms are also effective in preventing coronary heart disease, aiding digestion, and relieving mental fatigue (29, 30).

However, few studies have been reported on the isolation and purification, structure and lipid-lowering efficacy of the polysaccharides from *S. rugosoannulata*. Therefore, the aim of this study was to extract new polysaccharides from *S. rugosoannulata* and to investigate their physicochemical properties and structure. Its potential as a lipid-lowering agent was investigated by *in vitro* antioxidant assays and *in vitro* lipid-lowering assays.

## 2 Materials and methods

### 2.1 Materials

*Stropharia rugosoannulata* was obtained from the Jilin Institute of Agricultural Science (Changchun, China) and

harvested in September 2021 in Gongzhuling (Jilin Province, China). HepG2 cells were purchased and characterized at Meixuan Biological Science Co., Ltd. (Shanghai, China). Diethylaminoethyl-Sepharose Fast Flow was purchased from Shanghai Hengxin Chemical Reagent Co., Ltd. (Shanghai, China) and Sephacryl S-200 High Resolution gel (Sephacryl S-200) was purchased from GE-healthcare. Relevant analytical purity grade was purchased from Sinopharm Chemical Reagent Co., Ltd. (Shanghai, China), including NaCl, phenol, sulfuric acid, potassium bromide, hydrochloric acid, anhydrous methanol, anhydrous ethanol, trifluoroacetic acid, PMP reagent, NaOH, acetonitrile, DMSO, iodomethane, formic acid, hydrogen sodium boride, and glacial acetic acid.

### 2.2 Extraction, isolation, and purification of polysaccharides from *S. rugosoannulata*

The plant material was fresh *S. rugosoannulata*, freeze–thaw 30 min (one time) and hot water extracting 30 min (1:100, m/m). The extracts were combined and centrifuged at 3,000 g for 10 min, concentrated to 15% of the original volume in a rotary evaporator at 60°C and precipitated overnight in a final concentration of 90% (v/v) ethanol at 4°C. After centrifugation, the separated precipitate was re-dissolved using ultrapure water and deproteinized enzymatically (neutral protease, 37°C, 2 h). Hydrodialysis (MWCO 3000 Da) for 24 h and lyophilization gave the crude polysaccharides (31).

Crude polysaccharides were prepared in distilled water to 0.2 g/ml and fractionated using the DEAE (45 mm × 260 mm) column on AKTA Pura 25 with distilled water and 0–0.5 M NaCl as eluent at a flow rate of 1 ml/min, collecting one tube every 4 min. The total polysaccharides content was determined by phenol-sulfuric acid method, and two fractions (SRF-1 and SRF-2) were extracted and freeze-dried. SRF-1 was identified as the major lipid-lowering fraction by assay and further purified using Sephacryl S-200 HR (26 mm × 1,000 mm) column at a flow rate of 0.4 ml/min with a mobile phase of 0.15 M NaCl solution and a collector for 10 min to collect one tube. The distribution curves of its sugar content were examined and obtain two target polysaccharides, SRF-3 and SRF-4, of which SRF-3 was the major fraction, which were then lyophilized and stored in a dry environment for subsequent studies.

### 2.3 Homogeneity and molecular weight of SRF-3

Distilled water was used as a blank for zeroing and used as a solvent to configure SRF-3 to the 1 mg/ml solution used,

then SRF-3 solution was placed in a quartz colorimetric cup and scanned at 190–900 nm at full UV-visible wavelength (UV-2700, Shimadzu, Japan).

High performance gel permeation chromatography (HPGPC, LC-10Avp, Japan) was used to determine the relative molecular mass of SRF-3. The SRF-3 sample solution was prepared at a concentration of 5 mg/ml and dextran was used as a standard, and all samples were filtered using a 0.45  $\mu$ m filter membrane prior to detection. The chromatographic column was a Shimadzu CLASS-Vp system with a TSK-gel G-3000 PWXL 7.8  $\times$  300 mm, a RID-10A parallax refractive detector, a mobile phase of 0.2 M NaCl aqueous solution, the injection volume of 20  $\mu$ l with flow rate of 0.6 ml/min and temperature of 40°C.

## 2.4 Monosaccharide composition analysis

The monosaccharide composition of SRF-3 was determined by PMP derivatization combined with ultra-high performance liquid chromatography (UHPLC). The SRF-3 sample was weighed 2 mg, 1 ml of anhydrous methanol solution containing 1 M hydrochloric acid was added, the tube was filled with N<sub>2</sub> and sealed, hydrolyzed at 80°C for 16 h. After blowing dry with nitrogen, add 1 ml of 2 M trifluoroacetic acid, hydrolyzed at 120°C for 1 h. A small amount of ethanol was added and dried in a water bath at 60°C and repeated 3–5 times to completely evaporate the trifluoroacetic acid. Add 0.5 ml of PMP reagent and 0.3 M NaOH solution to the dried sample obtained after complete acid hydrolysis, and after the sample is fully dissolved, take 0.2 ml of it in a small centrifuge tube, water bath at 70°C for 30 min. After centrifugation at 10,000 g for 5 min, add 0.3 M of hydrochloric acid solution 0.1 ml and distilled water 0.1 ml, mix thoroughly. Add 1 ml of dichloromethane, mix well and then extract the remaining PMP reagent, aspirate the dichloromethane layer, retain the aqueous layer and repeat three times (32, 33). The samples were filtered through 0.22  $\mu$ m membrane and then assayed. The chromatography was performed on a Shimadzu UHPLC system with a Compass C18 (150  $\times$  4.6 mm) column using a mobile phase of PBS (0.1 M, pH 7): acetonitrile 81:19 (v/v) at a flow rate of 1.0 ml/min with a sample volume of 10  $\mu$ l and a detection wavelength of 245 nm.

## 2.5 Infrared spectroscopy

The dried SRF-3 samples were mixed well with KBr, then pressed into thin slices for FT-IR analysis, then scanned with a PerkinElmer Spectrum Two spectrometer (PerkinElmer, USA) to record FT-IR spectra from 4,000 to 400  $\text{cm}^{-1}$ . The data

were analyzed and processed using OMSNIC spectroscopy software (34).

## 2.6 Structural characterization

### 2.6.1 Methylation analysis

A total of 10 mg of SRF-3 was dissolved in 1 ml DMSO, 0.5 ml NaOH-DMSO suspension was added and mixed well. Slowly add 1 ml of iodomethane in an ice bath, protected from light, stirring magnetically for 30 min and add 2 ml distilled water to abort the reaction. Dialysis was performed for 24 h each in flowing tap water and distilled water, respectively. After repeating the above steps for the second methylation, the extraction was carried out three times using dichloromethane, followed by reverse extraction using water, blowing the organic phase dry with an air pump, dissolving in distilled water and lyophilizing. The methylated samples were subjected to infrared spectroscopy to examine the methylation. To the above dried sample of methylated sugars, 1 ml of mixed acid (HCOOH:H<sub>2</sub>O:TFA = 3:2:1) was added, sealed with N<sub>2</sub> and hydrolyzed at 100°C for 6 h. After hydrolysis, anhydrous ethanol was added repeatedly to evaporate the mixed acid to pH = 7 (at temperatures below 40°C). Add 1 ml of 30 mg/ml NaBH<sub>4</sub> solution at room temperature and stir for 12 h. Neutralize by adding about 100  $\mu$ l of 50% glacial acetic acid, add an appropriate amount of strong acidic cation exchange resin, stir magnetically for 20 min, filter (remove the resin), add methanol repeatedly to the filtrate and evaporate the boric acid to neutral (temperature below 40°C). Add 0.5 ml each of acetic anhydride and anhydrous pyridine, seal with N<sub>2</sub> and react at 100°C for 2 h, then the reaction was terminated by adding 1 ml of distilled water to an ice bath, which was sealed for 5 min. A total of 2 ml of dichloromethane and 2 ml of distilled water were added, and the organic phase was reverse extracted three times, the aqueous phase was removed, the organic phase was blown dry, dissolved in 1 ml of chromatographically pure dichloromethane, filtered, and analyzed by Gas Chromatography–Mass Spectrometer (GC-MS). The chromatographic column was an Agilent DB-35 ms with an injection temperature of 300°C and an auxiliary heater temperature of 280°C. The ramp-up procedure: initial temperature 140°C with 2 min retention, 5°C/min to 170°C with 3 min retention, 1°C/min to 180°C with 5 min retention, 3°C/min to 220°C with 1 min retention, 20°C/min to 295°C with 3 min retention.

### 2.6.2 NMR spectroscopy analysis

A total of 20 mg of dried SRF-3 sample was dissolved in 0.5 ml of D<sub>2</sub>O and left at 20°C for 12 h to dissolve completely. The one-dimensional nuclear magnetic resonance (NMR) spectra (1H NMR, 13C NMR) and two-dimensional

NMR spectra (HSQC, HMBC) were measured at 20°C (Bruker Avance 600 MHz, Bruker, Switzerland). <sup>1</sup>H NMR was detected at 600 MHz and <sup>13</sup>C NMR was detected at 150 MHz.

## 2.7 Antioxidant activity

### 2.7.1 Hydroxyl radical scavenging capacity

One milliliter sample solution was mixed with an equal volume of ferrous sulfate solution (Fe·SO<sub>4</sub>·7H<sub>2</sub>O, 9 mM/L) and hydrogen peroxide solution (10 mM/L). After 10 min of reaction at 37°C, 1 ml of salicylic acid solution (9 mM/L) was added, mixed well and reacted at 37°C for 30 min. Pure water as a blank control, the absorbance of the reaction solution at 510 nm was recorded (35).

$$\text{Hydroxyl radical scavenging capacity (\%)} = (A_0 - A_1) / A_0 \times 100$$

where A<sub>0</sub> is the absorbance of control reaction (without addition of the sample), A<sub>1</sub> was absorbance of sample solution in reaction mixture.

### 2.7.2 DPPH\* radical scavenging capacity

DPPH solution was prepared with anhydrous ethanol at 0.1 mM/L and stored away from light. Two milliliter sample solution was mixed with equal amount of DPPH solution and shaken well and left to stand for 30 min in the dark at 20°C. The DPPH solution was used as a blank control and the absorbance was measured at 520 nm (35).

$$\text{DPPH* radical scavenging capacity (\%)} = (A_0 - A_1) / A_0 \times 100$$

where A<sub>0</sub> is the absorbance of the control reaction (without addition of the sample), A<sub>1</sub> was the absorbance of sample solution in the reaction mixture.

### 2.7.3 Lipid peroxidation inhibition capacity

Egg yolk homogenate (10%, v/v) was used as the lipid medium for the reaction. A total of 0.1 ml test solution was mixed with 0.5 ml of egg yolk homogenate, 0.4 ml of pure water and 50 μl of ferrous sulfate solution (Fe·SO<sub>4</sub>·7H<sub>2</sub>O, 70 mM/L). After incubation at 37°C for 30 min, 1.5 ml of acetic acid solution (20%, v/v, pH 3.5) and 1.5 ml of thiobarbituric acid solution (0.8% by mass, prepared with 1.1% sodium dodecyl sulfate solution) were added. Five milliliter of n-butanol was added and centrifuged at 5,000 r/min for 15 min. The absorbance of the supernatant was measured at 532 nm (36).

$$\text{Lipid peroxidation inhibition capacity (\%)} = (A_0 - A_1) / A_0 \times 100$$

where A<sub>0</sub> is the absorbance of control reaction (without addition of the sample), A<sub>1</sub> was the absorbance of sample solution in reaction mixture.

## 2.8 Hypolipidemic activities *in vitro*

### 2.8.1 Cholesterol adsorption capacity

Samples were added to 30 ml of fresh egg yolk solution (10%, v/v), adjusted to pH 7 using NaOH and HCl solution (simulate the environment of intestine), shaken for 2 h at 37°C, centrifuged at 3,000 g for 20 min, the supernatant was combined and fixed to 100 ml, then 1 ml was diluted by adding 9 ml of glacial acetic acid, and the cholesterol content in the diluted solution was determined by phthalaldehyde method (2).

### 2.8.2 Pancreatic lipase inhibitory capacity

The sample was mixed with 3 ml of PBS (0.1 M, pH = 7.4), 0.5 ml of 1.2 mg/ml pancreatic lipase and 0.5 ml of 0.08% p-NPP (p-nitrophenyl phosphate disodium salt), then shake for 30 min at 37°C in a water bath and record the absorbance value at 410 nm, recorded as A<sub>1</sub>. No sample plus lipase solution is denoted as A<sub>0</sub>. Add the sample without lipase solution and write A<sub>2</sub> (3).

$$\text{Pancreatic lipase inhibitory capacity (\%)} = [1 - (A_1 - A_2) / A_0] \times 100\%$$

### 2.8.3 Bile acid salt binding capacity

The sample was taken in a conical flask, 30 mg pepsin and 1 ml of 0.01 M hydrochloric acid solution were added and shaken in a water bath at 37°C for 1 h. The pH of the system was adjusted to 6.3 with NaOH solution, 40 mg trypsin was added and shaken at 37°C for 1 h (simulate the environment of intestinal). Add 4 ml of sodium glycocholate/sodium taurocholate and shake in a water bath at 37°C for 1 h, then centrifuge at 3,000 g for 20 min, take 2.5 ml of the supernatant and add 7.5 ml of 60% sulfuric acid and measure the absorbance value at 387 nm (4).

## 2.9 Cellular assays

The toxicity of the polysaccharides to HepG2 cells was determined by measuring cell viability with the CCK-8 kit. HepG2 cells were treated with 1 mM free fatty acid (FFA) mixture (oleic acid/palmitic acid, 2:1) for 24 h (37). A hepatocyte fat accumulation model was established, and three administration concentrations of 25 μg/ml (LD), 100 μg/ml (MD), and 400 μg/ml (HD) were selected to intervene in FFA-induced HepG2 cells based on the results of cytotoxicity assay. Cellular activity, extracellular glutamic-pyruvic transaminase (ALT) content and intracellular

triglyceride (TG) levels were measured using CCK-8, ALT and TG kits (Nanjing Jiancheng Institute of Biological Engineering, Nanjing, China), respectively.

## 2.10 Statistical analysis

GraphPad Prism 7.0 was used to perform statistical analysis of the data. The results of the Shapiro–Wilk normality test were used to ensure that the numbers were normally distributed. ANOVA with Tukey's test was used to assess whether there were any significant differences between the groups. Results were expressed as mean  $\pm$  SD with at least six biological replicates for each independent experiment. The threshold for statistical significance was set at  $p < 0.05$ .

## 3. Results

### 3.1 Purification and screening of polysaccharides fractions with hypolipidemic activity

The crude polysaccharides (SRF) were extracted from *S. rugosoannulata* by freeze–thaw combine with hot water, and purified by ethanol precipitation, protein removal, and freeze-drying steps. Then cellular experiments were conducted to screen the polysaccharides with hypolipidemic efficacy from SRF. HepG2 lipid accumulation model was prepared by FFA-induced, and the lipid-lowering efficacy of SRF-1 and SRF-2 isolated from DEAE-Sepharose Fast Flow columns (Figure 1A) was compared by detecting the cell viability, intracellular TG content and extracellular AST content of FFA-induced HepG2 cells.

As shown in Figure 2, SRF-1 significantly increased FFA-induced HepG2 cell viability and decreased extracellular ALT content and intracellular TG content, implying that SRF-1 can reduce FFA-induced hepatocyte injury and lipid accumulation. Therefore, we chose Sephacryl S-200 HR ion exchange column for further purification and study of SRF-1. As shown in Figures 1B, a 0.15 M NaCl solution eluted SRF-1, and two fractions, named SRF-3 and SRF-4, were obtained, with SRF-3 as the main fraction. Therefore, the present study focused on the structure and activity of SRF-3.

The purity and average relative molecular mass of SRF-3 were further determined by HPGPC. The HPGPC spectrum of SRF-3 was a sharp and symmetric single elution peak, indicating that SRF-3 was a relatively homogeneous fraction (Figure 3B). The average relative molecular mass of SRF-3 was 24 kDa.

### 3.2 Monosaccharide composition analysis of SRF-3

The phenol-sulfate method was used to determine the total sugar content, while the BCA method was used to determine the protein content. The results showed that SRF-3 contained 95.43% total sugars and 0.2% protein (Table 1). Scanning of the SRF-3 using full wavelength UV spectroscopy showed that SRF-3 had no absorption peaks at 260–280 nm, indicating that SRF-3 was almost free of protein and nucleic acids (Figure 3A).

The primary structure of polysaccharides determines the secondary, tertiary and even quaternary structure of polysaccharides, which in turn influences the physicochemical properties and biological activity of polysaccharides (38). The monosaccharide composition of SRF-3 was determined by PMP derivatization combined with UHPLC, by comparing the retention time and peak area with each monosaccharide

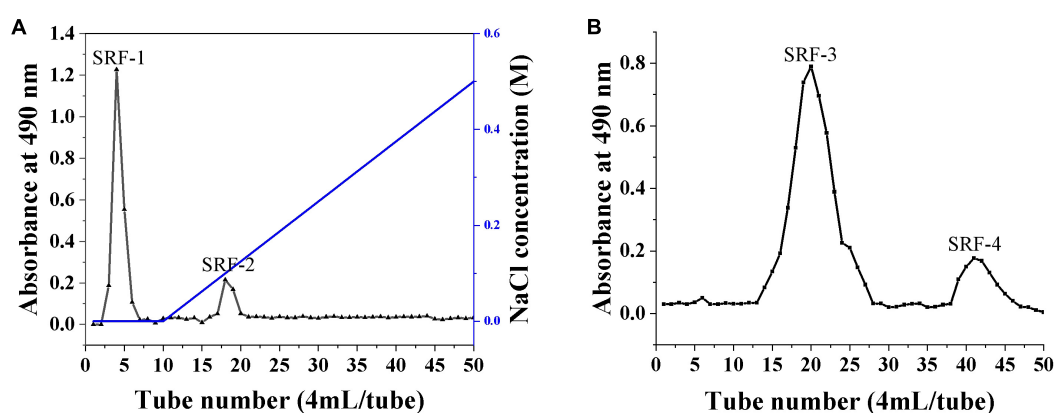


FIGURE 1  
Isolation and purification of polysaccharides from *S. rugosoannulata* by gel column. (A) DEAE cellulose column for the separation of crude polysaccharides. (B) SRF-1 was further separated by a Sephacryl S-200 high-resolution column.



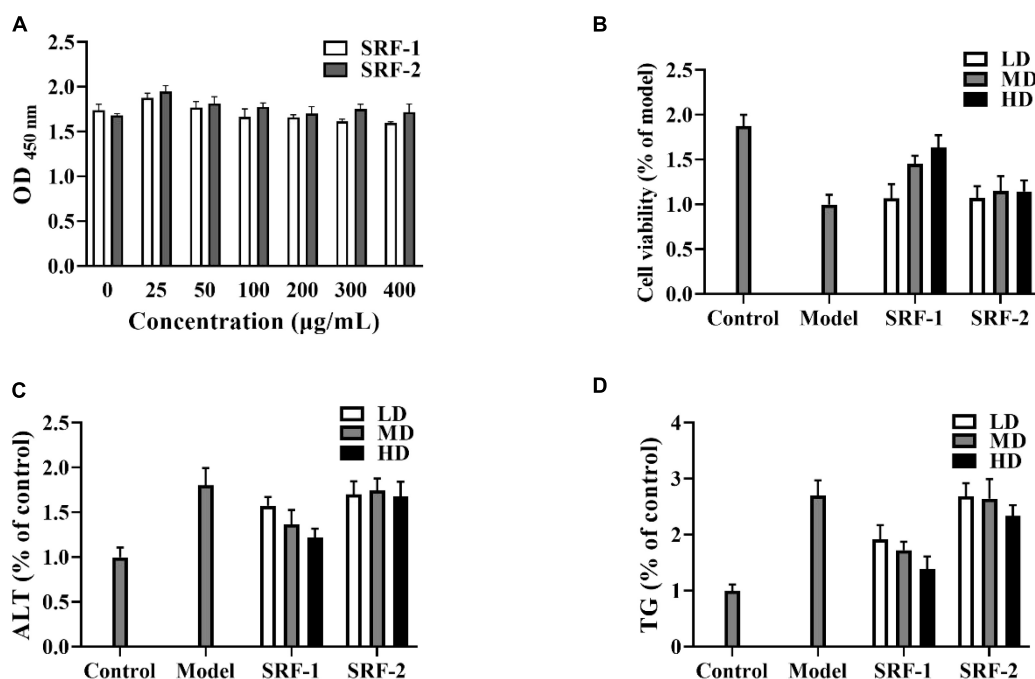


FIGURE 2

Effects of SRF-1 and SRF-2 on FFA-induced HepG2 cells. (A) Cell viability of HepG2 cells. (B) Cell viability of FFA-induced HepG2 cells. (C) Extracellular ALT levels. (D) Intracellular TG levels.

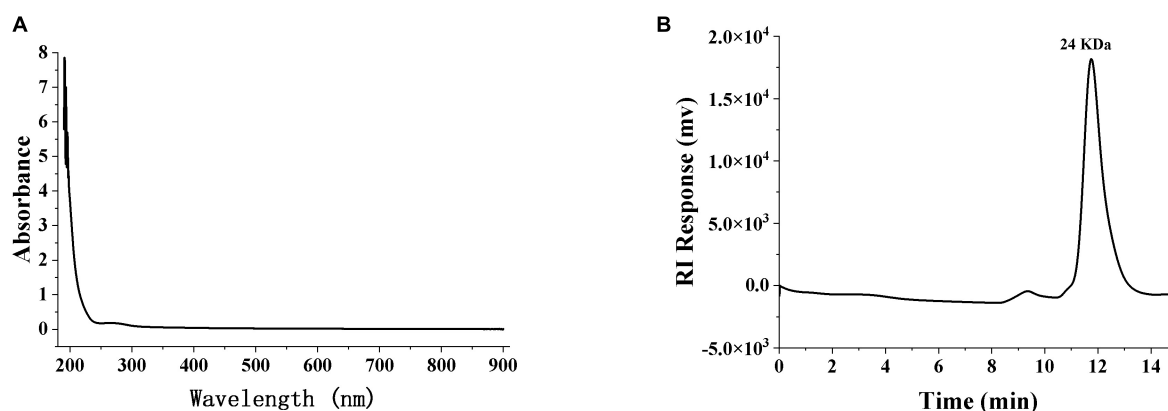


FIGURE 3

The ultraviolet spectroscopy (A) and HPGPC (B) of SRF-3. SRF-3 was configured as a 1 mg/ml solution, samples were scanned in a quartz colorimetric cup at 190–900 nm for UV-vis full wavelength, and zeroed with distilled water as a blank.

standard (Figure 4 and Table 1), it was determined that SRF-3 consisted of mannose, glucose, galactose, and methyl galactose in a molar ratio of 8:12:58:12.

Currently, a wide variety of polysaccharides are extracted from edible mushrooms. Liang et al. reported that the PGP-1c extracted from the *Pleurotus geesteranus* was composed of galactose (36.4%), 3-O-methylgalactose (20.8%), mannose (20.7%), glucose (19.9%), and fucose (2.2%) (39). Chen et al. reported that the polysaccharides EP-1 extracted from *Pleurotus*

*eryngii* consisted of D-Glc, D-Gal, and D-Man in the molar ratio: 96.39:2.26:1.35 (11). Manna et al. reported that the polysaccharides extracted from the *L. edodes* consisted of a (1→6)-linked galactose group, a (1→6)-linked (1→3,6)-linked glucose residue, and a terminal pyranose groups in a molar ratio close to 3:1:1, respectively (40). The high content of galactose, mannose and glucose in edible mushroom polysaccharides and the agreement of SRF-3 to contain these three monosaccharides, but with a higher content of galactose,

TABLE 1 Component characterization of SRF-3.

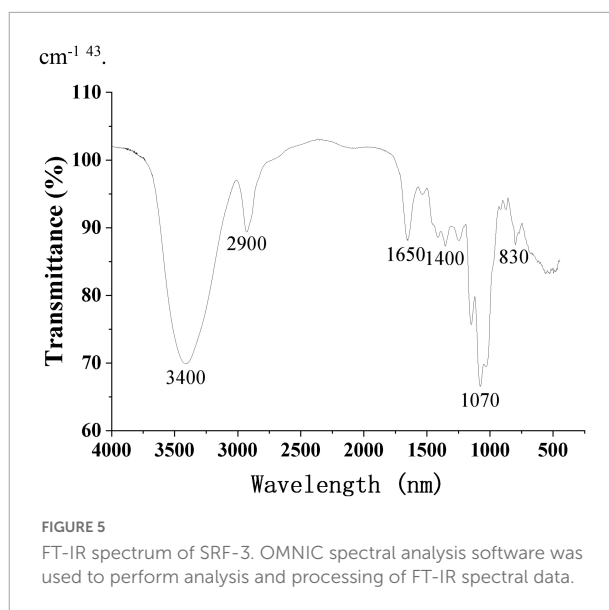
Index	SRF-3
Total sugar content (%)	95.43 ± 2.84
Protein content (%)	0.2 ± 0.04
Monosaccharide composition (molar ratio)	
Mannose	0.16
Glucose	0.12
Galactose	0.58
Methyl galactose	0.12
Fucose	0.02

indicating that SRF-3 is very different from other typical edible mushroom polysaccharides, which may be related to the properties of the *S. rugosoannulata* itself or the method of polysaccharides extraction.

### 3.3 Structure of SRF-3

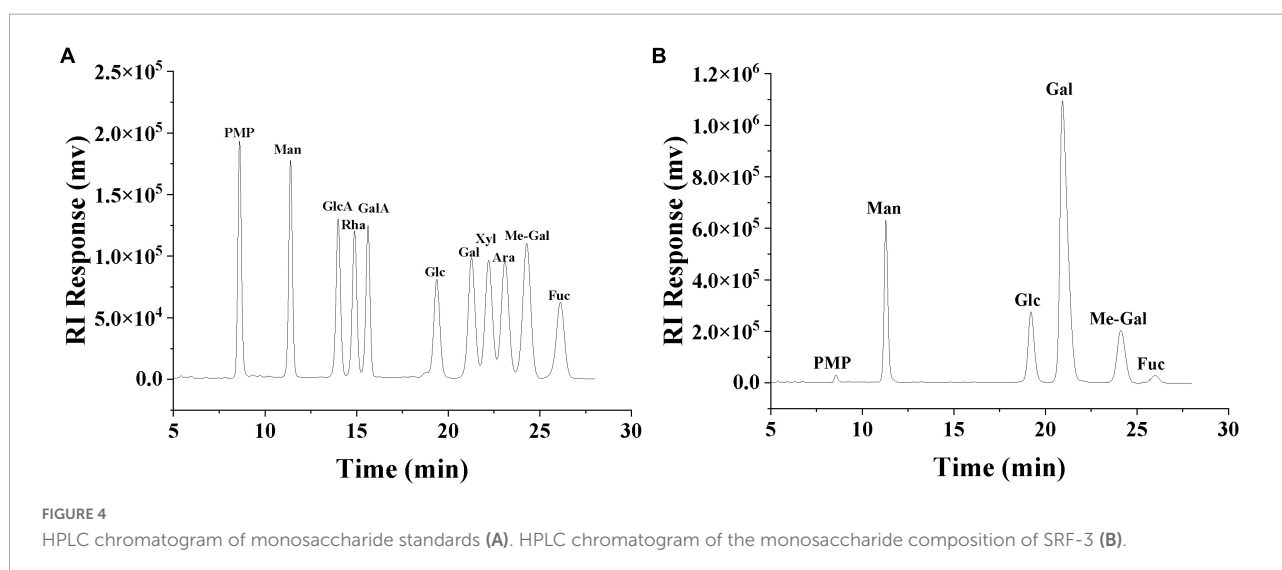
#### 3.3.1 FT-IR spectroscopy

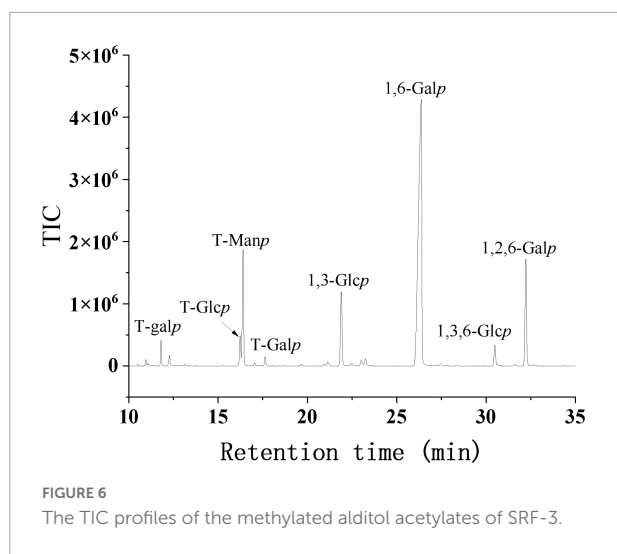
Figure 5 shows the FT-IR spectra of purified SRF-3 from 1,650 to 4,000  $\text{cm}^{-1}$ . The sample exhibits a distinct polysaccharides characteristic absorption peak with a broad and strong absorption peak of -OH stretching vibration detected near 3,400  $\text{cm}^{-1}$ . A narrow and weak C-H stretching vibration absorption peak was detected near 2,900  $\text{cm}^{-1}$ , and a bending vibration absorption peak of OH was shown near 1,650  $\text{cm}^{-1}$ . In addition, a weak C-H deformation vibration peak was detected around 1,400  $\text{cm}^{-1}$ , as well as a clear pyran ring absorption peak near 1,070  $\text{cm}^{-1}$ , and C-H variable angle vibration of the differential isomerization of the  $\alpha$ -terminus of pyranose at 855–810  $\text{cm}^{-1}$  (40).



#### 3.3.2 Methylation analysis

Methylation analysis is the complete methylation of free hydroxyl groups in polysaccharides and is often used to determine the glycosyl bonds and thus resolve the structure of polysaccharides. The methylation, hydrolysis, reduction and acetylation of SRF-3 were carried out and the type of glycosidic bond was determined by GC-MS analysis. The methylation results of SRF-3 are shown in Figure 6 and Table 2. SRF-3 contains mainly 1,6-Gal (60.3%) and 1,2,6-Gal (11.0%), t-Man (10.4%) and t-Fuc (1.6%) were detected indicating that they were mainly present in the non-reducing end form. It is assumed that this homogeneous component is mainly 1,6-Gal as the main chain with substitution at the O-2 position of Gal with a branching degree of 15.4%, and the side chain structure is





dominated by t-Man with a small amount of t-Fuc present, indicating that this homogeneous component is a rockweed mannogalactan. In addition, a small amount of 1,3-Glc and 1,3,6-Glc indicated that a small amount of glucan structure was also present in this sample (39).

### 3.3.3 NMR analysis

Nuclear magnetic resonance is one of the commonly used methods to analyze the structure of polysaccharides and can provide accurate structural information of polysaccharides (41). In the present study, the fine structure of SRF-3 was analyzed using one-dimensional NMR ( $^1\text{H}$  and  $^{13}\text{C}$ ) and two-dimensional NMR (HSQC and HMBC), and the results are shown in Figure 7 and Tables 3, 4. In the  $^1\text{H}$ -NMR spectrum, 4.93 ppm is attributed to the heterohead proton signal peaks of  $\alpha$ -D-1,6-Galp and  $\alpha$ -D-1,6-Me-Galp sugar residues, the signal peak located at 3.38 ppm is the signal peak of H in O-CH<sub>3</sub>, the heterohead proton signal peak of  $\beta$ -D-Manp appears at 4.75 ppm. In the  $^{13}\text{C}$ -NMR spectrum, the heterohead carbon of  $\alpha$ -D-1,6-Galp or  $\alpha$ -D-1,6-Me-Galp and  $\alpha$ -D-1,2,6-Galp are located at 96.79 and 97.35 ppm, respectively. The signal peak

at 75.87 ppm located in the low field is attributed to the C-2 position of  $\alpha$ -D-1,2,6-Galp, the signal peak of C in O-CH<sub>3</sub> peak is located at 54.98 ppm, the hetero-headed carbon signal peak of  $\beta$ -D-Manp appears at 100.65 ppm, and the hetero-headed carbon signal peak of  $\beta$ -D-Glcp appears at 102.24 ppm (34). Other chemical shifts and connections were attributed by HSQC and HMBC.

In HSQC, the H-1/C-1 to H-6/C-6 of Gal, Glc and Man were attributed sequentially, which revealed the presence of  $\alpha$ -D-1,6-Galp,  $\alpha$ -D-1,6-Me-Galp and  $\alpha$ -D-1,2,6-Galp in the sample, as well as a small amount of  $\beta$ -1,6-D-Glcp composed of Glc and Man consisting of t- $\beta$ -D-Manp, named below with the letters A, B, C, D, and E, respectively. The linkage order between the individual sugar residues was analyzed by the long-range coupling correlation spectrum HMBC: BH-1/EC-2, CH-1/DC-6, DC-1/CH-6a/6b, CC-1/DH-6a/6b, DH-1/CC-6, DC3-O-CH<sub>3</sub>H, DH3-O-CH<sub>3</sub>C, FH-6/FC-4, FH-6/FC-5. In summary, we can obtain the structural characteristics of this sample as follows:  $\alpha$ -D-1,6-Galp and  $\alpha$ -D-1,6-Me-Galp are linked to form the main chain structure, with a branch at the O-2 position of Gal, and a small amount of t- $\beta$ -D-Manp and a trace amount of t- $\alpha$ -L-Fucp structure in the form of side chains, which is the rockweed mannogalactan (39).

### 3.4 *In vitro* antioxidant activity of SRF-3

The antioxidant capacity of SRF-3 was evaluated by three complementary tests on hydroxyl and DPPH radical scavenging capacity and lipid peroxidation inhibition. Scavenging of free radicals is considered to be one of the main mechanisms by which antioxidants slow down the oxidative process, while inhibition of lipid peroxidation can directly reduce the oxidative damage caused by fat accumulation. As shown in Figure 8, the antioxidant capacity of SRF-1 and SRF-3 showed a significant positive correlation with their concentrations.

The scavenging rates of hydroxyl radicals by SRF-1 and SRF-3 were 60.84 and 70.35% at 2 mg/ml, respectively. The IC<sub>50</sub> values of SRF-1 and SRF-3 were  $1.62 \pm 0.02$  and  $0.96 \pm 0.04$  mg/ml, respectively (Figure 8A). The DPPH

TABLE 2 Results of SRF-3 methylation analysis.

Retention time (min)	PMAAs	Linkage	Molar ratios
11.801	1,5-Di-O-acetyl-1-deuterio-6-deoxy-2,3,4-tri-O-methyl-L-galactitol	L-Fucp-( $\rightarrow$ 1)	1.6
16.232	1,5-Di-O-acetyl-1-deuterio-2,3,4,6-tetra-O-methyl-D-glucitol	Glcp-( $\rightarrow$ 1)	2.5
16.398	1,5-Di-O-acetyl-1-deuterio-2,3,4,6-tetra-O-methyl-D-mannitol	Manp-( $\rightarrow$ 1)	10.4
17.633	1,5-Di-O-acetyl-1-deuterio-2,3,4,6-tetra-O-methyl-D-galactitol	Galp-( $\rightarrow$ 1)	0.9
21.904	1,3,5-Tri-O-acetyl-1-deuterio-2,4,6-tri-O-methyl-D-glucitol	$\rightarrow$ 3)-Glcp-( $\rightarrow$ 1)	8.3
26.371	1,5,6-Tri-O-acetyl-1-deuterio-2,3,4-tri-O-methyl-D-galactitol	$\rightarrow$ 6)-Galp-( $\rightarrow$ 1)	60.3
30.491	1,3,5,6-Tetra-O-acetyl-1-deuterio-2,4-di-O-methyl-D-glucitol	$\rightarrow$ 3,6)-Glcp-( $\rightarrow$ 1)	2.4
32.229	1,2,5,6-Tetra-O-acetyl-1-deuterio-3,4-di-O-methyl-D-galactitol	$\rightarrow$ 2,6)-Galp-( $\rightarrow$ 1)	11.0

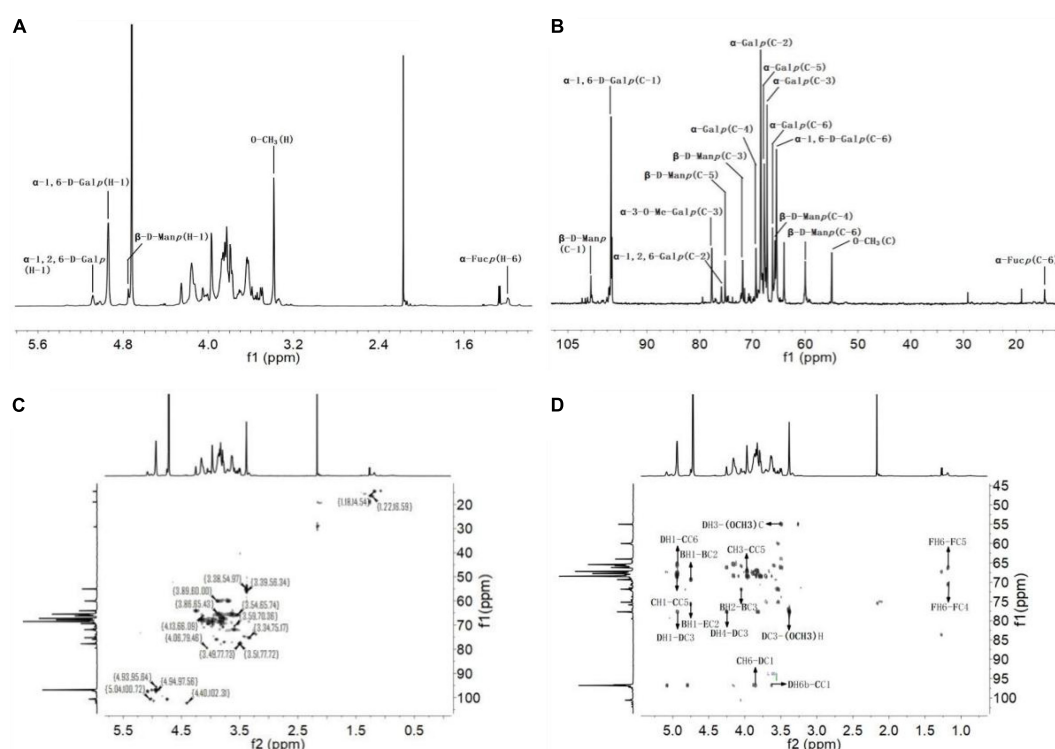


FIGURE 7  
Nuclear magnetic resonance analysis of SRF-3. (A) <sup>1</sup>H NMR spectrum. (B) <sup>13</sup>C NMR spectrum. (C) HSQC spectrum. (D) HMBC spectrum.

TABLE 3 <sup>1</sup>H and <sup>13</sup>C NMR spectra assignments for SRF-3 (ppm).

Sugar residues		1	2	3	4	5	6	O-CH <sub>3</sub>
(A)β-1,6-D-Glcp	H	4.41	3.22	3.42	3.34	3.42	3.97, 3.83	–
	C	102.24	73.79	74.61	68.56	75.42	69.12	–
(B)t-β-D-Manp	H	4.75	4.05	3.61	3.54	3.34	3.86, 3.69	–
	C	100.65	70.22	71.83	65.73	75.17	59.99	–
(C)α-1,6-D-Galp	H	4.93	3.84	3.97	4.03	4.15	3.85, 3.63	–
	C	96.79	68.45	67.22	69.33	67.76	66.21	–
(D)α-1,6-D-3-Me-Galp	H	4.93	3.84	3.51	4.25	4.15	3.85, 3.63	3.38
	C	96.79	68.45	77.72	65.44	67.76	66.21	54.98
(E)α-1,2,6-D-Galp	H	5.08	3.91	3.97	4.05	4.15	3.85, 3.51	–
	C	97.35	75.87	67.22	69.33	67.76	64.01	–
(F)t-α-L-Fucp	H	5.03	3.56	4.02	3.78	4.12	1.18	–
	C	101.6	71.54	67.48	70.64	66.23	14.63	–

scavenging activities of SRF-1 and SRF-3 were significantly different, with 10.22 and 45.22% scavenging of DPPH radicals at low concentrations (0.4 mg/ml) for SRF-1 and SRF-3, respectively. The IC<sub>50</sub> was 1.32 ± 0.05 and 0.80 ± 0.03 mg/ml, respectively. But at a concentration of 5 mg/ml, both DPPH radical scavenging rates were similar (Figure 8B). At low concentrations, there was no significant difference in the lipid

peroxidation inhibitory capacity of SRF-1 and SRF-3, but as the concentration increased, the lipid peroxidation inhibitory capacity of SRF-3 was significantly higher than that of SRF-1, and at 2 mg/ml, the inhibitory capacity of SRF-1 and SRF-3 lipid peroxidation was 65.34 and 78.25%, respectively. The IC<sub>50</sub> values of SRF-1 and SRF-3 were 0.81 ± 0.01 and 0.69 ± 0.02, respectively (Figure 8C). Overall, the antioxidant

TABLE 4 HMBC spectrum chemical shifts of SRF-3.

Sugar residues	H-6/C-6	H-3/C-3	H-1/C-1	Coupling relationship		
				$\delta$ H/ $\delta$ C	Residue	Atom
(B)t- $\beta$ -D-Manp			4.75	69.33	B	C2
				75.87	E	C2
		71.83		4.05	B	H2
(C) $\alpha$ -1,6-D-Galp			4.93	66.21	D	C6
				67.76	C	C5
		4.97		67.76	C	C5
			96.79	3.85	D	H6a
				3.63	D	H6b
(D) $\alpha$ -1,6-D-3-Me-Galp			4.93	66.21	C	C6
				67.76	D	C5
				77.72	D	C3
		3.51		54.98	O-CH <sub>3</sub>	C
		77.72		3.38	O-CH <sub>3</sub>	H
				4.25	D	H4
			97.56	3.85	C	H6a
				3.63	C	H6b
(F)t- $\alpha$ -L-Fucp	1.18			70.64	F	C4
				66.23	F	C5

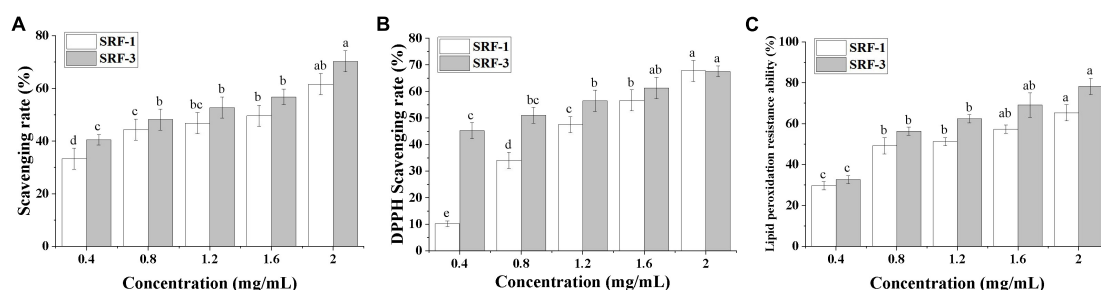


FIGURE 8

*In vitro* determination of the antioxidant capacity. (A) Hydroxyl radical scavenging capacity. (B) DPPH scavenging capacity. (C) Lipid peroxidation resistance capacity. Values with different letters (a–d) were significantly different ( $p < 0.05$ ).

activity of SRF-3 was significantly higher than that of SRF-1, predicting that SRF-3 may be the main antioxidant component of SRF.

### 3.5 *In vitro* hypolipidemic effects of SRF-3

Numerous studies have shown that polysaccharides can modulate blood lipids in a variety of ways, including lowering serum total cholesterol (TC), low-density lipoprotein cholesterol

(LDL-C), and increasing bile acid efflux (42). The *in vitro* lipid-lowering ability of SRF-3 was verified by testing the cholesterol adsorption ability, pancreatic lipase inhibition ability, and bile acid salt binding ability of SRF-3. As seen in Figure 9A, the adsorption capacity of SRF-3 for cholesterol adsorption showed a positive correlation with its concentration, and the cholesterol adsorption capacity was higher at pH 7 than pH 2 at the same concentration, and the cholesterol binding capacity of SRF-3 reached 60% at 10 mg/ml in the pH 7 environment, indicating that the cholesterol adsorption capacity of SRF-3 was higher in the intestinal environment than in the gastric environment. The small intestine is an important pathway for the biological



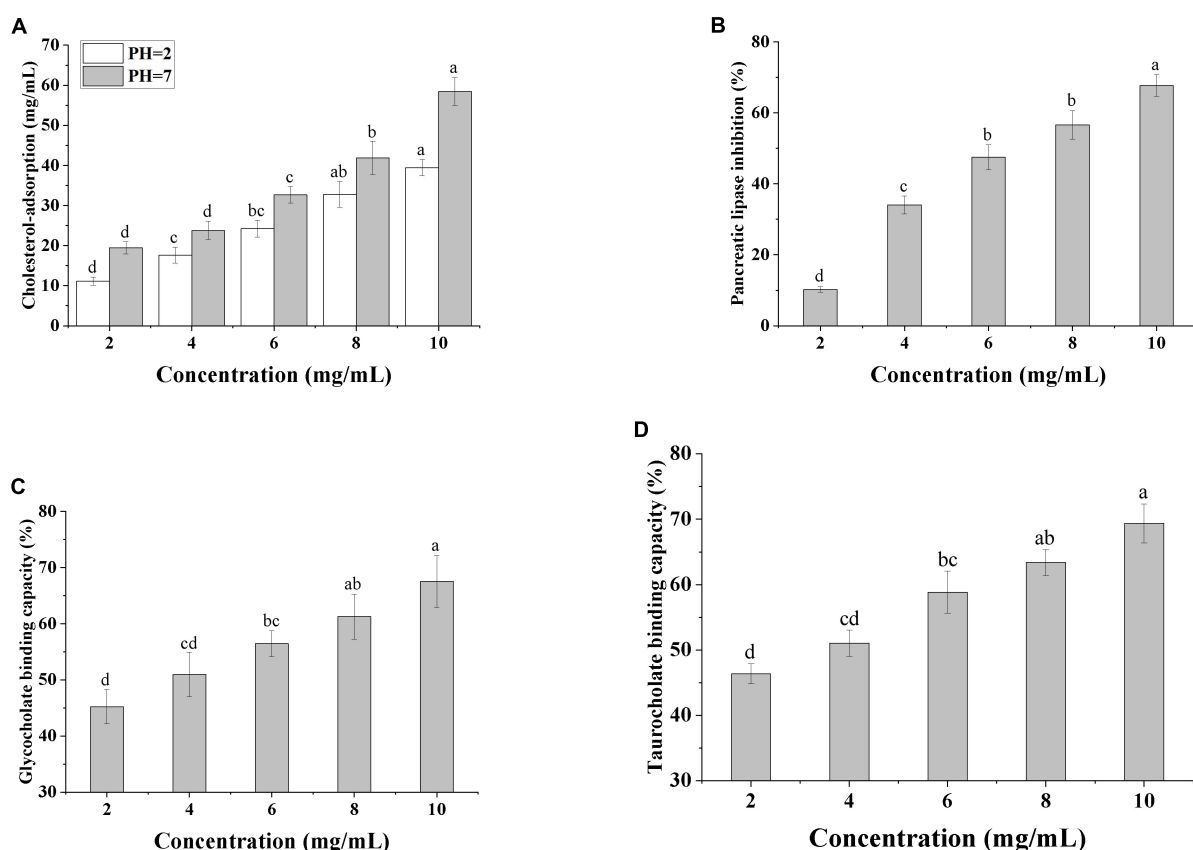


FIGURE 9

*In vitro* determination of the hypolipidemic capacity. (A) Cholesterol-adsorption capacities of SRF-3. (B) Pancreatic Lipase inhibition capacity of SRF-3. (C) Glycocholate binding capacity of SRF-3. (D) Taurocholate binding capacity of SRF-3. Values with different letters (a–d) were significantly different ( $p < 0.05$ ).

organism to obtain exogenous cholesterol from food, it can be judged that SRF-3 can reduce blood lipids by affecting the absorption of exogenous cholesterol by the biological organism. **Figure 9B** shows that as the concentration of SRF-3 increases, its inhibition of pancreatic lipase activity is enhanced, implying that SRF-3 has some potential in reducing exogenous fat digestion. **Figures 9C, D** show the binding ability of SRF-3 for glycocholate and taurocholate, respectively, and the results indicate that the bile acid salt binding ability also showed a significant positive correlation with SRF-3 concentration, implying that SRF-3 can reduce the circulation of bile acids in the body by binding bile acid salt in bile acids, thus promoting the excretion of lipids and lowering blood lipids (6).

## 4 Discussion and conclusion

In this article, two crude polysaccharides fractions, SRF-1 and SRF-2, were isolated from *S. rugosoannulata* by DEAE Sepharose Fast Flow chromatography, and SRF-1 was identified

as an effective lipid-lowering fraction by cellular assay, and then Sephacryl S-200 high resolution column Chromatography was used to separate and purify to obtain the fractions SRF-3 and SRF-4, with SRF-3 being the major fraction. SRF-3 was characterized by UHPLC, acid hydrolysis, methylation and one/two-dimensional NMR, and its hypolipidemic potential was evaluated by *in vitro* experiments. The results showed that SRF-3 consists of five monosaccharides (Rha, Ara, Man, Glc, and Gal) with an average weight of 24 kDa. Structural analysis showed that SRF-3 consists of  $\alpha$ -D-1,6-Galp and  $\alpha$ -D-1,6-Me-Galp linked to form the main chain structure, with a branch at the O-2 position of Gal with 15.4% branching, and a small amount of t- $\beta$ -D-Manp and a trace amount of t- $\alpha$ -L-Fucp are present as side chains. The production and removal of reactive oxygen species in living organisms is in a dynamic equilibrium, and lipid peroxidation resulting from fat accumulation can upset this equilibrium, thus allowing the concentration of reactive oxygen species to exceed physiological limits and causing damage to the body's cells. Therefore, lipid-lowering ingredients must not only have lipid-lowering effects, but also have the ability to reduce

the damage caused by lipid accumulation in the organism. SRF-3 exhibited free radical scavenging ability in antioxidant assays *in vitro*. This phenomenon also occurs in other edible fungal polysaccharides. Zhang et al. (35) isolated three crude polysaccharides from *Agaricus blazei* that also showed good antioxidant activity and concentration-dependent properties. Liu et al. (43) isolated water-soluble polysaccharides and alkali-soluble polysaccharides from the *Oudemansiella radiata*, whose main components were mannose, glucose, and galactose, and showed good antioxidant activity and antioxidant activity with concentration dependence. Through *in vitro* lipid-lowering experiments, we speculate that SRF-3 can reduce the intake and accumulation of lipids *in vivo* by binding exogenous cholesterol, reducing the digestion and decomposition of exogenous lipids by lipase and binding bile acid salts in bile acids (4). Our results suggest that SRF-3 has potential as a raw material for a lipid-lowering drug.

The structure and biological activity of polysaccharides in mushrooms are diverse and the biological activity of mushroom polysaccharides depends on the molecular weight of the polysaccharide, the monosaccharide composition, the degree of branching and the type of glycosidic bond. Previous investigations have revealed that mushroom polysaccharides such as *Auricularia auricula*, *A. blazei*, *Agaricus bisporus*, *Cordyceps sinensis*, *Grifola frondosa*, *Ganoderma lucidum*, *Morchella esculenta*, *Pleurotus eryngii*, *Pleurotus ostreatus*, *Pholiota nameko*, and *Collybia albuminosa* both have a substantial influence on antioxidant, anti-inflammatory, immunomodulatory, hypoglycemic, and hypolipidaemic effects (44–51). Liu et al. (30) used macroporous adsorption resin and ion exchange chromatography to isolate two structurally different glucose-based polysaccharides, SRP-1 and SRP-2, from *S. rugosoannulata*. Both polysaccharides contained a (1→, 6)- $\alpha$ -D-glucan backbone, but the monosaccharides of SRP-1 and SRP-2 molar ratios and glycosidic bond types were different, and both polysaccharides exhibited antioxidant activity. Their extraction and elution methods were similar to our study, but the extracted polysaccharides differed significantly in structure from those obtained by our isolation. Liang et al. (39) isolated a glucomannan galactan with a glycan chain structure similar to SRP-3 from *P. ostreatus*, with  $\alpha$ -(1→6)Gal as the main chain and  $\beta$ -D-Manp-(1→, →3)- $\alpha$ -D-Glcp-(1→ and a small amount of Fucp as the side chain, and *in vitro* experiments showed that the polysaccharides has immunomodulatory activity. Ge et al. (52) isolated a mannogalactan composed of glucose, galactose, and mannose from *Helvella leucopus*, which showed significant lipid-lowering activity in high-fat fed mice. We suggest that the monosaccharide composition of glucose, galactose, and mannose and the main chain of (1→, 6)- $\alpha$ -D-glucan may be responsible for the hypolipidemic and antioxidant effects of SRF-3, but further experiments are needed to verify this.

Different extraction and isolation methods may result in differences in the structure and activity of polysaccharides. In this study, SRF-3 was isolated and purified by DEAE Sepharose Fast Flow and Sephacryl S-200 high-resolution column chromatography, and its chemical structure and lipid-lowering activity were investigated, which could be useful for its future application development in lipid-lowering. However, the biological activity of polysaccharides depends not only on their structure and molecular size, but also on their conformation. Therefore, additional conformational analyses of the polysaccharides of *S. rugosoannulata* are needed in the future.

## Data availability statement

The original contributions presented in this study are included in the article/supplementary material, further inquiries can be directed to the corresponding authors.

## Author contributions

DW and YZ established the research direction. TL, HF, and HL guided the thesis writing. YG carried out the experiments and wrote the manuscript. SZ helped to consult the literature. GA, CY, XT, and CB assisted in experimental operation and data recording. All authors contributed to the article and approved the submitted version.

## Funding

This research was funded by the Science and Technology Projects of Jilin Provincial Department of Education (JJKH20210617KJ).

## Conflict of interest

The authors declare that the research was conducted in the absence of any commercial or financial relationships that could be construed as a potential conflict of interest.

## Publisher's note

All claims expressed in this article are solely those of the authors and do not necessarily represent those of their affiliated organizations, or those of the publisher, the editors and the reviewers. Any product that may be evaluated in this article, or claim that may be made by its manufacturer, is not guaranteed or endorsed by the publisher.

## References

1. Thu ZM, Myo KK, Aung HT, Clericuzio M, Armijos C, Vidari G. Bioactive phytochemical constituents of wild edible mushrooms from Southeast Asia. *Molecules*. (2020) 25:1972. doi: 10.3390/molecules25081972
2. Zhang YZ, Wang DW, Chen YT, Liu TT, Zhang SS, Fan HX, et al. Healthy function and high valued utilization of edible fungi. *Food Sci Hum Wellness*. (2021) 10:408–20.
3. Xue ZH, Hao JF, Yu WC, Kou XH. Effects of processing and storage preservation technologies on nutritional quality and biological activities of edible fungi: a review. *Food Process Eng*. (2017) 40:e12437.
4. Tyler JB, Cao L, Pan ZL, Zhang RH. Fungi for future foods. *J Future Foods*. (2021) 1:25–7.
5. Yin ZH, Sun-W DX, Wang JM, Ma CY, Geoffrey INW, Kang WY. Polysaccharides from edible fungi *Pleurotus* spp.: advances and perspectives. *J Future Foods*. (2021) 1:128–40.
6. Song Z, Zhao R, Zhang H, Wei P, Qi L, Chen G, et al. Rapid and accurate screening of lysine-producing edible mushrooms via the homocitrate synthase gene as a universal molecular marker. *ACS Omega*. (2021) 6:26910–8. doi: 10.1021/acsomega.1c03175
7. Machado AR, Teixeira MF, de Souza Kirsch L, Campelo Mda C, de Aguiar Oliveira IM. Nutritional value and proteases of *Lentinus citrinus* produced by solid state fermentation of lignocellulosic waste from tropical region. *Saudi J Biol Sci*. (2016) 23:621–7. doi: 10.1016/j.sjbs.2015.07.002
8. Fogarasi M, Socaci SA, Dulf FV, Diaconeasa ZM, Farcas AC, Tofana M, et al. Bioactive compounds and volatile profiles of five Transylvanian wild edible mushrooms. *Molecules*. (2018) 23:3272. doi: 10.3390/molecules23123272
9. Barros L, Baptista P, Estevinho L, Ferreira I. Effect of fruiting body maturity stage on chemical composition and antimicrobial activity of *Lactarius* sp. Mushrooms. *J Agric Food Chem*. (2007) 55:8766–71. doi: 10.1021/jf071435+
10. Cheng XD, Wu QX, Zhao J, Su T, Lu YM, Zhang WN, et al. Immunomodulatory effect of a polysaccharide fraction on RAW 264.7 macrophages extracted from the wild *Lactarius deliciosus*. *Int J Biol Macromol*. (2019) 128:732–9. doi: 10.1016/j.ijbiomac.2019.01.201
11. Chen J, Yong Y, Xia X, Wang Z, Liang Y, Zhang S, et al. The excreted polysaccharide of *Pleurotus eryngii* inhibits the foam-cell formation via down-regulation of CD36. *Carbohydr Polym*. (2014) 112:16–23. doi: 10.1016/j.carbpol.2014.05.068
12. Chen J, Yong Y, Xing M, Gu Y, Zhang Z, Zhang S, et al. Characterization of polysaccharides with marked inhibitory effect on lipid accumulation in *Pleurotus eryngii*. *Carbohydr Polym*. (2013) 97:604–13. doi: 10.1016/j.carbpol.2013.05.028
13. Zhang C, Zhang L, Liu H, Zhang J, Hu C, Jia L. Antioxidation, anti-hyperglycaemia and renoprotective effects of extracellular polysaccharides from *Pleurotus eryngii* SI-04. *Int J Biol Macromol*. (2018) 111:219–28. doi: 10.1016/j.ijbiomac.2018.01.009
14. He L, He X, Liu X, Shi W, Xu X, Zhang Z. A sensitive, precise and rapid LC-MS/MS method for determination of ergosterol peroxide in *Paecilomyces cicadae* mycelium. *Steroids*. (2020) 164:108751. doi: 10.1016/j.steroids.2020.108751
15. Lee SO, Lee MH, Lee KR, Lee EO, Lee HJ. *Fomes fomentarius* ethanol extract exerts inhibition of cell growth and motility induction of apoptosis via targeting AKT in human breast cancer MDA-MB-231 cells. *Int J Mol Sci*. (2019) 20:1147. doi: 10.3390/ijms20051147
16. Wong JH, Ng TB, Chan HHL, Liu Q, Man GCW, Zhang CZ, et al. Mushroom extracts and compounds with suppressive action on breast cancer: evidence from studies using cultured cancer cells, tumor-bearing animals, and clinical trials. *Appl Microbiol Biotechnol*. (2020) 104:4675–703. doi: 10.1007/s00253-020-10476-4
17. Xu TT, Robert BB, Joshua DL. The cancer effects of edible mushrooms. *Anti Cancer Agents Med Chem*. (2012) 12:1255–63.
18. Zhang B, Li Y, Zhang F, Linhardt RJ, Zeng G, Zhang A. Extraction, structure and bioactivities of the polysaccharides from *Pleurotus eryngii*: a review. *Int J Biol Macromol*. (2020) 150:1342–7. doi: 10.1016/j.ijbiomac.2019.10.144
19. Song AX, Mao YH, Siu KC, Wu JY. Bifidogenic effects of *Cordyceps sinensis* fungal exopolysaccharide and konjac glucomannan after ultrasound and acid degradation. *Int J Biol Macromol*. (2018) 111:587–94. doi: 10.1016/j.ijbiomac.2018.01.052
20. Geng X, Yang D, Zhang Q, Chang M, Xu L, Cheng Y, et al. Good hydrolysis activity on raffinose family oligosaccharides by a novel alpha-galactosidase from *Tremella aurantialba*. *Int J Biol Macromol*. (2020) 150:1249–57. doi: 10.1016/j.ijbiomac.2019.10.136
21. Zheng Y, Wang WD, Li Y. Antitumor and immunomodulatory activity of polysaccharide isolated from *Trametes orientalis*. *Carbohydr Polym*. (2015) 131:248–54. doi: 10.1016/j.carbpol.2015.05.074
22. Qian Y, Wang D, Fan M, Xu Y, Sun X, Wang J. Effects of intrinsic metal ions of lentinan with different molecular weights from *Lentinus edodes* on the antioxidant capacity and activity against proliferation of cancer cells. *Int J Biol Macromol*. (2018) 120:73–81. doi: 10.1016/j.ijbiomac.2018.06.203
23. Lee KF, Chen JH, Teng CC, Shen CH, Hsieh MC, Lu CC, et al. Protective effects of *Hericium erinaceus* mycelium and its isolated erinacine A against ischemia-injury-induced neuronal cell death via the inhibition of iNOS/p38 MAPK and nitrotyrosine. *Int J Mol Sci*. (2014) 15:15073–89. doi: 10.3390/ijms150915073
24. Amara I, Scuto M, Zappala A, Ontario ML, Petralia A, Abid-Essefi S, et al. *Hericium erinaceus* prevents DEHP-induced mitochondrial dysfunction and apoptosis in PC12 cells. *Int J Mol Sci*. (2020) 21:2138. doi: 10.3390/ijms21062138
25. Yin ZH, Liang ZH, Li CQ, Wang JM, Ma CY, Kang WY. Immunomodulatory effects of polysaccharides from edible fungus: a review. *Food Sci Hum Wellness*. (2021) 10:393–400.
26. Zhang SS, Xu XL, Cao X, Liu TT. The structural characteristics of dietary fibers from *Tremella fuciformis* and their hypolipidemic effects in mice. *Food Sci Hum Wellness*. (2023) 12:503–11.
27. Subbulakshmi M, Dhanasekaran Sugapriya S, Abirami M, Kannan R, Divya V. Phylogenetic analysis and protective effects of thymol and its chromatographic fractions from a novel wild mushroom in combating oxidative stress. *Food Sci Hum Wellness*. (2021) 10:452–9.
28. Zhao SZ, Lei M, Xu H, He HL, Alexander S, Wang JH, et al. The normal cell proliferation and wound healing effect of polysaccharides from *Ganderma amboinense*. *Food Sci Hum Wellness*. (2021) 10:508–13.
29. Zhang W, Tian G, Geng X, Zhao Y, Ng TB, Zhao L, et al. Isolation and characterization of a novel lectin from the edible mushroom *Stropharia rugosoannulata*. *Molecules*. (2014) 19:19880–91. doi: 10.3390/molecules191219880
30. Liu Y, Hu CF, Feng X, Cheng L, Ibrahim SA, Wang CT, et al. Isolation, characterization and antioxidant of polysaccharides from *Stropharia rugosoannulata*. *Int J Biol Macromol*. (2020) 155:883–9. doi: 10.1016/j.ijbiomac.2019.11.045
31. Wu JW, Chen XT, Qiao K, Su YC, Liu Z. Purification, structural elucidation, and *in vitro* antitumor effects of novel polysaccharides from *Bangia fuscopurpurea*. *Food Sci Hum Wellness*. (2021) 10:63–71.
32. Liu M, Shan S, Gao X, Zeng D, Lu W. Structure characterization and lipid-lowering activity of a homogeneous heteropolysaccharide from sweet tea (*Rubus suavisissimus* S. Lee). *Carbohydr Polym*. (2022) 277:118757. doi: 10.1016/j.carbpol.2021.118757
33. Susumu H, Eiko A, Shigeo S, Masahiro O, Kazuaki K, Jun N. High-performance liquid chromatography of reducing carbohydrates as strongly ultraviolet-absorbing and electrochemically sensitive 1-phenyl-3-methyl-5-pyrazolone derivatives. *Anal Biochem*. (1989) 180:351–7. doi: 10.1016/0003-2697(89)90444-2
34. Liu B, Shang ZZ, Li QM, Zha XQ, Wu DL, Yu NJ, et al. Structural features and anti-gastric cancer activity of polysaccharides from stem, root, leaf and flower of cultivated *Dendrobium huoshanense*. *Int J Biol Macromol*. (2020) 143:651–64. doi: 10.1016/j.ijbiomac.2019.12.041
35. Zhang A, Li X, Xing C, Yang J, Sun P. Antioxidant activity of polysaccharide extracted from *Pleurotus eryngii* using response surface methodology. *Int J Biol Macromol*. (2014) 65:28–32. doi: 10.1016/j.ijbiomac.2014.01.013
36. Tang W, Xing Z, Li C, Wang J, Wang Y. Molecular mechanisms and *in vitro* antioxidant effects of *Lactobacillus plantarum* MA2. *Food Chem*. (2017) 221:1642–9.
37. Lee MS, Han HJ, Han SY, Kim IY, Chae S, Lee CS, et al. Loss of the E3 ubiquitin ligase MKRN1 represses diet-induced metabolic syndrome through AMPK activation. *Nat Commun*. (2018) 9:3404. doi: 10.1038/s41467-018-05721-4
38. Huang F, Hong R, Zhang R, Dong L, Bai Y, Liu L, et al. Dynamic variation in biochemical properties and prebiotic activities of polysaccharides from *Longan pulp* during fermentation process. *Int J Biol Macromol*. (2019) 132:915–21. doi: 10.1016/j.ijbiomac.2019.04.032
39. Liang Z, Yin Z, Liu X, Ma C, Wang J, Zhang Y, et al. A glucomannogalactan from *Pleurotus geesteranus*: structural characterization, chain conformation and immunological effect. *Carbohydr Polym*. (2022) 287:119346. doi: 10.1016/j.carbpol.2022.119346

40. Manna DK, Maity P, Nandi AK, Pattanayak M, Panda BC, Mandal AK, et al. Structural elucidation and immunostimulating property of a novel polysaccharide extracted from an edible mushroom *Lentinus fusipes*. *Carbohydr Polym.* (2017) 157:1657–65. doi: 10.1016/j.carbpol.2016.11.048
41. Wu Q, Luo M, Yao X, Yu L. Purification, structural characterization, and antioxidant activity of the COP-W1 polysaccharide from *Codonopsis tangshen* oliv. *Carbohydr Polym.* (2020) 236:116020. doi: 10.1016/j.carbpol.2020.11.6020
42. Gunness P, Gidley MJ. Mechanisms underlying the cholesterol-lowering properties of soluble dietary fibre polysaccharides. *Food Funct.* (2010) 1:149–55.
43. Liu Q, Zhu M, Geng X, Wang H, Ng TB. Characterization of polysaccharides with antioxidant and hepatoprotective activities from the edible mushroom *Oudemansiella radicata*. *Molecules.* (2017) 22:234. doi: 10.3390/molecules22020234
44. Fu Y, Feng KL, Wei SY, Xiang XR, Ding Y, Li HY, et al. Comparison of structural characteristics and bioactivities of polysaccharides from loquat leaves prepared by different drying techniques. *Int J Biol Macromol.* (2020) 145:611–9. doi: 10.1016/j.ijbiomac.2019.12.226
45. Amirullah N, Rahmat S, Dzulkarnain A, Maamor N, Jamaludin M, Che Azemin M. The potential applications of mushrooms against some facets of atherosclerosis: a review. *Food Res Int.* (2018) 105:517–36. doi: 10.1016/j.foodres.2017.11.023
46. Wang D, Sun SQ, Wu WZ, Yang SL, Tan JM. Characterization of a water-soluble polysaccharide from *Boletus edulis* and its antitumor and immunomodulatory activities on renal cancer in mice. *Carbohydr Polym.* (2014) 105:127–34. doi: 10.1016/j.carbpol.2013.12.085
47. Wang L, Xu N, Zhang J, Zhao H, Lin L, Jia S, et al. Antihyperlipidemic and hepatoprotective activities of residue polysaccharide from *Cordyceps militaris* SU-12. *Carbohydr Polym.* (2015) 131:355–62. doi: 10.1016/j.carbpol.2015.06.016
48. Yang J, Dong H, Wang Y, Jiang Y, Zhang W, Lu Y, et al. *Cordyceps cicadae* polysaccharides ameliorated renal interstitial fibrosis in diabetic nephropathy rats by repressing inflammation and modulating gut microbiota dysbiosis. *Int J Biol Macromol.* (2020) 163:442–56. doi: 10.1016/j.ijbiomac.2020.06.153
49. Zaid, RM, Mishra P, Wahid ZA, Sakinah AMM. *Hylocereus polyrhizus* peel's high-methoxyl pectin: a potential source of hypolipidemic agent. *Int J Biol Macromol.* (2019) 134:361–7. doi: 10.1016/j.ijbiomac.2019.03.143
50. Yuan Y, Xu X, Jing C, Zou P, Zhang C, Li Y. Microwave assisted hydrothermal extraction of polysaccharides from *Ulva prolifera*: functional properties and bioactivities. *Carbohydr Polym.* (2018) 181:902–10. doi: 10.1016/j.carbpol.2017.11.061
51. Long H, Gu X, Zhou N, Zhu Z, Wang C, Liu X, et al. Physicochemical characterization and bile acid-binding capacity of water-extract polysaccharides fractionated by stepwise ethanol precipitation from *Caulerpa lentillifera*. *Int J Biol Macromol.* (2020) 150:654–61. doi: 10.1016/j.ijbiomac.2020.02.121
52. Ge YZ, Qiu HM, Zheng JX. Physicochemical characteristics and anti-hyperlipidemic effect of polysaccharide from BaChu mushroom (*Helvella leucopus*). *Food Chem.* (2022) 15:100443. doi: 10.1016/j.fochx.2022.10.0443



## OPEN ACCESS

## EDITED BY

Wenyi Kang,  
Henan University, China

## REVIEWED BY

Wenhao Li,  
Northwest A&F University, China  
Jiao Liu,  
South-Central University for  
Nationalities, China

## \*CORRESPONDENCE

Wen-jie Yan  
✉ meyanwenjie@126.com  
Jing Wang  
✉ wangjing07@caas.cn

## SPECIALTY SECTION

This article was submitted to  
Food Chemistry,  
a section of the journal  
Frontiers in Nutrition

RECEIVED 06 December 2022

ACCEPTED 09 January 2023

PUBLISHED 06 February 2023

## CITATION

Feng D, Zhou S-q, Zhou Y-x, Jiang Y-j, Sun Q-d,  
Song W, Cui Q-q, Yan W-j and Wang J (2023)  
Effect of total glycosides of *Cistanche*  
*deserticola* on the energy metabolism of  
human HepG2 cells. *Front. Nutr.* 10:1117364.  
doi: 10.3389/fnut.2023.1117364

## COPYRIGHT

© 2023 Feng, Zhou, Zhou, Jiang, Sun, Song,  
Cui, Yan and Wang. This is an open-access  
article distributed under the terms of the  
Creative Commons Attribution License (CC BY).  
The use, distribution or reproduction in other  
forums is permitted, provided the original  
author(s) and the copyright owner(s) are  
credited and that the original publication in this  
journal is cited, in accordance with accepted  
academic practice. No use, distribution or  
reproduction is permitted which does not  
comply with these terms.

# Effect of total glycosides of *Cistanche deserticola* on the energy metabolism of human HepG2 cells

Duo Feng<sup>1,2,3</sup>, Shi-qi Zhou<sup>1,2</sup>, Ya-xi Zhou<sup>1,2</sup>, Yong-jun Jiang<sup>4</sup>,  
Qiao-di Sun<sup>1,2</sup>, Wei Song<sup>1,2</sup>, Qian-qian Cui<sup>1,2</sup>, Wen-jie Yan<sup>1,2\*</sup> and  
Jing Wang<sup>3\*</sup>

<sup>1</sup>College of Biochemical Engineering, Beijing Union University, Beijing, China, <sup>2</sup>Beijing Key Laboratory of Bioactive Substances and Functional Food, College of Biochemical Engineering, Beijing Union University, Beijing, China, <sup>3</sup>Institute of Food and Nutrition Development, Ministry of Agriculture and Rural Affairs, Beijing, China, <sup>4</sup>Inner Mongolia Sankou Biotechnology Co., Ltd., Ordos City, Inner Mongolia, China

To study the anti-tumor effect of *Cistanche deserticola* Y. Ma, HepG2 cells were treated with 0, 3.5, 10.5, 21, 31.5, and 42  $\mu\text{g/ml}$  of total glycosides (TG) from *Cistanche deserticola*. The HepG2 cell survival rate and 50% inhibition concentration ( $\text{IC}_{50}$ ) were detected using the CCK-8 method, and the level of reactive oxygen species (ROS) was detected by using a DCFH-DA fluorescence probe. Finally, a Seahorse XFe24 energy analyzer (Agilent, United States) was used to detect cell mitochondrial pressure and glycolytic pressure. The results showed that TG could reduce the survival rate of HepG2 cells and that the  $\text{IC}_{50}$  level was 35.28  $\mu\text{g/ml}$ . With increasing TG concentration, the level of ROS showed a concentration-dependent upward trend. Energy metabolism showed that each dose group of TG could significantly decline the mitochondrial respiratory and glycolytic functions of HepG2 cells. In conclusion, TG could significantly inhibit the mitochondrial respiration and glycolysis functions of HepG2 cells, increase the level of ROS, and inhibit cell proliferation. Thus, this experiment pointed out that *Cistanche deserticola* can be used as a source of anti-cancer foods or drugs in the future. However, further studies on its mechanisms and clinical applications are needed.

## KEYWORDS

*Cistanche deserticola*, total glycosides, HepG2 cells, mitochondrial respiration, glycolytic pressure

## 1. Introduction

*Cistanche deserticola* Y. Ma is a homologous medicine and food substance. It is a perennial parasitic plant of the family Orobanchaceae and is called “desert ginseng” (1). Most importantly, nutrients such as fat and protein provided by *Cistanche* can meet the basic energy metabolism needs of normal human tissues and reduce the energy supply of tumor cells and thus achieve the purpose of inhibiting tumor cell growth. Moreover, *Cistanche* has the functions of antioxidation, suppression of inflammatory response, and enhancement of immunity (1, 2). Since the National Health Commission of the People's Republic of China and the State Administration for Market Regulation officially announced the production and operation of *Cistanche deserticola*. Y. Ma as a homologous substance of medicine and food was piloted in 2021, and there has been more in-depth research on its development.



Liver cancer is a common malignant tumor of the digestive system, and its mortality ranks at the forefront of malignant tumors (3, 4), which can be divided into primary and secondary. Nowadays, there is still a lack of safe and effective therapeutic drugs in the clinic. If sorafenib and other therapeutic drugs are taken for a long time, they will be prone to drug resistance and adverse reactions (5). Because the symptoms of early liver cancer are non-specific and most of the symptoms are in the middle and late stages, people are more active in the treatment of liver cancer with traditional Chinese medicine. Among patients with tumors and patients with unsatisfactory curative effects, such as chemoradiotherapy, traditional Chinese medicine reflects its advantages, such as, it can enhance immunity and be an adjuvant in early and medium-term tumor treatment.

In recent years, it has been reported that *Cistanche* has anticancer effects (6–11). Ye et al. (6) found that echinacoside extracted from *Cistanches herba* (*Cistanche salsa*) could inhibit the proliferation of HepG2 cells by reducing the expression of TREM2 and blocking the PI3K/Akt signal pathway. Li et al. (7) also found that echinacoside exerted an antitumor activity via the miR-503-3p/TGF- $\beta$ 1/Smad axis against liver cancer. Meanwhile, *Verbascoside* could regulate oxidative stress and apoptosis of HepG2 cells through STAT-3 and has the potential to be developed as a chemopreventive agent (8–10). Besides, researchers found that phenylethanol glycoside could also inhibit the proliferation effect of HepG2 cells (11). In addition, echinacoside inhibited the proliferation of renal cancer 786-O cells and SW480 colon cancer cells (12, 13). In another study, phenylethanol glycosides from *Cistanche* have also been shown to reduce liver injury in H22 tumor-bearing mice (14, 15) and to improve immune function by reducing AFP levels, thereby adversely affecting tumor growth (16). It is worth noting that altered energy metabolism is one of the characteristics of tumor cells, which is manifested as the fact that tumor cells use glucose glycolysis as a way of energy supply regardless of the aerobic or anaerobic environment, and this phenomenon is known as the “Warburg effect.” Therefore, it is theoretically possible to selectively starve tumor cells to limit tumor cell growth by limiting glucose uptake (17).

Although many studies have studied the anti-tumor effect of phenylethanol glycosides, such as *Echinacoside* and *Verbascoside*, the anti-tumor activity of TG (phenylethanoid glycosides, and other glycosides) (18) is not common. There are only a few studies on whether TG affects the energy metabolism of tumor cells. Thus, this experiment analyzed the relationship between energy metabolism, oxidative damage, and cell survival through glycolytic ability and mitochondrial pressure so as to explore the inhibitory activity of TG on HepG2 cells.

## 2. Materials and methods

### 2.1. Cell culture and treatment

HepG2 cells were purchased from the Cell Center of the Institute of Basic Medicine, Peking Union Medical University (Beijing, China), and DMEM complete medium containing 10% fetal bovine serum and 1% antibiotic (penicillin, streptomycin, and gentamicin) was used. The cells were cultured in a 37°C and 5% CO<sub>2</sub> saturated humidity incubator (19). After the cells grew to a confluence of

80–90%, they were digested with 0.25% trypsin without EDTA and subcultured in 1:3. After 2–3 days of cell growth, the cells in the logarithmic growth stage were taken for a subculture or for subsequent experiments. In each experiment, HepG2 cells were exposed to different concentrations of TG.

Total glycosides of *Cistanche deserticola* were provided by Inner Mongolia Sankou Technology Co., Ltd (Ordos, Inner Mongolia, China) (20). TG was dissolved in a DMEM culture medium until the final concentrations were 0, 3.5, 10.5, 21, 31.5, and 42  $\mu$ g/ml.

### 2.2. Effect of TG on HepG2 cell morphology

HepG2 cells in the logarithmic growth phase were inoculated into 24-well plates at a concentration of  $5 \times 10^4$ /well. After the cells adhered to the wall, TG was added until the final concentrations were 0, 21, and 42  $\mu$ g/ml and cultured for 24 h. Then, the cell morphology of each group was observed under the fluorescence microscope.

### 2.3. Effect of TG on the proliferation of HepG2 cells

The logarithm of the cell growth phase of HepG2 cells was taken as  $1 \times 10^4$ /well, inoculated in 96-well plates, and each well was inoculated with 100  $\mu$ l. After the cells adhered to the wall, they were dissolved in a serum-free DMEM medium such that the final drug concentrations were 0, 3.5, 10.5, 21, 31.5, and 42  $\mu$ g/ml. Each concentration was allotted six multiple wells and then incubated at 37°C under 5% CO<sub>2</sub> in an incubator for 24 h. Finally, to each well, 100  $\mu$ l of DMEM culture medium containing 10% CCK8 solution was added, and then, the wells were incubated in an incubator for 30 min to detect the absorbance value (A) at 450 nm.

### 2.4. Measurement of intracellular ROS levels

The system of 2 ml per well containing  $4 \times 10^5$  cells was laid in a 6-well plate and placed in an incubator at 37°C under 5% CO<sub>2</sub>. After 24 h of treatment, the intracellular ROS level was measured. Then, 1 ml of DCFH-DA (10  $\mu$ M) was added and incubated in the dark at 37°C for 30 min. Then, we washed them with PBS three times, and finally, the ROS activity was detected by flow cytometry.

### 2.5. Effect of TG on the energy metabolism of HepG2 cells

(A) Optimization of test conditions: HepG2 cells in the logarithmic growth period were selected and inoculated on the cell culture plate of a Seahorse XFe 24 bioenergy analyzer at 500  $\mu$ l per well such that the number of cells was 1, 2, 4, and 8 ( $\times 10^4$ ). Five replicates of each group were made, of which only A1, B3, C4, and D6 were added with culture medium. (B) Mitochondrial pressure detection: a mitochondrial pressure kit was

taken out in advance, which included oligomycin, carbonyl cyanide-trifluoromethoxy phenylhydrazone (FCCP), and rotenone/antimycin A (Rot/AA). They were diluted with the detection medium to make their concentrations 1  $\mu$ M, 0.5  $\mu$ M, and 0.5  $\mu$ M, separately. Then, the hydrated probe plate was removed and added to ports A, B, and C, respectively, with a volume of 56  $\mu$ l, 62  $\mu$ l, and 69  $\mu$ l. The oxygen consumption rate (OCR) values at different time intervals were measured to reflect the level of oxidative phosphorylation. (C) Glycolysis pressure detection: Glucose, oligomycin, and 2-deoxyglucose (2-DG) were diluted with the detection medium to make the concentrations 10 mM, 1  $\mu$ M, and 50 mM, respectively. Then, the hydrated probe plate was removed and added to ports A, B, and C, respectively, with the aforementioned volumes. The extracellular acidification rate (ECAR) values at different time intervals were measured to reflect the glycolytic function of the cells (21).

## 2.6. Western blot

The treated cells were plated with 80  $\mu$ l of lysis buffer (RIPA:PMSF = 100:1) that was used to lyse proteins, and then, sodium dodecyl sulfate-polyacrylamide gel electrophoresis (SDS-PAGE) was performed to separate the protein samples (50  $\mu$ g loading volume per well). Later, the protein transfer to the PVDF membrane was accomplished using an ice bath, the proteins were blocked by BSA for 1 h at room temperature, and the primary antibodies (Bcl-2, Bax, caspase-3) were added proportionally and incubated overnight at 4°C. Afterward, the PVDF membranes were then incubated with diluted secondary antibodies for 1–2 h at room temperature.  $\beta$ -Actin was used as an internal reference protein, and PVDF membranes were developed and fixed to observe target protein expression changes (22, 23).

## 2.7. Statistical processing

The test data were expressed as  $\bar{x} \pm SD$  (standard deviation) and analyzed by one-way analysis of variance (ANOVA) using SPSS 25.0 (SPSS, United States). Flowjo10 and Graphpad prism 8.0.2 were the software used to draw the figures. \* $P < 0.05$  and \*\* $P < 0.01$ .

# 3. Results

## 3.1. Effect of TG on HepG2 cell morphology

In the process of apoptosis, first, the cell volume will slowly decrease and deform and then cells growing closer to the wall will slowly shrink, become round, fall off, and result in chromosome pyknosis. Some nuclei will break, marginalize, and form apoptotic vesicles. It was observed from Figure 1 that, when HepG2 cells were treated with TG, the cell volume gradually decreased. It was intuitively observed that the nuclei of cells treated with 21  $\mu$ g/ml of TG began to shrink and the volume became smaller. With 42  $\mu$ g/ml TG, the cells were accompanied by floating and cell fragmentation; the cell membrane was completely broken, cracked, necrotic, with unclear boundary, and in a state of imminent collapse and death.

## 3.2. Effect of TG on the proliferation of HepG2 cells

To confirm the antitumor effect of TG *in vitro*, HepG2 cells were treated with a series of concentrations of TG (0, 3.5, 10.5, 21, 31.5, and 42  $\mu$ g/ml) for 24 h. Then, the CCK8 assay method was used to explore the effect of TG on the proliferation of HepG2 cells.

Figure 2 shows that the proliferation of HepG2 was affected to varying degrees after treatment with different concentrations of TG for 24 h. Compared with the cell survival rate of the control group, the cell survival rates of the treatment group were 96.95%, 92.59%, 92.78%, 77.28%, and 31.04%, respectively. With the increase in concentration, the cell survival rate showed a downward trend, but there was no significant difference ( $P > 0.05$ ) in the concentrations of 3.5, 10.5, and 21  $\mu$ g/ml, and the inhibition range was small. There were significant differences between the concentrations 31.5 and 42  $\mu$ g/ml ( $P < 0.01$ ), and the inhibition rate was as high as 68.96% at 42  $\mu$ g/ml. Therefore, this experiment showed that TG could significantly inhibit the survival of HepG2 cells in a concentration-dependent manner, and further experiments may be needed to confirm the cytotoxicity of TG.

## 3.3. Measurement of intracellular ROS levels

As shown in Figure 3, with the increase in TG concentration, higher relative contents of ROS were detected by the DCFH-DA fluorescence probe method, showing a dose gradient trend. After TG treatment for 24 h, the relative fluorescence intensity of DCF increased by 0.91%, 13.64%, 24.61%, 45.91%, and 105.33%, and there were highly significant differences at 10.5, 21, 31.5, and 42  $\mu$ g/ml ( $P < 0.01$ ). When TG concentration was 42  $\mu$ g/ml, the maximum ROS accumulation level was observed to be about two times higher than that in the control group. Therefore, we speculated that the stable and high ROS production capacity may be the reason for the better cytotoxicity of TG. These results may also indicate a close relationship between ROS production ability and cell cytotoxicity.

## 3.4. Effect of TG on mitochondrial aerobic respiration of Hep2 cells

### 3.4.1. Determination of cell number

In the detection of mitochondrial pressure and glycolytic pressure, it was first necessary to determine the optimal cell seeding density (21). In this experiment, it is recommended that the basic oxygen consumption rate (OCR) value and the extracellular acidification rate (ECAR) be used to characterize the cell density. First, visual evaluation was used to approximate the optimal cell density: cells should be evenly distributed in each well with a fusion degree of 50–90%. On the one hand, when using a 24-well bioenergy analyzer to determine the cell OCR or ECAR values, the cell inoculation density should be  $1 \times 10^4$ – $8 \times 10^4$  cells/well. On the other hand, the basic OCR and ECAR values can be used to determine the best sowing density and ensure the accuracy of the data. According to the product description of a Seahorse XFe24 analyzer, the cell OCR in the normal growth state should be in the

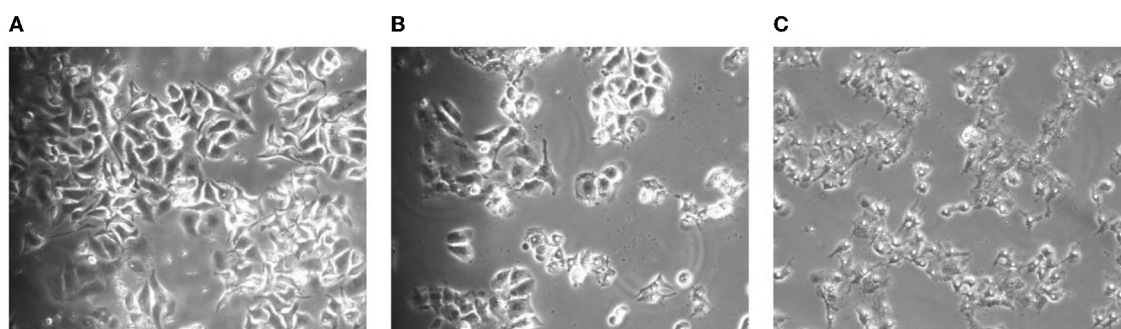


FIGURE 1

Morphological changes of the cells after TG treatment for 24 h. (A) Cell morphology after treatment with 0  $\mu\text{g/ml}$  TG. (B) Cell morphology after treatment with 21  $\mu\text{g/ml}$  TG. (C) Cell morphology after treatment with 42  $\mu\text{g/ml}$  TG.

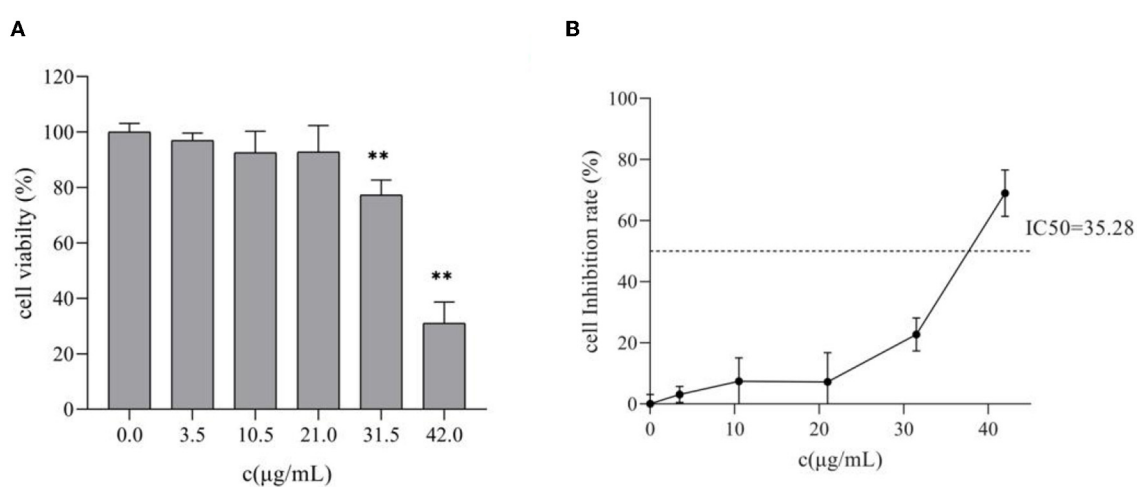


FIGURE 2

Effects of different concentrations of TG on the proliferation of HepG2 cells. (A) The survival rate of HepG2 cells. (B) The inhibition rate of HepG2 cells; IC<sub>50</sub> represents the 50% inhibition of cell viability. \*\* $P < 0.01$ .

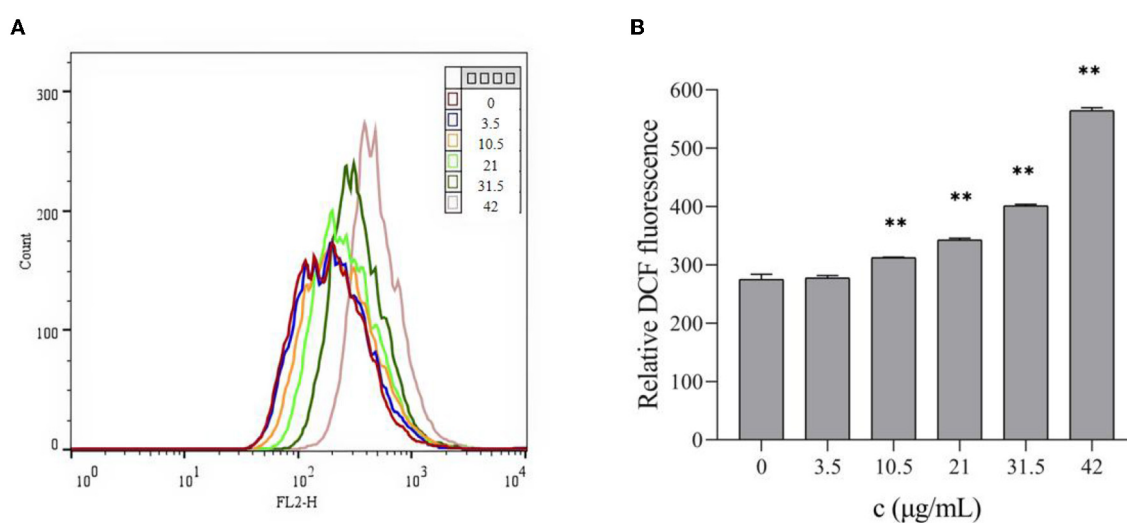


FIGURE 3

Effects of different concentrations of TG on the ROS levels of HepG2 cells. (A) The level of ROS was detected by flow cytometry. (B) Different concentrations of TG induced relative ROS production in HepG2 cells. \*\* $P < 0.01$ .

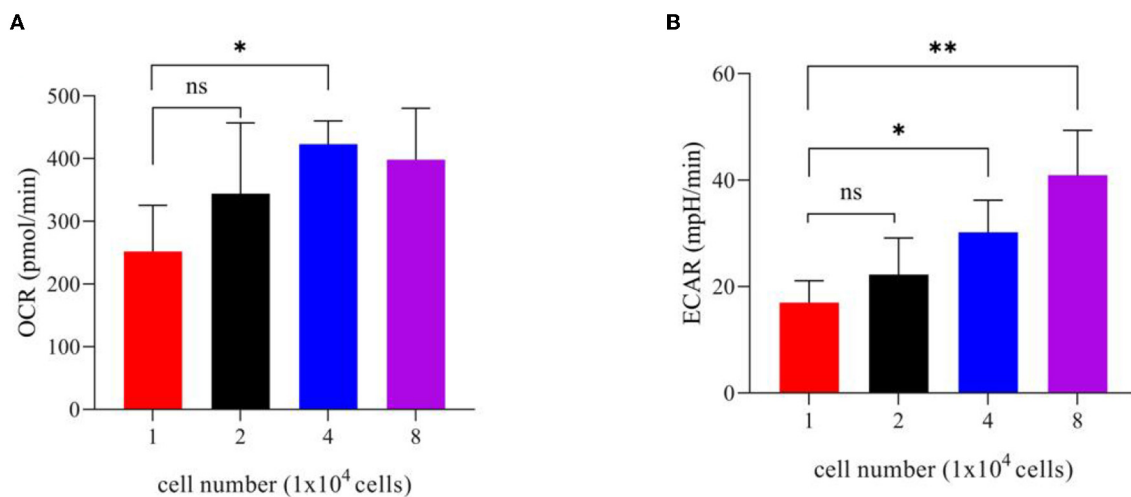


FIGURE 4  
Bar chart of different cell numbers. (A) OCR values of different cell numbers. (B) ECAR values of different cell numbers. \* $P < 0.05$  and \*\* $P < 0.01$ .

range of 50–400 pmol/min and the normal basic ECAR range should be in the range of 20–120 mpH/min. Therefore, combining the two aspects, maintaining the cells at  $8 \times 10^4$ /well will be more suitable (Figure 4) (21).

### 3.4.2. Effect of TG on oxidative phosphorylation of HepG2 cells

The evaluation of mitochondrial function is essential for understanding the diseases related to cell energy metabolism and the development of corresponding drugs, and OCR is one of the most important evaluation indexes. To study the effect of TG on the oxidative phosphorylation process of HepG2 cells, we used a Seahorse XFe24 analyzer to detect the OCR levels of the cells treated with TG and analyzed the relevant indices. With an increase in TG concentration, the OCR level gradually decreased (Figures 5A, B), and especially, after the addition of FCCP, the difference in the OCR values between the dosing group and the control group became larger. At the same time, Figures 5C–F and Table 1 show that basal respiration decreased gradually; compared with  $0 \mu\text{g/ml}$ , it decreased by 39.24%, 41.43%, 47.10%, 78.22%, and 95.26%, respectively, for each dosing group. The maximum respiration rate decreased by 52.95%, 65.06%, 77.76%, 94.48%, and 98.61%, respectively; Non-mitochondrial oxygen consumption decreased by 37.34%, 37.45%, 47.27%, 76.10%, and 79.79%, respectively. ATP production decreased by 42.49%, 47.91%, 57.83%, 87.28%, and 98.16%, respectively. The reasons for the decrease may be that the cells treated with TG were in the state of apoptosis and the level of ROS increased, which may increase the oxidative damage of the cells, reduce the activity of the mitochondrial respiratory chain complex, and affect the ability of mitochondrial ATP synthesis. The results showed that TG could significantly inhibit the overall level of aerobic respiration of cell mitochondria, and the cell survival rate after TG treatment was significantly reduced, which may be directly related to the disorder of mitochondrial energy metabolism. However, there is a need for more in-depth studies of the mechanisms.

### 3.4.3. Effect of TG on the glycolytic ability of HepG2 cells

The glycolysis process is carried out in the cell matrix, and the produced lactic acid releases  $\text{H}^+$  to the outside of the cell. Moreover, a Seahorse XFe24 analyzer was used to analyze the glycolytic function by detecting the ECAR values after TG treatment and the relevant assay parameters to determine the specific method by which TG affects the glycolytic process of HepG2 cells. Over time, with the addition of glucose and oligomycin, the ECAR value increased gradually and showed a downward trend upon adding 2-DG (Figure 6A). With the increase in TG concentration, the overall ECAR level gradually decreased (Figure 6B), which was reflected by the gradual decline in glycolytic capacity and glycolytic reserve value (Figures 6D, E; Table 2). The non-glycosylation level was mostly lower than that of the control group but there was no concentration dependence (Figure 6C). Compared with the control group, the glycolytic capacity of the TG treatment group decreased by 1.12%, 9.29%, 34.46%, 92.15%, and 100.00%, respectively; the glycolytic reserve value decreased by 4.78%, 34.17%, 79.50%, 93.39%, and 98.63%, respectively. The results showed that TG could inhibit the proliferation and growth of HepG2 cells by reducing the glycolytic function of HepG2 and producing cytotoxicity. Of note, the damage degree of glycolytic function at low dose was lower than the decline degree of various parameters of cell oxidative phosphorylation, while glycolytic function and cell oxidative phosphorylation both were significantly reduced at high dose. Therefore, it was suggested that TG mainly damaged mitochondrial function at low dose, while at high dose both damaged mitochondrial function and glycolytic function at the same time, so as to accelerate the degree of apoptosis and necrosis of tumor cells and inhibit cell proliferation.

### 3.5. Expression of HepG2 cell proteins after TG treatment

Figure 7 shows that, after treatment with different concentrations of TG for 24 h, the protein expression levels of HepG2 cells



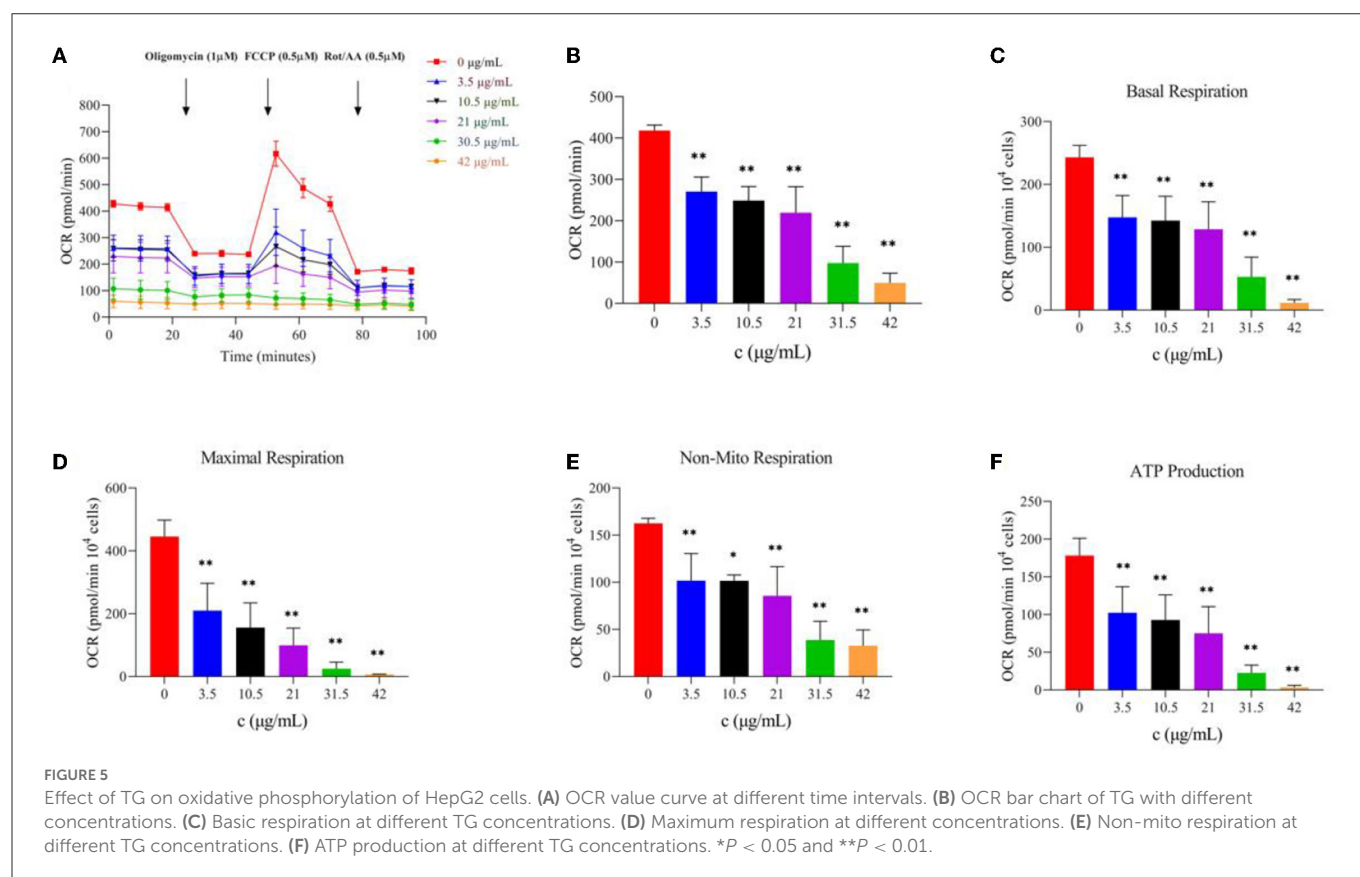


TABLE 1 Parameters of mitochondrial oxidative phosphorylation.

OCR (pmol/min)	Basal respiration	Maximal respiration	Non-mito respiration	ATP production
0 $\mu\text{g/ml}$	243.04 $\pm$ 19.08	445.41 $\pm$ 52.32	162.36 $\pm$ 5.55	178.15 $\pm$ 22.99
3.5 $\mu\text{g/ml}$	147.66 $\pm$ 34.76**	209.55 $\pm$ 87.16**	101.73 $\pm$ 28.63**	102.46 $\pm$ 34.59**
10.5 $\mu\text{g/ml}$	142.36 $\pm$ 38.85**	155.64 $\pm$ 78.37**	101.55 $\pm$ 6.20*	92.8 $\pm$ 33.29**
21 $\mu\text{g/ml}$	128.58 $\pm$ 43.77**	99.07 $\pm$ 54.95**	85.61 $\pm$ 31.01**	75.13 $\pm$ 35.34**
31.5 $\mu\text{g/ml}$	52.94 $\pm$ 31.55**	24.59 $\pm$ 21.24**	38.8 $\pm$ 19.71**	22.66 $\pm$ 10.39**
42 $\mu\text{g/ml}$	11.52 $\pm$ 5.24**	6.18 $\pm$ 1.72**	32.81 $\pm$ 16.56**	3.27 $\pm$ 2.83**

\*There is a significant difference ( $P < 0.05$ ) between the treatment group and the 0  $\mu\text{g/ml}$  group.

\*\* $P < 0.01$ .

change concomitantly. As the concentration of TG increased, the expression levels of the proapoptotic factors Bax and Caspase-3 increased, and the relative protein expression was the highest when the concentrations were 31.5  $\mu\text{g/ml}$  and 10.5  $\mu\text{g/ml}$ , respectively. In addition, when the concentration was low (0, 3.5, 10.5, and 21  $\mu\text{g/ml}$  TG), the relative expression of the anti-apoptotic factor Bcl-2 increased. When the TG concentration was 31.5  $\mu\text{g/ml}$  and 42  $\mu\text{g/ml}$ , it showed a significant downward trend. Therefore, we inferred that TG may promote the apoptosis of HepG2 cells.

## 4. Discussion and conclusion

Studies proved that *Cistanche deserticola* and its effective components have antioxidant, anti-fatigue, antiaging, antitumor,

memory-improving properties and promote bone formation (11, 12). At present, the treatment for liver cancer still lacks effective means. It is often based on comprehensive treatment such as surgery, radiotherapy, and chemotherapy. Chemotherapy has large toxic and side effects and is easy to develop drug resistance. Traditional Chinese medicine has less effective antitumor toxicity and side effects. At the same time, it can enhance organic immunity and prevent cancer (24).

Cancer meets the biosynthesis and redox needs of tumor cells by changing the metabolism, tumor cell reprogramming, nutrient acquisition, and metabolic pathways, making it possible for tumor cells to proliferate without restriction (25). Therefore, restricting the proliferation of tumor cells through the above ways was the focus of our subsequent experiments. A certain concentration of TG was found to significantly inhibit the growth and proliferation



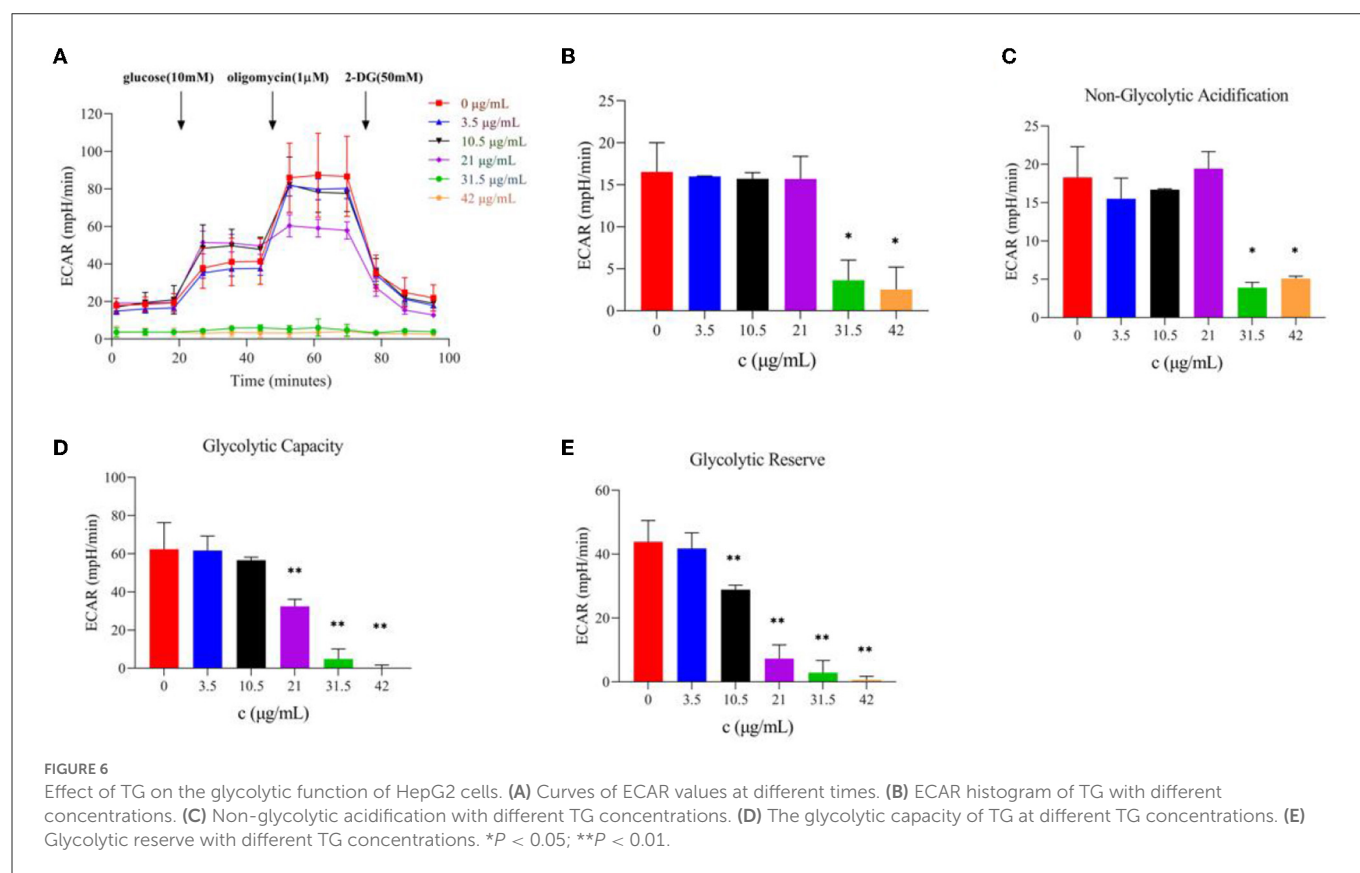


TABLE 2 Parameters of glycolytic stress.

ECAR (mpH/min)	Non-glycolytic acidification	Glycolytic capacity	Glycolytic reserve
0 µg/ml	18.3 ± 4.0	62.4 ± 13.9	43.9 ± 6.6
3.5 µg/ml	15.5 ± 2.7	61.7 ± 7.6	41.8 ± 4.9
10.5 µg/ml	16.7 ± 0.1	56.6 ± 1.6	28.9 ± 1.4**
21 µg/ml	19.4 ± 2.2	40.0 ± 3.7**	9.0 ± 1.7**
31.5 µg/ml	3.9 ± 0.7*	4.9 ± 5.2**	2.9 ± 3.8**
42 µg/ml	5.1 ± 0.3*	0.0 ± 1.7**	0.6 ± 1.1**

\*There is a significant difference ( $P < 0.05$ ) between the treatment group and the 0 µg/ml group.

\*\* $P < 0.01$ .

of HepG2 cells in a dose-dependent manner with the increase in concentration.

Under normal circumstances, a slight increase in ROS level can promote the proliferation of normal cells. However, a significant ROS level increase in cancer cells can trigger cell death (26). High doses of ROS could cause cell growth inhibition, injury, apoptosis, and even death, which was consistent with the inhibitory effect of TG on the proliferation of HepG2 cells. There is also evidence that ROS production usually inhibits the proliferation of cancer cells (27). The survival or death of cells largely depends on the functional state of mitochondria (28). ROS is an inevitable product in the process of cell metabolism as it acts on mitochondria and is one of the main ways to cause mitochondrial damage. The main function of mitochondria in cells is to provide energy for cell metabolism and biosynthesis by producing ATP, which is very

important for the survival of normal cells and tumor cells (29). If the ROS level increases in the body and is not decomposed by cells, ROS will affect the activity of the mitochondrial respiratory chain complex (30) and, thus, affect the oxidative phosphorylation of mitochondria and reduce ATP synthesis in cells (31), resulting in the imbalance of the intracellular redox system and inhibition of the proliferation of tumor cells (32). Indeed, chemopreventive agents could enhance the level of ROS to reach the toxicity threshold and promote cancer cell apoptosis with the least toxicity to normal cells (33). The results also confirmed that the increase in the relative content of ROS could significantly reduce the survival rate of HepG2 cells.

To adapt to changing external environments, an organism must adjust the biological activities of cells at any time. Correspondingly, the regulation of cell biological activities by the organism is

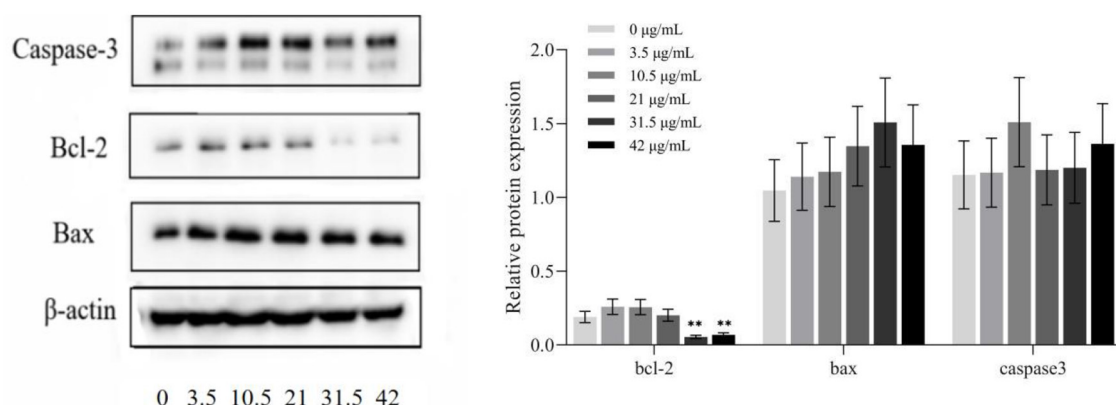


FIGURE 7  
Protein expression in HepG2 cells treated with different concentrations of TG. \* $P < 0.05$ ; \*\* $P < 0.01$ .

based on its regulation of cellular metabolic networks. Therefore, the energy state of cells is always regulated and maintained in a certain range of dynamic balance under normal physiological conditions, which is the steady state of cell energy metabolism (34). In addition, the mitochondria are considered one of the main targets of drug-induced hepatocyte injury (35). At the same time, researchers believe that the energy needs of cells can be met through glycolysis and oxidative phosphorylation (OXPHOS). When OXPHOS is no longer available, for example, due to hypoxic effects or mitochondrial damage, these cell lines can switch to glycolysis to produce sufficient ATP for continued survival (36).

Otto Warburg (37, 38) observed that, in the presence of oxygen, tumor cells exhibited unusual characteristics of absorbing glucose and fermenting it into lactic acid. This characteristic, aerobic glycolysis indicates that, with sufficient oxygen, tumor cells preferred to use glycolysis for glucose metabolism instead of mitochondrial oxidative phosphorylation to produce more ATP. This will help tumor cells to quickly produce enough energy for their rapid growth, release more lactic acid, maintain their acidic microenvironment, escape immune surveillance, and easily metastasize (39, 40). Therefore, Warburg proposed that mitochondrial respiratory defects are a potential basis for aerobic glycolysis and cancer (37, 38). In this study, all concentrations of TG significantly inhibited the overall level of aerobic respiration of mitochondria and limited the glycolytic function, which may be directly related to the disorder of mitochondrial energy metabolism. However, there is a need for more in-depth studies of the mechanisms.

Bax is the main regulator of Bcl-2 activity and its expression levels are directly related to apoptosis regulation, with increased Bax expression indicating the promotion of apoptosis by drugs and increased Bcl-2 indicating the inhibition of apoptosis (41). In addition, caspase protease highly influences apoptosis and its activation represents the progression of cells into the irreversible apoptosis phase (42). Thus, in HepG2 cells treated with TG, the extent of caspase-3 activation was clearly increased,

indicating that TG could cause irreversible apoptosis and prevent cell proliferation.

In conclusion, this study has significant reference to in-depth research on the anti-tumor mechanism of *Cistanche deserticola*. It has the potential to be a raw material of drugs for the clinical treatment of liver cancer and to effectively prevent tumors with consumption in daily diet.

## Data availability statement

The datasets presented in this study can be found in online repositories. The names of the repository/repositories and accession number(s) can be found in the article/Supplementary material.

## Author contributions

DF: investigation, writing original draft, and plot analyses. S-qZ and Y-xZ: formal analysis and visualization. Y-jJ: investigation. Q-dS, WS, and Q-qC: resources and material support. W-jY: writing review and editing, project supervision, and funding acquisition. JW: writing review and editing and validation. All authors approved the final version of the manuscript.

## Funding

This work was supported by the National Natural Science Foundation of China (32172244) and the Academic Research Projects of Beijing Union University (JB202101).

## Conflict of interest

Y-jJ was employed by Inner Mongolia Sankou Biotechnology Co., Ltd.

The remaining authors declare that the research was conducted in the absence of any commercial or financial relationships that could be construed as a potential conflict of interest.

## Publisher's note

All claims expressed in this article are solely those of the authors and do not necessarily represent those of their affiliated organizations, or those of the publisher, the editors and the reviewers.

## References

- Feng D, He Y, Jiang Y-J, Wang Y-J, Yan W-J. Research progress on anti-aging function of *Cistanche*. *J Food Saf Qual.* (2021) 12:4429–37. doi: 10.19812/j.cnki.jfsq11-5956/ts.2021.11.018
- Feng D, Duan H, Lv Y-N, Jiang Y-J, Wang Y-J, Yan W-J. Application of *Cistanche deserticola* Ma in functional food in China. *Food Sci Technol.* (2021) 46:76–81. doi: 10.13684/j.cnki.spkj.2021.12.012
- Ma G-Z, Chen J-R, Wei T-T, Wang J, Chen W-S. Inhibiting roles of FOXA2 in liver cancer cell migration and invasion by transcriptionally suppressing microRNA103a-3p and activating the GREM2/LATS2/YAP axis. *Cytotechnology.* (2021) 73:523–37. doi: 10.1007/s10616-021-00475-2
- Zheng R-S, Zhang S-W, Zeng H-M, Wang S-M, Sun K-X, Chen R, et al. Cancer incidence and mortality in China, 2016. *J Natl Cancer Center.* (2022) 2:1–9. doi: 10.1016/j.jncc.2022.02.002
- Sun Y, Song Y-Y, Zhang C, Lu Y-Z, Zheng G-H, Tian X-X, et al. Effects and mechanism of celastrol on the proliferation of hepatocellular carcinoma HepG2 cells by activating AMPK signal pathway. *China Pharmacist.* (2021). 24:1961–6. doi: 10.19962/j.cnki.issn1008-049X.2021.11.001
- Ye Y, Song Y, Zhuang J, Wang G, Ni J, Xia W. Anticancer effects of echinacoside in hepatocellular carcinoma mouse model and HepG2 cells. *J Cell Physiol.* (2019) 234:1880–8. doi: 10.1002/jcp.27063
- Li W, Zhou J, Zhang Y, Zhang J, Li X, Yan Q, et al. Echinacoside exerts anti-tumor activity via the miR-503-3p/TGF- $\beta$ 1/Smad axis in liver cancer. *Cancer Cell Int.* (2021) 21:304. doi: 10.1186/s12935-021-01890-3
- Zhang Y, Zhu B-L, Yang X-J, Hui J, Ma Q, Yu X-H. Research progress on inhibition of malignant tumors of verbascode. *Res Pract Chin Med.* (2019) 33:78–82. doi: 10.13728/j.1673-6427.2019.06.018
- Alipieva K, Korkina L, Orhan I-E, Georgiev MI. Verbascode—a review of its occurrence, (bio)synthesis and pharmacological significance. *Biotechnol Adv.* (2014) 32:1065–76. doi: 10.1016/j.biotechadv.2014.07.001
- Peerzada K-J, Faridi A-H, Sharma L, Bhardwaj S-C, Satti N-K, Shashi B, et al. Acteoside mediates chemoprevention of experimental liver carcinogenesis through STAT-3 regulated oxidative stress and apoptosis. *Environ Toxicol.* (2016) 31:782–98. doi: 10.1002/tox.22089
- Qi X-X, You S-P, He Z-X, Zhao J, Liu T. Effect of *Cistanche deserticola* phenylethanolic glycoside on proliferation and apoptosis of HepG2 cells in vitro. *J Xinjiang Med Univ.* (2021) 44:1041–7.
- Xie Y-T. *Effects of Echinacoside on 786-O Cells Apoptosis and Inductive Mechanisms In Vitro*. New York: Baotou Teachers' College (2020).
- Han Y-M, Jin W-M, Zeng H, Wang C, Zhang H. Effects of echinacoside on proliferation, invasion and metastasis of colon cancer SW480 cells in vitro and in vivo. *J Guangzhou Univ Trad Chin Med.* (2020) 37:1542–9. doi: 10.13359/j.cnki.gzxbtcm.2020.08.024
- Hou X-T, Liu T, Su D-Q. Anti-tumor effect of phenylethanolic glycosides from *Cistanche deserticola* on H22 tumor-bearing mice. *J Toxicol.* (2021) 35:231–40. doi: 10.16421/j.cnki.1002-3127.2021.03.010
- Hou X-T, Su D-Q, Qi X-X, Liu T. Effect of phenylethanolic glycosides from *Cistanche deserticola* on autophagy of tumor cells in H22 tumor-bearing mice. *J Toxicol.* (2022) 36:137–41. doi: 10.1155/2022/3993445
- Hu Q, You S-P, Liu T, Wang B, Liu X, Jiang Y-D. An investigation on the anti-liver cancer effect of *Cistanche*. *Carcinog Teratog Mutag.* (2018) 30:194–9.
- Kamalian L, Douglas O, Jolly CE, Snoeys J, Simic D, Monshouwer M, et al. The utility of HepaRG cells for bioenergetic investigation and detection of drug-induced mitochondrial toxicity. *Toxicol In Vitro.* (2018) 53:136–47. doi: 10.1016/j.tiv.2018.08.001
- Wang F-J, Li R-Y, Tu P-F, Chen J-P, Zeng K-W, Jiang Y. Total glycosides of *Cistanche deserticola* promote neurological function recovery by inducing

Any product that may be evaluated in this article, or claim that may be made by its manufacturer, is not guaranteed or endorsed by the publisher.

## Supplementary material

The Supplementary Material for this article can be found online at: <https://www.frontiersin.org/articles/10.3389/fnut.2023.1117364/full#supplementary-material>

- neurovascular regeneration via Nrf-2/Keap-1 pathway in MCAO/R rats. (2020) 11:236. doi: 10.3389/fphar.2020.00236
- Wang J, Zhang X-X, Ni Z-J, Elam E, Thakur Kiran, Li K-X, et al. The anti-cancerous mechanism of Licochalcone A on human hepatoma cell HepG2 based on the miRNA omics. *Food Sci Hum Well.* (2023) 12:1136–48. doi: 10.1016/j.fshw.2022.10.039
- Feng D, Chang X, Jiang Y-J, Guo Y, Zhao J, Zhao J-Y, et al. Optimization of aqueous extraction preparation technology of *Cistanche deserticola* by response surface methodology and its activity research. *Sci Technol Food Ind.* (2023) 5:1–16. doi: 10.13386/j.issn1002-0306.2022050033
- Ji X-J, Wang J, Ma A-J, Feng D, He Y, Yan W-J. Effects of silkworm pupa protein on apoptosis and energy metabolism in human colon cancer DLD-1 cells. *Food Sci Hum Well.* (2022). 2022:1171–6. doi: 10.1016/j.fshw.2022.04.011
- Zhang Z-G, Wang M-L, Xing S, Zhang C. Flavonoids of *Rosa rugosa* Thunb inhibit tumor proliferation and metastasis in human hepatocellular carcinoma HepG2 cells *Food Sci Hum Well.* (2022) 11:374–82. doi: 10.1016/j.fshw.2021.11.016
- Liu X, Jiang N, Xu X, Liu C, Liu Z, Zhang Y, et al. Anti-hepatoma compound determination by the method of spectrum effect relationship, component knock-out, and UPLC-MS2 in *Schefflera heptaphylla* (L) frodin harms and its mechanism. *Front Pharmacol.* (2020) 11:1342. doi: 10.3389/fphar.2020.01342
- Liu X-Q, Wang S-Y, Cui L-L, Zhou H-H, Liu Y-H, Meng L-J, et al. Flowers: precious food and medicine resources. *Food Sci Hum Well.* (2023) 12:1020–52. doi: 10.1016/j.fshw.2022.10.022
- Yin X-Z, Liu Z-J, Guo Y. Evaluation of effects on tetrahydropalmatine on human hepatocellular carcinoma cells by cellular energy metabolism analysis. *Chin J Immunol.* (2021) 37:426–30.
- Liu GY, Sun YZ, Zhou N, Du XM, Yang J, Guo SJ. 3,3'-OH curcumin causes apoptosis in HepG2 cells through ROS-mediated pathway. *Eur J Med Chem.* (2016) 112:157–63. doi: 10.1016/j.ejmech.2016.02.019
- Pal LC, Prateeksha, Singh BN, Pande V, Rao CV. Phenolics-enriched fraction of *Pterospermum lanceifolium* Roxb. efficiently reverses the Hepatocellular carcinoma in NDEA-induced HCC rats. *Nutrition Cancer.* (2022) 74:1106–21. doi: 10.1080/01635581.2021.1922716
- Bras M, Queenan B, Susin SA. Programmed cell death via mitochondria: different modes of dying. *Biochemistry (Mosc).* (2005). 70:231–9. doi: 10.1007/s10541-005-0105-4
- Galber C, Acosta MJ, Minervini G, Giorgio V. The role of mitochondrial ATP synthase in cancer. *Biol Chem.* (2020) 401:1199–214. doi: 10.1515/hsz-2020-0157
- Piantadosi CA, Zhang J. Mitochondrial generation of reactive oxygen species after brain ischemia in the rat. *Stroke.* (1996) 27:327–31. doi: 10.1161/01.STR.27.2.327
- Avery SV. Molecular targets of oxidative stress. *Biochem J.* (2011) 434:201–10. doi: 10.1042/BJ20101695
- Cui Z, Li S, Wang H-J, Ma J, Qin T-T, Shi H, et al. Effect of dihydroartemisinin on oxidative damage and energy metabolism of HepG2 cells and its synergistic effect with Sorafenib. *Chin J Exp Trad Med Formul.* (2021) 27:24–32. doi: 10.13422/j.cnki.syfjx.20211202
- Hail N Jr, Cortes M, Drake EN, Spallholz JE. Cancer chemoprevention: a radical perspective. *Free Radic Biol Med.* (2008) 45:97–110. doi: 10.1016/j.freeradbiomed.2008.04.004
- Jiang B, Zhao W-T, Ouyang C, Wang H-H, Zhang F-Q, Zhao G-H, et al. Regulation network of cellular metabolism. *J Xiamen Univ (Nat Sci).* (2022) 61:346–64.
- Dragovic S, Vermeulen N-P, Gerets H-H, Hewitt P-G, Ingelman-Sundberg M, Park B-K, et al. Evidence-based selection of training compounds for use in the mechanism-based integrated prediction of drug-induced liver injury in man. *Arch Toxicol.* (2016) 90:2979–3003. doi: 10.1007/s00204-016-1845-1
- Diaz-Ruiz R, Rigoulet M, Devin A. The Warburg and Crabtree effects: on the origin of cancer cell energy metabolism and of yeast glucose repression. *Biochim Biophys Acta.* (2011) 1807:568–76. doi: 10.1016/j.bbabo.2010.08.010

37. Warburg O. On respiratory impairment in cancer cells. *Science*. (1956) 124:269–70. doi: 10.1126/science.124.3215.269
38. Warburg O. On the origin of cancer cells. *Science*. (1956) 123:309–14. doi: 10.1126/science.123.3191.309
39. Zhang X, Fryknäs M, Hernlund E, Fayad W, De Mito A, Olofsson M-H, et al. Induction of mitochondrial dysfunction as a strategy for targeting tumour cells in metabolically compromised microenvironments. *Nat Commun*. (2014) 5:3295. doi: 10.1038/ncomms4295
40. Rios Garcia M, Steinbauer B, Srivastava K, Singhal M, Mattijssen F, Maida A, et al. Acetyl-CoA carboxylase 1-dependent protein acetylation controls breast cancer metastasis and recurrence. *Cell Metab*. (2017) 26:842–55.e5. doi: 10.1016/j.cmet.2017.09.018
41. Yang E, Zha J, Jocker J, Boise LH, Thompson CB, Korsmeyer SJ. Bad, a heterodimeric partner for Bcl-XL and Bcl-2, displaces bax and promotes cell death. *Cell*. (1995) 80:285–91. doi: 10.1016/0092-8674(95)90411-5
42. Liang K, Cao B-Z. Progress on cell apoptosis of mitochondrial regulation. *Biomed Eng Clin Med*. (2014) 18:501–5. doi: 10.13339/j.cnki.sglc.2014.05.049



## OPEN ACCESS

EDITED BY  
Wenyi Kang,  
Henan University, China

REVIEWED BY  
Peiyu Qin,  
Institute of Crop Sciences (CAAS),  
China  
Yilong Ma,  
Hefei University of Technology, China

\*CORRESPONDENCE  
Hongzhi Yang  
✉ Yhz5070679@163.com  
Changyuan Wang  
✉ byndwcy@163.com

†These authors have contributed  
equally to this work and share first  
authorship

SPECIALTY SECTION  
This article was submitted to  
Food Chemistry,  
a section of the journal  
Frontiers in Nutrition

RECEIVED 19 November 2022  
ACCEPTED 19 December 2022  
PUBLISHED 20 February 2023

CITATION  
Feng Y, Fan X, Suo D, Zhang S, Ma Y,  
Wang H, Guan X, Yang H and Wang C  
(2023) Screening of heat  
stress-regulating active fractions  
in mung beans.  
*Front. Nutr.* 9:1102752.  
doi: 10.3389/fnut.2022.1102752

COPYRIGHT  
© 2023 Feng, Fan, Suo, Zhang, Ma,  
Wang, Guan, Yang and Wang. This is an  
open-access article distributed under  
the terms of the [Creative Commons  
Attribution License \(CC BY\)](https://creativecommons.org/licenses/by/4.0/). The use,  
distribution or reproduction in other  
forums is permitted, provided the  
original author(s) and the copyright  
owner(s) are credited and that the  
original publication in this journal is  
cited, in accordance with accepted  
academic practice. No use, distribution  
or reproduction is permitted which  
does not comply with these terms.

# Screening of heat stress-regulating active fractions in mung beans

Yuchao Feng<sup>1,2,3†</sup>, Xia Fan<sup>2†</sup>, Dengcheng Suo<sup>2</sup>, Shu Zhang<sup>1,3</sup>,  
Yantao Ma<sup>1,3</sup>, Haoyu Wang<sup>1,3</sup>, Xin Guan<sup>1</sup>, Hongzhi Yang<sup>1,3\*</sup>  
and Changyuan Wang<sup>1,3\*</sup>

<sup>1</sup>College of Food, Heilongjiang Bayi Agricultural University, Daqing, China, <sup>2</sup>Institute of Quality Standard and Testing Technology for Agro-Products, Chinese Academy of Agricultural Sciences, Beijing, China, <sup>3</sup>Chinese National Engineering Research Center, Daqing, China

**Introduction:** Heat stress caused by high temperatures has important adverse effects on the safety and health status of humans and animals, and dietary interventions to alleviate heat stress in daily life are highly feasible.

**Methods:** In this study, the components of mung bean that have heat stress-regulating effects were characterized by in vitro antioxidant indicators and heat stress cell models.

**Results:** As a result, 15 target monomeric polyphenol fractions were identified based on untargeted analysis on an ultra performance liquid chromatography coupled with high field quadrupole orbit high resolution mass spectrometry (UHPLC-QE-HF-HRMS) platform and available reports. The results of DPPH and ABTS radical scavenging showed that mung bean polyphenols (crude extract) and 15 monomeric polyphenols had better antioxidant activity, followed by oil and mung bean peptides, while protein and polysaccharides had relatively poor antioxidant activity. Qualitative and quantitative assays for 20 polyphenols (15 polyphenols and 5 isomers) were then established based on platform targets. Vitexin, orientin, and caffeic acid were identified as monomeric polyphenols for heat stress control in mung beans based on their content. Finally, mild (39°C), moderate (41°C), and severe (43°C) heat stress models were successfully constructed based on mouse intestinal epithelial Mode-k cells and human colorectal adenocarcinoma Caco-2 cell lines, all with an optimal heat stress modeling time of 6 h. Screening of mung bean fractions using HSP70 mRNA content, a key indicator of heat stress. As a result, HSP70 mRNA content was significantly up-regulated by different levels of heat stress in both cell models. The addition of mung bean polyphenols (crude extract), vitexin, orientin, and caffeic acid resulted in significant down-regulation of HSP70 mRNA content, and the higher the level of heat stress, the more significant the regulation effect, with orientin having the best effect. Mung bean proteins, peptides, polysaccharides, oils and mung bean soup resulted in increased or no change in HSP70 mRNA levels after most heat stresses.



**Discussion:** The polyphenols were shown to be the main heat stress regulating components in mung bean. The results of the validation experiments confirm that the above three monomeric polyphenols may be the main heat stress regulating substances in mung bean. The role of polyphenols in the regulation of heat stress is closely linked to their antioxidant properties.

#### KEYWORDS

heat stress, polyphenols, cells, HSP70, mung bean, UHPLC-QE-HF-HRMS

## Highlights

- Studies have confirmed that polyphenols are the main heat stress regulating component in mung beans, and that both flavonoids and phenolic acids have heat stress regulating effects.
- Orientin, vitexin and caffeic acid may be the main heat stress-regulating components in mung bean multi-fraction, with orientin being the most effective.
- The study was based on Mode-k cells and Caco-2 cells to model mild, moderate, and severe heat stress, respectively, with a modelling time of 6 h.
- A qualitative and quantitative method for the determination of 20 polyphenols, based on the UHPLC-QE-HF-HRMS platform, was targeted and found to be high in vitexin/isovitexin orientin and caffeic acid in mung beans.

## 1. Introduction

Heat is an important environmental stressor. Heat stress is the sum of non-specific responses that occur in humans or animals to excessive temperature stimuli that exceed their thermoregulatory capacity (1). Previous research has shown that the effects of heat stress is expected to be more severe in the future and that adaptation to increasing heat stress in urban areas is highly necessary (2, 3). Excessive heat exposure during daily activities can have harmful effects on the health of the body, such as heat stroke and heat cramps in humans, which can lead to death in severe cases (4). Decreased animal performance, death, and even outbreaks of various infectious diseases (5, 6). This shows that heat stress also has an important impact on the safety and health of the livestock and within poultry economic industries, food, and the environment (7). Therefore, reducing the impact of heat stress on humans and animals has become a hot topic in scientific research.

Safer and more effective dietary interventions to reduce heat stress in the food sector are highly feasible. The prevention of

heat stress in animals is mostly done by adding polyphenols, vitamins, trace elements, etc. to the basic feed. Most of the heat stress studies related to humans comprise investigative reports and a few *in vivo* tests, however, no studies on dietary interventions have been reported. The intensity and duration of high temperatures have increased significantly in recent years, making it necessary to take precautions against heat stress in daily life. Mung beans are a traditional and recognized food for the prevention and elimination of heat stroke and are a preferred ingredient for dietary interventions to relieve heat stress. Mung beans also contain high levels of polyphenols, although some studies have shown that flavonoids in mung beans have heat stress-modulating effects (8). However, similar studies are rare and need to be supported by a large amount of data. Additionally, the scientific basis for the reduction of heat stress by mung beans and the primary components responsible for their effectiveness are still unclear. Heat stress as an inducer of oxidative stress has also been shown (9–12). Polyphenols have received renewed attention in recent years for their good anti-stress effects in animal models and human trials (13, 14). However, there are few reports of interventional stress studies using polyphenols in humans or epidemiological studies on the relationship between dietary polyphenol intake and stress. Cellular peroxidation has also been a focus of research in recent years in the pharmacological management of heat stroke, both nationally and internationally. It is therefore conjectured that the heat stress-regulating effect of mung beans is closely related to their high polyphenol content.

The digestion and absorption of the intestinal tract is necessary to prevent and control heat stress through dietary intervention. The intestinal tissues are also sensitive to heat stress (15), especially when animals are exposed to high temperatures for long periods of time without alleviation. Therefore, it is of practical significance to investigate the components of heat stress regulation at the cell level within the intestinal tract. Under high temperature environment, the integrity of the intestinal mucosa is disrupted, resulting in oxidative stress and massive apoptosis of the intestinal cells. Heat shock proteins (HSPs) are highly conserved proteins that are rapidly synthesized to protect the body under heat stress

conditions and play a key role in the survival of stressed cells and in the repair and protection of the internal environment (16). Heat stress induces the accumulation of HSP70 in cells and is a marker of thermal tolerance in animals and cellular models (17). It can be used as a key indicator of heat stress regulation effect.

*In summary*, this study will screen the heat stress regulatory components in mung bean through *in vitro* antioxidant index and intestinal heat stress cell model to identify their main components and provide a theoretical basis for the mitigation and prevention of heat stress in mung bean.

## 2. Materials and methods

### 2.1. Materials

Plant material: mung beans comprised Ming mung beans from Shanxi, a geographical indication product of China, which were samples were collected in 2021, full-grained, and free of pests and diseases. Mung bean powder was sieved through an 80 mesh and defatted with petroleum ether for the next step of the experiment.

The mouse intestinal epithelial MODE-K cells and human colorectal adenocarcinoma Caco-2 cell line used in this experiment were provided by the College of Animal Science and Technology, Heilongjiang Bayi Agricultural University, China.

### 2.2. Experimental apparatus and reagents

SW-CJ-1FDG ultra-clean bench, LAYTE; BPN-150CH(UV) CO<sub>2</sub> incubator, bluepard; MF52-N inverted microscope, Mshot; L3-5K low-speed centrifuge, Kecheng; HH-2 water bath, Changzhou Aohua Instruments Co. FlexStation 3 Multifunctional Enzyme Labeler, Molecular Devices; H1650-W Centrifuge, Xiang Yi; Tissulyser-24 Tissue Grinder, Shanghai Jingxin; 752 Spectrophotometer, Shanghai Q EXACTIVE HF, Heraeus Fresco Centrifuge, Thermo Fisher Scientific; Smart Sample Grinder, Beijing Newport Biotechnology Co., Ltd.; PS-60AL Ultrasonic Cleaner, Shenzhen Redbone Electronics Co. A TU-1800 UV-Visible Spectrophotometer from Beijing Pu-Analysis Instrument Co.

DMEM, penicillin-streptomycin solution (double antibody, 100 ×), and 0.25% trypsin solution (containing EDTA, dissolved in PBS) were purchased from Procell; Fetal Bovine Serum, ExCell Bio; MTT, MCE; cell culture dishes, cell culture bottles, Corning; malondialdehyde (MDA) test kit, lactate Total Antioxidant Capacity (T-AOC), and Superoxide Dismutase (SOD) kits were purchased from Nanjing Jiancheng Institute of Biological Engineering; Mitochondrial Membrane Potential

Assay Kit, Biyuntian; methanol, acetonitrile, formic acid, purified water; all reagents were LC-MS grade and all other chemical reagents were analytically pure.

### 2.3. Mung bean fraction extraction methods

#### 2.3.1. Mung bean protein, peptide, polysaccharide, and oil extraction methods

Mung bean total protein (18), mung bean globulin (19), mung bean trypsin-hydrolyzed peptide, mung bean pepsin-pepsin-hydrolyzed peptide (20), mung bean polysaccharide (21), mung bean oil (22), and mung bean soup were prepared in the laboratory by referring to the relevant literature and making some improvements. The detailed extraction procedure is shown in [Supplementary Appendix](#)—Experimental methods.

#### 2.3.2. Mung bean polyphenol extraction method

Three grams of defatted mung bean flour was weighed and extracted with 80% ethanol at a ratio of 1:10 for 60 min under ultrasonic conditions at 40°C and 400 W. The supernatant was collected after centrifugation at 10,000 r/min for 5 min, and the residue was extracted twice as described above, for a total of three times. The ethanol was removed from the supernatant at 45°C by rotary evaporation under reduced pressure to obtain a polyphenol extract. The residue of the free phenol extraction was collected and hydrolyzed in 2 mol/L NaOH solution for 1 h. The pH was adjusted to between 2 and 3 with hydrochloric acid and then extracted three times with ethyl acetate. The supernatant was centrifuged, evaporated to until dry, and dissolved in methanol to obtain the extract of bound phenols. The free phenol and bound phenol extracts were combined and fixed to 10 ml, freeze-dried, and stored in a refrigerator at −80°C (23).

### 2.4. Antioxidant test

#### 2.4.1. DPPH free radical scavenging rate measurement

A total of 3.9 mL of DPPH was added to a working solution to 0.1 mL of the solution to be measured (the absorbance of DPPH working solution was  $0.70 \pm 0.02$  at this time), this was shaken well and left to stand for 30 min away from light. Anhydrous ethanol was chosen as the blank reference, and absorbance value A1 was measured at 515 nm. Anhydrous ethanol (0.1 mL) was added to 3.9 mL of the DPPH working solution, and the absorbance value A2 was measured under the same conditions: 0.1 mL of the solution to be measured was added to 3.9 mL of anhydrous ethanol, and the absorbance value

marked as A3 was measured under the same conditions. The DPPH radical-scavenging rate was calculated as follows:

$$DPPH(\%) = (1 - \frac{A1 - A3}{A2}) \times 100\%$$

### 2.4.2. ABTS free radical scavenging assay

The method of Lahouar et al. (24) was used for determination, with slight modifications. The prepared ABTS<sup>+</sup> stock solution was incubated overnight protected from light and diluted with ethanol before use to give an absorbance value of  $0.70 \pm 0.02$  at 734 nm. Zero point one milliliters of the sample solution was mixed with 3.9 mL of freshly prepared ABTS<sup>+</sup> free radical working solution, and the absorbance was measured at 734 nm and labeled AX. The results were expressed as % activity (%).

$$ABTS \text{ free radical scavenging } (\%) = (1 - \frac{Ax - Ax_0}{A_0}) \times 100\%$$

Note: Ax0 is a 0.1 mL sample solution + 3.9 mL solvent; A0 is 0.1 mL solvent + 3.9 mL ABTS<sup>+</sup> working solution.

## 2.5. Mung bean polyphenol assay establishment

### 2.5.1. Preparation of 20 polyphenol standards

The appropriate amount of the 20 standards were dissolved in dimethyl sulfoxide and the standard stock solution was configured at a concentration of 1 mg/mL. Next, 1 mL of each of the 20 standard stock solutions was removed and placed in a 100 mL volumetric flask. These stock solutions were then configured as a standard intermediate mixture of 10 µg/mL. This intermediate solution was further diluted into solutions with concentrations of 50, 100, 250, 500, 750, 1,000, and 1,500 ng/mL, respectively, after which the standard curves were plotted using the standard concentration and peak area as the horizontal and vertical axes, respectively. In this case, the method was established using a mixed standard solution of 1,000 ng/mL.

### 2.5.2. Establishment of the method

Instrument platform: Q Exactive HF spectrometer; Column: aqueous. BEH C18, 1.7 µm/3.00 × 100 mm. Based on the non-targeted detection method established in a previous study, a mixture of 20 polyphenol standards was tested. Polyphenols were detected using full MS/dd-MS 2 (top-n) detection in positive/negative ion mode. Chromatographic conditions: mobile phase A for liquid chromatography comprised 1% formic acid in water, mobile phase B comprised acetonitrile, and the sample tray temperature was 4°C. Mass spectrometric conditions: electrospray voltage, 3.5 kV; sheath gas, 30 Arb; auxiliary gas, 20 Arb; ion transport tube temperature, 350°C; auxiliary gas heater temperature, 300°C; full mass spectrometric resolution, 120,000; MS/MS resolution, 60,000.

The scanning mode of the QE-HF-HRMS was changed to negative ionization (HEI-) and parallel reaction monitoring (PRM) modes after the detection of 20 specimens. The chromatographic conditions were maintained. The mass spectrometry conditions were as follows: electrospray voltage, 3.5 kV; sheath gas, 30 Arb; auxiliary gas, 20 Arb; ion transfer tube temperature, 350°C; auxiliary gas heater temperature, 300°C; MS/MS resolution ratio, 60,000. The target determination was performed according to the molecular weight of the polyphenols.

Finally, the main influencing factor collision energy (CE) is optimized. A simple optimization of the column temperature, flow Rate and mobile phase gradient was carried out, the rest is automatically optimized by the instrument.

## 2.6. Cell modeling methods

### 2.6.1. Cell recovery and passaging methods

Caco-2 cell medium: DMEM + 10% FBS + 1% (penicillin-streptomycin solution). ModeK cell medium: DMEM + 10% FBS + 1% (penicillin-streptomycin solution). Resuscitate cells: Caco-2 and ModeK cells were removed from liquid nitrogen, and quickly placed in a 37°C water bath and shaken in a tube to gently dissolve the freezing solution; after dissolution, the cells were transferred to a centrifuge tube containing 5 ml of medium, centrifuged, the cells were collected, centrifuged at 1,000 r/min for 5 min at room temperature, and the supernatant was discarded. The cells were then suspended in complete medium containing 10% fetal bovine serum, inoculated into culture dishes, gently blown, and mixed, and incubated at 37°C with 5% CO<sub>2</sub> saturation humidity.

#### 2.6.1.1. Cell passages

When the density of the cells reached 80%, the cells were passaged. The medium was discarded, and the cells were washed with PBS; 1–2 ml of 0.25% trypsin was added to digest the cells which were observed under a microscope. 1–2 min of digestion was seen when the cells were separated from each other and rounded, i.e., the digestion was complete; the trypsin was then quickly discarded, the complete medium was added, the cells were blown to make a single cell suspension, the cells were then passed at a ratio of 1:3, and the culture was expanded at 37°C and 5% CO<sub>2</sub> saturated humidity.

### 2.6.2. Cell model construction method

Caco-2 and mode-k cells were added to DMEM high sugar complete medium and placed in an incubator (37°C, 5%). Cell assays were performed when the cells were 80–90% fused. The control cells were incubated at 37°C with 5% CO<sub>2</sub> concentration; the heat stress group was treated at 39°C, 41°C, and 43°C with 5% CO<sub>2</sub> concentration for 2, 4, 6, and 8 h. The cells were first tested for cell morphology, cell viability, mRNA

content of the HSP70 gene, and cellular glutathione peroxidase (GSH-Px) activity, lactate dehydrogenase (LDH) activity, total antioxidant activity, and total antioxidant activity. The time required for heat stress modeling was determined by changes in cell morphology, cell viability, HSP70 mRNA content, cellular GSH-Px, LDH activity, T-AOC, SOD, and MDA content.

### 2.6.3. Cell viability MTT assay

Caco-2 and ModeK cells in the logarithmic growth phase were inoculated at  $3 \times 10^3$  cells/well in a 96-well cell culture plate (16 plates) and incubated overnight at 37°C in a 5% CO<sub>2</sub> incubator (100 µL sterile PBS was added to the wells around the cell wells); grouping: Group A, blank wells; Group B, modeK cells; and Group C, Caco-2 clls. Duration of action: incubate at 37°C, 39°C, 41°C, and 43°C for 2, 4, 6, and 8 h. Then, 10 µL MTT was added to each well and incubated at 37°C for 4 h. The medium was aspirated, 150 µL DMSO was added, and shaken for 10 min. The absorbance value of each well was then measured with the enzyme marker OD 570.

### 2.6.4. Mitochondrial membrane potential and antioxidant index assay

The cells were cultured to the experimental state at different treatment temperatures or at the same treatment temperature for different treatment times. The assays were then performed according to the MDA, LDH, GSH-PX, T-AOC, SOD, and mitochondrial membrane potential assay kits.

### 2.6.5. Changes in the relative mRNA expression of HSP27, HSP70, HSP90, Claudin-1, ZO-1, TNF-α, IL-1β, Bcl-2, and Bax genes

#### 2.6.5.1. Trizol method for RNA extraction

One milliliter of Trizol reagent was added to the cells, blown, mixed with a gun, transferred to a 1.5 ml RNase-free EP tube, and lysed for 10 min. 200 µL of chloroform was added, mixed several times *via* vigorous inversion, and left at room temperature for 5 min. The mixture was centrifuged for 15 min (4°C, 12,000 r/min), visible division into upper (RNA), middle (protein), and lower (DNA). The upper aqueous phase (approximately 400 µL) was transferred to a new 1.5 ml EP tube, 400 µL of isopropanol was added, mixed well, and left at room temperature for 10 min. The mixture was then centrifuged at 4°C, 12,000 r/min for 10 min, a white RNA precipitate was visible at the bottom of the tube. The supernatant was discarded, 1 ml of RNase-free 75% ethanol was added, vortexed, and centrifuged at 10,000 r/min for 5 min at 4°C. This was repeated only once. The supernatant was discarded and the RNA precipitate was dried in air for 5–10 min and dissolved in 20 µL of DEPC water. Two microliter of the dissolved RNA was then used to measure the OD260, OD280, and OD260/OD280 values using a microspectrophotometer to calculate the purity and concentration of RNA. The RNA mass was estimated according to the OD260/OD280 ratio, which was between 1.8 and 2.0, to

TABLE 1 Primer sequence list.

Gene	Primer	Sequence (5'-3')	PCR products
b-actin	Forward	CACGATGGAGGGGCCGGA CTCATC	240 bp
	Reverse	TAAAGACCTCTATGCCAACACAGT	
Mus IL-1b	Forward	TCAGGCAGGCAGTATCACTC	250 bp
	Reverse	AGCTCATATGGGTCCGACAG	
Mus TNF-α	Forward	CGTCAGCCGATTGTCTATCT	206 bp
	Reverse	CGGACTCCGCAAAGTCTAAG	
Mus Bax	Forward	TTTGTCTACAGGGTTTCATCCA	181 bp
	Reverse	GTGTCCACGTCAGCAATCATC	
Mus Bcl2	Forward	AGCCACCGTAACAATCAAG	147 bp
	Reverse	CCTGTCCCTTTGTCTTCAGC	
Mus ZO-1	Forward	CCAGCAACTTTCAGACCACC	154 bp
	Reverse	TTGTGTACGGCTTTGGTGTG	
Mus HSP70	Forward	GCAGACCTTCACCACCTACT	248 bp
	Reverse	CCTTGTCTGTTGGTGATGGTG	
Mus HSP90	Forward	CTCCATGATCGGGCAGTTTG	239 bp
	Reverse	TCACCACTTCCTTGACCCTC	
Mus Claudin-1	Forward	GATGTGGATGGCTGTCATTG	246 bp
	Reverse	CGTGGTGTGGGTAAGAGGT	
Mus HSP27	Forward	AGCGCTTCGAGAAGATGT	150 bp
	Reverse	GGTCAGGAGGAGCAGGAAG	

meet experimental requirements. The concentration of sample RNA was calculated from the absorbance values according to the following formula:

$$\text{Total RNA concentration } (\mu\text{g}/\mu\text{L}) = \text{OD}_{260} \times 40 \times 10^{-3}.$$

The total RNA was stored in a refrigerator at −80°C for backup.

The primer sequences, used for genetic testing (Table 1).

### 2.6.6. Analysis of significance

Univariate analysis of variance (ANOVA) and Duncan's test ( $p < 0.05$ ) using the SPSS 21 software were used for data calculation and significance analysis.

## 3. Results and analysis

### 3.1. Selection of mung bean components

In this study, total mung bean protein and mung bean globulin, which are the main storage proteins in mung

TABLE 2 Mass spectrometric signature ion list of 20 mung bean polyphenols.

	Name	Molecular formula	Molecular weight	Precursor ion	Retention time (min)	Characteristic ion 1	Characteristic ion 2
1	Caffeic acid	C <sub>9</sub> H <sub>8</sub> O <sub>4</sub>	180.16	179.03498	5.28	135.0441	107.0497
2	Ferulic acid	C <sub>10</sub> H <sub>10</sub> O <sub>4</sub>	194.18	193.05063	8.61	134.0363	178.0262
3	Naringenin	C <sub>15</sub> H <sub>12</sub> O <sub>5</sub>	272.25	271.0612	13.68	151.0026	119.0491
4	Hesperetin	C <sub>16</sub> H <sub>14</sub> O <sub>6</sub>	304.27	301.07176	14.31	164.0106	151.0027
5	Quercetin	C <sub>15</sub> H <sub>10</sub> O <sub>7</sub>	302.236	301.03538	12.60	151.0026	178.9976
6	Cryptochlorogenic acid	C <sub>16</sub> H <sub>18</sub> O <sub>9</sub>	354.31	353.08781	6.10	173.0446	135.0441
7	Chlorogenic acid	C <sub>16</sub> H <sub>18</sub> O <sub>9</sub>	354.31	353.08781	4.77	191.0553	161.0235
8	Neochlorogenic acid	C <sub>16</sub> H <sub>18</sub> O <sub>9</sub>	354.31	353.08781	2.11	191.0553	179.0341
9	Curcumin	C <sub>21</sub> H <sub>20</sub> O <sub>6</sub>	368.39	367.11871	12.61	301.0712	164.0106
10	Puerain	C <sub>21</sub> H <sub>20</sub> O <sub>9</sub>	416.378	415.10346	7.41	267.0657	295.0605
11	Vitexin	C <sub>21</sub> H <sub>20</sub> O <sub>10</sub>	432.378	431.09837	9.36	311.0555	283.0605
12	Isovitexin	C <sub>21</sub> H <sub>20</sub> O <sub>10</sub>	432.38	415.10346	9.36	311.0555	283.0605
13	Naringin	C <sub>27</sub> H <sub>32</sub> O <sub>14</sub>	580.535	579.17193	10.40	151.0026	271.0605
14	Neohesperidin	C <sub>28</sub> H <sub>34</sub> O <sub>15</sub>	610.56	609.18249	11.01	301.0712	151.0027
15	Rutinium	C <sub>27</sub> H <sub>30</sub> O <sub>16</sub>	610.52	609.1468	9.35	300.0269	271.0142
16	Isochlorogenic acid A	C <sub>25</sub> H <sub>24</sub> O <sub>12</sub>	516.453	515.1213	10.40	191.0552	179.0552
17	Isochlorogenic acid B	C <sub>25</sub> H <sub>24</sub> O <sub>12</sub>	516.453	515.0517	10.21	173.0447	191.0553
18	Isochlorogenic acid C	C <sub>25</sub> H <sub>24</sub> O <sub>12</sub>	516.45	515.1206	10.90	173.0446	135.0441
19	Orientin	C <sub>21</sub> H <sub>20</sub> O <sub>11</sub>	448.09	447.0932	8.74	327.0502	357.0607
20	Gallic acid	C <sub>7</sub> H <sub>6</sub> O <sub>5</sub>	170.01	169.01425	0.82	125.0233	169.0133

beans, were selected. These two components represent the two types of crude protein and purified mung bean isolate proteins, respectively. Mung bean peptides also have good immunomodulatory activity as well as good antioxidant properties (25, 26), and the types of peptides chosen to mimic the digestion and absorption of the gastrointestinal tract after digestion were mung bean trypsin-hydrolyzed peptide and pepsin-hydrolyzed peptide, respectively. Polysaccharides also exhibit important physiological activities in organisms. Mung bean polysaccharides have been less studied, but differences have been found in the functional properties of mung bean polysaccharides obtained by different treatments. Mung bean polysaccharides obtained by aqueous extraction (solvent-free) and (hot) water-soluble polysaccharides exhibit antioxidant and immunomodulatory activities (27). Therefore, in this study, polysaccharides prepared by water extraction were chosen for the heat stress studies. Lipids supply energy and essential fatty acids to the body. Mung beans are low in lipids, including fat, phospholipids, and soy sterols. Polyphenols can be subdivided into crude extracts of mung bean polyphenols and monomeric polyphenols from mung beans. As heat stress can cause oxidative stress, *in vitro* antioxidant indicators were used in the prescreening process to screen for effective fractions of mung bean heat stress.

The polyphenols contained in mung beans from several origins were identified non-targeted by UHPLC-QE HF. The aim was to screen for polyphenolic substances contained simultaneously in mung beans from multiple origins. A total of 57 polyphenol fractions were screened as a result, (see [Supplementary Table 1](#)). There are currently 21 accurately detected polyphenols in mung beans (28–30), while mung bean polyphenols identified by non-targeted screening in this study were more abundant. Due to the large number of fractions, preliminary screening was carried out by reviewing the literature to select fractions with known heat stress modulating effects and polyphenolic substances without heat stress modulation-related studies, but with antioxidant properties. Fifteen polyphenolic substances were Caffeic acid, Ferulic Acid, Naringenin, Hesperetin, Quercetin, Chlorogenic acid, Curcumin, Puerain, Vitexin, Isovitexin, Naringin, Neohesperidin, Rutinium, Orientin, Gallic acid.

### 3.2. Determination of polyphenol content of mung bean monomers

The results from section “3.2 Determination of polyphenol content of mung bean monomers” show that the *in vitro*



antioxidant properties of mung bean monomeric polyphenols are highly similar, but mung bean, as a daily dietary food for heat relief, should also have a higher content of fractions with heat stress-modulating effects. Therefore, the content of monomeric polyphenols in mung beans needs to be used as an indicator for the screening of major heat-stress-modulating polyphenol fractions. The 15 monomeric polyphenols screened in section “3.2 Determination of polyphenol content of mung bean monomers” were used as targets. Chlorogenic acid also contains five isomeric forms, cryptochlorogenic acid, neochlorogenic acid, isochlorogenic acid A, isochlorogenic acid B, and isochlorogenic acid C, were also added to the method development, a method for the detection of 20 polyphenols was developed based on UHPLC-QE HF.

The HRMS parameters of the 20 polyphenols were optimized by injecting QE-HF-HRMS with a continuous microflow jet pump in the PRM mode of negative ionization (HEI-). The detection results obtained a high sensitivity. In this study, the capillary voltage and characteristic fragment ions were fully optimized, and the carbon-equivalent (CE) values were 20, 30, 40, 50, and 60. The mass spectra are shown in [Supplementary Figure 2](#). High response intensities for the parent ions of ferulic acid, naringenin, hesperetin, quercetin, and rutin at CE = 20 and 30, and better results at CE = 40, 50, and 60, when the parent is not fully broken up and the target daughter ions have high response intensities. At CE = 20, 30, and 40, the parent ions of curcumin, orientin, cryptochlorogenic acid, neochlorogenic acid, and isochlorogenic acid B dissociated well, it CE > 40, the parent ion is completely broken up or there is too much fragmentation of the daughter ion. Gallic acid varied insignificantly at five collision energies, both of which were better. it CE = 30, 40, and 50, neohesperidin, puerarin, caffeic acid, ellagic acid, isochlorogenic acid A, and isochlorogenic acid C were dissociated with high corresponding intensity of the target daughter ions. It CE = 40 and 50, vitexin, and Isoviteixin were most effective with high corresponding intensity of the target daughter ions. At CE = 30 and 40, naringenin dissociated best, with high parent ion response intensity and low daughter ion response intensity at CE < 30, and at CE > 40, the parent ion was completely broken up. Therefore, combining the effects of the 20 polyphenols, the optimized CE values were set to 30, 40, and 50. The mass spectrometric ion characteristics of the 20 mung bean polyphenols are shown in [Table 2](#). The chromatograms of the 20 polyphenols under optimal conditions are shown in [Supplementary Figure 4](#).

As the instrument is a combination of the parent ion selectivity of a high-performance quadrupole and the high-resolution accurate mass number (HR/AM) orbitrap detection technique, it exhibits excellent performance, and the MS conditions are crucial to the establishment of the method. Further, the LC conditions, including the flow rate, column temperature, and elution gradient, were also optimized. The flow rates were set as 0.3, 0.35, and 0.4 ml/min, it was observed

TABLE 3 Optimal chromatographic conditions.

Time (min)	Flow (mL/min)	%B	Cure (μL)
0	0.4	5	5
3.5	0.4	5	5
15.5	0.4	38	5
17	0.4	38	5
17.1	0.4	5	5
18	0.4	5	5

that the higher the flow rate, the shorter the peak time, there was no significant change in the separation of the chromatographic peaks. Therefore, the flow rate was set as 0.4 ml/min. The column temperatures were set as 35°C, 40°C, and 45°C, The higher the temperature, the better the separation of the peaks. The column temperatures rate was set as 45°C. The mobile phase B was set to 28, 38, 48, and 58%, respectively. The best peak response intensities were found at 38 and 58%, with 38% being more stable, the Volume of mobile phase B es rate was set as 38%. The optimum chromatographic conditions are shown in [Table 3](#). The chromatogram under optimal conditions is shown in [Supplementary Figure 4](#). Qualitative and quantitative determination of 20 polyphenols in 18 min. The linearity results of the 20 polyphenol standard curves are shown in [Supplementary Table 2](#).

Detection of heat-stress-regulated polyphenolic fractions in mung beans was conducted using direct injection-mass spectrometry fingerprinting. After simple extraction, the samples were directly analyzed by mass spectrometry without excessive chromatographic separation. These 20 polyphenols can be detected and distinguished with great effectiveness and precise quantification. This method is a highly characteristic mass spectrometric fingerprinting technique. Among them, it was not possible to distinguish the two due to the mutual isomerization of vitexin and Isoviteixin and the almost identical mass spectral fragments, the two isomers were also not separated in the chromatogram, which may be related to the column, and a chiral column should be chosen for the separation. But the mass spectra and chromatographic separation of the other components were very good. The method was then used to test the polyphenol content of mung beans and the results are shown in [Figure 1](#) (The quantification results are the average of three parallel sample determinations). Polyphenolic substances with high content in mung beans are mucuna vitexin/Isoviteixin, caffeic acid, and Orientin. Ferulic acid, Curcumin, quercetin, gallic acid, chlorogenic acid, and naringin are present in small amounts. The remaining components are present in very small amounts, Cryptochlorogenic acid is not present in mung beans. Vitexin/Isoviteixin is a major polyphenol in mung beans. Caffeic acid was also detected. Individual studies have detected orientin in mung beans using non-targeted analysis (31), but there is no precise qualitative and quantitative method with corroboration,

the present study confirms this. As shown by the DPPH radical scavenging rate of the monomeric polyphenols, the antioxidant properties of isovitexin are very poor. Therefore, from the point of view of content, vitexin, caffeic acid, and orientin were selected as mung bean monomeric polyphenol heat stress modulating components.

### 3.3. *In vitro* antioxidant activity of mung bean fractions

First, the antioxidant properties of each fraction of mung bean and 15 monomeric polyphenols were measured at high concentrations (10 mg/mL) using the DPPH scavenging rate as an indicator, the results of which are shown in [Supplementary Figure 1A](#). Among the monomeric polyphenols, neohesperidin, hesperidin, naringenin, puerarin, isovitexin, and naringenin had relatively low DPPH clearance, so these were initially excluded. The total proteins, globulins, and polysaccharides in mung beans have lower antioxidant activity than most of the monomeric polyphenols, but given that they are nutritional fractions, subsequent experiments were continued. The antioxidant properties of the mung bean fractions were then compared based on the concentrations of DPPH and ABTS clearance at 50%. The results are shown in [Supplementary Figure 1B](#). The scavenging rates of both free radicals increased with increasing concentration in the concentration range of each fraction, reaching over 90%. However, the strength of the antioxidant properties of the different fractions can be seen from the corresponding concentration range differences, with curcumin, orientin, rutin, gallic acid, quercetin, caffeic acid, ferulic acid, and chlorogenic acid in the range of 0.004–0.1 mg/mL. Vitexin in the range of 0.1–1.6 mg/mL. Among the mung bean fractions, the DPPH radical scavenging rate of mung bean polysaccharide, tryptase peptide, pepsin peptide, globulin, and total protein increased with increasing concentration. However, certain maximum values did not exceed 90%. The ABTS scavenging rate of the two mung bean proteins also increased with concentration, whereas the ABTS scavenging rate of the polysaccharide and the two mung bean peptides did not increase with concentration and tended to decrease slightly.

The scavenging rates of both free radicals from mung bean oil did not vary with concentration, and were relatively stable, ranging from 60 to 85%. Using a 50% scavenging rate of both free radicals as a criterion, combined with the range of scavenging rates of both free radicals, it can be seen that mung bean mixed polyphenols and monomeric polyphenols have good antioxidant properties, followed by oil and mung bean peptides, with proteins and polysaccharides having relatively poor antioxidant properties. Therefore, mixed polyphenols, oils, and two polypeptides were selected from the mung bean fraction for subsequent cellular experiments.

### 3.4. Screening of heat stress regulatory components in mung beans

The study first selected mode-K mouse small intestine epithelial cells for the construction of a heat stress model. Based on the results of the mode-K cell heat stress model screening, Caco-2 human colorectal adenocarcinoma cells were used to confirm the results of the mung bean fraction screening. Although many cellular heat stress models are available ([32](#), [33](#)), the conditions for heat stress construction differ for cells of different origins. Therefore, the conditions were based on the imbalance of oxidative stress Superoxide dismutase (SOD), GSH-PX, LDH, T-AOC, and MDA, loosening and “leakage” of intestinal epithelial junctions ZO-1 protein and Claudin protein, changes in intestinal inflammation, intestinal serum physicochemical parameters [Interleukin (IL-1 $\beta$ ) and tumor necrosis factor (TNF- $\alpha$ )], apoptosis and changes in heat shock protein content due to heat stress-induced intestinal damage (HSP70, HSP27, HSP90). The above key indicators were used to construct and verify the cell model of heat stress. In this study, mild (39°C), moderate (41°C), and severe (43°C) heat stress models were constructed for both types of cells. For detailed results, see [Supplementary Appendix](#)—Experimental methods.

#### 3.4.1. Screening results of heat stress regulatory components of mung bean based on mode-k cell heat stress model

The effect of heat stress regulation investigated using the previously screened mung bean polyphenols, oils and fats, pepsin-hydrolyzed peptides, trypsin-hydrolyzed peptides, vitexin, orientin, and Caffeic acid using HSP70 mRNA content change as an indicator of heat stress. In addition, mung bean soup, a representative food in the daily diet to relieve heat, was compared with mung bean soup for heat stress regulation. The effect of each fraction on cell viability was determined by preliminary experiments, and a concentration of 30  $\mu$ mol/L of each fraction was selected for the investigation of the regulatory effect of cellular heat stress. The results are shown in [Figure 2A](#). When the components were co-cultured with cells at 37°C, mung bean polyphenols, vitexin, and orientin could decrease the HSP70 mRNA content, while the other components could increase the HSP70 mRNA content. Mung bean soup, vitexin and orientin decreased HSP70 mRNA content at 39°C, whereas other components increased HSP70 mRNA content. Mung bean polyphenols, mung bean oil, trypsin-hydrolyzed peptide, vitexin, orientin and caffeic acid decreased HSP70 mRNA content significantly at 41°C, whereas other components increased HSP70 mRNA content. Mung bean polyphenols, pepsin peptides, vitexin, orientin and caffeic acid decreased HSP70 mRNA content significantly at 43°C. The other components increased HSP70 mRNA content. The combined analysis revealed that mung bean polyphenols, vitexin, orientin, and caffeic acid almost all

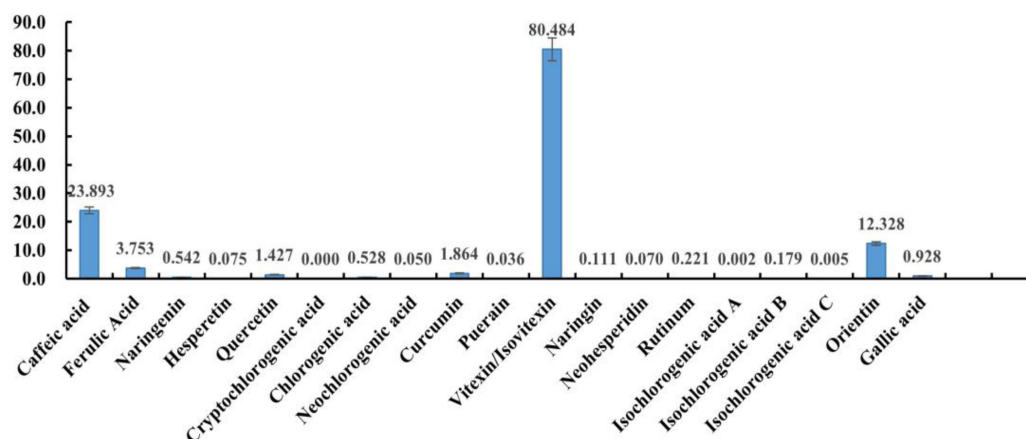


FIGURE 1  
The content of 20 phenolics.

caused a downregulation of HSP70 mRNA content compared to the control group at each heat stress temperature. Although statistically not reaching the level of significant difference, the preventive and regulatory effects were better. Although green bean soup is useful in the daily diet to relieve heat stroke, a comparison shows that mung bean soup is not as effective as mixed and monomeric polyphenols in regulating cellular heat stress. Proteins, peptides, polysaccharides and lipids do not regulate HSP70 mRNA content well. These four substances are the components of mung beans screened for their heat stress regulatory group effects.

Figure 2B shows the effects of modulation of the cell morphology. The morphology of mode-k cells with the four components added at 37°C did not change, which initially indicated no significant toxicity to the cells, and the morphology of the control cells and cells with the four components added at 39°C under mild heat stress was not significantly different from that of the cells at 37°C. The cells under moderate heat stress at 41°C showed a shrinkage of cell morphology and a reduction in growth density compared to the control group, while the cell morphology of the cells with the four mung bean fractions improved significantly compared to the control group at 41°C. Cell morphology did not differ significantly from normal cells, and the effect of the three monomeric polyphenols was slightly better than that of mung bean polyphenols. Cells under severe heat stress at 43°C were significantly shrunken and oval in shape compared to those at 37°C. In contrast, the cells treated with the four mung bean fractions had significantly improved morphology and increased growth density. This indicates that the four mung bean fractions have significant effects on the regulation of cellular heat stress. Further, orientin has the best effect on the regulation of heat stress. All four fractions comprised polyphenols, which further indicates that

polyphenols in mung beans are substances that regulate heat stress.

### 3.4.2. Screening and verification results of heat stress regulatory components of mung bean based on Caco-2 cell heat stress model

Based on the Caco-2 cell heat stress model, the heat stress regulatory components of mung bean were screened and verified by the change of HSP70 mRNA content. The results are shown in Figure 3A. Co-culture of the fractions with cells at 37°C showed that the mung bean polyphenols were at the same level as the control group. Mung bean broth, vitexin, and orientin decreased HSP70 mRNA content, while the other fractions increased HSP70 mRNA content. Mung bean polyphenols, vitexin, caffeic acid and orientin decreased HSP70 mRNA content, whereas other components increased HSP70 mRNA content at 39°C. At 41°C, mung bean polyphenols, mung bean oil, vitexin, orientin, and caffeic acid decreased the HSP70 mRNA content significantly, while the other components increased the HSP70 mRNA content. The HSP70 mRNA content of all fractions was lower than that of the control group at 43°C, however, mung bean polyphenols, vitexin, orientin, caffeic acid reduced the HSP70 mRNA content to a greater extent. The combined analysis revealed that mung bean polyphenols, vitexin, orientin, and caffeic acid almost all resulted in the downregulation of HSP70 mRNA content at each heat stress temperature compared to the control group. Although the degree of heat stress regulation did not reach statistical significance, its regulation improved. Among them, orientin was the most effective, with results identical to those of mode-k cells. The same can be found for mung bean soup is not as effective as mixed and monomeric polyphenols in regulating cellular heat stress. Proteins, peptides, polysaccharides and lipids do not regulate HSP70 mRNA content well. Confirming once

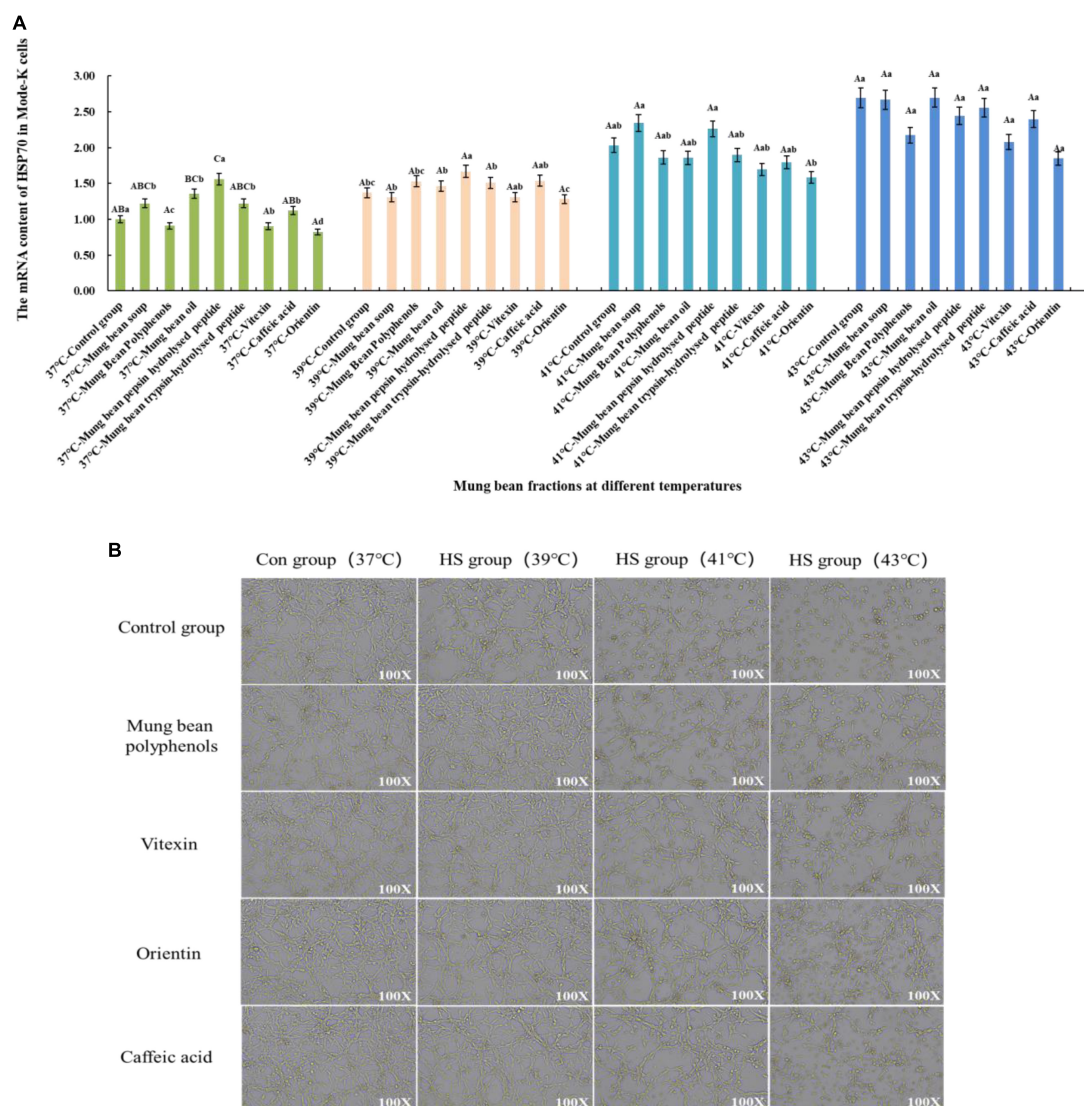


FIGURE 2

(A) Effect of mung bean components on HSP70 mRNA content in Mode-k cells. (B) Effect of key mung bean components on Mode-k cell morphology at different heat stress temperatures.

again that these four substances were the fractions of mung beans screened for their heat stress regulatory group effects.

**Figure 3B** shows the cell morphology of the modulation effect. It can be clearly seen from the control group that the Caco-2 cells gradually shrink with the increase in heat stress temperature, the cell gap becomes larger, and the cell boundary becomes blurred. The morphology of the cells in the control group with the four fractions added at 37°C did not change, which tentatively indicated that there was no significant toxicity to Caco-2 cells. The morphology of the cells in the treatment group with the four fractions added at 39°C was similar to that of the cells at 37°C. Compared with the control group at 41°C, the cells with the four mung bean fractions showed less contraction of morphology and smaller cell gaps, and the regulation effect

was better. The cell morphology was significantly improved by the addition of the four mung bean fractions compared with the control group at 43°C. Less cell shrinkage, clearer boundaries between cells, and increased cell growth density were observed. This indicated that the four mung bean fractions had a significant effect on the regulation of heat stress in Caco-2 cells. The effect of the four monomeric polyphenols was slightly better than that of mung bean polyphenols in terms of cell morphology.

The mung bean fractions screened by the mode-k cell heat stress model were validated in the Caco-2 cell heat stress model by combining the results of all indicators under six heat stress models for both cells. Very few studies have been conducted on the regulation of heat stress by mung beans and



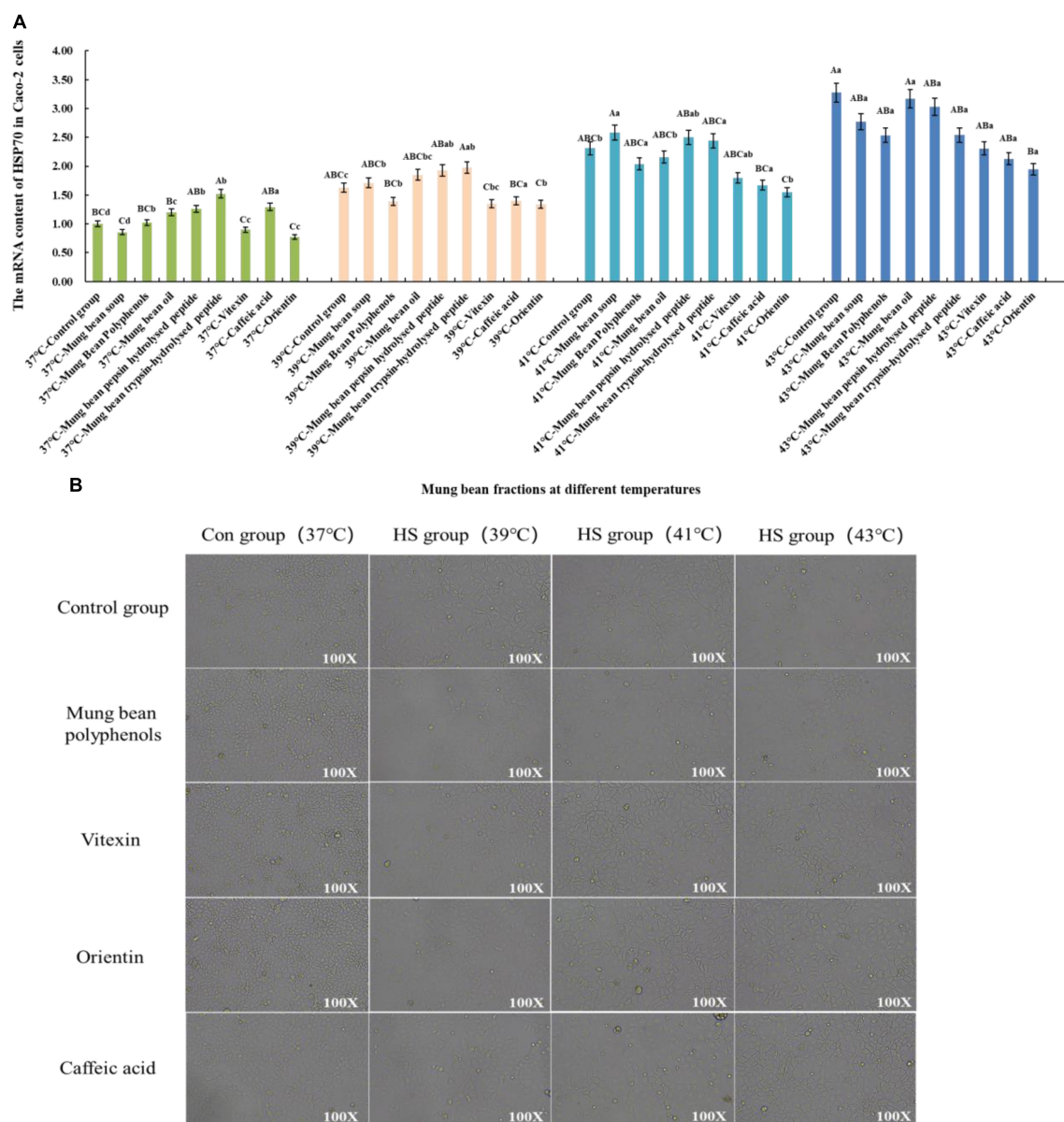


FIGURE 3

(A) Effect of mung bean components on HSP70 mRNA content in Caco-2 cells. (B) Effect of key mung bean components on Caco-2 cell morphology at different heat stress temperatures.

their foods. Cao et al. (8) found that vitexin and isovitexin were the main antioxidant components of mung beans (more than 96% of which was present in the seed coat of the beans), both of which could be absorbed into rat plasma through gavage. The plasma levels of MDA and the activities of LDH and nitric oxide synthase (NOS) were significantly reduced in rats fed mung bean peel extract before and after heat stress, whereas the levels of T-AOC and GSH-Px (a quantitative assessment of oxidative stress) were significantly increased. It was confirmed that mung bean flavonoids could alleviate heat stress in rats by modulating the antioxidant levels in the

body. In this study, the heat stress-modulating effects of the screened mung bean fractions were investigated at the cellular level. In addition to vitexin, orientin, and caffeic acid have been found to be effective in heat stress regulation. Orientin is a flavonoid, caffeic acid are phenolic acid compounds. This suggests that phenolic acid compounds also have heat stress-modulating effects. The results of this study were similar to those reported by Cao et al. Once again, it was confirmed that mung bean polyphenols are a major substance in their heat stress-modulating effect and are closely related to the antioxidant properties of polyphenols.



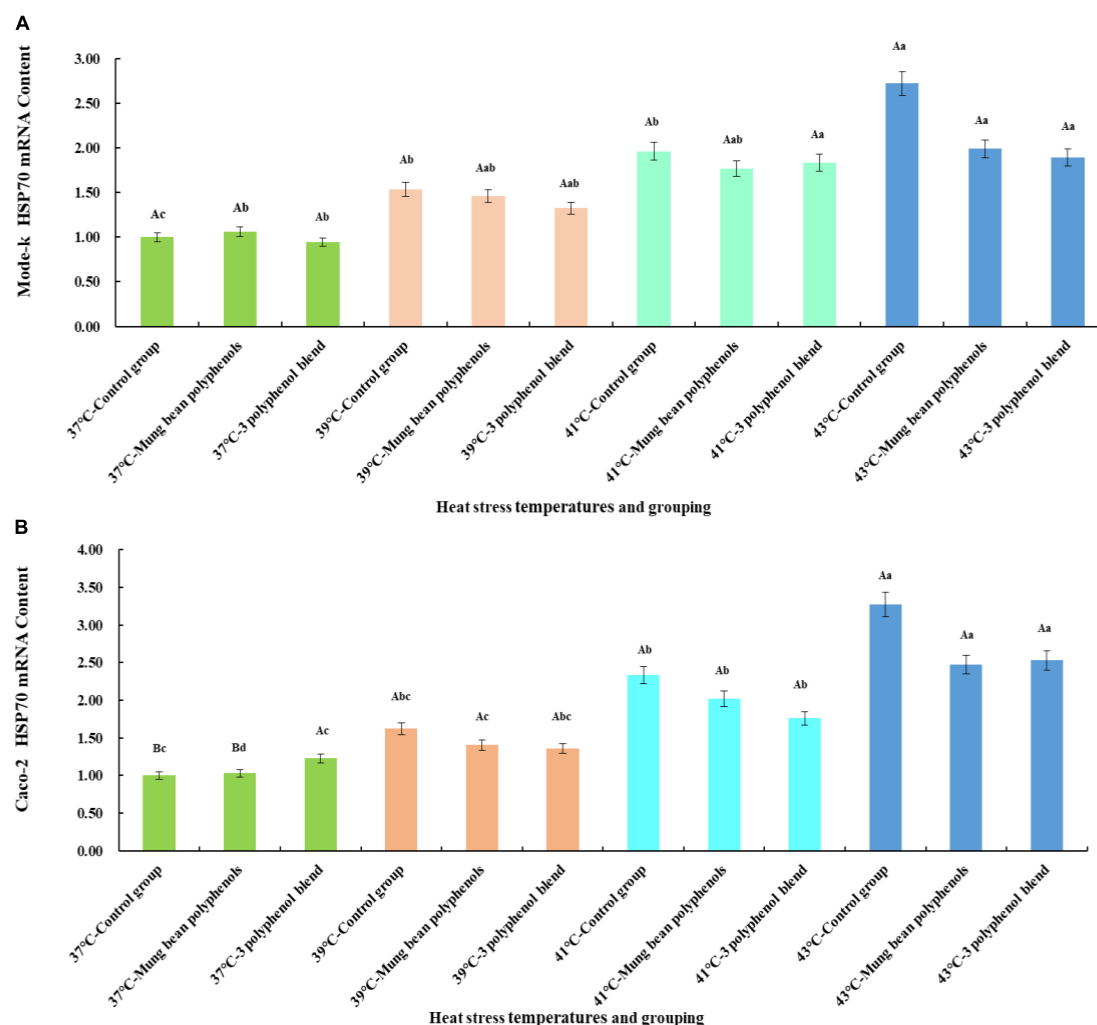


FIGURE 4

(A) Results of the regulation of HSP70 mRNA content in Mode-k cells by mung bean polyphenols and a mixture of three monomeric mung bean polyphenols. (B) Results of the regulation of HSP70 mRNA content in Caco-2 cells by mung bean polyphenols and a mixture of three monomeric mung bean polyphenols.

Orientin has been shown to have anti-inflammatory, antibacterial, antiviral, and antioxidant properties (34–36). Clinical studies have shown that Orientin is a potential treatment for Alzheimer's disease (37), as well as an anti-tumor agent (38). However, studies on the Orientin of heat stress by herbicides have not been reported. Polyphenols, as secondary metabolites, are also a source of feedback from plants to adapt to environmental changes. Wang et al. (39) found that short-term heat stress in plants resulted in a significant increase in caffeic acid content, suggesting a potential role for caffeic acid as an emergent signaling molecule. Bhardwaj Rachana and Ramandeep (40) study confirmed that protective Role of Pre-treatment with Caffeic acid in Wheat Seedlings Against Heat Stress Induced Oxidative Damage. Caffeic acid has a heat stress resistance effect, and its antioxidant properties

have been extensively demonstrated (41). However, caffeic acid has not been reported at the cellular or animal level in response to heat stress.

The results showed that the modeling time for both cell models was 6 h. The modeling time in the existing heat stress cell models was also variable, ranging from 1, 2, 4, to 6 h, which was closely related to the cell source and type. However, many of the available reports did not provide a clear explanation of the basis for the choice of modeling time or only used cell viability as an indicator. There was also some variation in the choice of heat stress temperature, ranging from 38 to 43°C. Many reports have only selected a single heat stress temperature for the study, and the temperature settings for different levels of heat stress have not been adequately studied. The results of this study also confirmed that 39°C,

41°C, and 43°C had different levels of heat stress and that statistically significant differences existed in all indicators at all three temperatures.

### 3.4.3. Confirmation of the main heat stress components

From the quantitative results, it is clear that a high proportion of vitexin, orientin, and caffeic acid was screened. Therefore, to confirm whether the three monomeric polyphenols might be the main components of mung bean that regulate heat stress, the three monomeric polyphenols were formulated in proportion to their content. The HSP70 mRNA content was then compared with that of mung bean polyphenols. The results are shown in [Figure 4](#).

The mode-k cell and Caco-2 cell heat stress model is shown in [Figure 4](#). A significant increase in HSP70 mRNA levels occurred in all three control groups at heat stress temperatures compared to the 37°C control group, indicating that the two types of cells heat stress model was valid. Mung bean polyphenols at 37°C slightly increased HSP70 mRNA content in mode-k cells, and a mixture of three monomeric polyphenols slightly decreased HSP70 mRNA content, but the differences between them were not significant. The mixture of mung bean polyphenols and three monomeric polyphenols reduced HSP70 mRNA content in mode-k and Caco-2 cells at all three heat stress temperatures, and the reduction was greater at higher heat stress temperatures but did not reach a significant reduction. A comparison of the regulatory effect of mung bean polyphenols with that of the three monomeric polyphenols showed that they are similar, with a mixture of the three monomeric polyphenols being somewhat more effective. The results were the same for both cell types, indicating that the mixture of the three monomeric polyphenols was similarly or better regulated than the mung bean polyphenols. The mung bean polyphenols contained other classes of polyphenols in addition to the three monomeric polyphenols. However, the mixture of the three monomeric polyphenols was more effective than the mung bean polyphenols, suggesting that the three monomeric polyphenols are likely to be the main components of heat stress regulation in mung beans. These results reaffirm that mung bean polyphenols have a heat stress-modulating effect.

## 4. Conclusion

The study was based on the mode-k mouse intestinal epithelial cell heat stress model and Caco-2 human rectal colon cancer cells, and six heat stress cell models were successfully constructed at 39°C (mild), 41°C (moderate), and 43°C (severe) using a combination of real-time quantitative PCR and physicochemical index assays. The main nutrient fractions and polyphenolic substances in mung beans were screened for heat stress regulatory fractions, using HSP70 as a key indicator. The results confirmed that polyphenols were the

main heat stress-regulating components in mung beans, among which orientin, vitexin, and caffeic acid were likely the main components. The higher the degree of heat stress, the more significant the regulation effect. Both flavonoids and phenolic acids in mung beans have heat stress-modulating effects. The heat-stress-modulating effects of polyphenols are closely related to their antioxidant properties. A qualitative and quantitative assay for 20 polyphenols was established using targeted analysis. The results of this study provide theoretical support for the regulation of heat stress by polyphenols. However, the present study was a preliminary screening, and the components in mung bean were diverse, with interactions among them. Whether the complexes of components in mung beans have heat stress-modulating effects or other effects requires further investigation. The mechanism of heat stress regulation by mung bean polyphenolic substances at the cellular and *in vivo* levels in animals was the next step in the research program.

## Data availability statement

The data presented in the study are deposited in the Figshare repository, accession number <https://figshare.com/s/7b59de689f7699d41a22>.

## Author contributions

YF: writing—original draft, methodology, and visualization. XF: conceptualization and writing—review and editing. SZ and DS: formal analysis and methodology. YM: data curation and visualization. HW: data curation and investigation. XG: formal analysis and investigation. CW and HY: supervision, project administration, and funding acquisition. All authors contributed to the article and approved the submitted version.

## Funding

This work was supported by the Key Technology and Industrialization of Green and Safe Manufacture of Legumes Health Food (ZY22D050), the Study on Metabolomics of Rice from Different Producing Areas based on GC-MS (XDB-2016-15), the Effect of Mung Bean Peptide on Intestinal Immune Function Induced by Inflammation in *Drosophila Melanogaster* (BYND2020CG002), and the Heilongjiang Bayi Agricultural University Graduate Innovation Project (YJSCX2021-Z04).

## Acknowledgments

We thank Dr. Xu Bin, College of Animal Science and Technology, Heilongjiang Bayi Agricultural University, for providing the cell lines for this experiment.

## Conflict of interest

The authors declare that the research was conducted in the absence of any commercial or financial relationships that could be construed as a potential conflict of interest.

## Publisher's note

All claims expressed in this article are solely those of the authors and do not necessarily represent those of their affiliated

organizations, or those of the publisher, the editors and the reviewers. Any product that may be evaluated in this article, or claim that may be made by its manufacturer, is not guaranteed or endorsed by the publisher.

## Supplementary material

The Supplementary Material for this article can be found online at: <https://www.frontiersin.org/articles/10.3389/fnut.2022.1102752/full#supplementary-material>

## References

- Pawar SS, Sajjanar B, Lonkar VD, Nitin KP, Kadam AS, Nirmale AV, et al. Assessing and mitigating the impact of heat stress in poultry. *Adv Anim Vet Sci.* (2016) 4:332–41. doi: 10.14737/journal.aavs/2016/4.6.332.341
- Wouters H, De Ridder K, Poelmans L, Willems P, Brouwers J, Hosseinzadehtalaei P, et al. Heat stress increase under climate change twice as large in cities as in rural areas: a study for a densely populated midlatitude maritime region. *Geophys Res Lett.* (2017) 44:8997–9007. doi: 10.1002/2017gl074889
- Lemonsu A, Viguié V, Daniel M, Masson V. Vulnerability to heat waves: impact of urban expansion scenarios on urban heat island and heat stress in Paris (France). *Urban Clim.* (2015) 14:586–605. doi: 10.1016/j.uclim.2015.10.007
- Salata F, Golasi I, Petitti D, de Lieto Vollaro E, Coppi M, de Lieto Vollaro A. Relating microclimate, human thermal comfort and health during heat waves: an analysis of heat Island mitigation strategies through a case study in an urban outdoor environment. *Sustain Cities Soc.* (2017) 30:79–96. doi: 10.1016/j.scs.2017.01.006
- Caulfield MP, Cambridge H, Foster SF, McGreevy PD. Heat stress: a major contributor to poor animal welfare associated with long-haul live export voyages. *Vet J.* (2014) 199:223–8. doi: 10.1016/j.tvjl.2013.09.018
- Ellamie AM, Fouda WA, Ibrahim WM, Ramadan G. Dietary supplementation of brown seaweed (*Sargassum latifolium*) alleviates the environmental heat stress-induced toxicity in male *Barki sheep* (*Ovis aries*). *J Therm Biol.* (2020) 89:102561. doi: 10.1016/j.jtherbio.2020.102561
- Watts N, Adger WN, Agnolucci P, Blackstock J, Byass P, Cai W, et al. Health and climate change: policy responses to protect public health. *Lancet.* (2015) 386:1861–914. doi: 10.1016/s0140-6736(15)60854-6
- Cao D, Li H, Yi J, Zhang J, Che H, Cao J, et al. Antioxidant properties of the *Mung bean* flavonoids on alleviating heat stress. *PLoS One.* (2011) 6:e21071. doi: 10.1371/journal.pone.0021071
- Lord-Fontaine S, Averill-Bates DA. Heat shock inactivates cellular antioxidant defenses against hydrogen peroxide: protection by glucose. *Free Radic Biol Med.* (2002) 32:752–65. doi: 10.1016/s0891-5849(02)00769-4
- Altan Ö, Pabuçcuoğlu A, Altan A, Konyalıoğlu S, Bayraktar H. Effect of heat stress on oxidative stress, lipid peroxidation and some stress parameters in broilers. *Br Poult Sci.* (2003) 44:545–50. doi: 10.1080/00071660310001618334
- Mujahid A, Yoshiki Y, Akiba Y, Toyomizu M. Superoxide radical production in chicken skeletal muscle induced by acute heat stress. *Poult Sci.* (2005) 84:307–14. doi: 10.1093/ps/84.2.307
- Lin H, Decuyper E, Buyse J. Acute heat stress induces oxidative stress in broiler chickens. *Comp Biochem Physiol Part A.* (2006) 144:11–7. doi: 10.1016/j.cbpa.2006.01.032
- Sakakibara H, Shimoi K. Anti-stress effects of polyphenols: animal models and human trials. *Food Funct.* (2020) 11:5702–17. doi: 10.1039/d0fo01129k
- Peng X, Zheng Z, Cheng KW, Shan F, Ren GX, Chen F, et al. Inhibitory effect of *Mung bean* extract and its constituents vitexin and isovitexin on the formation of advanced glycation endproducts. *Food Chem.* (2008) 106:475–81. doi: 10.1016/j.foodchem.2007.06.016
- Slawinska A, Mendes S, Dunislawski A, Siwek M, Zampiga M, Sirri F, et al. Avian model to mitigate gut-derived immune response and oxidative stress during heat. *Biosystems.* (2019) 178:10–5. doi: 10.1016/j.biosystems.2019.01.007
- Gilles C, Helen B, Hella H, Sue C. The *Drosophila* Dpit47 protein is a nuclear Hsp90 co-chaperone that interacts with DNA polymerase alpha. *J Cell Sci.* (2001) 114:2015–25. doi: 10.1242/jcs.114.11.2015
- Beckham JT, Wilmink GJ, Mackanos MA, Takahashi K, Contag CH, Takahashi T, et al. Role of HSP70 in cellular thermotolerance. *Lasers Surg Med.* (2008) 40:704–15.
- Du M, Xie J, Gong B, Xu X, Tang W, Li X, et al. Extraction, physicochemical characteristics and functional properties of *Mung bean* protein. *Food Hydrocoll.* (2018) 76:131–40. doi: 10.1016/j.foodhyd.2017.01.003
- Zhang S, Sheng Y, Feng Y, Diao J, Wang C, Zhang D. Changes in structural and functional properties of globulin-polyphenol complexes in *Mung beans*: exploration under different interaction ratios and heat treatment conditions. *Int J Food Sci Technol.* (2021) 57:1–34. doi: 10.1111/ijfs.15180
- Ye HZ. *Preparation, separation, purification and structural identification of Mung bean antioxidant peptides*. Nanchang: Nanchang University (2021). p. 14–25.
- Song QQ. *Research on physicochemical, antioxidant properties of Mung bean polysaccharides activity and its effects on intestinal health of mice*. Nanchang: Nanchang University (2020). p. 12–3.
- Dou KN, Bai CQ. Extraction process optimization and fatty acid composition analysis of glycyrrhiza oil. *J Chin Cereals Oils Assoc.* (2018) 33:102–6.
- Zhang S. *Study on the processing methods on the functional properties and their interaction of polyphenols and proteins in Mung bean*. Heilongjiang: Heilongjiang Bayi Agricultural University (2021). p. 17–8.
- Lahouar L, El Arem A, Ghrairi F, Chahdoura H, Ben Salem H, El Felah M, et al. Phytochemical content and antioxidant properties of diverse varieties of whole barley (*Hordeum vulgare* L.) grown in Tunisia. *Food Chem.* (2014) 145:578–83. doi: 10.1016/j.foodchem.2013.08.102
- Li M, Zhang Y, Xia S, Ding X. Finding and isolation of novel peptides with anti-proliferation ability of hepatocellular carcinoma cells from *Mung bean* protein hydrolysates. *J Funct Foods.* (2019) 62:103557. doi: 10.1016/j.jff.2019.10.3557
- Xie J, Du M, Shen M, Wu T, Lin L. Physico-chemical properties, antioxidant activities and angiotensin-I converting enzyme inhibitory of protein hydrolysates from *Mung bean* (*Vigna radiata*). *Food Chem.* (2019) 270:243–50. doi: 10.1016/j.foodchem.2018.07.103
- Yao Y, Zhu Y, Ren G. Immunoregulatory activities of polysaccharides from *Mung bean*. *Carbohydr Polym.* (2016) 139:61–6. doi: 10.1016/j.carbpol.2015.12.001
- Yao Y, Yang X, Tian J, Liu C, Cheng X, Ren G. Antioxidant and antidiabetic activities of black *Mung bean* (*Vigna radiata* L.). *J Agric Food Chem.* (2013) 61:8104–9. doi: 10.1021/jf401812z
- Pajak P, Socha R, Galkowska D, Rożnowski J, Fortuna T. Phenolic profile and antioxidant activity in selected seeds and sprouts. *Food Chem.* (2014) 143:300–6. doi: 10.1016/j.foodchem.2013.07.064
- Bai Y, Zhang Q, Wang B, Zhang M, Xu Y, Li S, et al. Plasma pharmacokinetics, bioavailability, and tissue distribution of four c-glycosyl flavones from *Mung bean* (*Vigna radiata* L.) seed extracts in rat by ultrahigh-performance liquid chromatography–tandem mass spectrometry. *J Agric Food Chem.* (2017) 65:5570–80. doi: 10.1021/acs.jafc.7b02053

31. Xiao ZM. *The inhibitory effect of orientin in Mung bean on liver cancer and the effect of processing mode on its activity*. Heilongjiang: Heilongjiang Bayi Agricultural University (2020). p. 30–1.
32. Pan ZG, He X, Shao Y, Chen WD, Fang BJ. ROS/JNK-mediated lysosomal injury in rat intestinal epithelial-6 cells during heat stress. *J Therm Biol.* (2022) 109:103326. doi: 10.1016/j.jtherbio.2022.103326
33. Hooper HB, dos Santos Silva P, de Oliveira SA, Merighe GKF, Negrão JA. Acute heat stress induces changes in physiological and cellular responses in *Saanen* goats. *Int J Biometeorol.* (2018) 62:2257–65. doi: 10.1007/s00484-018-1630-3
34. Du SK, Yu XZ, Li ZX. *In vitro* antioxidative activity of ethanol extracts of food legume. *J Chin Inst Food Sci Technol.* (2012) 12:14–9.
35. Liang SL, Liang Q, Zhong WH, Li QY, Yan FG, Zhou XG. Anti-inflammatory and analgesic effects of *Polygonum orientale* extract. *Chin Tradit Herb Drugs.* (2014) 45:3131–5.
36. Xiao Q, Qu Z, Zhao Y, Yang L, Gao P. Orientin ameliorates LPS-induced inflammatory responses through the inhibitory of the NF- $\kappa$ B pathway and NLRP3 inflammasome. *Evid Based Complement Altern Med.* (2017) 2017:2495496. doi: 10.1155/2017/2495496
37. Zhong Y, Zheng Q, Sun C, Zhang Z, Han K, Jia N. Orientin improves cognition by enhancing autophagosome clearance in an Alzheimer's mouse model. *J Mol Neurosci.* (2019) 69:246–53. doi: 10.1007/s12031-019-01353-5
38. Fang AN, Wang SH, Tian QQ, Zhu DX. Effects of orientin and vitexin from *Trollius chinensis* on the growth and apoptosis of esophageal cancer EC-109 cells. *Oncol Lett.* (2015) 10:2627–33. doi: 10.3892/ol.2015.3618
39. Wang J, Yuan B, Huang B. Differential heat-induced changes in phenolic acids associated with genotypic variations in heat tolerance for hard fescue. *Crop Sci.* (2019) 59:667. doi: 10.2135/cropsci2018.01.0063
40. Bhardwaj Rachana D, Ramandeep K. Protective role of pre-treatment with different phenolic acids in wheat seedlings against heat stress induced oxidative damage. *Indian J Agric Biochem.* (2017) 30:147–55. doi: 10.5958/0974-4479.2017.00024.7
41. Khan FA, Maalik A, Murtaza G. Inhibitory mechanism against oxidative stress of caffeic acid. *J Food Drug Anal.* (2016) 24:695–702. doi: 10.1016/j.jfda.2016.05.003
42. Ali NM, Mohd Yusof H, Yeap SK, Ho WY, Beh BK, Long K, et al. Anti-inflammatory and antinociceptive activities of untreated, germinated, and fermented *Mung bean* aqueous extract. *Evid Based Complement Altern Med.* (2014) 2014:350507. doi: 10.1155/2014/350507
43. Chai WM, Wei QM, Deng WL, Zheng YL, Chen XY, Huang Q, et al. Anti-melanogenesis properties of condensed tannins from *Vigna angularis* seeds with potent antioxidant and DNA damage protection activities. *Food Funct.* (2019) 10:99–111. doi: 10.1039/c8fo01979g
44. Das A. Heat stress-induced hepatotoxicity and its prevention by resveratrol in rats. *Toxicol Mech Methods.* (2011) 21:393–9. doi: 10.3109/15376516.2010.550016
45. Frijhoff J, Winyard PG, Zarkovic N, Davies SS, Stocker R, Cheng D, et al. Clinical relevance of biomarkers of oxidative stress. *Antioxid Redox Signal.* (2015) 23:1144–70. doi: 10.1089/ars.2015.6317
46. Giusti F, Caprioli G, Ricciutelli M, Torregiani E, Vittori S, Sagratini G. Analysis of 17 polyphenolic compounds in organic and conventional legumes by high-performance liquid chromatography-diode array detection (HPLC-DAD) and evaluation of their antioxidant activity. *Int J Food Sci Nutr.* (2017) 69:557–65. doi: 10.1080/09637486.2017.1399258
47. Gupta N, Srivastava N, Bhagyawant SS. Vicilin—A major storage protein of mungbean exhibits antioxidative potential, antiproliferative effects and ACE inhibitory activity. *PLoS One.* (2018) 13:e0191265. doi: 10.1371/journal.pone.0191265
48. He S, Li S, Arowolo MA, Yu Q, Chen F, Hu R, et al. Effect of resveratrol on growth performance, rectal temperature and serum parameters of yellow-feather broilers under heat stress. *Anim Sci J.* (2019) 90:401–11. doi: 10.1111/asj.13161
49. Ketha K, Gudipati M. Immunomodulatory activity of non starch polysaccharides isolated from green gram (*Vigna radiata*). *Food Res Int.* (2018) 113:269–76. doi: 10.1016/j.foodres.2018.07.010
50. Li X, Yang Y, Liu S, Yang J, Chen C, Sun Z. Grape seed extract supplementation attenuates the heat stress-induced responses of jejunum epithelial cells in Simmental  $\times$  qinchuan steers. *Br J Nutr.* (2014) 112:347–57. doi: 10.1017/s0007114514001032
51. Liyanage R, Kiramagge C, Visvanathan R, Jayathilake C, Wethasinghe P, Bangamuwage R, et al. Hypolipidemic and hypoglycemic potential of raw, boiled, and sprouted *Mung beans* (*Vigna radiata* L. Wilczek) in rats. *J Food Biochem.* (2017) 42:e12457. doi: 10.1111/jfbc.12457
52. Lopes L, Martins M, Farias L, Brito A, Lima G, Carvalho V, et al. Cholesterol-lowering and liver-protective effects of cooked and germinated *Mung Beans* (*Vigna radiata* L.). *Nutrients.* (2018) 10:821. doi: 10.3390/nu10070821
53. Nakatani A, Li X, Miyamoto J, Igarashi M, Watanabe H, Sutou A, et al. Dietary *Mung bean* protein reduces high-fat diet-induced weight gain by modulating host bile acid metabolism in a gut microbiota-dependent manner. *Biochem Biophys Res Commun.* (2018) 501:955–61. doi: 10.1016/j.bbrc.2018.05.090
54. Sordillo LM, Aitken SL. Impact of oxidative stress on the health and immune function of dairy cattle. *Vet Immunol Immunopathol.* (2009) 128:104–9. doi: 10.1016/j.vetimm.2008.10.305
55. Sahin K, Orhan C, Tuzcu M, Ali S, Sahin N, Hayirli A. Epigallocatechin-3-gallate prevents lipid peroxidation and enhances antioxidant defense system via modulating hepatic nuclear transcription factors in heat-stressed quails. *Poult Sci.* (2010) 89:2251–8. doi: 10.3382/ps.2010-00749
56. Sonklin C, Laohakunjit N, Kerdchoechuen O. Assessment of antioxidant properties of membrane ultrafiltration peptides from *Mungbean* meal protein hydrolysates. *PeerJ.* (2018) 6:e5337. doi: 10.7717/peerj.5337
57. Vandana GD, Bagath M, Sejian V, Krishnan G, Beena V, Bhatta R. Summer season induced heat stress impact on the expression patterns of different toll-like receptor genes in *Malabari goats*. *Biol Rhythm Res.* (2018) 50:466–82. doi: 10.1080/09291016.2018.1464638
58. Watanabe H, Inaba Y, Kimura K, Asahara S, Kido Y, Matsumoto M, et al. Dietary *Mung bean* protein reduces hepatic steatosis, fibrosis, and inflammation in male mice with diet-induced, nonalcoholic fatty liver disease. *J Nutr.* (2016) 147:52–60. doi: 10.3945/jn.116.231662
59. Xie J, Ye H, Du M, Yu Q, Chen Y, Shen M. *Mung bean* protein hydrolysates protect mouse liver cell line Nctc-1469 cell from hydrogen peroxide-induced cell injury. *Foods.* (2019) 9:14. doi: 10.3390/foods9010014
60. Zhu YG. Technical measures to alleviate heat stress in pigs. *China Anim Health.* (2021) 23:79. doi: 10.3969/j.issn.1008-4754.2021.04.05



## OPEN ACCESS

EDITED BY  
Wenyi Kang,  
Henan University, China

REVIEWED BY  
Liyan Zhao,  
Nanjing Agricultural University, China  
Biao Yuan,  
China Pharmaceutical University, China

\*CORRESPONDENCE  
Xuebing Wang  
✉ xbwang74@163.com  
Yue Wei  
✉ 67430218@qq.com

<sup>†</sup>These authors have contributed equally to this work

SPECIALTY SECTION  
This article was submitted to  
Food Chemistry,  
a section of the journal  
Frontiers in Nutrition

RECEIVED 06 January 2023

ACCEPTED 30 January 2023

PUBLISHED 23 February 2023

CITATION  
Li X, Gui R, Wang X, Ning E, Zhang L, Fan Y,  
Chen L, Yu L, Zhu J, Li Z, Wei L, Wang W, Li Z,  
Wei Y and Wang X (2023) Oligosaccharides  
isolated from *Rehmannia glutinosa* protect  
LPS-induced intestinal inflammation and barrier  
injury in mice. *Front. Nutr.* 10:1139006.  
doi: 10.3389/fnut.2023.1139006

COPYRIGHT  
© 2023 Li, Gui, Wang, Ning, Zhang, Fan, Chen,  
Yu, Zhu, Li, Wei, Wang, Li, Wei and Wang. This is  
an open-access article distributed under the  
terms of the [Creative Commons Attribution  
License \(CC BY\)](#). The use, distribution or  
reproduction in other forums is permitted,  
provided the original author(s) and the  
copyright owner(s) are credited and that the  
original publication in this journal is cited, in  
accordance with accepted academic practice.  
No use, distribution or reproduction is  
permitted which does not comply with these  
terms.

# Oligosaccharides isolated from *Rehmannia glutinosa* protect LPS-induced intestinal inflammation and barrier injury in mice

Xiao Li<sup>1,2†</sup>, Rong Gui<sup>2,3†</sup>, Xuefang Wang<sup>1,3</sup>, Erjuan Ning<sup>1,2</sup>,  
Lixian Zhang<sup>1,2</sup>, Yi Fan<sup>2,4</sup>, Ling Chen<sup>1,2</sup>, Liqin Yu<sup>1,2</sup>, Jie Zhu<sup>1,2</sup>,  
Zhining Li<sup>1,2</sup>, Lei Wei<sup>1,2</sup>, Wei Wang<sup>1,2</sup>, Zihong Li<sup>1,2</sup>, Yue Wei<sup>1,2\*</sup> and  
Xuebing Wang<sup>3\*</sup>

<sup>1</sup>Henan Natural Products Biotechnology Co., Ltd., Zhengzhou, China, <sup>2</sup>Biological Center of Henan Academy of Sciences, Zhengzhou, China, <sup>3</sup>College of Animal Medicine, Henan Agricultural University, Zhengzhou, China, <sup>4</sup>Henan High Tech Industry Co., Ltd., Zhengzhou, China

**Objectives:** We investigated the protective effect of *Rehmannia glutinosa* oligosaccharides (RGO) on lipopolysaccharide (LPS)-induced intestinal inflammation and barrier injury among mice.

**Methods:** RGO is prepared from fresh *rehmannia glutinosa* by water extraction, active carbon decolorization, ion exchange resin impurity removal, macroporous adsorption resin purification, and decompression drying. LPS could establish the model for intestinal inflammation and barrier injury in mice. Three different doses of RGO were administered for three consecutive weeks. Then the weight, feces, and health status of the mice were recorded. After sacrificing the mice, their colon length and immune organ index were determined. The morphological changes of the ileum and colon were observed using Hematoxylin-eosin (H&E) staining, followed by measuring the villus length and recess depth. RT-qPCR was utilized to detect the relative mRNA expression of intestinal zonula occludens-1 (*ZO-1*) and *occludin*. The expression of inflammatory factors and oxidation markers within ileum and colon tissues and the digestive enzyme activities in the ileum contents were detected using ELISA. The content of short-chain fatty acids (SCFAs) in the colon was determined with GC. The gut microbial composition and diversity changes were determined with 16S-rRNA high-throughput sequencing. The association between intestinal microorganisms and SCFAs, occludins, digestive enzymes, inflammatory factor contents, and antioxidant indexes was also analyzed.

**Results:** RGO significantly increased the weight, pancreatic index, thymus index, and colon length of mice compared with the model group. Moreover, it also improved the intestinal tissue structure and increased the expression of intestinal barrier-related junction proteins *ZO-1* and *Occludin*. The contents of IL-6, IL-17, IL-1 $\beta$ , and TNF- $\alpha$  in the intestinal tissues of mice were significantly reduced. Additionally, the activities of superoxide dismutase (SOD), glutathione peroxidase (GSH-Px), and catalase (CAT) were elevated. In contrast, the malondialdehyde (MDA) content decreased. Trypsin and pancreatic lipase activities in the ileum enhanced, and the SCFA contents such as acetic acid, propionic acid, and butyric acid in the colon increased. The study on intestinal flora revealed that RGO could enhance the abundance of intestinal flora and improve the flora structure. After RGO intervention, the relative abundance of Firmicutes, *Lactobacillus*, and *Akkermansia* bacteria in the intestinal tract of mice increased compared with the model group, while that of Actinomycetes decreased. The intestinal microbiota structure changed to the case, with probiotics playing a dominant role. The correlation analysis indicated that *Lactobacillus* and *Akkermansia* bacteria in the intestinal tract of mice were positively associated with SCFAs, *Occludin*, *ZO-1*, pancreatic amylase, SOD, and CAT activities. Moreover, they were negatively correlated with inflammatory factors IL-6, IL-17, IL-1 $\beta$ , and TNF- $\alpha$ .



**Conclusions:** RGO can decrease LPS-induced intestinal inflammation and intestinal barrier injury in mice and protect their intestinal function. RGO can ameliorate intestinal inflammation and maintain the intestinal barrier by regulating intestinal flora.

#### KEYWORDS

*Rehmannia glutinosa* oligosaccharide, LPS, intestinal inflammation, barrier injury, intestinal flora

## Introduction

The incidence rate of intestinal inflammatory diseases has gradually increased in recent years, becoming a global health management problem (1). The intestinal tract is the leading site of digestion and absorption, and the intestinal mucosa has rich blood vessels. Inflammation will lead to intestinal barrier injury. Simultaneously, intestinal barrier injury is also involved in various intestinal diseases, closely associated with inflammatory bowel disease, bacterial enteritis, and Crohn's disease (2). Intestinal injury can cause emaciation, malnutrition, stunted growth, and even death of patients, among severe cases (3). The timely and appropriate application of enteral nutrition can effectively enhance the nutritional status of patients and alleviate the release of intestinal inflammatory factors. Moreover, it effectively improves intestinal mucosal injury, significantly maintaining the health of the intestinal system (4). Hormones and antibiotics for treating intestinal inflammation have noticeable therapeutic effects, but they can also cause potential damage to the body. Therefore, using natural nutritional agents without side effects for treatment and prevention is a new method for treating intestinal inflammatory diseases.

*Rehmannia glutinosa* is the root tuber of the Scrophulariaceae plant *Rehmannia*. It is a traditional Chinese medicine with the functions of nourishing Yin, clearing heat, tonifying blood, and stopping bleeding. *Rehmannia* has a long history of consumption in China. Around 1,000 years ago, in Huaqing Prefecture and other *Rehmannia*-producing areas in Henan Province, people "pickled the *Rehmannia* into pickles, and soaked in wine and tea for consumption." *Rehmannia* is still shredded and served cold or boiled into porridge. Studies have depicted that the main chemical components of *Rehmannia glutinosa* are iridoid glycosides, oligosaccharides, polysaccharides, and amino acids, which are the material basis for it to play its role (5). Oligosaccharides are low molecular weight sugar polymers formed by the condensation of 3–9 monosaccharides by glycosidic bonds (6). These oligosaccharides cannot be easily digested and hydrolyzed in the small intestine. Instead, they are utilized by probiotics after entering the hindgut to enhance the proliferation of beneficial bacteria and contribute to the stability of intestinal microecology (7). Several studies have demonstrated that intestinal microorganisms are closely related to intestinal health and function. Once the balance of intestinal flora is destroyed, it can lead to excessive consumption of the mucosal layer and accelerated apoptosis of intestinal mucosal epithelial cells, thereby damaging the intestinal mucosal barrier. Many pathogenic bacteria could invade to trigger a strong intestinal immune response, increasing the secretion of various intestinal inflammatory factors and ultimately inducing digestive and absorption dysfunction (8–10). However, it has not been reported whether RGO can ameliorate intestinal inflammation and maintain the intestinal barrier by regulating intestinal microbiota.

LPS comprises lipids and polysaccharides at the outermost layer of the cell wall of gram-negative bacteria and is an inflammatory stimulator (9). Studies have indicated that LPS can bind to TLR4 receptors on the cell surface. They activate nuclear factor- $\kappa$ B (NF- $\kappa$ B) through the MyD88 pathway and then enter the nucleus to induce the synthesis and release of cytokines. These include tumor necrosis factor- $\alpha$  (TNF- $\alpha$ ), interferon- $\gamma$  (IFN- $\gamma$ ), interleukin-6 (IL-6), etc., which causes intestinal inflammation (11). Long-term exposure to heterogeneous LPS can destroy the intestinal mucosal barrier, causing intestinal flora homeostasis (12). The amount of SCFAs produced can indirectly reflect the balance of intestinal flora, and the content of intestinal tight junction protein can also reflect the health of intestinal barrier. Therefore, in this study, LPS was used to construct an animal model for intestinal inflammation and barrier injury using mice to explore the protective effect of RGO on LPS-induced intestinal inflammation and barrier injury in mice. Moreover, the relationship between RGO and intestinal microorganisms was also assessed, thus providing the theoretical basis for applying RGO in intestinal inflammatory diseases.

## Materials and methods

### Materials and reagents

Fresh Rhizomes of *Rehmannia glutinosa* were obtained from Wuzhi County, Henan Province, China (35° 1' 23" north latitude, 113° 18' 76" east longitude) in December 2021. Stachyose (NO. 112031-201701), sucrose (NO. 11507-202105), raffinose (NO. 190225-201901), and verbascose (NO. 111530-201914) were purchased from China Institute for Food and Drug Control.

Dexamethasone tablets were purchased from Tangshan Longkang Pharmaceutical Co., Ltd.

The lipopolysaccharide (LPS) was purchased from Sigma Company in the United States. The detection kits for TNF- $\alpha$ , IL-6, IL-17, and IL-1 $\beta$  were purchased from Shanghai Enzyme-linked Biotechnology Co., Ltd. Moreover, the detection kits for SOD, MDA, GSH-Px, and CAT were purchased from the Nanjing Jiancheng Bioengineering Research Institute. Additionally, the digestion enzyme test kits were purchased from Beijing SOLEBAR Technology Co., Ltd. All other chemicals, solvents, and reagents were of pure analytical grade.

### Preparation of RGO

Fresh Rhizomes of *Rehmannia glutinosa* were cut into small pieces of 5–10 mm after being washed, added four times the amount of water, and extracted twice at 90°C, at 1 h duration. The two extracts were combined, adding activated carbon (2 g/100 ml) and activated

clay (2 g/100 ml) to the extract. It was stirred and decolorized at 80°C for 30 min, then centrifuged. The supernatant was passed through 001 × 7 cation exchange resin column (diameter: high = 6:1), D201 type anion exchange resin column (diameter: high = 6:1), D101 macroporous adsorption resin column (diameter: high = 10:1) one by one, sample volume (mL): resin column volume = 1:1.5, flow rate was 500 mL/h. Finally, the macroporous adsorption resin effluent was collected and concentrated and dried at 60°C to get white powder, that is RGO.

The type and content of oligosaccharides in RGO were detected using high-performance liquid chromatography (HPLC) (Agilent1260), configured using a Refractive Index Detector (RID) (13). The standard reference substances of sucrose, stachyose, raffinose, and mulberry sugar were weighed precisely and prepared with 70% acetonitrile aqueous solution into the standard reference solution with a concentration of 0.5 mg/mL, respectively. The RGO powder was also weighed precisely, and prepared with 70% acetonitrile aqueous solution into the sample solution with a concentration of 1 mg/mL. The chromatographic column was Agilent ZORBOX NH2 (4.6 mm × 250 mm, 5 μm); the mobile phase was acetonitrile: water (7:3); the injection volume was 10 μL, the flow rate was 1.0 mL/min, and the temperature of column incubator was 40°C. The temperature of the detection was 50°C with RID. The types of oligosaccharides in RGO were determined by comparing the HPLC peaks of reference substance with those in RGO, and the content of oligosaccharides was calculated by external standard method.

## Animal and experimental design

We purchased 36 KM mice from Henan Scribes Biotechnology Co., Ltd. The mice were fed for 7 days before the experiment to acclimate to the environment. The mice were randomly divided into six groups, namely normal (N), model (M), treatment (T), RGO low dose (RL, 0.25 g/kg), RGO medium dose (RM, 0.5 g/kg), and RGO high dose (RH, 1 g/kg) groups. Six mice were in each group, and the test period was 21 days. Except for the normal group, on the 9th, 13th, 17th, and 21st days, 0.2 mL of normal saline was injected intraperitoneally. 0.2 mL of 1 mg/kg LPS was injected intraperitoneally in all other groups to develop mice models of intestinal inflammation and barrier injury (14, 15). From the first day of the test, mice in RL, RM, and RH groups were provided 0.2 mL of RGO solution by gavage once a day for 21 days. The mice in the N, M, and T groups were gavaged with an equal volume of normal saline daily. After each intraperitoneal LPS injection, the mice in the T group were gavaged with 0.2 mL dexamethasone solution at 0.5 mg/kg dose 30 min. All the groups were fed adequate food and free to drink water. The weight of mice was determined on the 1<sup>st</sup>, 7<sup>th</sup>, 14<sup>th</sup>, and 21<sup>st</sup> days of the test. Additionally, the food intake,

fecal properties, and health status of mice were observed and recorded daily.

## Sample collection

On the 21<sup>st</sup> day of the test, the mice were sacrificed under ether anesthesia after 6 h of LPS treatment and dissected. The thymus, spleen, and liver tissues were collected, rinsed with PBS solution, blotted dry using filter paper, and weighed. Then the immune organ index of the mice was calculated. The whole colon was taken, and the length of the colon was measured. The ileum and colon tissues and their contents were collected to detect related indicators. A part of the intestinal tissue was placed in 4% paraformaldehyde for histopathological analysis. Then, the rest of the intestinal tissue and contents were stored at −80°C.

Immune organ index = weight of organ (mg)/body weight (g).

## Histopathology

The ileum and colon tissues of mice were extracted from a 4% paraformaldehyde solution. About 1 cm of the middle segment was dehydrated using ethanol, hyalinized in xylene, embedded in paraffin, and sectioned (4–6 μm). The pathologic slices were made with Hematoxylin-eosin (H&E) staining, and the morphology of intestinal tissues was observed using a light microscope (Olympus, DP-72, Tokyo, Japan). The jejunum villus length, the colonic fold height, and the depth of the crypt of the ileum and colon were evaluated.

## RT-qPCR detection

The total RNA of the ileum and colon mucosa was extracted using the Trizol method. Then, 1,000 ng of total RNA was reverse transcribed into cDNA with RT Super Mix and stored at −80°C. β-actin was utilized as the reference gene. The primer sequences of the target gene and the reference gene are shown in Table 1. The cDNA was used as the template for real-time PCR (16). Reaction procedures: High-temperature denaturation was performed at 95°C for 10 min, renaturation at 95°C for 15 s, and primer extension at 60°C for the 60 s. This was repeated for 40 cycles. Cycle threshold (Ct) values were utilized for the relative quantification of RT-qPCR amplification. The Ct value method compared the expression of target genes associated with β-actin.

TABLE 1 Primer sequence.

Gene name	Upstream primer	Downstream primer
ZO-1	5'-GGGTCATCATCTCTGCACCT-3'	5'-GGTCATAAGTCCCTCCACGA-3'
Occludin	5'-AACAAACCCTTCCAAGTTCC-3'	5'-CTCCCAGAGTTCCGATTAC-3'
β-actin	5'-ACCTCCAGGACGACGACTTTGAT-3'	5'-GTGTCTTCTGCACGTACTCCA-3'

## Enzyme-linked immunosorbent assay

Precooled normal saline was added to the ileum and colon tissues of mice at the ratio of weight (g): volume (ml) = 1:10, respectively. The homogenate was mechanically homogenized at 3,000 r/min and centrifuged for 15 min under ice-water bath conditions. The supernatant was taken, and according to the kit's instructions, the contents of IL-6, IL-17, TNF- $\alpha$ , IL-1 $\beta$ , MDA, SOD, GSH-Px, and CAT were determined.

## Digestive enzyme detection

Precooled normal saline was added to the middle ileum of mice at the ratio of weight (g): volume (ml) = 1:10. A high-speed grinder centrifuged them at 3,000 r/min for 15 min, and the supernatant was taken. The activities of trypsin, lipase and amylase were determined based on the kit's instructions.

## SCFA content in feces

The colon contents of mice were weighed accurately. Methanol was added at a ratio of 1:5 (mg:  $\mu$ L). The mixture was stirred for 30 s to form a uniform suspension. A small amount of concentrated sulfuric acid solution was added to adjust the pH to 2–3. The samples were left at room temperature for 10 min through continuous shaking. Then, the samples were centrifuged at 12,000 rpm for 10 min. Ten microliter of supernatant was taken, and the content of SCFA was determined through the Shimadzu GC-2014C gas chromatograph (Shimadzu, Japan), the flame ionization detector, and the DB-FFAP capillary column (30 m  $\times$  0.25 mm  $\times$  0.25 mm) (17).

## 16S rRNA high-throughput sequencing analysis of intestinal flora

The colonic contents of mice were obtained through 16S rRNA high-throughput sequencing, commissioned by Shanghai Parsono Biotechnology Co., Ltd.

## Statistical analysis

Microsoft Excel software were used for Preliminary statistical. GraphPad Prism 8 software was used for image processing. All data were collected in triplicate and the average value was used for analysis and the data were statistically compared for significant differences by one-way analysis of variance (One-Way ANOVA) and Duncan's multiple comparisons using SPSS 22.0 software.

## Results

### Identification and content determination of RGO

Determination of main components of RGO by HPLC, The peak positions of sucrose, raffinose, stachyose and verbascode were 7.164, 10.052, 15.001, 22.778 min, respectively, The RGO isolated in this experiment have chromatographic peaks in the corresponding position. The contents of sucrose, raffinose, stachyose, and verbascode in the prepared RGO were 7.52, 5.19, 81.02, and 4.85%, respectively, Moreover, the total amount of oligosaccharides was 91.06%. The HPLC chromatogram is shown in Figure 1.

### Effects of RGO on body weight, organ index, and colon length in LPS mice

As shown in Figure 1, no significant difference was observed in the body mass of mice from each group before the intraperitoneal LPS injection. After the LPS injection, the mice in the M group showed symptoms of movement retardation, in appetite, soft stools, tears, listlessness, and messy fur. During the experiment, the body weight gain of mice in the M group was significantly decreased ( $P < 0.01$ ) compared with the N group. Moreover, the body weight gain of mice in RL, RM, RH, and T groups was significantly increased compared with the M group ( $P < 0.01$ ). Among them, the weight gain in the RL and T groups was significantly lower than in the N group ( $P < 0.05$ ). The body weight gain in the RH group revealed no significant difference from that in the N group ( $P < 0.05$ ). The body weight gain in the

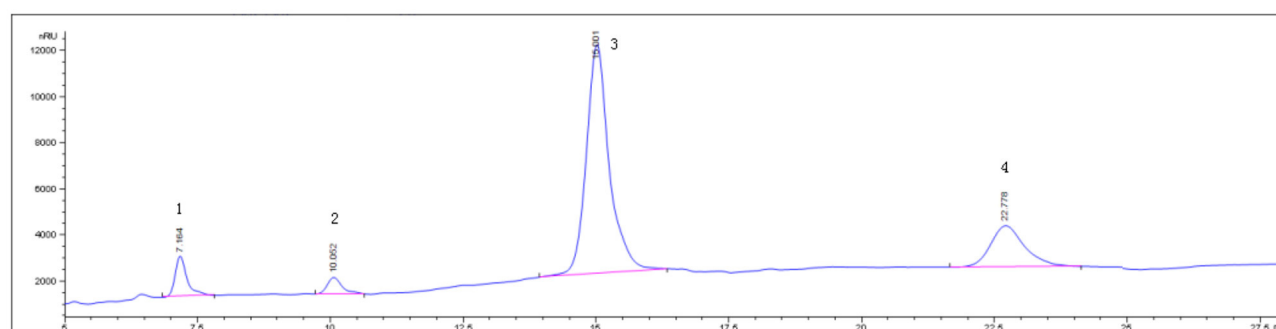


FIGURE 1  
RGO HPLC chromatogram (1 sucrose, 2 raffinose, 3 stachyose, 4 verbascode).

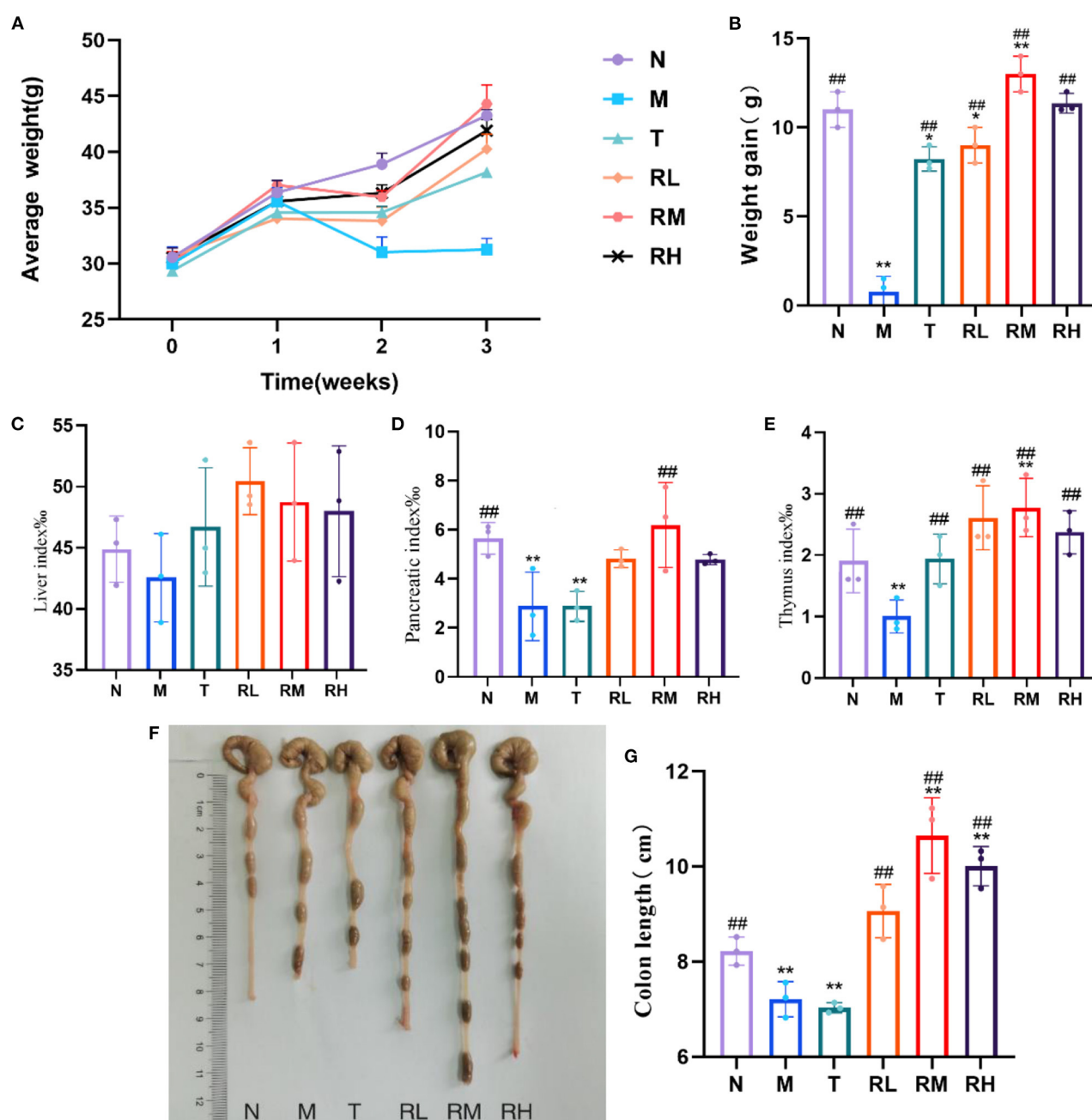


FIGURE 2

Changes of body weight, immune organ index and colon length in mice during the test. (A) Weekly body weight of mice. (B) Body weight gain of mice. (C) Liver index. (D) Pancreatic index. (E) Thymus index. (F) Colon of mice. (G) Length of colon. Compared with group N: \* $P < 0.05$ , \*\* $P < 0.01$ ; compared with group M. # $P < 0.05$ , ## $P < 0.01$ .

RM group was significantly higher than the N group ( $P < 0.05$ ) (Figures 2A, B). Thus, RGO could inhibit LPS-induced weight loss within mice.

The liver index of mice in each experimental group had no significant difference compared with group N. In contrast, the pancreas and thymus indexes of mice in the M and T groups were significantly reduced ( $P < 0.01$ ). Compared with the M group, the pancreas index of mice in the RM group was significantly elevated ( $P < 0.01$ ). Moreover, the thymus index of mice in RL, RM, RH, and T groups was significantly

increased ( $P < 0.01$ ) (Figures 2C–E). We also determined the colon length of mice within each experimental group. Compared with the N group, the colon length of mice in the M and T groups was significantly reduced ( $P < 0.01$ ). However, the colon length of mice in RL, RM, and RH groups increased significantly compared with the M group ( $P < 0.01$ ) (Figures 2F, G). These results demonstrated that LPS induced atrophy of the pancreas, thymus, and colon in mice. RGO intervention could decrease the atrophy of the pancreas, thymus, and colon in LPS mice and protect them.



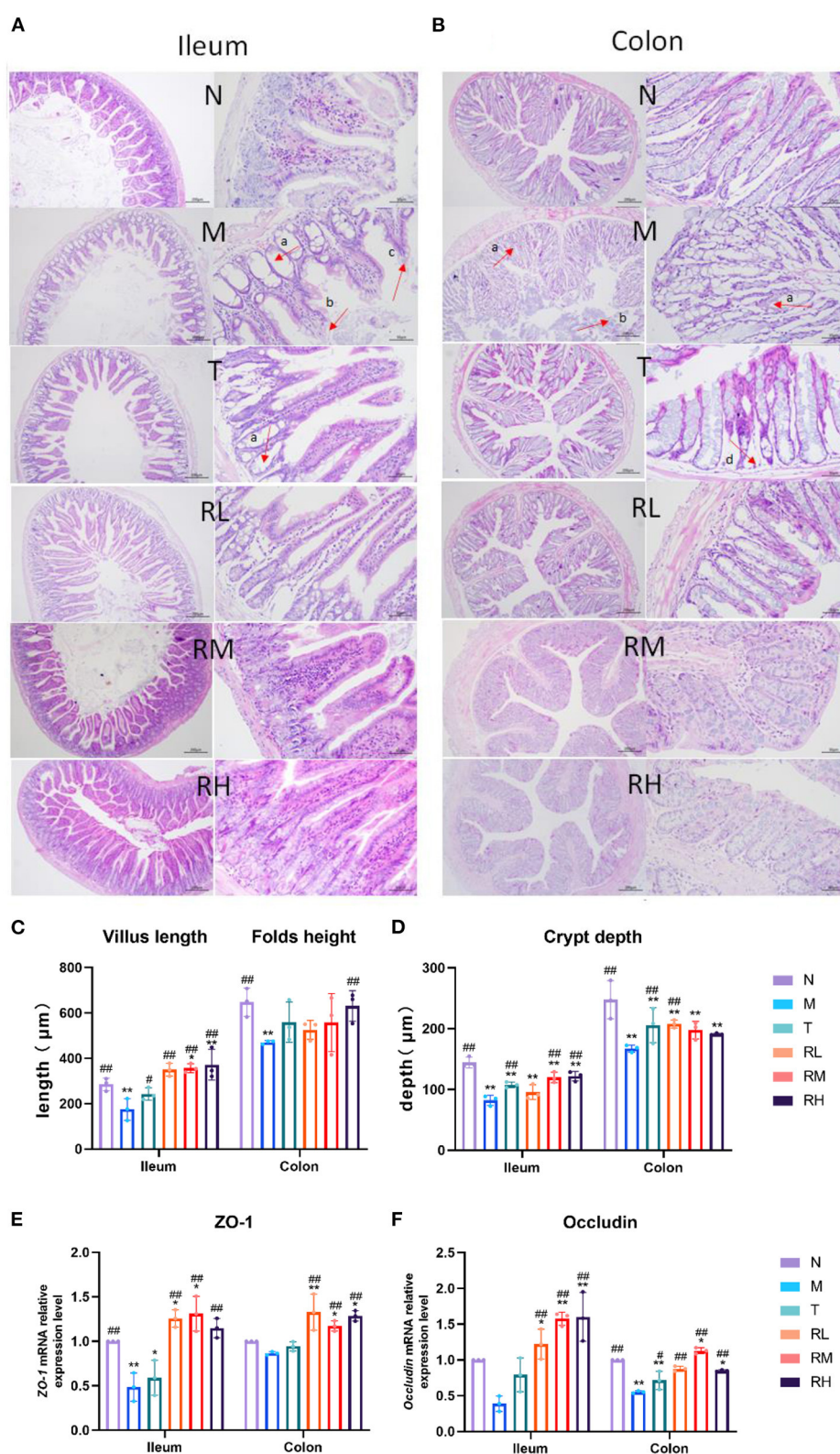


FIGURE 3

Effect of RGO on intestinal epithelial barrier in LPS mice. (A) Pathological assessment of H&E-stained mice ileum sections; magnification 10× and 40×. (B) Pathological assessment of H&E-stained mice colon sections; magnification 10× and 40×. (C) Villus length and folds height. (D) Crypt depth. (E) ZO-1 mRNA relative expression level. (F) Occludin mRNA relative expression level (a. Intestinal gland necrosis; b. Epithelial cell exfoliation; c. The villus becomes shorter; d. Necrosis of intestinal gland basal layer). Compared with group N: \* $P < 0.05$ , \*\* $P < 0.01$ ; compared with group M: # $P < 0.05$ , ## $P < 0.01$ .



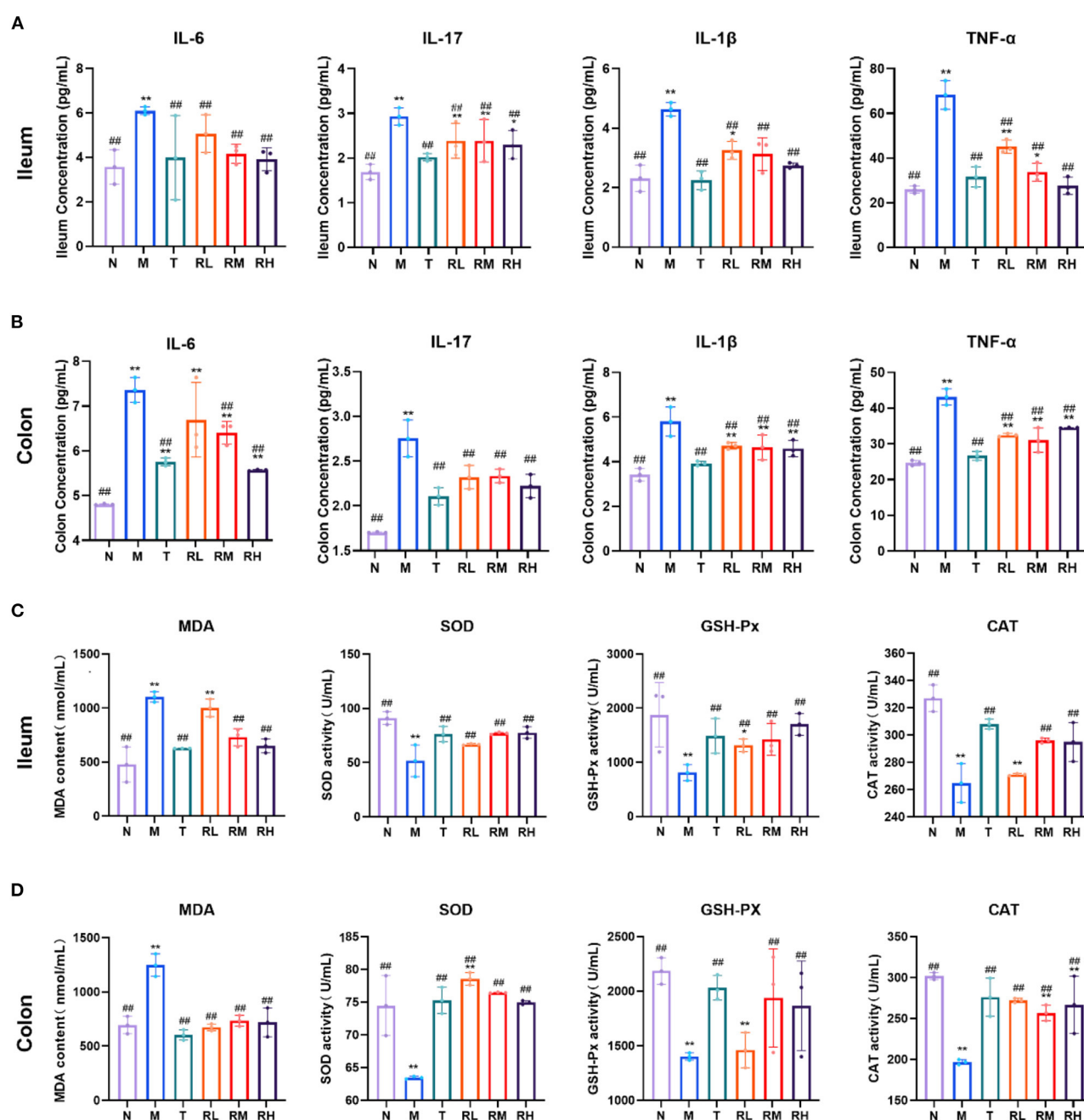


FIGURE 4

The effect of RGO on intestinal inflammatory factors and oxidative indexes in LPS mice. (A) IL-6, IL-17, IL-1β, and TNF-α levels in the ileum. (B) IL-6, IL-17, IL-1β, and TNF-α levels in the colon. (C) MDA, SOD, GSH-Px, and CAT levels in the ileum. (D) MDA, SOD, GSH-Px, and CAT levels in the colon. Compared with group N: \* $P < 0.05$ , \*\* $P < 0.01$ ; compared with group M: # $P < 0.05$ , ## $P < 0.01$ .

## Effects of RGO on intestinal epithelial barrier in LPS mice

We used H&E-stained to detect the pathological changes in the ileum and colon and investigate the effect of RGO on the intestinal epithelial barrier of LPS mice (Figures 3A, B). From the pathological section of the ileum and colon, it could be observed that the intestinal mucosa of mice in the N group was intact. Moreover, the villi of the small intestine were arranged closely and regularly, and the morphology of epithelial cells was normal. In the

M group, intestinal gland necrosis, villus shortening, necrosis, and abscission of part of villous epithelium in the ileum, intestinal gland necrosis, goblet cell abscission, and other pathological conditions in the colon were observed. In each administration group, the exfoliation of intestinal epithelial cells was milder, the villus was arranged orderly, inflammatory cell infiltration was reduced, and infection symptoms were alleviated. The villus length and crypt depth of the ileum and the height and crypt depth of colonic folds were evaluated (Figures 3C, D). Compared with group N, the ileal villi length of mice in group M was significantly shortened ( $P <$

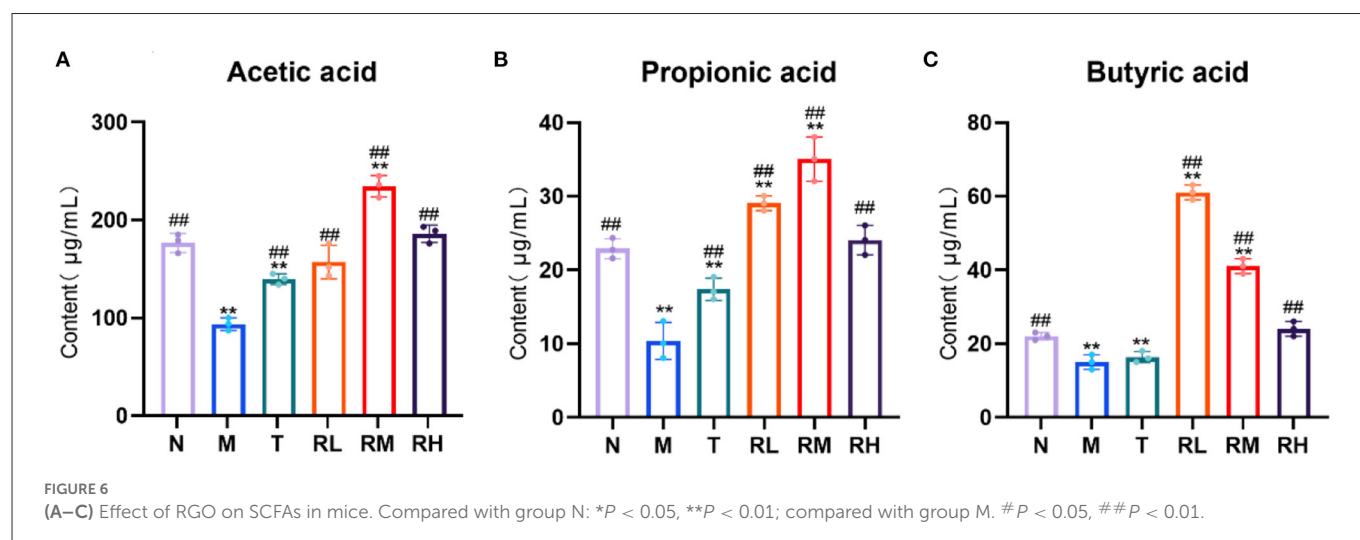
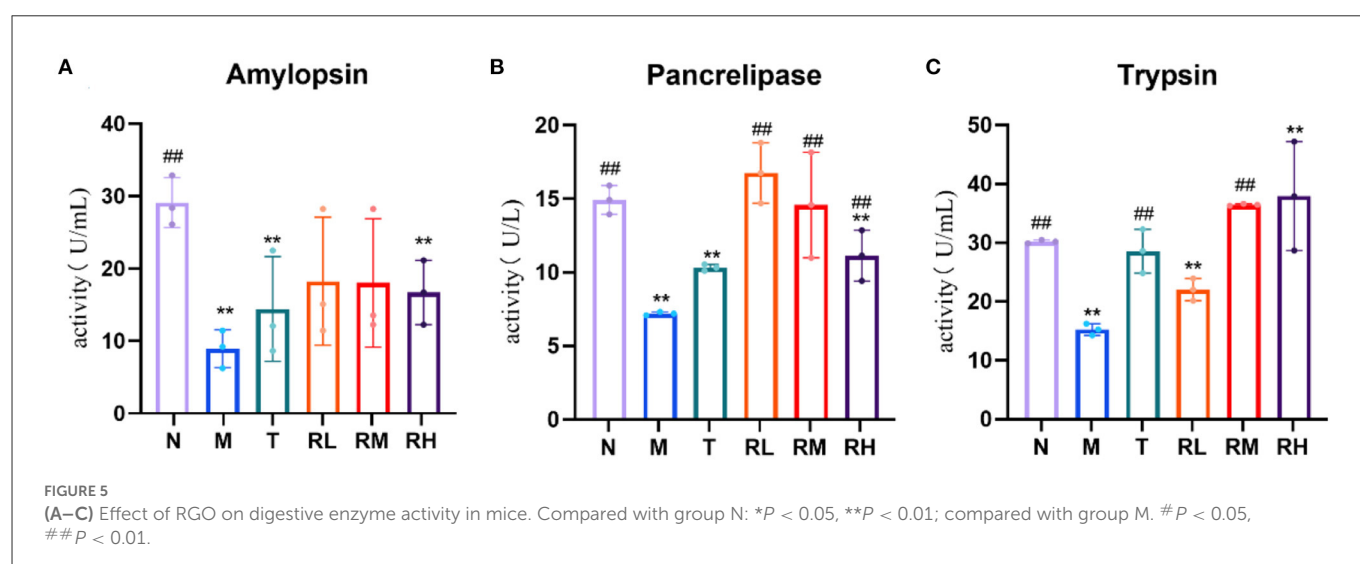
0.01). Additionally, the height of colonic folds was significantly reduced ( $P < 0.01$ ), and the depth of the ileal colonic recess was significantly enhanced ( $P < 0.01$ ). This indicated that LPS caused intestinal villi damage, recess deepening, and intestinal epithelial barrier injury among mice. The villus length of the ileum of the mice in the RM and RH groups increased significantly ( $P < 0.01$ ) compared with the M group. Moreover, the height of colonic folds in the RH group increased significantly ( $P < 0.01$ ), and the depth of the ileal crypt in the RL, RM, and RH groups significantly decreased ( $P < 0.01$ ).

RT-qPCR detected the relative mRNA expression of the intestinal barrier-related junction proteins *Occludin* and *ZO-1* (Figures 3E, F). The results indicated that the relative mRNA expression of *Occludin* and *ZO-1* in mice ileum and colon mucosa in group M was lower than in group N. The relative mRNA expression of *Occludin* and *ZO-1* in mice ileum and colon mucosa in RL, RM, and RH groups was significantly increased compared with the M group ( $P < 0.01$ ). These results indicated that RGO could enhance the intestinal morphology of LPS mice, increase the length of the intestinal villus, the height of the colonic fold, and the depth of the ileocolic crypt. Furthermore, it can increase the relative mRNA expression of intestinal tight junction

protein and alleviate intestinal morphology and epithelial barrier damage in LPS mice.

## Effects of RGO on intestinal inflammation and oxidative indexes in LPS mice

ELISA could detect the expression of related inflammatory factors in the ileum and colon and identify the effect of RGO on intestinal inflammation in LPS mice (Figures 4A, B). The results indicated that compared with the N group, the levels of IL-6, IL-17, IL-1 $\beta$ , and TNF- $\alpha$  in the ileum and colon tissues of the M group elevated significantly ( $P < 0.01$ ). Compared with the M group, the levels of IL-6, IL-17, IL-1 $\beta$ , and TNF- $\alpha$  in the ileum of mice in RL, RM, and RH groups were significantly decreased ( $P < 0.01$ ). However, there was no significant difference in the level of IL-6 in the colon between the RL and M groups. IL-6, IL-17, IL-1 $\beta$ , and TNF- $\alpha$  levels in the colon of RL, RM, and RH groups were significantly reduced ( $P < 0.01$ ). These results depicted that RGO intervention could decrease the levels of intestinal inflammatory factors in LPS mice.



Inflammatory injury is often accompanied by oxidative damage to LPS-induced intestinal mucosal injury. Therefore, intestinal oxidative indicators were also measured in LPS mice. The results indicated that in the ileum tissue of mice, compared with group N, the MDA level in group M increased significantly ( $P < 0.01$ ). In contrast, the SOD, GSH-Px, and CAT levels decreased significantly ( $P < 0.01$ ). Compared with the M group, the MDA levels in RL, RM, RH, and T groups decreased significantly ( $P < 0.01$ ). However, the SOD and GSH-Px levels increased significantly ( $P < 0.01$ ). CAT levels in RL, RM and T groups also increased significantly ( $P < 0.01$ ) (Figure 4C). In the colon tissue of mice, the level of MDA in group M was significantly elevated compared with group N ( $P < 0.01$ ). In contrast, the SOD, GSH-Px, and CAT levels were significantly decreased ( $P < 0.01$ ). After RGO intervention, the SOD, GSH-Px, and CAT levels in T, RM, and RH groups were significantly increased compared with group M ( $P < 0.01$ ). The SOD and CAT levels in group RL were also significantly enhanced ( $P < 0.01$ ), but the GSH-Px levels were insignificant (Figure 4D). These results indicated that RGO intervention could improve the antioxidant capacity of the intestinal tract of mice.

## Effects of RGO on intestinal digestive enzymes in LPS mice

Compared with the N group, the pancreatic amylase, lipase, and trypsin activities in the ileum of mice in the M group were significantly decreased ( $P < 0.01$ ). Compared with the M group, the activities of pancreatic lipase in RL, RM, and RH groups were significantly enhanced ( $P < 0.01$ ). Trypsin activity in group RM was significantly increased ( $P < 0.01$ ). However, there was no significant difference in pancreatic amylase activity (Figure 5). These results indicated that RGO intervention could restore the activities of trypsin and lipase within the intestinal tract of LPS mice.

## Effects of RGO on the content of intestinal SCFAs in LPS mice

SCFAs are metabolites of the intestinal flora. Compared with the N group, acetic acid, propionic acid, and butyric acid in the colon contents of the mice in the M group were significantly decreased ( $P < 0.01$ ). It depicted that LPS had an inhibitory effect on the production of SCFAs. Compared with the M group, acetic acid, propionic acid, and butyric acid in RL, RM, and RH groups were significantly elevated ( $P < 0.01$ ). Among them, the contents of acetic acid and propionic acid in the RM group were the highest, while the butyric acid in the RL group was the highest (Figure 6). These results indicated that RGO intervention could enhance the content of SCFAs in the intestinal tract of LPS mice. Moreover, we also suggested that RGO could elevate the content of SCFAs by controlling the composition of the intestinal microorganisms.

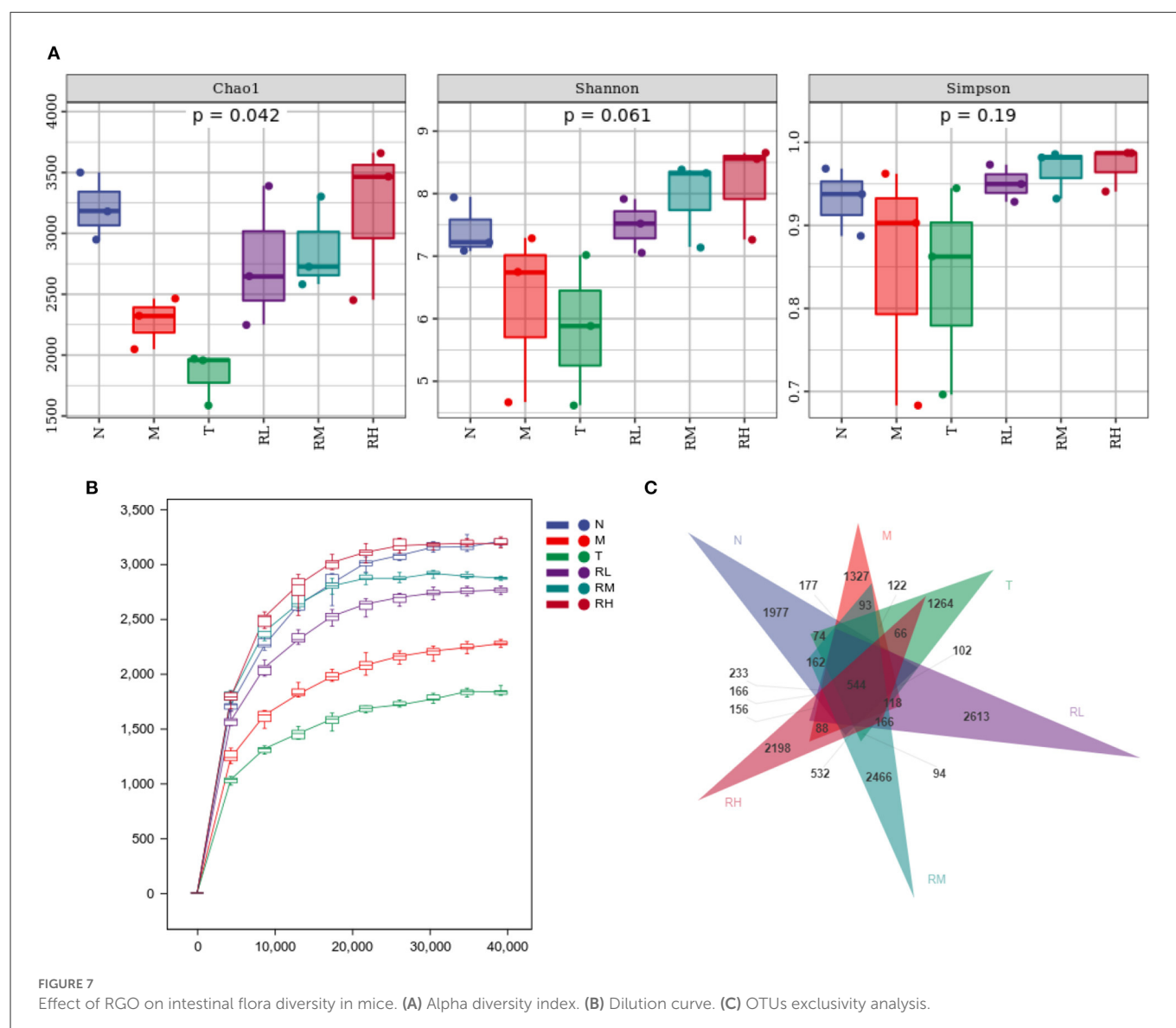
## Effects of RGO on intestinal flora of LPS mice

16S rRNA could determine the diversity and species richness of intestinal microorganisms in mice from different treatment groups. Alpha diversity analysis revealed that the species richness index Chao1 of N, RL, RM, and RH groups was much higher than that of M and T groups, showing significant differences ( $P < 0.05$ ). At the same time, the Shannon diversity index and Simpson diversity index were also higher than the M and T groups, without any significant difference (Figure 7A). The Rarefaction curves revealed that all curves tended to be parallel as the number of sequences increased, depicting that the sequencing data met the analysis needs (Figure 7B). Exclusivity analysis of OTUs showed that 14,738 OTUs were obtained using alignment. The proportions of annotated OTUs at the phyla, genus, and species levels were 98.14, 40.73, and 5.68%, respectively. The number of bacterial species in the RL, RM, RH, and N groups was significantly higher than in M and T groups ( $P < 0.05$ ). There was no significant difference between the M and T groups. Compared with the M group, the number of species in RL, RM, and RH groups elevated by 14.55% ( $P < 0.05$ ), 19.09% ( $P < 0.05$ ), and 22.74% ( $P < 0.05$ ), respectively (Figure 7C).

At the phyla level, the microflora with a larger abundance of mouse intestinal microbes was mainly *Firmicutes*, *Bacteroides*, *Proteobacteria*, and *Actinobacteria*. *Firmicutes* and *Bacteroides* had the highest relative abundance, having more than 90% of the total microbial biomass (Figure 8A). Compared with group N, the relative abundance of *Firmicutes* among intestinal microorganisms of mice in group M was significantly decreased. The relative abundance of *Proteobacteria* was significantly enhanced ( $P < 0.01$ ). The abnormal expansion of *Proteobacteria* reduced the ability to regulate the balance of the intestinal microbial community. The increase in *Proteobacteria* was considered a potential feature of ecological imbalance and disease risk (18). After RGO intervention, compared with the M group, the relative abundance of *Proteobacteria* in RL, RM, and RH groups decreased significantly ( $P < 0.01$ ), while the relative abundance of *Firmicutes* increased. The relative abundance of *Firmicutes* in the RH group increased significantly ( $P < 0.01$ ).

At the genus level, *Lactobacillus* and *Bacteroides* were the primary genera of intestinal microorganisms in mice (Figure 8B). The relative abundance of the two genera in group N was 41.40 and 7.10%, respectively. Compared with group N, the relative abundance of *Lactobacillus* in the M and T groups was reduced to 29.87 and 17.68%, respectively. Lactic acid bacteria have been a common probiotic to regulate intestinal ecological balance. After RGO intervention, the relative abundance of *Lactobacillus* in the RH group (57.12%) was significantly higher than that in the M group ( $P < 0.01$ ). In contrast, the relative abundance of *Bacteroides*, *Prevotella*, and *Oscillospira* had no significant change.

At the species level, intestinal microorganisms among mice with relatively high abundance included *Bacteroides barnesiae*, *Lactobacillus vaginalis*, *Lactobacillus hamsteri*, *Akkermania musciniphila*, and *Lactobacillus salivarius*. Compared with the M group, the relative abundance of *Akkermania musciniphila* in the RM and RH groups was significantly enhanced ( $P < 0.01$ ). Moreover, the relative abundance of *Lactobacillus vaginalis*, *Lactobacillus hamsteri*, and *Lactobacillus salivarius* in the RH group



significantly increased ( $P < 0.01$ ). Cluster analysis revealed that the intestinal flora structure of the *Rehmannia glutinosa* oligosaccharides group was clustered into one group. Thus, the effects of different doses of RGO on intestinal microorganisms were consistent (Figure 8C). Therefore, RGO regulates intestinal flora imbalance in LPS mice.

## Correlation between intestinal microorganisms and SCFAs, tight junction proteins, digestive enzymes, inflammatory factors, and antioxidant indexes

The analysis revealed that *Lactobacillus*, *Akkermansia*, and *Alistipes massiliensis* in the intestinal tract of mice were positively associated with SCFAs, *Occludin*, *ZO-1*, pancreatic amylase, and SOD activities (Figure 9). Moreover, they were negatively correlated with inflammatory factors. Such as IL-6, IL-17, IL-1 $\beta$ , and TNF- $\alpha$ . However, *Mucispirillum schaedleri* and *Desulfovibrio* have been

negatively associated with SCFAs, tight junction associated proteins, digestive enzymes, and SOD activities and positively correlated with inflammatory factors. RGO intervention significantly elevated the relative abundance of *Lactobacillus*, *Lactobacillus*, and *Akkermansia*, combined with the structural changes of intestinal flora. Therefore, we speculate that RGO may be by increasing the proportion of beneficial bacteria in the intestine to enhance SCFA production, enhance the expression of intestinal tight junction proteins, inhibit the release of inflammatory factors, and elevate antioxidant activity. Moreover, RGO alleviated intestinal inflammation and barrier injury due to LPS. The mechanism of RGO relieving intestinal inflammation in mice needs to be further analyzed.

## Discussion

The difficulty in preventing intestinal inflammation and the strong recurrence are the problems in treating this disease (19). Therefore, human health must appropriately apply natural and non-irritating bioactive substances to enhance intestinal

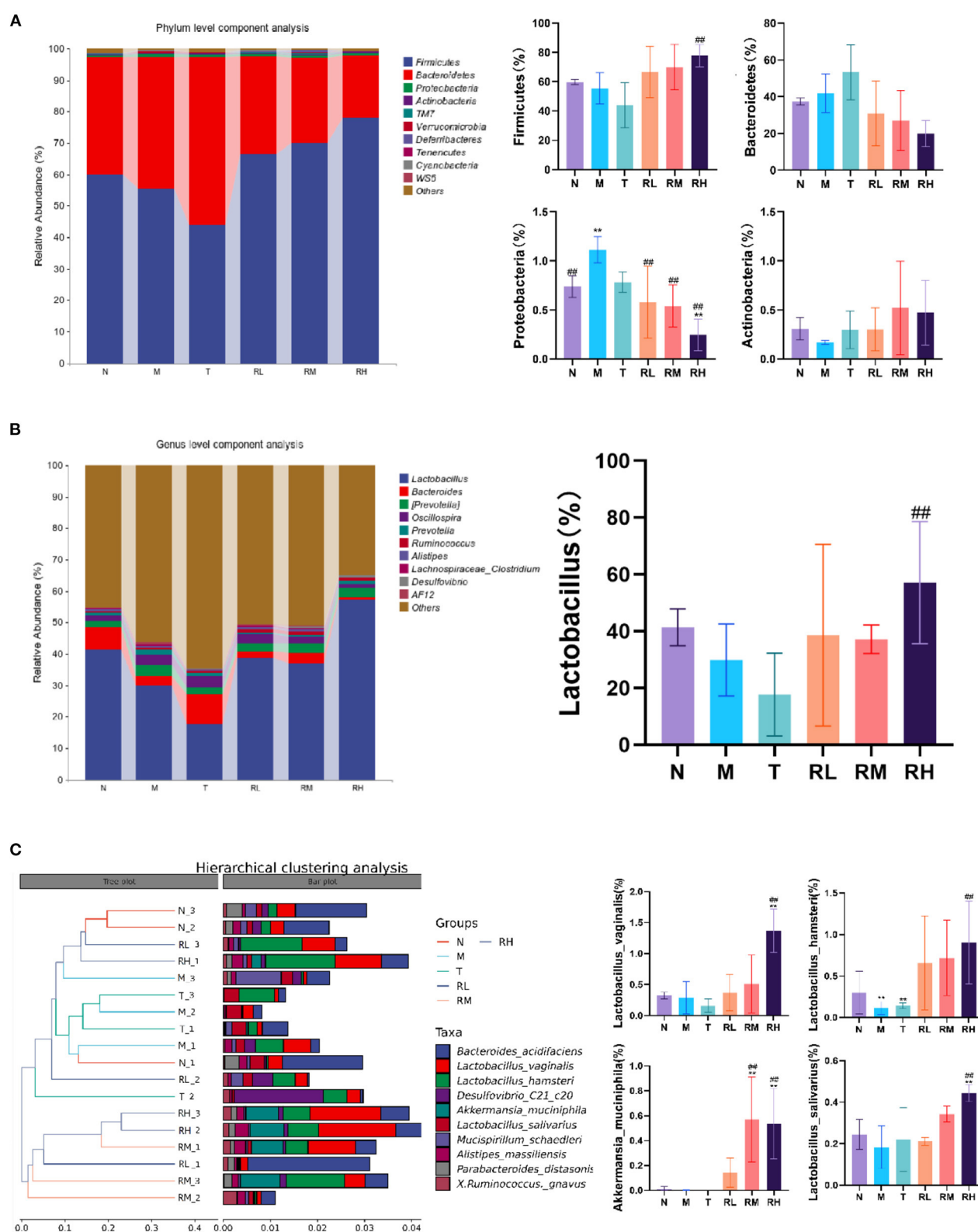


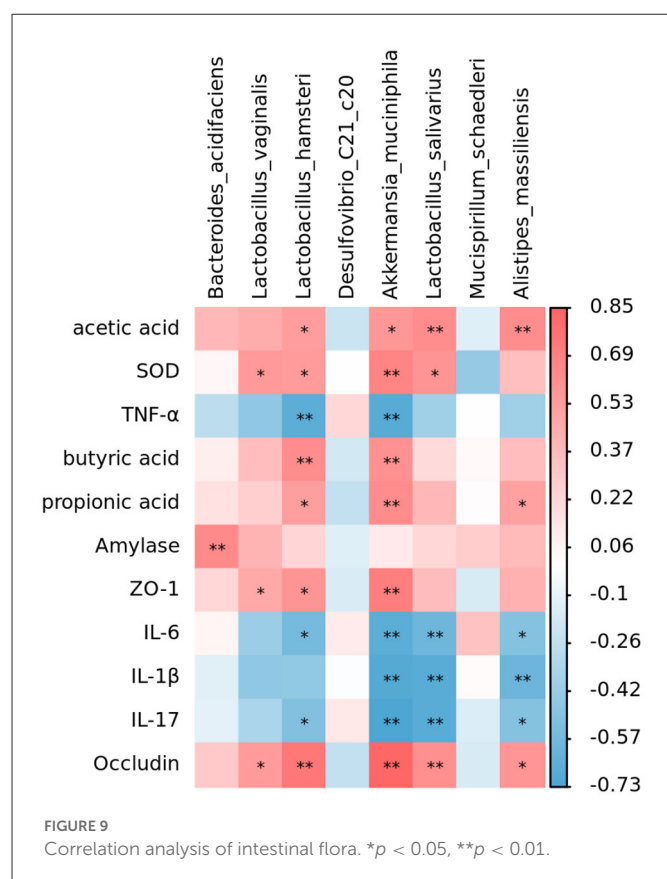
FIGURE 8

Effect of RGO on intestinal microflora structure in mice. (A) Phylum level composition analysis. (B) Genus level composition analysis. (C) Species level cluster analysis. Compared with group N: \* $P < 0.05$ , \*\* $P < 0.01$ ; compared with group M. # $P < 0.05$ , ## $P < 0.01$ .

inflammation and maintain intestinal barrier function (1). *Rehmannia glutinosa* oligosaccharide, a natural bioactive substance, can proliferate probiotics and improve immunity (6), with high

application value. Therefore, this study explored the effects of RGO on LPS-induced intestinal inflammation and barrier injury among mice.





LPS exists in the outer membrane of Gram-negative bacteria, stimulating macrophages to secrete proinflammatory cytokines, including IL-6, IL-1 $\beta$ , and TNF- $\alpha$ , while promoting the synthesis and release of inflammatory cytokines (20). The excessive secretion of IL-6, IL-17, IL-1 $\beta$ , and TNF- $\alpha$  has a crucial role in the pathogenesis of intestinal inflammation (21). TNF- $\alpha$  can enhance intestinal permeability by regulating the integrity of intestinal epithelial cells (22, 23). Therefore, blocking the secretion of these cytokines can be an effective strategy for treating intestinal inflammation. This study revealed that RGO could reduce the excessive secretion of inflammatory factors IL-6, IL-17 and IL-1 $\beta$ , and TNF- $\alpha$  within the intestine due to LPS.

Studies have indicated that the body has a strong oxidative stress response, and the antioxidant capacity of cells will be reduced when intestinal inflammation occurs. Excessive free radicals will act on lipid peroxidation, producing a large amount of MDA, thereby damaging the structure and function of proteins (12). SOD, GSH-Px, and CAT are the most important antioxidant enzymes in the body. Their main functions are to eliminate free radicals and reactive oxygen species, thus preventing peroxide production (24). RGO can alleviate the oxidative stress due to LPS, specifically manifested by enhancing the activities of SOD, GSH-Px, and CAT and inhibiting the enhancement of MDA levels.

The villus height and crypt depth could reflect the digestion and absorption ability of the small intestine. The higher the villus, the larger the number of peripheral intestinal epithelial cells. Moreover, the larger the contact area between the intestine and nutrients, the stronger the digestion and absorption of nutrients. The depth of

the crypt becomes shallow, depicting that the maturation rate of intestinal epithelial tissue increases (25). Additionally, the ability to secrete digestive fluid is more substantial, and the intestinal absorption capacity is stronger. The plica is rich in glands and lymphoid tissue; the higher the plicae, the more excellent intestinal transport, and absorption capacity. Therefore, the higher the villi and plicae, the shallower the crypts and has better the capacity of the intestinal tract to digest and absorb nutrients. This experiment showed that the intervention of RGO could enhance the length of the ileal villi and the height of the colonic plicae. Moreover, it can reduce the depth of crypts in LPS mice, suggesting that RGO could restore the structural damage from the LPS-induced intestinal inflammation among mice.

*Occludin* and *ZO-1* are essential tight junction proteins of the intestinal barrier structure (26). They have an important role in maintaining epithelial cell structure, regulating the transport of related ions, and controlling and regulating intestinal permeability (27). The results indicated that LPS could significantly reduce the expression of *Occludin* and *ZO-1* in the intestinal tight junction and increase intestinal permeability. Therefore, there is increased fecal water content and soft and loose stool in LPS mice (26). After the RGO intervention, the expression of *Occludin* and *ZO-1* was significantly enhanced. In combination with the results of intestinal tissue sections, RGO could improve intestinal permeability and water reabsorption capacity. Moreover, it can adjust the balance of water and salt and alleviate diarrhea symptoms by up-regulating the content of intestinal tight junction proteins. Thus, it maintains the integrity of intestinal tissue.

Digestive enzyme activity is one of the essential indicators to evaluate intestinal function, and its primary role is to aid digestion (28, 29). LPS can significantly decrease the activity of pancreatic digestive enzymes in mice. At the same time, the intervention of RGO can substantially improve the activity of pancreatic digestive enzymes, demonstrating that RGO plays a significant role in restoring intestinal dysfunction.

Ninety-five percent of SCFAs in the intestine are acetic acid, propionic acid, and butyric acid, and after being absorbed by the intestine, they store energy and reduce osmotic pressure. SCFAs play an essential role in regulating the normal function of the large intestine and the morphology and function of colonic epithelial cells (30, 31). SCFAs can also enhance the absorption of sodium, especially butyric acid, which can increase the production of *Lactobacillus*. It also reduces the number of *Escherichia coli* and serves as a significant energy source for intestinal mucosal cells (32). This study found that RGO could significantly up-regulate the production of acetic acid, propionic acid, and butyric acid in the intestine. SCFAs can promote the repair of intestinal mucosa damage, restore its function, regulate oxidative stress response, and inhibit the production of inflammatory cytokines as the energy source of intestinal epithelial cells, thus exerting anti-inflammatory effects.

When intestinal inflammation occurs, it can cause an imbalance of intestinal flora. Therefore, it is also crucial to correct intestinal flora and treat intestinal diseases and eliminate inflammation (33). The study observed that endogenous specific anaerobes (*Lactobacillus*, *Bifidobacterium*, etc.) could compete against potential aerobic pathogenic bacteria (*Enterococcus faecalis*, *Escherichia coli*, etc.), and their content could reflect the balance of intestinal flora (34). The results showed that RGO could regulate the intestinal floral structure and restore the balance of intestinal flora

in LPS-induced inflammatory mice. This may be facilitated by increasing the relative expression of 16S rRNA genes of intestinal probiotics, including *Firmicutes*, *Lactobacillus*, and *Akkermansia*. Most *Firmicutes* are beneficial bacteria, such as *Lactobacillus*, *Fecal bacilli*, and *Lactobacillus*. They produce acetic acid and butyric acid in the intestine to enhance the development of intestinal epithelial cells while preventing pathogens from interfering with intestinal health (35, 36). *Bacteroides* can promote the digestion and absorption of lipids, proteins, and carbohydrates. Moreover, they resist the adhesion of invasive intestinal pathogens by colonizing the intestinal mucosa surface (37, 38). Studies have revealed that *Akkermansia* can delay aging, inhibit neurodegenerative diseases, lower lipids, and weight loss, and assist cancer immunotherapy (39). These results indicated that RGO could induce changes in the composition or metabolism of intestinal microbiota, enhance the proliferation of probiotics in intestinal microbiota, and inhibit the growth of harmful bacteria such as *Proteobacteria*. Thus, it affects the structure of intestinal microbiota, regulates the intestinal microecological balance, and maintains the richness and diversity of intestinal microbiota while promoting the health of the host organism. Simultaneously, correlation analysis revealed that beneficial bacteria in the intestine (including *Lactobacillus*, *Akkermansia*, etc.) were positively associated with intestinal SCFA, tight junction protein, digestive enzyme, and SOD activity. Moreover, they were negatively correlated with the content of inflammatory factors. Thus, RGO may improve intestinal function, reduce inflammation and restore intestinal health by controlling the homeostasis of intestinal flora.

Therefore, RGO can regulate the intestinal floral structure in LPS mice and increase the abundance of intestinal flora. At the same time, it can increase the production of SCFAs in the intestine, decreasing intestinal inflammation, repairing intestinal barrier injury, and maintaining intestinal health. RGO has potential application value in treating and preventing intestinal inflammatory diseases.

## Data availability statement

The original contributions presented in the study are included in the article/supplementary material, further inquiries can be directed to the corresponding authors.

## References

- Wang X. Protective Effect of Pilose Antler Protein on LPS Induced Intestinal Inflammation in Mice. Jilin Agricultural University (2021) 13–48. doi: 10.27163/d.cnki.gjlnu.2021.000699
- Jia T, Xing Z, Wang HJ, Li GL. Dexmedetomidine reduces lipopolysaccharide-induced intestinal barrier damage in mice by regulating TXNIP/NLRP3 inflammasome pathway. *Chin J Pathophysiol*. (2021) 37:1589–95. doi: 10.3969/j.issn.1000-4718.2021.09.007
- Liu F, Smith AD, Solano-Aguilar G, Wang TTY, Pham Q, Beshah E, et al. Mechanistic insights into the attenuation of intestinal inflammation and modulation of the gut microbiome by krill oil using *in vitro* and *in vivo* models. *Microbiome*. (2020) 8:83–9. doi: 10.1186/s40168-020-00843-8
- Yin S, Yang H, Tao Y, Wei S, Li L, Liu M, et al. Artesunate ameliorates DSS-induced ulcerative colitis by protecting intestinal barrier and inhibiting inflammatory response. *Inflammation*. (2020) 43:765–76. doi: 10.1007/s10753-019-01164-1
- Chen JP, Zhang KX, Liu Y, Gai XH, Ren T, Liu SX, et al. Research progress on chemical constituents and pharmacological actions of *Rehmannia glutinosa*. *Chin Trad Herbal Drugs*. (2021) 52:1772–84. doi: 10.7501/j.issn.0253-2670.2021.06.028
- Qian YY, Wang L, Wen CN, Zhou Y, Li X, Zhang LX, et al. Purification, physicochemical property and antioxidant activity analysis of oligosaccharides from the fresh roots of *Rehmannia glutinosa* Libosch. *Nat Prod Res Dev*. (2021) 33:1470–7. doi: 10.16333/j.1001-6880.2021.9.004
- Ma LN, Luo BL, Shi JJ, Ma Y. Progress on regulation mechanism of intestinal flora by several common functional oligosaccharides. *Progr Microbiol Immunol*. (2017) 45:89–92. doi: 10.13309/j.cnki.pmi.2017.06.016
- Chorawala MR, Chauhan S, Patel R, Shah G. Cell wall contents of probiotics (*Lactobacillus* species) protect against lipopolysaccharide (LPS)-induced murine colitis by limiting immuno-inflammation and oxidative stress. *Probiot Antimicrobial Proteins*. (2021) 13:1005–17. doi: 10.1007/s12602-020-09738-4
- Li LY, Guo YN, Huang Q, Shi X, Liu Q, Wang F, et al. GPP (composition of *Ganoderma lucidum* polysaccharides and *Polyporus umbellatus* polysaccharides)

## Ethics statement

The animal study was reviewed and approved by Animal Ethics of the Henan Agricultural University.

## Author contributions

XL and XuefW provided experimental plans and ideas. XL, RG, XuefW, EN, LZ, LC, JZ, ZhL, and YW conducted experiments, sorted out data, and drew drawings. XL, RG, YF, LY, LW, WW, and ZiL helped analyze data and participated in paper writing. All authors have read and agreed to submit the manuscript.

## Funding

This research was funded by Henan Academy of Sciences Research and Development Project (210213014, 210913009, and 220613105).

## Conflict of interest

XL, XuefW, EN, LZ, LC, LY, JZ, ZhL, LW, WW, ZiL, and YW were employed by Henan Natural Products Biotechnology Co., Ltd. YF was employed by Henan High Tech Industry Co., Ltd.

The remaining authors declare that the research was conducted in the absence of any commercial or financial relationships that could be construed as a potential conflict of interest.

## Publisher's note

All claims expressed in this article are solely those of the authors and do not necessarily represent those of their affiliated organizations, or those of the publisher, the editors and the reviewers. Any product that may be evaluated in this article, or claim that may be made by its manufacturer, is not guaranteed or endorsed by the publisher.

- protects against DSS-induced murine colitis by enhancing immune function and regulating intestinal flora. *Food Science and Human Wellness*. (2022) 11:795–805. doi: 10.1016/j.fshw.2022.03.010
10. Pan DF, Cang YZ, Shen F, Lin HX. Effect of combination of invigorating spleen recipes and enteric nutrition on intestinal flora in rats with ulcerative colitis. *J N Med*. (2020) 51:691–6. doi: 10.3969/j.issn.0253-9802.2020.09.010
11. Zhang M, Pan H, Xu Y, Wang X, Qiu Z, Jiang L. Allicin decreases lipopolysaccharide-induced oxidative stress and inflammation in human umbilical vein endothelial cells through suppression of mitochondrial dysfunction and activation of Nrf2. *Cell Physiol Biochem*. (2017) 41:2255–67. doi: 10.1159/000475640
12. Gil-Cardoso K, Comitato R, Ginés I, Ardévol A, Pinet M, Virgili F, et al. Protective effect of proanthocyanidins in a rat model of mild intestinal inflammation and impaired intestinal permeability induced by LPS. *Mol Nutr Food Res*. (2019) 63:e1800720. doi: 10.1002/mnfr.201800720
13. Li W, Zhao Z, Zhao H, Liu M, Lin C, Li L, et al. Pectin polysaccharide from *Flos Magnoliae* (Xin Yi, *Magnolia biondii* Pamp. flower buds): hot-compressed water extraction, purification and partial structural characterization. *Food Hydrocolloids*. (2022) 122:107061. doi: 10.1016/j.foodhyd.2021.107061
14. Li C. Effects of Lipopolysaccharide On morphology and Defense Function Of intestinal Mucosal Epithelial Barrier in Mice. Northwest A&F University (2021) 17–41. doi: 10.27409/d.cnki.gxbnu.2021.000741
15. Zhao KL, Xu JX, Chen XL, Wang XC. The use composite antioxidants to repair intestinal tract injuries of rats induced by lipopolysaccharide. *Chin J Anim Nutr*. (2011) 23:670–6. doi: 10.3969/j.issn.1006-267x.2011.04.019
16. Li RL, Zhao DY, Li PP, Lei MK, Wu JQ, Wu JM, et al. Effects of thymol and rosmarinic acid combination on growth performance, inflammatory response and intestinal health of lipopolysaccharide- challenged rats. *Chin J Anim Nutr*. (2022) 34:2009–22. doi: 10.3969/j.issn.1006-267x.2022.03.059
17. Dong J, Liang QX, Niu Y, Jiang SJ, Zhou L, Wang JM, et al. Effects of *Nigella sativa* seed polysaccharides on type 2 diabetic mice and gut microbiota. *Int J Biol Macromol*. (2020) 159:725–38. doi: 10.1016/j.ijbiomac.2020.05.042
18. Shin NR, Whon TW, Bae JW. Proteobacteria: microbial signature of dysbiosis in gut microbiota. *Trends Biotechnol*. (2015) 33:496–503. doi: 10.1016/j.tibtech.2015.06.011
19. Li M, Li P, Tang RX, Lu H. Resveratrol and its derivative improve inflammatory bowel disease by targeting gut microbiota and inflammatory signaling pathways. *Food Sci Hum Wellness*. (2022) 11: 22–31. doi: 10.1016/j.fshw.2021.07.003
20. Shi L, Dai Y, Jia B, Han Y, Guo Y, Xie T, et al. The inhibitory effects of Qingchang Wenzhong granule on the interactive network of inflammation, oxidative stress, and apoptosis in rats with dextran sulfate sodium-induced colitis. *J Cell Biochem*. (2019) 120:9979–91. doi: 10.1002/jcb.28280
21. Li T, Zhang T, Gao H, Liu R, Gu M, Yang Y, et al. Tempol ameliorates polycystic ovary syndrome through attenuating intestinal oxidative stress and modulating of gut microbiota composition-serum metabolites interaction. *Redox Biol*. (2021) 41:101886. doi: 10.1016/j.redox.2021.101886
22. Liang Q, Zhao Q, Hao X, Wang J, Ma C, Xi X, et al. The effect of flammulina velutipes polysaccharide on immunization analyzed by intestinal flora and proteomics. *Front Nutr*. (2022) 9:841230. doi: 10.3389/fnut.2022.841230
23. Lu N, Xiu H, Xu YB, Dong J, Shi H, Li M, et al. Mechanism of invigorating spleen and clearing intestines method inhibiting chemotherapy-induced intestinal mucositis by regulating TLRs/NF-KB pathway. *Chinese Archives of Traditional Chinese Medicine*. (2022) 40:47–50+261. doi: 10.13193/j.issn.1673-7717.2022.07.012
24. Zhou X, Du H-H, Jiang M, Zhou C, Deng Y, Long X, et al. Antioxidant effect of *Lactobacillus fermentum* HFY02- fermented soy milk on D-galactose-induced aging mouse model. *Food Sci Hum Wellness*. (2022) 11:1362–72. doi: 10.1016/j.fshw.2022.04.036
25. Xu TT, Zhang CD, Lin LX. Research progress on the effect of probiotics on bone metabolism by gut microbiota in chickens. *Chin J Anim Sci*. (2022) 58:31–6. doi: 10.19556/j.0258-7033.20210305-06
26. Zhang YQ, Gan JF, Wang YF, et al. Regulation of Jianpi Qushi ointment on gastrointestinal function in rats. *Chin Trad Patent Med*. (2021) 43:191–5. doi: 10.3969/j.issn.1001-1528.2021.01.039
27. Pan M, Barua N, Ip M. Mucin-degrading gut commensals isolated from healthy faecal donor suppress intestinal epithelial inflammation and regulate tight junction barrier function. *Front Immunol*. (2022) 13:1021094. doi: 10.3389/fimmu.2022.1021094
28. Xie GZ, Tang Y, Wu Y, Huang LL, Tan ZJ. Effects of total glycosides of Qiwei Baizhu powder on intestinal microbiota and enzyme activities in diarrhea mice. *Biotechnol Bull*. (2021) 37:124–31. doi: 10.13560/j.cnki.biotech.bull.1985.2021-0149
29. He L, Liu YW, Guo YF, Xiao N, Tan Z. Influences of Aflatoxin B1 on main intestinal bacteria communities and enzyme activities in mice. *Toxin Rev*. (2018) 38:121–6. doi: 10.1080/15569543.2018.1426611
30. Zhao MQ, Wang J, Cui NL, et al. Research progress on the relationship between short chain fatty acids and intestinal diseases. *Modern Med J China*. (2020) 22:105–8. doi: 10.3969/j.issn.1672-9463.2020.09.029
31. Cui M, Wang Y, Elango J, Wu J, Liu K, Jin Y. *Cereus sinensis* polysaccharide alleviates antibiotic- associated diarrhea based on modulating the gut microbiota in C57BL/6 mice. *Front Nutr*. (2021) 8:751992. doi: 10.3389/fnut.2021.751992
32. Ma Y, Fei Y, Han X, Liu G, Fang J. *Lactobacillus plantarum* alleviates obesity by altering the composition of the gut microbiota in high-fat diet-fed mice. *Front Nutr*. (2022) 9:947367. doi: 10.3389/fnut.2022.947367
33. Wang J, Liang Q, Zhao Q, Tang Q, Ahmed AF, Zhang Y, et al. The effect of microbial composition and proteomic on improvement of functional constipation by *Chrysanthemum morifolium* polysaccharide. *Food Chem Toxicol*. (2021) 153:112305. doi: 10.1016/j.fct.2021.112305
34. Huang SY, Xu P, Hong ZY, Zhong SZ. Experimental study on improvement of bacterial enteritis and regulation of intestinal flora in mice by punicalagin. *Chinese Trad Herbal Drugs*. (2022) 53:3044–52. doi: 10.7501/j.issn.0253-2670.2022.10.014
35. Shen X, Jiang X, Qian L, Zhang A, Zuo F, Zhang D. Polyphenol extracts from germinated mung beans can improve type 2 diabetes in mice by regulating intestinal microflora and inhibiting inflammation. *Front Nutr*. (2022) 9:846409. doi: 10.3389/fnut.2022.846409
36. Jiang H, Dong J, Jiang S, Liang Q, Zhang Y, Liu Z, et al. Effect of Durio Zibethinus rind polysaccharide on functional constipation and intestinal microbiota in rats. *Food Res Int*. (2020) 136:109316. doi: 10.1016/j.foodres.2020.109316
37. Cheng JB, Hu JL, Geng F, Nie S. Bacteroides utilization for dietary polysaccharides and their beneficial effects on gut health. *Food Sci Hum Wellness*. (2022) 11:1101–10. doi: 10.1016/j.fshw.2022.04.002
38. Ji X, Su L, Zhang P, Yue Q, Zhao C, Sun X, et al. Lentinan improves intestinal inflammation and gut dysbiosis in antibiotics-induced mice. *Sci Rep*. (2022) 12:19609. doi: 10.1038/s41598-022-23469-2
39. Liu Y. Regulation of Akkermansia muciniphila on Intestinal Barrier and Related Genes. Jiangnan University (2021) 1–12. doi: 10.27169/d.cnki.gwqgu.2021.000845



## OPEN ACCESS

## EDITED BY

Haining Zhuang,  
Shanghai Urban Construction  
Vocational College,  
China

## REVIEWED BY

Carlos L. Cespedes-Acuña,  
University of Bio-Bio,  
Chile  
Kit Leong Cheong,  
Guangdong Ocean University,  
China

## \*CORRESPONDENCE

Wenjie Yan  
✉ meyanwenjie@126.com

## SPECIALTY SECTION

This article was submitted to  
Food Chemistry,  
a section of the journal  
Frontiers in Nutrition

RECEIVED 17 November 2022

ACCEPTED 07 February 2023

PUBLISHED 03 March 2023

## CITATION

Zhou S, Feng D, Zhou Y, Duan H, Jiang Y and  
Yan W (2023) Analysis of the active ingredients  
and health applications of cistanche.  
*Front. Nutr.* 10:1101182.  
doi: 10.3389/fnut.2023.1101182

## COPYRIGHT

© 2023 Zhou, Feng, Zhou, Duan, Jiang and  
Yan. This is an open-access article distributed  
under the terms of the [Creative Commons  
Attribution License \(CC BY\)](#). The use,  
distribution or reproduction in other forums is  
permitted, provided the original author(s) and  
the copyright owner(s) are credited and that  
the original publication in this journal is cited,  
in accordance with accepted academic  
practice. No use, distribution or reproduction is  
permitted which does not comply with these  
terms.

# Analysis of the active ingredients and health applications of cistanche

Shiqi Zhou<sup>1,2</sup>, Duo Feng<sup>1,2</sup>, Yaxi Zhou<sup>1,2</sup>, Hao Duan<sup>1,2</sup>,  
Yongjun Jiang<sup>3</sup> and Wenjie Yan<sup>1,2\*</sup>

<sup>1</sup>College of Biochemical Engineering, Beijing Union University, Beijing, China, <sup>2</sup>Beijing Key Laboratory of Bioactive Substances and Functional Food, College of Biochemical Engineering, Beijing Union University, Beijing, China, <sup>3</sup>Inner Mongolia Sankou Biotechnology Co., Ltd., Ordos City, Inner Mongolia, China

Cistanche is a tonic Chinese medicine commonly used in traditional Chinese medicine, with 2016, CFSA through the alxa desert cistanche safety evaluation, cistanche began to officially enter the food field. At present, the research on cistanche mainly focuses on the extraction, isolation and purification and pharmacological effects, and its pharmacological effects such as neuroprotective effects, immunomodulation, antioxidant anticancer and hepatoprotective liver protection have attracted the attention of researchers. This review mainly reviews the research status, chemical composition and health benefits, analyzes its application prospects in food, and aims to provide certain theoretical support for the safe application of cistanche in functional food.

## KEYWORDS

Cistanche, homology of medicine and food, active ingredient, PHG, health benefits

## 1. Introduction

Cistanche (*Cistanche deserticola* Ma) is a perennial parasitic herb of cistanches in the family *Orobanchaceae*, also known as golden shoots, goblins, and brassica, which is mainly produced in China in inner Mongolia, Xinjiang, Ningxia, Gansu, and Qinghai (1). There are about 22 species of cistanche in the world, mostly distributed in dry areas such as warm deserts and deserts in the northern hemisphere. According to the flora of China, there are currently 6 species of cistanche recorded in China. They are *Cistanche deserticola* (*Cistanche deserticola* Y.C.M), *Cistanche lanzhouensis* (*Cistanche lanzhouensis* Z. Y. Zhang), *Cistanche mongolica* (*Cistanche mongolica* Beck), *Cistanche salsa* [*Cistanche salsa* (C. A. Mey.) G.Beck], *Cistanche sinensis* (*Cistanche sinensis* G.Beck), and *Cistanche tubulosa* [*Cistanche tubulosa* (Schenk) Wight] (2). Chinese edible cistanche has a long history, first recorded in the “Shennong Materia Medica” and was listed as a superior product, which has the effect of tonifying kidney yang, improving sperm and blood, and moisturizing the intestines and laxatives.

In 2016, the expert review committee of the China National Center for Food Safety Risk Assessment (CFSA) reviewed in accordance with legal procedures and found that Alxa Desert Cistanche meets food safety requirements based on existing hygienic and toxicological tests and related safety data. In 2018, the desert cistanche was included in the Catalog of Substances That are both food and chinese medicinal materials according to tradition by the National Health Commission, which shows that cistanche can be used as a daily food for the health care of the general population (3). In 2020, the National Health Commission and the State Administration of Market Supervision officially issued a notice on the pilot work on the material management



of 9 substances such as party ginseng, which are both food and Chinese medicinal materials in accordance with tradition. And *cistanche* (*Cistanche deserticola*) is listed among them. Since then *cistanche* has been officially approved to enter the list of new food raw materials as a medicinal and food homologous substance. At present, China has carried out pilot work on *cistanche* food and drug substances in Inner Mongolia, Inner Mongolia Ordos, Ningxia Hui Autonomous Region, Gansu and Qinghai, while the published local food safety standards are DBS62/003-2021 in Gansu and DBS63/00016-2021 in Qinghai Province, of which the standard in Qinghai Province stipulates that the daily recommended consumption is 6 to 10 g/d. As of June 29, 2022, there are 60 registered health foods with *cistanche*, *cistanche* and *cistanche* extract as the main raw materials available on the national “special food information inquiry platform.” Their main health care functions are to relieve physical fatigue, regulate immunity and antioxidants, which greatly enriches the sales market of *cistanche* products.

To put it briefly, *cistanche* has a variety of nutritional and functional properties, and its application in functional food processing is increasing. At present, the research on the bioactive substances in *cistanche* is still deepening. This article will review the nutritional and bioactive components of *cistanche* and its impact on health. So as to better expound the potential impact of *cistanche* on human health and provide theoretical reference for its safe application in the food field.

## 2. Nutritional value and bioactive compounds of *cistanche*

With the growing awareness of health care among consumers, this has increased the application of *cistanche* and its extracts in food. As a food, one of the most important points of consumers is the nutritional value of food. Because health food needs to declare the health function of the product when declaring, it is necessary to understand the bioactive ingredients of *cistanche*.

### 2.1. Nutritional value of *cistanche*

*Cistanche*, as a common Chinese medicinal material for the prescription of Traditional Chinese medicine tonics, weighs, is hard, not easy to break, and is mostly flat cylindrical in shape, slightly curved, and the surface is tan or gray-brown and arranged with wavy rings. In order to further promote the application of *cistanche* in food, Kurban et al. (4) used burning method, Philin's method, alkali titration method, Sox extraction method, ultraviolet spectrophotometry to determine the content of general nutrients, vitamin A, vitamin C and cholesterol in *cistanche*, and also used atomic absorption spectrophotometry to determine the content of trace elements in *cistanche*. As can be seen from Table 1, *cistanche* has the highest total acid content and the lowest cholesterol content. Among the elements tested, the macro element Na had the highest content, followed by potassium, the content of manganese, iron, copper and zinc in the essential trace elements was higher, and the content of nickel was the lowest.

At present, the literature shows that vitamin A, as an essential fat-soluble micronutrient that the human body cannot synthesize, must be obtained from the diet, and  $V_A$  supplementation can delay

TABLE 1 General nutrient and trace element content in *cistanche*.

Nutrient	Content (per 100 g of original fruit)	Element	Content ( $\mu\text{g/g}$ original fruit)
Moisture (g)	7.16	K	$7.60 \times 10^4$
Fat (mg)	12	Na	$1.14 \times 10^5$
Cholesterol ( $\mu\text{g}$ )	102	Ca	$3.63 \times 10^4$
Ash (g)	0.24	Fe	$1.05 \times 10^4$
Dietary fiber (g)	0.19	Mg	$9.09 \times 10^3$
Reducing sugar (mg)	7.34	Mn	$2.02 \times 10^2$
Total acid (g)	1.56	Zn	$1.07 \times 10^2$
$V_A$ (mg)	2.42	Cu	$9.42 \times 10^2$
$V_C$ (mg)	3.12	Sr	$1.55 \times 10^2$
		Ni	11.53

cellular aging, promote wound healing, anti-inflammatory, and can also be used for xerophthalmia and blindness prevention (5–7). Vitamin C is a water-soluble vitamin, which can be obtained from fresh fruits and vegetables, is mostly used for preservatives in food to prolong the shelf life of food, can play an antioxidant and strengthen the immune system in the human body, and is clinically used to treat scurvy (6, 8). Dietary fiber is a polysaccharide, and proper intake can help improve intestinal function, promote intestinal health, regulate the body's immunity, and effectively control blood sugar and blood lipid levels (9). Trace elements are found in smaller amounts in the human body, but play an important role in maintaining the body's normal physiological functions, such as participating in antioxidant defense, immune response, and wound healing (10). Therefore, *cistanche* has a high health value in food processing.

### 2.2. Bioactive ingredient of *cistanche*

So far, the literature has shown that the health value of *cistanche* is closely related to the bioactive ingredients it contains, and more than 120 compounds have been isolated from *cistanche*, including phenethyl glycosides, cycloenne ether terpenes and their glycosides, lignans and their glycosides, oligosaccharide esters, polyols and polysaccharides (11, 12). Among them, studies have shown that phenylethanoid glycoside (PhG) extracted from *cistanche* exceed 80%. As the main active ingredient of *cistanche*, PhGs have a significant effect on the quality of vascular dementia, and play a positive role in the prevention and treatment of Alzheimer's disease (AD) (13). *Cistanche* polysaccharides have a positive effect on immune regulation and can play an anti-peroxidant role in the body (14).

#### 2.2.1. Phenylethanoid glycosides

PhGs are currently the most studied class of compounds among the active ingredients of *cistanche*, as one of the main components of *cistanche*, it plays an active role in antioxidants, protecting liver, myocardium, nerve cells and enhancing memory (15, 16). At present, Zhang et al. (17) established a novel HPLC-LTQ-Orbitrap-based strategy, 69 PhGs (LTQ) isolated from *cistanche* and *cistanche*. Li et al.



(18) used LC/QTOF-MS/MS to find 21 phenethyl alcohol glycosides in *cistanche*. Ai et al. (19) found 10 PhGs by using UHPLC-MS/MS. Li et al. (20) used quantitative analysis of multi-components by single marker (QAMS) to determine the content of 5 phenethyl alcohol glycosides in 10 batches of *cistanche*, providing an economical and reliable method for quality control. Yan-xia et al. (21) and Lu et al. (22) used high performance liquid chromatography (HPLC) method to determine the phenethyl alcohol glycoside compounds in *cistanche*. It was clear that the phenethyl alcohol compounds of different types of medicinal materials were different. And Jian-song et al. (23) used ultra performance liquid chromatography (UPLC) method to determine 6 phenethyl alcohol glycoside components in *cistanche*, which provided an obvious basis for the quality evaluation of genuine and counterfeit products. Besides Xie et al. (24) used a solvent system of ethyl acetate-n-butanol-glacial acetic acid-water (1, 1.2, 0.2, 2,  $v=v=v=v$ ) to isolate and purify echinacoside and acteoside. And Yang et al. (25) established PhGs chemical fingerprints of *cistanche* from different regions of China. At present, through literature search, it has been found that more than 70 PhGs can be isolated, including 4 monoglycosides, 41 disaccharides and 25 triglycosides (Table 2). It can be concluded that the study of the purification and extraction of the active ingredient of PhGs in *cistanche*. They are helpful to the study of the medicinal value of *cistanche* and also have guiding value for the study of the mechanism of action of the body.

## 2.2.2. Iridoids

Iridoid is one of the main chemical constituents of *cistanche* and has antibacterial, anti-inflammatory and analgesic effects (44). Jianghua et al. (45) used column chromatography techniques such as macroporous resin and activated carbon to separate cycloen ether mushroom compounds from purified salt *cistanche* and successfully isolated two compounds. Li et al. (18) found 2 iridoids by using LC/QTOF MS/MS. Wenjing et al. (46) used the HPLC-IT-TOF-MS method to qualitatively analyze the chemical composition of desert *cistanche* flowers and lignified stems, and found that there were more cycloen ether terpenoids in the flowers and stems of *cistanche* than in the fleshy stems. At present, there are 27 kinds of cycloen ether terpenoid active substances isolated from *cistanche* (Table 3). And the structure of these active substances contain glucose monoglycosides, which provides new ideas for the drug research and development of *cistanche*, and also promotes the research of *cistanche* in neuroprotective, hepatoprotective and hypoglycemic blood lipids (52).

## 2.2.3. Lignans

Lignan is a large class of compounds containing two phenyl propane units (53), basically present in plants, is a plant hormone, which has been found to have biological properties such as scavenging free radicals, antioxidants, and antivirals in the body (54). Zedong et al. (55) conducted a chemical composition study of desert *cistanche* by using chromatographic analysis techniques, and isolated 11 lignan compounds, providing new discoveries for the study of lignans in *cistanche*. At present, there are 17 lignan compounds isolated from *cistanche* (Table 4), of which syringin, syringaresinol O- $\beta$ -D-glucopyranoside and pineoresinol are the earliest discovery, which greatly promotes scientists' research on the estrogen effects of *cistanche* and provides an alternative for finding alternative synthetic estrogen research.

## 2.2.4. Polysaccharides

Polysaccharides are widely present in the composition of animals, plants and microbial cells (57, 58). And polysaccharides can be used as a substance for storing energy in organisms, playing a role in immunomodulation, antiviral, anti-cancer, hypoglycemic, prevention and treatment of heart disease and laxative (59, 60). At present, the research on *cistanche* polysaccharides is mostly isolated and purified, and the research on the pharmacological effects of polysaccharides has gradually begun to deepen. Xing-hui et al. (61) took Xinjiang desert *cistanche* as raw material, after process optimization and extraction. It is finally concluded that the use of water immersion extraction method at 75°C, the material-to-liquid ratio is 1:55, the extraction rate of 165 min polysaccharide extraction is the highest, and combined with papain to remove protein, macroporous resin decolorization has the highest polysaccharide recovery rate and the best purification effect. Table 5 is one of the 11 species of *cistanche* polysaccharides that have been studied so far, and most *cistanche* polysaccharides are composed of glucose, galactose, rhamnose, arabinose, and fructose. The study of *cistanche* polysaccharides provided a basic basis for understanding its structure, composition and chemical properties, and also has a huge impact on its biological activity research.

## 2.2.5. Other compounds

In addition, *cistanche* also contains many other chemical components, Li et al. (18) used LC/QTOF-MS/MS to identify and analyze 1 monoterpenoids. Qing-Qing et al. (12) used mass spectrometry analysis method, but also isolated benzyl alcohol glycosides, phenylacryl oligosaccharides, monoterpenoids and nitrogen-containing compounds, etc., of which the chemical structure of benzool glycoside compounds and phenylacryl oligosaccharides has similarities with the structure of phenylethanol glycoside compounds, and contains glucose in the structure. These compounds are described in Table 6 (Figure 1) and provide a reference for quality control of *cistanche* by analyzing these chemical components.

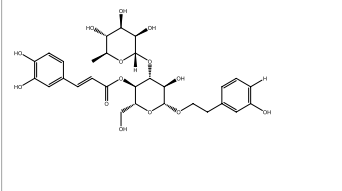
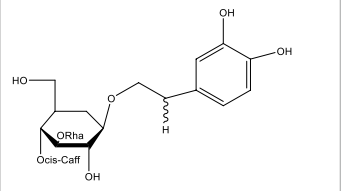
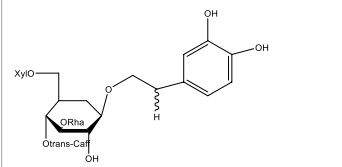
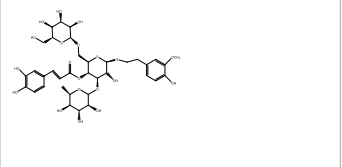
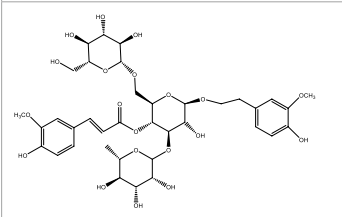
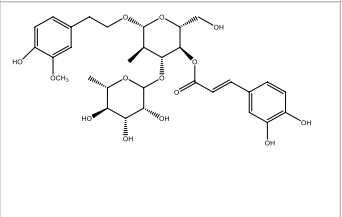
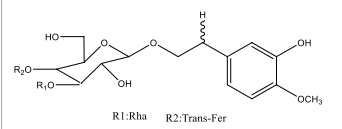
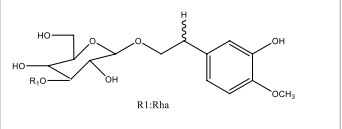
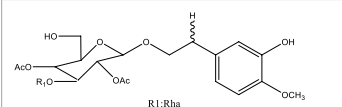
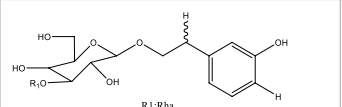
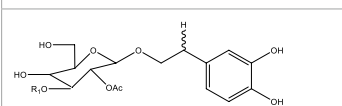
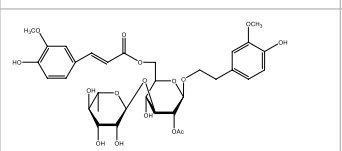
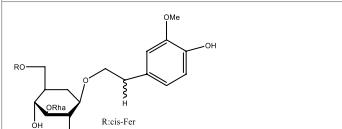
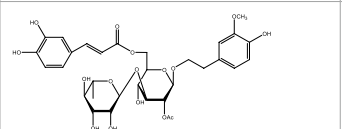
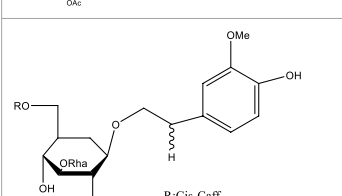
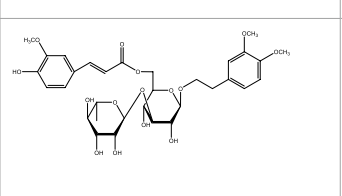
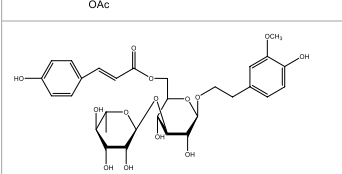
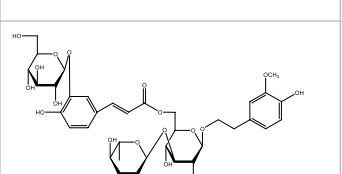
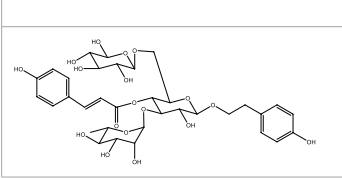
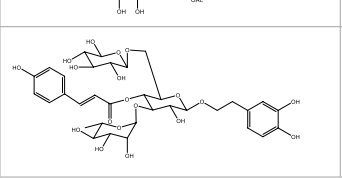
# 3. Health benefits of *cistanche* consumption

*Cistanche* contains a variety of biologically active ingredients. It has different pharmacological mechanisms of action in the body, has been studied that *cistanche* not only plays an important role in lowering lipids and hypoglycemicity, preventing osteoporosis, but also plays an active role in antioxidant, liver protection, anti-cancer, immunomodulation, Figure 2 briefly summarizes some of the mechanisms of action of *cistanche*. It can be seen that eating *cistanche* has many benefits for health.

## 3.1. Immunomodulatory effects

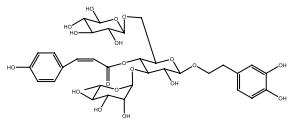
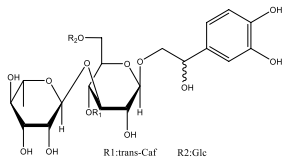
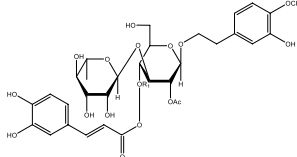
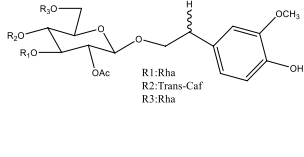
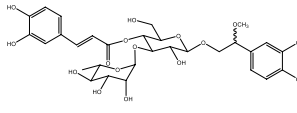
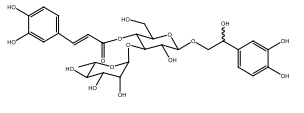
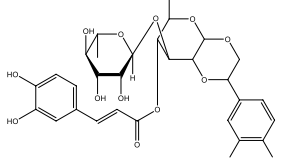
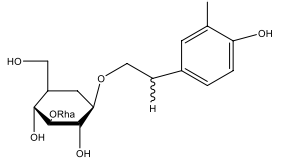
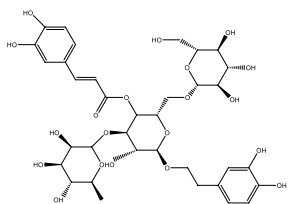
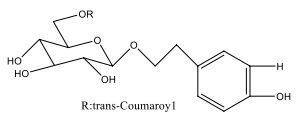
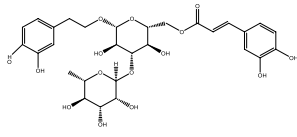
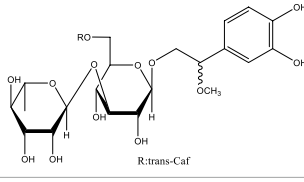
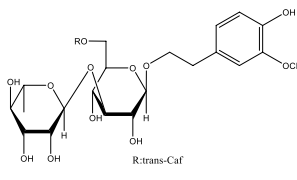
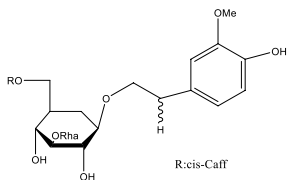
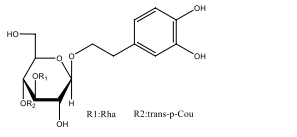
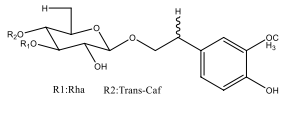
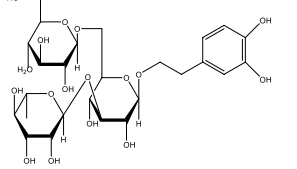
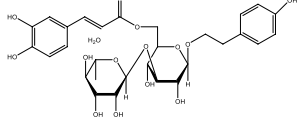
Long-term studies have shown that *cistanche* polysaccharide is the basis for *cistanche* to play an immunomodulatory role, which can play a role in regulating the body's immunity by promoting lymphocyte proliferation and enhancing phagocyte activity. Li et al. (76) evaluated the regulatory activity of crude polysaccharides of *Cistanche deserticola* (CPCD) on activating dendritic cells (DCs).

TABLE 2 Phenylethanoid glycosides from cistanche species.

Chemical structure	PhGs compound	Ref	Chemical structure	PhGs compound	Ref
	acteoside	(26)		Cis-acteoside	(27)
	arenarioside	(27)		Cistanoside A	(26, 28)
	Cistanoside B	(28, 29)		Cistanoside C	(26, 30)
	Cistanoside D	(30)		Cistanoside E	(28)
	Cistanoside F	(31, 32)		Cistanoside G	(32)
	Cistanoside H	(32)		Cistanoside J	(33)
	Cis-cistanoside J	(34)		Cistanoside K	(33)
	Cis-cistanoside K	(12)		Cistanoside L	(33)
	Cistanoside M	(33)		Cistanoside N	(33)
	Cistantubuloside A	(31)		Cistantubuloside B1	(31)

(Continued)

TABLE 2 (Continued)

Chemical structure	PhGs compound	Ref	Chemical structure	PhGs compound	Ref
	Cistantubuloside B2	(31)		Cistantubuloside C1/C2	(31)
	Cistansinenside A	(35)		Cistansinenside B	(35)
	Campneoside I	(36)		Campneoside II	(36)
	Crenatoside	(27)		Decaffeoylacteoside	(37)
	Echinacoside (ECH)	(26)		Eutigoside A	(38)
	Isoacteoside	(26)		Isocampneoside I	(36)
	Isocistanoside C	(39)		cis-isocistanoside C	(12)
	Isosyringalide A 3'-alpha-L-rhamnopyronoside	(39)		Jionoside D	(40)
	Kankanoside F	(32, 33)		Kankanoside G	(32)

(Continued)

TABLE 2 (Continued)

Chemical structure	PhGs compound	Ref	Chemical structure	PhGs compound	Ref
	Kankanosides H <sub>1</sub>	(27)		Kankanosides H <sub>2</sub>	(27)
	Kankanosides I	(27)		Kankanosides J1/ J2	(36)
	Kankanosides K1/ K2	(36)		Osmanthuside B	(41)
	Osmanthuside B6(E)	(12)		Osmanthuside B6(Z)	(26)
	Plantainoside C	(34)		Poliumoside	(40, 41)
	Pheliposide	(11)		Phenylethyl-glucopyranoside	(34)
	Salidroside	(32)		Salsasides D	(42)
	Salsasides E	(42)		Salsasides F	(42)

(Continued)

TABLE 2 (Continued)

Chemical structure	PhGs compound	Ref	Chemical structure	PhGs compound	Ref
	Syringalide A 3'- $\alpha$ -L-rhamnopyranoside	(43)		Tubuloside A	(32)
	Tubuloside B	(32)		Cis-Tubuloside B	(12)
	Tubuloside C	(11, 27)		Tubuloside D	(11, 27)
	Tubuloside E	(11, 27)		Wiedemanninoside C	(12, 27)
	2'-O-acetylpoliumoside	(40)		2'-Acetylacteoside	(26, 30)
	6'-Acetylacteoside	(26)		trans-Fer	
	trans-p-Cou			trans-Caf	

Glc:  $\beta$ -glucopyranose. Rha:  $\alpha$ -L-rhamnopyranose; Ac: acetyl; Cd: *C. deserticola*; Ct: *C. tubulosa*; Csa: *C. salsa*; Csi: *C. sinensis*; Cp: *C. phelpaia*.

And the final results showed that CPCD increased the specific antibody of foot-and-mouth disease vaccine (FMDV), promoted lymphocyte proliferation, and concluded that cistanche polysaccharide has a regulatory effect on cellular immunity. Feng et al. (77) extracted water-soluble polysaccharides from cistanche, studied the immune efficacy and efficacy of aqueous extracts of cultivated *Cistanche deserticola* Y.C. Ma(AECCD) through *in vitro* experiments *in vitro*. And the final test results showed that AECCD can activate a long-lasting and effective antigen-specific immune response through DC, and can also participate in regulating cytokine expression through TLR4-related NF- $\kappa$ B pathway, which can promote related cell proliferation, activate T cell response, and is a potential immunomodulator. Tian et al. (78) selected Wistar female mice, except for the blank group, the rest of the rats were

excised the left ovary, 80% of the right ovary was excised, administered by gastric lavage, phenylethanoid glycosides of cistanche herb (PGC) high, medium, low suspension which is 450 mg/(kg day), 133.33 mg/(kg day), 66.67 mg/(kg day), 33.33 mg/(kg day), the blank group was fed the same volume of distilled water for 30 consecutive days. After the last administration, blood was taken from the abdominal aorta and the levels of E-2, LH, FSH, GnRH, BGP and  $\beta$ -EP in serum were determined, respectively, and the final results showed that PGC increased the activity, the organ index (thymus, spleen, uterus), E2, T, BGP level in serum,  $\beta$ -EP level in plasma, AR level in hypothalamus, ER level in hypothalamus, pituitary. Zhang et al. (79) used water-extractable polysaccharides of CD(WPCD) to study, they found WPCD significantly promoted the maturation and function of murine marrow-derived dendritic

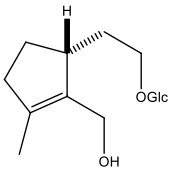
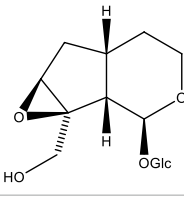
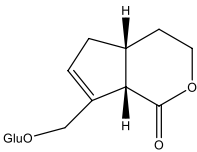
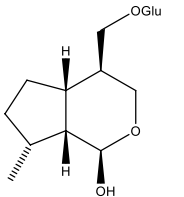
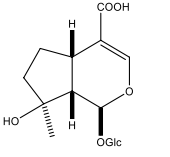
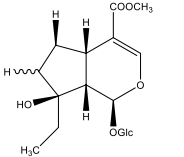
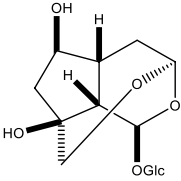
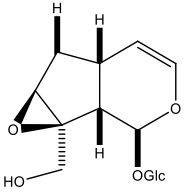
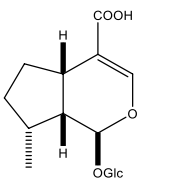
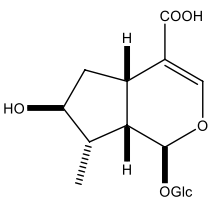
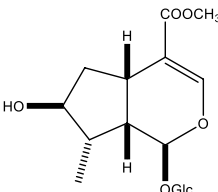


TABLE 3 Iridoids from *Cistanche* species.

Name	Chemical structure	Ref	Name	Chemical structure	Ref
Adoxosidic acid		(47)	Antirrhine		(48)
Ajugol/Leomuride		(35, 48)	Argyol		(48)
Bartsioside		(48, 49)	Catalpol		(48)
Cistanin		(50)	Cistachlorin		(50)
Cistadesertoside A		(51)	Geniposide		(35)
Geniposidic acid		(48, 49)	Glucoside		(30, 48, 49)
Kankanol		(48)	Kankanoside A		(48)
Kankanoside B		(48)	Kankanoside C		(48)

(Continued)

TABLE 3 (Continued)

Name	Chemical structure	Ref	Name	Chemical structure	Ref
Kankanoside D		(48)	Kankanoside L		(27)
Kankanoside M		(27)	Kankanoside N		(27)
Mussaenoidic acid		(44, 50)	Mussaenoside		(35)
Phelypaeside		(11)	6-Deoxycatalpol		(50)
8-Epideoxyloganic acid		(34, 49)	8-Epiloganic acid		(35)
8-Epiloganin		(35)			

Glc:  $\beta$ -glucopyranose. Rha:  $\alpha$ -L-rhamnopyranose; Ac: acetyl.

cells (BM-DCs) through up-regulating the expression levels of MHC-II, CD86, CD80, and CD40, allogenic T cell proliferation, and the yields of IL-12 and TNF- $\alpha$  *via* toll-like receptor4 (TLR4). So WPCD activates DCs through the TLR4 signaling pathway, triggering humoral and cellular immunity. Therefore, cistanche polysaccharides and PhG play an important role in immune regulation (Table 7).

### 3.2. Neuroprotective effect

Parkinson's disease is a chronic disease characterized by dysfunction of the central nervous system, from Table 8, it can be seen that cistanche has a protective effect on the nerves. By gavaging Wistar rats Herb Epimedii (Epimedium), Semen Cuscutae (Dodder Seed), or Herb Cistanches (Desertliving Cistanche), then the sera of different groups of

mice were compared and analyzed by enzyme-linked immunosorbent assay and MES23.5 cells in the logarithmic phase were cultured in medium with 15% drug-containing serum added for 24h. The results showed that serum containin Cistanches increased the expression of nerve growth factor, brain-derived neurotrophic factor, and glial cell line-derived neurotrophic factor in injured MES23.5 cells, so *Cistanche deserticola* can protect nerve cells by regulating the expression of apoptosis related factors and neurotrophic factors in MES23.5 cells (80). Echinacoside (ECA) is one of the main compounds of *Cistanche deserticola*. By intraperitoneal injection of echinacoside into rats, the results showed that the effect of pretreatment with echinacoside on the expression of proinflammatory factor genes in the hippocampus of kainic acid-induced epileptic rats would be weakened. Therefore, echinacoside is the potentially useful in the prevention of epilepsy (81). Ischemic stroke is a disease with high morbidity and mortality, cistanche deserticola polysaccharides (CDP) has always been considered to have

TABLE 4 Lignans from *Cistanche* species.

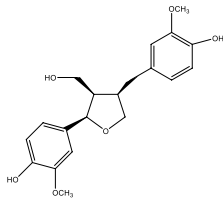
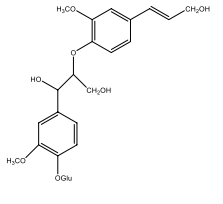
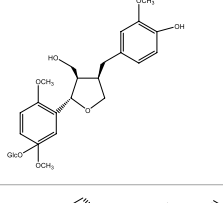
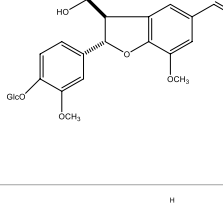
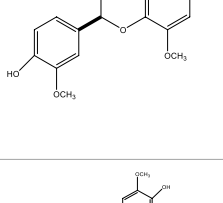
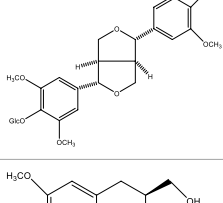
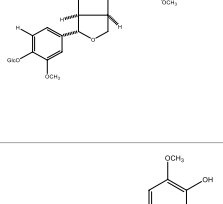
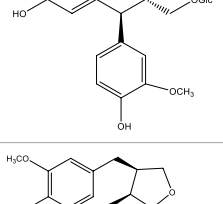
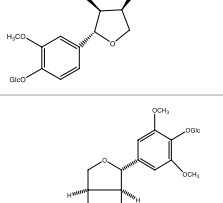
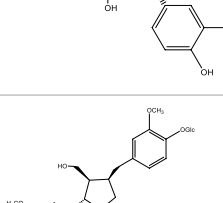
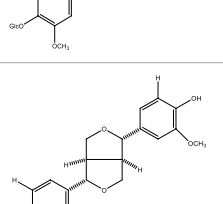
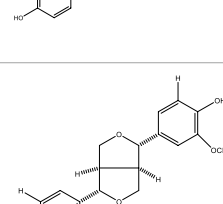
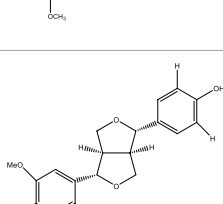
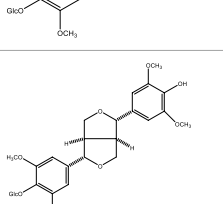
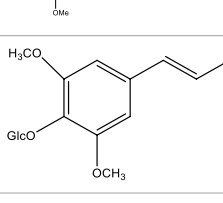
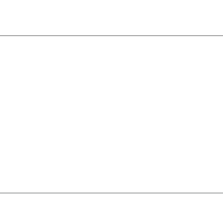

Compounds name	Chemical structure	Ref	Compounds name	Chemical structure	Ref
Alaschanoside A		(55)	Citrusin A		(55)
Conicaoside		(55)	Ddehydrodiconiferyl alcohol 4-O-β-D-glucopyranoside		(55)
Dehydrodiconiferyl alcohol γ'-O-β-D-glucopyranoside		(34, 55)	Eucommin A		(55)
Isoeucommin A		(55)	Isolariciresinol-9'-O-β-D-glucopyranoside		(48)
Lariciresinol 4-O-β-D-glucopyranoside		(55)	Lariciresinol 4'-O-β-D-glucopyranoside		(55)
Liriodendrin		(55)	Lariciresinol 4'-O-β-D-glucopyranoside		(55)
(+)-Pinoresinol		(56)	(+)-Pinoresinol O-β-D-glucopyranoside		(55)
(+)-syringaresinol		(12)	(+)-Syringaresinol O-β-D-glucopyranoside		(56)
Syringin		(56)			

TABLE 5 Polysaccharides from *Cistanche* species.

Name	Composition	Ref
ACDP-2	1,4-D-gal and D-glu, containing predominantly a branching point at the C6	(62)
CDA-0.05	contained 1, 4-linked $\alpha$ -D-Glcp, 1, 4, 6-linked $\alpha$ -D-Glcp and 1, 4-linked $\beta$ -D-Galp, with branches of T-linked $\alpha$ -D-Glcp attached at C-6 of 1, 4, 6-linked $\alpha$ -D-Glcp residues	(63)
CDA-1A	an $\alpha$ -(1 $\rightarrow$ 4)-D-glucan with $\alpha$ -(1 $\rightarrow$ 6)-linked branches attached to the O-6 of branch points	(64)
CDA-3B	an RG-I polysaccharide containing a typical rhamnogalacturonan backbone and arabinogalactan or arabinan branches	(64)
CLP-1	mannose 2.78%, galacturonic acid 4.07%, glucose 88.62%, galactose 1.80% and arabinose 2.39%	(65)
CLP2	rhamnose 5.79%, galacturonic acid 7.78%, glucose 9.99% and galactose 13.30%.	(65)
CTP	rhamnose, mannose, glucose, and galactose	(66)
CDP-4	straight-chain glucose	(66)
SPA	glucose and galactose are mainly composed of arabinose, rhamnose and mannose	(67)
-	$\alpha$ -1,4-D-glucan, $\alpha$ -L-arabino-3,6- $\beta$ -D-galactan, pectic polysaccharides and 4-O-methyl-D-glucurono-D-xylan.	(68)
-	glucose, galactose, rhamnose, arabinose and fructose	(69)

TABLE 6 Other compounds from *Cistanche* species.

Compound category	Name	R	Ref
Benzyl alcohol glycosides	salsaside A (Figure 1A)	$R_1 = H$ $R_2 = \text{trans-Caf}$	(42)
	salsaside B (Figure 1A)	$R_1 = \text{trans-Caf}$ $R_2 = H$	(42)
	salsaside C1 (Figure 1A)	$R_1 = \text{p-trans-Cou}$ $R_2 = H$	(42)
	salsaside C2 (Figure 1A)	$R_1 = \text{p-cis-Cou}$ $R_2 = H$	(42)
Phenylacetylated oligosugars	Cistanoside F (Figure 1B)	$R_1 = \text{trans-Caf}$ $R_2 = H$	(70)
	Cistanoside I (Figure 1B)	$R_1 = \text{p-trans-Cou}$ $R_2 = H$	(27)
	Cistantubulose A1/A2 (Figure 1B)	$R_1 = \text{trans-Caf}$ $R_2 = \text{Glc}$	(31)
	Cistansinense A1/A2 (Figure 1B)	$R_1 = \text{trans-Caf}$ $R_2 = \text{Rha}$	(40)
Monoterpenoids	8-hydroxygeraniol (Figure 1C)	$R = H$	(47)
	8-hydroxygeraniol-1- $\beta$ -D-glucopyranoside (Figure 1C)	$R = \text{Glc}$	(71)
	(2E,6R)-8-hydroxy-2,6-dimethyl-2-octenotic acid (Figure 1D)	$R = H$	(72)
	Kankanoside E (Figure 1D)	$R = \text{Glc}$	(48)
	(2E,6Z)-8-O- $\beta$ -D-glucopyranoside-2,6-dimethyl-2,6-octadienoic acid (Figure 1E)	$R = \text{Glc}$	(48)
	(2E)-2,6-dimethyl-2,7-octadiene-1,6-diol (Figure 1F)	$R_1 = \text{CH}_3$ $R_2 = \text{CH}_2\text{OH}$	(73)
Nitrogen-containing	(2Z)-2,6-dimethyl-2,7-octadiene-1,6-diol (Figure 1F)	$R_1 = \text{CH}_2\text{OH}$ $R_2 = \text{CH}_3$	(73)
	Uridine	-	(45)
	Inosine	-	(27)
	2'-O-methyladenosine	-	(27)
	(3R)-3-hydroxy-1-methyl-2-pyrrolidinone	-	(45)
	(3R)-3-hydroxy-2-pyrrolidinone	-	(45)
	(2,5-dioxo-4-imidazolidinyl)-carbamic acid	-	(74)
	Succinimide	-	(29)
	2-methanol-5-hydroxy-pyridine	-	(73)
	betaine	-	(75)

Caf: caffeoyl; Cou: coumaroyl; Glc:  $\beta$ -D-glucopyranosyl; Rha:  $\alpha$ -L-rhamnopyranosyl.

neuroprotective effects, through cell experiments have found that CDP can inhibit oxidative stress and regulate the secretion and expression of DJ-1 has a protective effect on nerve damage induced by OGD/RP. So it has clinical significance for the treatment of ischemic stroke diseases (82). The Parkinson's disease like model induced by the neurotoxin 1-methyl-4-phenyl-1,2,3,6-tetrahydropyridine(MPTP) is mainly based on the lack of its ability to produce dopamine in the striatum, resulting in the loss of dopaminergic neurons in the dense part of the substantia nigra, the study found that the mouse model pretreated with PhGs had obvious neuroprotective effect on dopaminergic neurons in substantia nigra by immunohistochemical analysis. Therefore, it is believed that PhG is conducive to the treatment of Parkinson's disease and plays a neuroprotective role in the human body (83).

### 3.3. Antioxidant effect

Among the existing health foods of *Cistanche deserticola* in the market, many products claim to have antioxidant effect (Table 9). In the research on the oxidation of *Cistanche deserticola*, Zhang et al. (86) compared and analyzed the chemical components and biological effects of the raw product of *Cistanche deserticola* slices (RCD) and its wine steam processed product (WSCD). The final results showed that both of them could restore the sex hormone level of model mice and improve the antioxidant effect. By comparing and analyzing the therapeutic effects of antioxidants and cistanche powder on cataracts with senescence accelerated OXYS rats as the test object. The experimental results showed that the antioxidant effect was related to

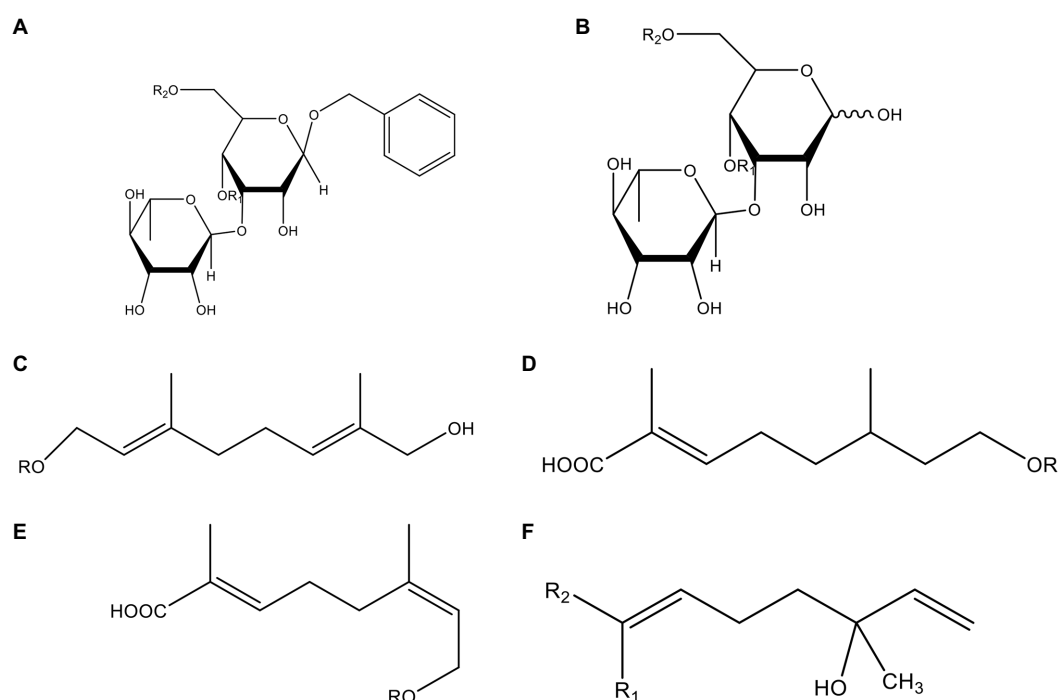


FIGURE 1  
Some chemical structures in *cistanche*.

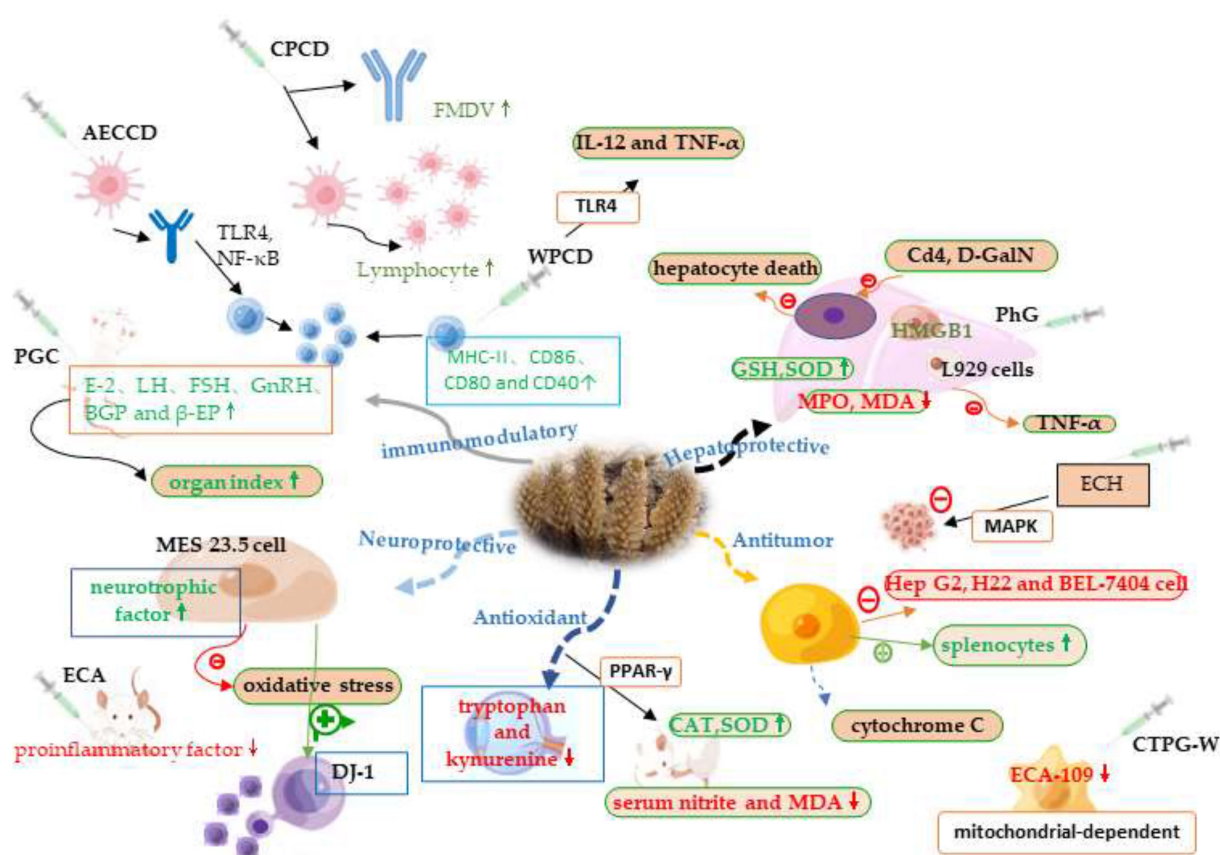


FIGURE 2  
Immunomodulatory effect mechanisms of *cistanche*.



TABLE 7 Immunomodulatory mechanism of *cistanche*.

Functional ingredients	Cell line/Animal model or method	Occurring mechanism or effect	Evaluation of research findings	Ref
CPCD	Modulator activities of CPCD on activating dendritic cells (DCs) and the adjuvant potential for foot and mouth disease vaccine (FMDV)	TLR-2 or TLR-4 antibodies suppressed levels of CPCD-mediated CD40 and CD86 as well as IL-6 and IL-1 $\beta$ in DCs. CPCD induced the phosphorylation of MAPKs related molecules and NF- $\kappa$ B.	CPCD could effectively stimulate stronger humoral and cellular responses by modulating DC activation through TLR-2/TLR-4 related MAPKs and NF- $\kappa$ B pathway.	(76)
AECCD(aqueous extracts of cultivated <i>Cistanche deserticola</i> )	ICR mice against ovalbumin (OVA), dendritic cells (DC) activation mechanism by AECCD	AECCD elicited vigorous and long-term IgG responses with mixed Th1/Th2 responses and up-regulated levels of Th-associated cytokines (CD4 + IL-4, CD4 + IFN- $\gamma$ and CD8 + IFN- $\gamma$ ).	AECCD could elicit potent and durable antigen specific immune responses through DC activation.	(77)
PGC	Wistar female rats were selected. The left ovaries for all rats except in the blank control group(BC) were removed, and the right ovaries were removed in 80%.	PGC increase the activity, the organ index (thymus, spleen, uterus), E-2, T, BGP level in serum, beta-EP level in plasma, AR level in hypothalamus, ER level in hypothalamus, pituitary, uterus in perimenopausal model rats. And it also reduced FSH, LH, GnRH level in serum, and improved uterine and ovarian lesions in perimenopausal model rats.	Each dose of PCG could counteract the disorder of sex hormone in perimenopausal model rats, correct the imbalance of ER and AR level, enhance and restore the effect of uterus and the nerve cells of hypothalamic, and improve immune function.	(78)
WPCD	DCs from C57BL/6 mice, ovalbumin (OVA) (Sigma) was used as the model antigen and female ICR mice	WPCD significantly promoted the maturation and function of murine marrow-derived dendritic cells (BM-DCs) through up-regulating the expression levels of MHC-II, CD86, CD80, and CD40, allogenic T cell proliferation, and the yields of IL-12 and TNF- $\alpha$ via toll-like receptor4 (TLR4), as indicated by <i>in vitro</i> experiments.	WPCD could modulate immune responses <i>in vitro</i> and <i>in vivo</i> .	(79)

TABLE 8 Neuroprotective effect mechanism of *cistanche*.

Functional ingredients	Cell line/Animal model or method	Occurring mechanism or effect	Evaluation of research findings	Ref
Herba Cistanches	Induced oxidative damage in MES23.5 cells using H2O2	All drug-containing serums improved the survival rate of H2O2-injured MES23.5 cells, inhibited pro-apoptotic FasL and caspase-3 expression, promoted anti-apoptotic Bcl-2 expression.	Chinese medicines used to tonify the kidney can protect nerve cells by regulating the expression of apoptosis-related factors and neurotrophic factors in MES23.5 cells.	(80)
ECA	Kainic acid-induced seizures in rats	Rats pre injected with Echinacea could reduce the effect of kainic acid on glutamate concentration in mice, slow down neuron loss and microglia activation, and inhibit the expression of proinflammatory cytokine genes in hippocampus	Echinacoside is the potentially useful in the prevention of epilepsy	(81)
CDP	PC12 cell model	CDP (0.05, 0.5 and 5 $\mu$ g/ml) attenuated PC12 cell death, preserved MMP and calcium homeostasis; inhibited oxidative stress and decreased cell apoptosis. Moreover, CDP (5 $\mu$ g/ml) markedly stimulated DJ-1 secretion and expression.	CDP exerts neuroprotective effect against OGD/RP-induced injury by inhibiting oxidative stress and regulating the DJ-1 pathway	(82)
PhG	Parkinson's mouse model induced by neurotoxin 1-methyl-4-phenyl-1,2,3,6-tetrahydropyridine (MPTP)	Neuroprotective effects of PhGs on nigral dopaminergic neurons were confirmed by the results of immunohistochemical staining.	PhG has neuroprotection	(83)

TABLE 9 Antioxidant effect mechanism of cistanche.

Functional ingredients	Cell line/animal model or method	Occurring mechanism or effect	Evaluation of research findings	Ref
<i>Cistanche deserticola</i>	Senescence accelerated OXYS rats	The oxidation rate of tryptophan and kynurenine in mice supplemented with <i>Cistanche deserticola</i> slowed down	<i>Cistanche deserticola</i> can slow down the development of cataract	(84)
Cistanche	Sevoflurane-induced aged cognitive dysfunction rat model	<i>Cistanche deserticola</i> can reduce oxidative stress by reducing nitrite and MDA and increasing SOD and CAT activities at the same time.	<i>Cistanche deserticola</i> can activate PPAR- $\gamma$ Signal transduction plays an antioxidant role in the development of sevoflurane induced cognitive dysfunction	(85)
PhG	Kidney yang deficiency model	The contents of SOD and MDA in treatment group were higher than those in other groups, the Level of Hormone (T and E2). were increasing	PhG can restore the level of neutral hormones in the kidney yang deficiency model and improve the antioxidant effect	(86)
PhG	AD senescence accelerated mouse prone 8 (SAMP8) model	PHG significantly increased the density of dendritic spines in hippocampal CA1 region, accompanied by increased expression levels of synaptophysin (SYN) and postsynaptic density 95 (PSD-95), decreased MDA content, and increased SOD and GSH PX activities	The ability of PhG to ameliorate cognitive deficits in SAMP8 mice may be related to promotion in synaptic plasticity involving antioxidant processes	(87)

the oxidation rate and level of tryptophan and kynurenine in the lens, and cistanche powder, like antioxidants, helped to slow down the oxidation rate of tryptophan and kynurenine, reduce the level, which can effectively reduce the oxidative stress in the lens and help cataract treatment (84). Some researchers also took rats with senile stress disorder as the research object, through the analysis of serum nitrite and MDA concentration, SOD and CAT activity, Cistanche can reduce nitrite and MDA concentration and increase SOD and CAT activity, so as to reduce the level of oxidative stress (85). Combined with the application of PPAR- $\gamma$  anti-caking agents, the results show that cistanche can exert antioxidant effects on the development of sevoflurane-induced cognitive dysfunction by activating PPAR- $\gamma$  signaling. (87) extracted PhG from cistanche, studied the cognitive protection mechanism of PhG pair (SAMP3) model mice, and by measuring MDA concentration, SOD and GSH-Px activity, the results showed that PhG has antioxidant effects. Therefore, cistanche has a positive role in antioxidant research, and studying antioxidant mechanisms helps to provide clinical guidance and recommendations for disease treatment.

### 3.4. Antitumor effect

Modern pharmacological studies have shown that Cistanche tubulosa phenylethanoid glycosides (CTPG) has anti-tumor effects on a variety of tumor cells (Table 10). At present, through cell experiments and H22 Tumor mouse model studies, CTPG can inhibit the normal growth of Hep G2 and BEL-7404 cells by inducing cell cycle arrest and apoptosis. And *in vivo* test results show that CTPG enhanced the proliferation of splenocytes and reduced the apoptosis of splenocytes induced by cisplatin. It can be seen that CTPG has the effect of inhibiting the growth of tumor cells (88). Yuan et al. (89) studied the anti-tumor mechanism and effect of CTPG on H22 liver cancer cells through a combination of *in vivo* and *in vitro* experiments. The final results showed that CTPG could inhibit the growth of H22 cells, promote the release of cytochrome C, and significantly enhance the signaling pathway. The level of caspase-8 and caspase-9 cleavage, which activates caspase-7 and -3 to cleave PARP, so CTPG can improve

the survival rate of liver cancer mice. Fu et al. (90) studied the effect of water-soluble phenylethanoid glycosides of *C. tubulosa* (CTPG-W) on ECA-109 cell, and the results showed that CTPG-W can significantly reduce cell viability, induce apoptosis of ECA-109 cells through mitochondrial-dependent pathways, and have a high-quality therapeutic effect on esophageal cancer. Echinacoside (ECH), one of the phenylethanoids, isolated from the stems of *Cistanche salsa*, has been shown to inhibit the proliferation of pancreatic cancer cells by promoting apoptosis, and revealed that ECH inhibits tumor cell growth by regulating MAPK activity (91). So, it can be seen that cistanche has development potential in cancer treatment.

### 3.5. Hepatoprotective effect

Liver damage, cirrhosis and fatty liver disease are currently more common liver diseases, affecting people's health (Table 11). Morikawa et al. (92) used the methanolic extract from fresh stems of Cistanche tubulosa to study the protective effect of PhG on the liver, they used a model of liver damage caused by D-galactosamine (D-GalN)/lipopolysaccharide (LPS) and found that PhG can inhibit hepatocyte death, reducing the toxic effect of TNF- $\alpha$  on L929 cells. It is believed that PhG has a hepatoprotective effect *in vivo*. Xiong et al. (93) used NADPH/CCl<sub>4</sub>-induced fatty liver rat model, observing the inhibitory effect of PhGs compounds on hepatocytes efficiently, they prevented cell damage induced by exposure to Cd<sub>4</sub> or o-galactosamine (D-GalN), thus it was proved that PhGs have a protective effect on liver cells. Cui et al. (94) used the GalN/LPS-induced-acute-hepatic-injury mouse model, found that the plasma ALT and AST levels of mice given to the ACT group were significantly reduced. The content of GSH and SOD was increased in the metabolites of liver tissue, the level of MPO and MDA was reduced, and the pathological changes of liver histopathology were effectively improved. And the inflammatory cytokine HMGB1 in serum was effectively improved. TNF- $\alpha$  and IL-6 levels have a regulatory effect, which suggests that ACT can effectively prevent liver damage. Because SOD is a typical antioxidant enzyme, GST is a soluble protein located in cytoplasm that plays an important role in liver detoxification. So SOD and GST are considered as

TABLE 10 Antitumor effect mechanism of cistanche.

Functional ingredients	Cell line/Animal model or method	Occurring mechanism or effect	Evaluation of research findings	Ref
CTPG	HepG2 and BEL-7404 hepatocellular carcinoma (HCC) cells, H22 tumor mouse model	CTPG significantly inhibited the growth of HepG2 and BEL-7404 cells through the induction of cell cycle arrest and apoptosis, which was associated with the activation of MAPK pathways characterized by the up-regulated phosphorylation of p38, JNK, and ERK1/2 and mitochondria-dependent pathway characterized by the reduction of mitochondrial membrane potential. The release of cytochrome c and the cleavage of caspase-3, -7, -9, and PARP were subsequently increased by CTPG treatment. CTPG combined with cisplatin further inhibited the growth of H22 cells and reduced the side effects of cisplatin.	CTPG inhibited the growth of HCC through direct antitumor effect and indirect immunoenhancement effect, and improved the antitumor efficacy of cisplatin	(88)
CTPG	H22 cells; tumor mouse model established using male Kunming mice	CTPG treatment significantly suppressed H22 cell growth in a dose and time dependent manner; significantly increased Bax/Bcl-2 ratio, reduced $\Delta\psi_m$ and enhanced the release of cytochrome c; the levels of cleaved caspase-8 and caspase-9 in both extrinsic and intrinsic signaling pathways were significantly increased that sequentially activated caspase-7 and -3 to cleave PARP.	CTPG suppressed H22 cell growth through both extrinsic and intrinsic apoptosis pathways	(89)
CTPG-W	Eca-109 cells	CTPG-W significantly reduced the viability of Eca-109 cells through the induction of apoptosis and cell cycle arrest; and the levels of cytochrome c and c-Jun NH2-terminal kinase were increased, which upregulated the levels of cleaved-poly (ADP-ribose) polymerase and cleaved-caspase-3, -7 and -9, but not caspase-8.	CTPG-W induced apoptosis of Eca-109 cells through a mitochondrial-dependent pathway	(90)
ECH	SW1990 pancreatic adeno- carcinoma cells	ECH can markedly inhibit the proliferation of pancreatic adenocarcinoma cells by inducing the production of reactive oxygen species and the perturbation of mitochondrial membrane potential and thus triggering apoptosis; and ECH represses tumor cell growth through modulating MAPK activity	ECH inhibits cancer development	(91)

TABLE 11 Hepatoprotective effect mechanism of cistanche.

Functional ingredients	Cell line/Animal model or method	Occurring mechanism or effect	Evaluation of research findings	Ref
PhG	D-galactosamine (D-GalN)/ lipopolysaccharide (LPS)- induced liver injury in mice	20-acetylacteoside and tubuloside A inhibited D-GalN-induced death of hepatocytes. isolates and cistantubuloside B1 also reduced TNF- $\alpha$ -induced cytotoxicity in L929 cells	Fresh cistanche extract has a protective effect on the liver	(92)
PhGs	NADPH/CCl4-induced lipid peroxidation in rat liver microsomes	The tested four phenylethanoids consecutively inhibited both hepatocytes lipid peroxidation and AST release to the medium and alleviated the cell death induced by CCl4	Phenylethanoids were potent hepatoprotective agents against CCl4 intoxication.	(93)
Acteoside (ACT)	GalN/LPS-induced-acute-hepatic-injury mouse model	GalN/LPS administration markedly increased MPO levels in liver tissues, indicating significant macrophage infiltration, whereas the CA, HT, and 3-HPP pretreatments reduced the levels of MPO; the ACT group reduced levels of HMGB1, TNF- $\alpha$ , and IL-6	ACT metabolites could be responsible for the potent hepatoprotective activity as well as the other therapeutic effects.	(94)
CDP-C	Hep G2 and Er Guo-tou white spirit was used to establish liver injury model in ICR mice	<i>In vitro</i> research, CDP-C promoted viability of HepG2 cells; CDP-C can reduce the contents of MDA and TG in liver, and modulate the enzyme activities	CDP-C can be used in the treatment of alcoholic liver disease	(95)

indicators of alcoholic hepatotoxicity, and liver MDA and TG can also be used as indicators of hepatotoxicity. In the end, alcohol has been found to significantly reduce SOD and GST levels and elevate MDA and TG levels in mice, while CDP-C mitigates this change, and

histopathological observations of liver slices suggest that CDP-C can significantly restore alcohol damage to liver tissue (95). Therefore, it is believed that cistanche products play a positive role in liver protection and liver protection.

### 3.6. Other pharmacological effects

In addition, cistanche has pharmacological effects such as immunomodulatory, antioxidant, anti-cancer and hepatoprotective liver protection. It also plays an active role in preventing osteoporosis, maintaining the health of the intestinal flora, and protecting heart health. By observing the effect of cistanche on the content and functional parameters of myocardial mitochondrial glutathione content and functional parameters in rats. It was found that cistanche alcohol extracts could increase mitochondrial glutathione content, reduce mitochondrial  $\text{Ca}^{2+}$  content, increase mitochondrial membrane potential, induce the production of unconjugated proteins. Thereby enhancing the cardiac mitochondrial glutathione status and respiration in rats, and playing a cardioprotective role (96). By giving rats with excision of ovaries, cistanche extract was found to significantly increase bone density (BMD), bone mineral content (BMC), maximum load, maximum load displacement, maximum load stress, self-breaking load, self-breaking displacement, self-breaking stress, and can significantly improve blood antioxidant enzyme activity, reduce blood calcium, zinc, copper levels. Thereby proving that cistanche has the effect of preventing osteoporosis (97). Fu et al. (98) fed rats cistanche polysaccharides, through pharmacokinetic parameters and intestinal microbial composition studies found that cistanche polysaccharides can increase the growth of intestinal beneficial flora, improve the production of short-chain fatty acids, promote the body's intestinal health. Zhu et al. (99) used diet/streptozotocin (STZ)-induced diabetic rats, the research found that total glycosides of cistanche tubulosa (TGCT) could improve oral glucose tolerance test (OGTT), area under curve of glucose (AUC-G) and insulin sensitivity, increase glycogen content and glucose metabolism enzyme activity, regulate blood lipid changes. So TGCT can be considered to have a lipid-lowering and glucose lowering effect. As a traditional tonic Chinese herbal medicine, cistanche has a far-reaching influence in regulating the function of the body, and its development as a food has far-reaching research value in nutrition and health research.

## 4. Conclusion

Cistanche is a kind of traditional Chinese medicine with high medicinal value in the history of Chinese medicine, known as “desert ginseng,” modern composition analysis studies have shown that cistanche contains hundreds of active ingredients, of which the content and type of phenethyl glycosides are the most extensively studied. In 2021, the European Food Safety Authority (EFSA) passed (EU) 2015/2283 (100), which means that cistanche water extract PhG has the potential to enter EFSA's novel food list and it may have the opportunity to be produced in Europe as a food supplement and food for special medical purposes. In conjunction with China, cistanche is listed as a dual-use substance for medicine and food, and is included in the list of food and drug homologous substances. And Liao et al. (101) conducted genotoxicity and 28-day repeated dose toxicity test, it is fully proved that cistanche has a certain degree of edible safety. This review summarized the composition of cistanche, briefly introduce the health benefits of cistanche on the human body, and describes its mechanism of bioactive ingredient. However, due to the

short time that cistanche has been included in the list of medicinal and food homologous substances, the current product processing technology is still based on processing drugs, slicing and synergistic, so the development of cistanche foods is limited. And its functional characteristics are limited to its pharmacokinetic research, which is different from the nutrition research of traditional foods. Therefore, we believe that cistanche has great potential for development in functional food applications, as a food and drug homologous substances. In the future, researchers should strengthen its functional characteristics research, further analyze the chemical composition, active ingredient quality control and influence mechanism of cistanche. To establish a standardized composition extraction and processing process and quality determination standards for cistanche. So as to better promote human health.

## Author contributions

SZ: conceptualization, methodology, writing—original draft preparation, and visualization. YZ and SZ: software and formal analysis. DF: validation. DF and HD: investigation. HD: resources. WY: data curation, writing—review and editing, and funding acquisition. WY and SZ: supervision. WY and YJ: project administration. All authors have read and agreed to the published version of the manuscript.

## Funding

This research was funded by Beijing Municipal University Classification Development Project.

## Conflict of interest

YJ was employed by Inner Mongolia Sankou Biotechnology Co., Ltd.

The remaining authors declare that the research was conducted in the absence of any commercial or financial relationships that could be construed as a potential conflict of interest.

## Publisher's note

All claims expressed in this article are solely those of the authors and do not necessarily represent those of their affiliated organizations, or those of the publisher, the editors and the reviewers. Any product that may be evaluated in this article, or claim that may be made by its manufacturer, is not guaranteed or endorsed by the publisher.

## Supplementary material

The Supplementary material for this article can be found online at: <https://www.frontiersin.org/articles/10.3389/fnut.2023.1101182/full#supplementary-material>



## References

- Gang, Z., Jia-Min, G., and Jin, C. Application of Cistanche in health food. *J Food Saf Qual.* (2021) 12:898–903. doi: 10.19812/j.cnki.jfsq11-5956/ts.2021.03.012
- Editorial Board of the Vegetation Map of China, C.A.O.S. *Flora of China*. Beijing: Science Press (1993).
- Dai-Qing, L., Rong, X., Xiu-Li, H., Ru, F., Chang-Qing, X., Tong-Ning, L., et al. Market investigation and study of standard grade of Cistanches Herba. *Mod Chin Med.* (2021) 23:1954:401–8. doi: 10.13313/j.issn.1673-4890.20200803006
- Kurban, G., Imerhasan, M., Osman, K., Helil, S., and Tursun, X. Determination of contents of nutrition and microelement in the Uyghur traditional health protection medicinal materials. *Herba Cistanches Sci Technol Food Ind.* (2009) 30:289–91. doi: 10.13386/j.issn1002-0306.2009.09.080
- De Medeiros, P., Pinto, DV, De Almeida, JZ, Rego, JMC, Rodrigues, FAP, Lima, AAM, et al. Modulation of intestinal immune and barrier functions by vitamin a: implications for current understanding of malnutrition and enteric infections in children. *Nutrients.* (2018) 10:128:1–14. doi: 10.3390/nu10091128
- Kazmierczak-Baranska, J., Boguszewska, K., Adamus-Grabicka, A., and Karwowski, BT. Two faces of vitamin C-Antioxidative and pro-oxidative agent. *Nutrients.* (2020) 12:1–19. doi: 10.3390/nu12051501
- Zinder, R., Cooley, R., Vlad, LG, and Molnar, JA. Vitamin a and wound healing. *Nutr Clin Pract.* (2019) 34:839–49. doi: 10.1002/ncp.10420
- Busso, D., David, A., Penailillo, R., Echeverria, G., Rigotti, A., Kovalskys, I., et al. Intake of vitamin E and C in women of reproductive age: results from the Latin American study of nutrition and health (ELANS). *Nutrients.* (2021) 13:1954:1–16. doi: 10.3390/nu13061954
- Klosterbuer, A., Roughead, ZF, and Slavin, J. Benefits of dietary fiber in clinical nutrition. *Nutr Clin Pract.* (2011) 26:625–35. doi: 10.1177/0884533611416126
- Zemrani, B., and Bines, JE. Recent insights into trace element deficiencies: causes, recognition and correction. *Curr Opin Gastroenterol.* (2020) 36:110–7. doi: 10.1097/MOG.0000000000000612
- Fu, ZF, Fan, X., Wang, XY, and Gao, XM. Cistanches Herba: an overview of its chemistry, pharmacology, and pharmacokinetics property. *J Ethnopharmacol.* (2018) 219:233–47. doi: 10.1016/j.jep.2017.10.015
- Qing-Qing, S., Ke, Z., Ting, L., Peng-Wei, G., Xing-Cheng, G., Xia, X., et al. Simultaneous determination of multiple components of Cistanches Herba based on reversed phase-hydrophilic interaction chromatography-tailored multiple reaction monitoring. *Chin J Anal Chem.* (2020) 48:1573–82. doi: 10.19756/j.issn.0253-3820.201104
- Zhou, XL, Xu, MB, Jin, TY, Rong, PQ, Zheng, GQ, and Lin, Y. Preclinical evidence and possible mechanisms of extracts or compounds from Cistanches for Alzheimer's disease. *Aging Dis.* (2019) 10:1075–93. doi: 10.14336/AD.2018.0815-1
- Wen-Ting, T., Xiao-Ming, W., Rong, X., Mei-Feng, S., Xiao-Mei, L., Xiao-Yan, C., et al. Content Determining of Phenylethanoid glycosides and polysaccharides in Cistanche deserticola and their antioxidant activity. *Mod Chin Med.* (2018) 20:426–31. doi: 10.13313/j.issn.1673-4890.20171209001
- Gu, C., Yang, X., and Huang, L. Cistanches Herba: a neuropharmacology review. *Front Pharmacol.* (2016) 7:289. doi: 10.3389/fphar.2016.00289
- Jiang, L., Zhou, B., Wang, X., Bi, Y., Guo, W., Wang, J., et al. The quality monitoring of Cistanches Herba (Cistanche deserticola Ma): a value chain perspective. *Front Pharmacol.* (2021) 12:782962. doi: 10.3389/fphar.2021.782962
- Zhang, J., Li, C., Che, Y., Wu, J., Wang, Z., Cai, W., et al. LTQ-Orbitrap-based strategy for traditional Chinese medicine targeted class discovery, identification and herbomics research: a case study on phenylethanoid glycosides in three different species of Herba Cistanches. *RSC Adv.* (2015) 5:80816–28. doi: 10.1039/c5ra13276b
- Li, W-L, Ding, J-X, Bai, J., Hu, Y., Song, H., Sun, X-M, et al. Research on correlation of compositions with oestrogenic activity of Cistanche based on LC/Q-TOF-MS/MS technology. *Open Chem.* (2019c) 17:1–12. doi: 10.1515/chem-2019-0001
- Ai, Z., Zhang, Y., Li, X., Sun, W., and Liu, Y. Widely targeted metabolomics analysis to reveal transformation mechanism of Cistanche deserticola active compounds during steaming and drying processes. *Front Nutr.* (2021) 8:742511. doi: 10.3389/fnut.2021.742511
- Li, R., Zhao, M., Tu, P., and Jiang, Y. Simultaneous determination of five phenylethanoid glycosides in Cistanches Herba using quantitative analysis of multi-components by single marker. *J Chin Pharm Sci.* (2019) 28:537–46. doi: 10.5246/jcps.2019.08.051
- Lu, D., Zhang, J., Yang, Z., Liu, H., Li, S., Wu, B., et al. Quantitative analysis of Cistanches Herba using high-performance liquid chromatography coupled with diode array detection and high-resolution mass spectrometry combined with chemometric methods. *J Sep Sci.* (2013) 36:1945–52. doi: 10.1002/jssc.201300135
- Yan-Xia, D., Xiao-Qin, W., and Ying, Z. Quantitative assay of six main phenylethanoid glycosides in Cistanche Herba by high performance liquid chromatography. *Lishizhen Med Materia Med Res.* (2020) 31:813–6. doi: 10.3969/j.issn.1008-0805.2020.04.012
- Jian-Song, L., Cui-Li, X., Meng-Hua, W., Ying, Z., Hui, C., and Zhi-Guo, M. Determination and chemometric evaluation of six phenylethanolic glycosides in Cistanche deserticola and Cistanche sinensis by UPLC. *Chin J Pharm Anal.* (2021) 41:266–35. doi: 10.16155/j.0254-1793.2021.02.06
- Xie, C., Xu, X., Liu, Q., Xie, Z., Yang, M., Huang, J., et al. Isolation and purification of Echinacoside and Acteoside from Cistanche tubulosa (Schrenk) Wight by high-speed counter-current chromatography. *J Liq Chromatogr Relat Technol.* (2012) 35:2602–9. doi: 10.1080/10826076.2011.637270
- Yang, Z., Lu, D., Yao, S., Zhang, R., Jiang, Z., and Ma, Z. Chemical fingerprint and quantitative analysis of Cistanche deserticola by HPLC-DAD-ESI-MS. *J Food Drug Anal.* (2013) 21:50–7. doi: 10.6227/jfda.2013210106
- Dong, Y., Guo, Q., Liu, J., and Ma, X. Simultaneous determination of seven phenylethanoid glycosides in Cistanches Herba by a single marker using a new calculation of relative correction factor. *J Sep Sci.* (2018) 41:1913–22. doi: 10.1002/jssc.201701219
- Pan, Y. *Studies on the constituents and bioactivity of fresh Cistanche tubulosa doctor.* Liaoning: Shenyang Pharmaceutical University (2011).
- Deyama, T., Kobayashi, H., Nishibe, S., and Tu, P. Isolation, structure elucidation and bioactivities of Phenylethanoid glycosides from Cistanche, forsythia and Plantago plants. *Chemistry.* (2006) 33:645–74. doi: 10.1016/S1572-5995(06)80036-0
- Zhaohui, X., Junshan, Y., Ruimian, L., Yang, L., Junguo, Z., Qitai, Z., et al. A new natural product from Cistanche deserticola Y.C. *Ma J Chin Pharma Sci.* (1999) 8:2167947:61–3.
- Kobayshi, H., Karasawa, H., Miyase, T., and Fukushima, S. Studies on the constituents of cistanche herba. IV. Isolation and structures of two new phenylpropanoid glycosides, cistanosides C and D. *Chem Pharm Bull.* (1984) 32:3880–5. doi: 10.1248/cpb.32.3880
- Tu, P-F, Song, Z-H, Shi, H-M, Jiang, Y., and Zhao, Y-Y. Arylethyl (= Phenylethanoid) glycosides and oligosaccharide from the stem of Cistanche tubulosa. *Helv Chim Acta.* (2006) 89:927–35. doi: 10.1002/hlca.200690096
- Yoshikawa, M., Matsuda, H., Morikawa, T., Xie, H., Nakamura, S., and Muraoka, O. Phenylethanoid oligoglycosides and acylated oligosugars with vasorelaxant activity from Cistanche tubulosa. *Bioorg Med Chem.* (2006) 14:7468–75. doi: 10.1016/j.bmc.2006.07.018
- Nan, ZD, Zeng, KW, Shi, SP, Zhao, MB, Jiang, Y., and Tu, PF. Phenylethanoid glycosides with anti-inflammatory activities from the stems of Cistanche deserticola cultured in Tarim desert. *Fitoterapia.* (2013) 89:167–74. doi: 10.1016/j.fitote.2013.05.008
- Qingqing, S. (2019). Study on the chemical composition of Chinese medicine cistanche and the in vivo pharmacodynamic substances against vascular dementia. Doctor. Beijing University of Traditional Chinese Medicine.
- Liu, X-M, Li, J., Jiang, Y., Zhao, M-B, and Tu, P-F. Chemical constituents from Cistanche sinensis (Orobanchaceae). *Biochem Syst Ecol.* (2013) 47:21–4. doi: 10.1016/j.bse.2012.09.003
- Pan, Y., Morikawa, T., Ninomiya, K., Imura, K., Yuan, D., Yoshikawa, M., et al. Bioactive constituents from Chinese natural medicines. XXXVI. Four new Acylated Phenylethanoid Oligoglycosides, Kankanosides J1, J2, K1, and K2, from stems of Cistanche tubulosa. *Chem Pharm Bull.* (2010) 58:575–8. doi: 10.1248/cpb.58.575
- Karasawa, H., Kobayashi, H., Takizawa, N., Miyase, T., and Fukushima, S. Studies on the constituents of Cistanche herba. VIII. *Yakugaku Zasshi.* (1986) 106:721–4. doi: 10.1248/yakushi1947.106.8\_721
- Yang, J., Du, N., and Kasimu, R. Phenylethanoid glycosides from cultivated Cistanche salsa. *J Chin Pharm Sci.* (2005):242–5.
- Zhengyi, Q., Chunlin, Y., Yinping, J., Hongqun, L., and Yingping, W. Research Progress in chemical constituents and pharmacological effects of Orobanchaceae. *Special Wild Econ Anim Plant Res.* (2010) 32:75. doi: 10.16720/j.cnki.tcyj.2010.01.009
- Tu, PF, Shi, HM, Song, ZH, Jiang, Y., and Zhao, YY. Chemical constituents of Cistanche sinensis. *J Asian Nat Prod Res.* (2007) 9:79–84. doi: 10.1080/10286020500384450
- Xiaoming, L., Yong, J., Yongqiang, S., Xinwen, X., and Pengfei, T. Study on cistanche constituents of Cistanche deserticola. *Chin Pharm J.* (2011) 46:1053–8.
- Lei, L., Jiang, Y., Liu, X-M, Tu, P-F, Wu, L-J, and Chen, F-K. New glycosides from Cistanche salsa. *Helv Chim Acta.* (2007) 90:79–85. doi: 10.1002/hlca.200790024
- Han, L., Ji, L., Boakye-Yiadom, M., Li, W., Song, X., and Gao, X. Preparative isolation and purification of four compounds from Cistanche deserticola Y.C. Ma by high-speed counter-current chromatography. *Mol Ther.* (2012) 17:8276–84. doi: 10.3390/molecules17078276
- Jiang, C., Wan, F., Zang, Z., Zhang, Q., Ma, G., and Huang, X. Effect of an ultrasound pre-treatment on the characteristics and quality of far-infrared vacuum drying with Cistanche slices. *Foods.* (2022) 11:866. doi: 10.3390/foods11060866
- Jianghua, Y., Junping, H., Kasimu, R., and Niansheng, D. Studies on the iridoid glycosides of cultivated Cistanche salsa. *Lishizhen Med Materia Med Res.* (2009) 20:522–3.
- Wenjing, L., Yan, C., Qingqing, S., Jian, Z., Yunfang, Z., Pengfei, T., et al. Chemical characterization for flowers and lignified stems of Cistanche deserticola. *China J Chin Materia Med.* (2018) 43:3708–14. doi: 10.19540/j.cnki.cjcmm.20180612.001



47. Hong, SZ-I, Shao-Hong, M, Yan, C, Peng-Fei, T, Yu-Ying, Z, and Jun-Hua, Z. Studies on chemical constituents of *Cistanche tubulosa* (Schenk) R. Wight. *China J Chin Materia Med.* (2000) 24:6.
48. Xie, H, Morikawa, T, Matsuda, H, Nakamura, S, Muraoka, O, and Yoshikawa, M. Monoterpene constituents from *Cistanche tubulosa*—chemical structures of Kankanosides A—E and Kankanol—. *Chem Pharm Bull.* (2006) 54:669–75. doi: 10.1248/cpb.54.669
49. Kobayashi, H, Karasawa, H, Miyase, T, and Fukushima, S. Studies on the constituents of *Cistanche herba*. III. Isolation and structures of new phenylpropanoid glycosides, cistanosides A and B. *Chem Pharm Bull.* (1984) 32:3009–14. doi: 10.1248/cpb.32.3009
50. Kobayashi, H, Karasawa, H, Miyase, T, and Fukushima, S. Studies on the constituents of *Cistanche herba*. II. Isolation and structures of new iridoids, cistanin and cistachlorin. *Chem Pharm Bull (Tokyo).* (1984) 32:1729–34. doi: 10.1248/cpb.32.1729
51. Nan, ZD, Zhao, MB, Zeng, KW, Tian, SH, Wang, WN, Jiang, Y, et al. Anti-inflammatory iridoids from the stems of *Cistanche deserticola* cultured in Tarim Desert. *Chin J Nat Med.* (2016) 14:61–5. doi: 10.3724/SPJ.1009.2016.00065
52. Kouda, R, and Yakushiji, F. Recent advances in Iridoid chemistry: biosynthesis and chemical synthesis. *Chem Asian J.* (2020) 15:3771–83. doi: 10.1002/asia.202001034
53. Xu, XY, Wang, DY, Li, YP, Deyrup, ST, and Zhang, HJ. Plant-derived lignans as potential antiviral agents: a systematic review. *Phytochem Rev.* (2022) 21:239–89. doi: 10.1007/s11101-021-09758-0
54. Yashin, AY, Yashinskii, DB, Vedenin, AN, Nifant'ev, NE, Nemzer, BV, and Yashin, YI. Chromatographic determination of Lignans (antioxidants) in food products. *J Anal Chem.* (2018) 73:399–406. doi: 10.1134/s106193481805012x
55. Zedong, N, Mingbo, Z, Yong, J, and Pengfei, T. Lignans from stems of *Cistanche deserticola* cultured in Tarim desert. *China J Chin Materia Med.* (2015) 40:463–8. doi: 10.4268/cjcm20150318
56. Yoshizawa, F, Deyama, T, Takizawa, N, Usmanghani, K, and Ahmad, M. The constituents of *Cistanche tubulosa* (SCHRENK) Hook.F. II. Isolation and structures of a new Phenylethanoid glycoside and a new Neolignan glycoside. *Chem Pharm Bull.* (1990) 38:1927–30. doi: 10.1248/cpb.38.1927
57. Chen, F, and Huang, G. Antioxidant activity of polysaccharides from different sources of ginseng. *Int J Biol Macromol.* (2019) 125:906–8. doi: 10.1016/j.ijbiomac.2018.12.134
58. Huang, S, and Huang, G. Extraction, structural analysis, and activities of rice bran polysaccharide. *Chem Biol Drug Des.* (2021) 98:631–8. doi: 10.1111/cbdd.13916
59. Cheong, K-I, Yu, B, Chen, J, and Zhong, S. A comprehensive review of the Cardioprotective effect of marine algae polysaccharide on the gut microbiota. *Foods.* (2022) 11:3550. doi: 10.3390/foods11223550
60. Li, N, Yu, X, Yu, Q, and Wang, M. Research progress on stability of polysaccharides in traditional Chinese medicine. *China J Chin Materia Med.* (2019) 44:4793–9. doi: 10.19540/j.cnki.cjcm.20190916.309
61. Xing-Hui, X, Hai-Xia, G, Hong-Hui, L, Xiao-Hui, J, Xiao-Nan, C, Gui-Fang, L, et al. Process optimization for extraction and purification of polysaccharides from *Cistanche deserticola*. *China J Chin Materia Med.* (2019) 44:475–81. doi: 10.19540/j.cnki.cjcm.20181129.004
62. Wu, XM, Gao, XM, Tsim, KW, and Tu, PF. An arabinogalactan isolated from the stems of *Cistanche deserticola* induces the proliferation of cultured lymphocytes. *Int J Biol Macromol.* (2005) 37:278–82. doi: 10.1016/j.ijbiomac.2005.11.001
63. Zeng, H, Huang, L, Zhou, L, Wang, P, Chen, X, and Ding, K. A galactoglucon isolated from *Cistanche deserticola* Y. C. Ma. And its bioactivity on intestinal bacteria strains. *Carbohydr Polym.* (2019) 223:115038. doi: 10.1016/j.carbpol.2019.115038
64. Dong, Q, Yao, J, Fang, JN, and Ding, K. Structural characterization and immunological activity of two cold-water extractable polysaccharides from *Cistanche deserticola* Y. C. Ma. *Carbohydr Res.* (2007) 342:1343–9. doi: 10.1016/j.carres.2007.03.017
65. Qiaoli, G, Zhibo, W, Yubi, Z, Lin, G, Xueqin, W, Jiachen, H, et al. Composition identification and antioxidant activity of *Cistanche lanzhouensis* polysaccharides. *Sci Technol Food Ind.* (2021) 42:96–103. doi: 10.13386/j.issn1002-0306.2021010193
66. Zhang, W, Huang, J, Wang, W, Li, Q, Chen, Y, Feng, W, et al. Extraction, purification, characterization and antioxidant activities of polysaccharides from *Cistanche tubulosa*. *Int J Biol Macromol.* (2016) 93:448–58. doi: 10.1016/j.ijbiomac.2016.08.079
67. Wei, Z, Hong, Y, Zhongyan, L, Yajun, Z, and Xinqian, J. Structural analysis of water-soluble polysaccharide SPA isolated from the stem of the *Cistanche Deserticola* Ma. *Chem J Chin Univ.* (2005) 461–3.
68. Naran, R, Ebringerova, A, Hromadkova, Z, and Patoprsty, V. Carbohydrate polymers from underground parts of *Cistanche deserticola*. *Phytochemistry.* (1995) 40:709–15. doi: 10.1016/0031-9422(95)00275-C
69. Sui, Z, Gu, T, Liu, B, Peng, S, Zhao, Z, Li, L, et al. Water-soluble carbohydrate compound from the bodies of *Herba Cistanche*: isolation and its scavenging effect on free radical in skin. *Carbohydr Polym.* (2011) 85:75–9. doi: 10.1016/j.carbpol.2011.01.053
70. Xiong, Q, Kadota, S, Tani, T, and Namba, T. Antioxidative effects of Phenylethanoids from *Cistanche deserticola*. *Biol Pharm Bull.* (1996) 19:1580–5. doi: 10.1248/bpb.19.1580
71. Kobayashi, H, and Komatsu, J. Studies on the constituents of *Cistanche herba*. I. *Yakugaku Zasshi.* (1983) 103:508–11. doi: 10.1248/yakushi1947.103.5\_508
72. Yamaguchi, K, Shinohara, C, Kojima, S, and Sodeoka, M. (2E,6R)-8-Hydroxy-2,6-dimethyl-2-octenoic acid, a novel anti-osteoporotic monoterpene, isolated from *Cistanche salsa*. *Biosci Biotechnol Biochem.* (1999) 63:731–5. doi: 10.1271/bbb.63.731
73. Jianhua, Y. (2006). Studies on chemical constituents and quality appraisalment of cultivated *Cistanche Salsa*. Doctor. Xinjiang, China: Xinjiang Medical University.
74. Li, L, Zhi-Hong, S, Peng-Fei, T, Li-Jun, W, and Fa-Kui, C. Studies on chemical constituents of *Cistanche salsa*. *Chin Tradit Herb Drug.* (2003) 34:293–4.
75. Miaohua, C, Fengshan, L, and Jianping, X. Tonic kidney aphrodisiac Chinese medicine meat from Rong chemical composition study. *China J Chin Materia Med.* (1993) 07:447.
76. Li, Q, Ba, X, Cao, H, Weng, X, Yang, Y, Wang, B, et al. Crude polysaccharides from *Cistanche deserticola* Y.C. Ma as an immunoregulator and an adjuvant for foot-and-mouth disease vaccine. *J Funct Foods.* (2021) 87:104800. doi: 10.1016/j.jff.2021.104800
77. Feng, S, Yang, X, Weng, X, Wang, B, and Zhang, A. Aqueous extracts from cultivated *Cistanche deserticola* Y.C. Ma as polysaccharide adjuvant promote immune responses via facilitating dendritic cell activation. *J Ethnopharmacol.* (2021) 277:114256. doi: 10.1016/j.jep.2021.114256
78. Tian, S, Miao, MS, Li, XM, Bai, M, Wu, YY, and Wei, ZZ. Study on neuroendocrine-immune function of Phenylethanoid glycosides of *Desertliving Cistanche herb* in perimenopausal rat model. *J Ethnopharmacol.* (2019) 238:111884. doi: 10.1016/j.jep.2019.111884
79. Zhang, A, Yang, X, Li, Q, Yang, Y, Zhao, G, Wang, B, et al. Immunostimulatory activity of water-extractable polysaccharides from *Cistanche deserticola* as a plant adjuvant in vitro and in vivo. *PLoS One.* (2018) 13:e0191356. doi: 10.1371/journal.pone.0191356
80. Lin, S, Ye, S, Huang, J, Tian, Y, Xu, Y, Wu, M, et al. How do Chinese medicines that tonify the kidney inhibit dopaminergic neuron apoptosis? *Neural Regen Res.* (2013) 8:2820–6. doi: 10.3969/j.issn.1673-5374.2013.30.004
81. Weilu, C, Hsieh, HL, Lin, TY, Hsieh, TY, Huang, SK, and Wang, SJ. Echinacoside, an active constituent of *Cistanche herba*, exerts a neuroprotective effect in a Kainic acid rat model by inhibiting inflammatory processes and activating the Akt/GSK3 $\beta$  pathway. *Biol Pharm Bull.* (2018) 41:1685–93. doi: 10.1248/bpb.b18-00407
82. Liu, Y, Wang, H, Yang, M, Liu, N, Zhao, Y, Qi, X, et al. *Cistanche deserticola* polysaccharides protects PC12 cells against OGD/RP-induced injury. *Biomed Pharmacother.* (2018) 99:671–80. doi: 10.1016/j.biopha.2018.01.114
83. Geng, X, Song, L, Pu, X, and Tu, P. Neuroprotective effects of Phenylethanoid glycosides from *Cistanche salsa* against 1-Methyl-4-phenyl-1,2,3,6-tetrahydropyridine (MPTP)-induced dopaminergic toxicity in C57 mice. *Biol Pharm Bull.* (2004) 27:797–801. doi: 10.1248/bpb.27.797
84. Snytnikova, OA, Tsentalovich, YP, Stefanova, NA, Fursova, A, Kaptein, R, Sagdeev, RZ, et al. The therapeutic effect of mitochondria-targeted antioxidant SkQ1 and *Cistanche deserticola* is associated with increased levels of tryptophan and kynurenine in the rat lens. *Dokl Biochem Biophys.* (2012) 447:300–3. doi: 10.1134/S1607672912060087
85. Peng, S, Li, P, Liu, P, Yan, H, Wang, J, Lu, W, et al. *Cistanche* alleviates sevoflurane-induced cognitive dysfunction by regulating PPAR- $\gamma$ -dependent antioxidant and anti-inflammatory in rats. *J Cell Mol Med.* (2020) 24:1345–59. doi: 10.1111/jcmm.14807
86. Zhang, Y, Wang, Y, Yang, S, Xiao, Y, Guan, H, Yue, X, et al. The difference of chemical components and biological activities of the raw products slices and the wine steam-processed product from *Cistanche deserticola*. *Evid Based Complement Alternat Med.* (2019) 2019:2167947:1–10. doi: 10.1155/2019/2167947
87. Jia, JX, Yan, XS, Cai, ZP, Song, W, Huo, DS, Zhang, BF, et al. The effects of phenylethanoid glycosides, derived from *Herba cistanche*, on cognitive deficits and antioxidant activities in male SAMP8 mice. *J Toxicol Environ Health A.* (2017) 80:1180–6. doi: 10.1080/15287394.2017.1367097
88. Yuan, P, Fu, C, Yang, Y, Adila, A, Zhou, F, Wei, X, et al. *Cistanche tubulosa* Phenylethanoid glycosides induce apoptosis of hepatocellular carcinoma cells by mitochondria-dependent and MAPK pathways and enhance antitumor effect through combination with cisplatin. *Integr Cancer Ther.* (2021) 20:15347354211013085. doi: 10.1177/15347354211013085
89. Yuan, P, Li, J, Aipire, A, Yang, Y, Xia, L, Wang, X, et al. *Cistanche tubulosa* phenylethanoid glycosides induce apoptosis in H22 hepatocellular carcinoma cells through both extrinsic and intrinsic signaling pathways. *BMC Complement Altern Med.* (2018) 18:275. doi: 10.1186/s12906-018-2201-1
90. Fu, C, Li, J, Aipire, A, Xia, L, Yang, Y, Chen, Q, et al. *Cistanche tubulosa* phenylethanoid glycosides induce apoptosis in Eca-109 cells via the mitochondria-dependent pathway. *Oncol Lett.* (2019) 17:303–13. doi: 10.3892/ol.2018.9635
91. Wang, W, Luo, J, Liang, Y, and Li, X. Echinacoside suppresses pancreatic adenocarcinoma cell growth by inducing apoptosis via the mitogen-activated protein kinase pathway. *Mol Med Rep.* (2016) 13:2613–8. doi: 10.3892/mmr.2016.4867
92. Morikawa, T, Pan, Y, Ninomiya, K, Imura, K, Matsuda, H, Yoshikawa, M, et al. Acylated phenylethanoid oligoglycosides with hepatoprotective activity from the desert plant *Cistanche tubulosa*. *Bioorg Med Chem.* (2010) 18:1882–90. doi: 10.1016/j.bmc.2010.01.047

93. Xiong, Q, Hase, K, Yasuhiroezuka, T, Namba, T, and Kadotal, S. Hepatoprotective activity of Phenylethanoids from *Cistanche deserticola*. *Planta Med.* (1998) 64:120–5. doi: 10.1055/s-2006-957387
94. Cui, Q, Pan, Y, Zhang, W, Zhang, Y, Ren, S, Wang, D, et al. Metabolites of dietary Acteoside: profiles, isolation, identification, and Hepatoprotective capacities. *J Agric Food Chem.* (2018) 66:2660–8. doi: 10.1021/acs.jafc.7b04650
95. Guo, Y, Cao, L, Zhao, Q, Zhang, L, Chen, J, Liu, B, et al. Preliminary characterizations, antioxidant and hepatoprotective activity of polysaccharide from *Cistanche deserticola*. *Int J Biol Macromol.* (2016) 93:678–85. doi: 10.1016/j.ijbiomac.2016.09.039
96. Siu, AH, and Ko, KM. Herba *Cistanche* extract enhances mitochondrial glutathione status and respiration in rat hearts, with possible induction of uncoupling proteins. *Pharm Biol.* (2010) 48:512–7. doi: 10.3109/13880200903190985
97. Liang, H, Yu, F, Tong, Z, and Huang, Z. Effect of *Cistanches* Herba aqueous extract on bone loss in ovariectomized rat. *Int J Mol Sci.* (2011) 12:5060–9. doi: 10.3390/ijms12085060
98. Fu, Z, Han, L, Zhang, P, Mao, H, Zhang, H, Wang, Y, et al. *Cistanche* polysaccharides enhance echinacoside absorption in vivo and affect the gut microbiota. *Int J Biol Macromol.* (2020) 149:732–40. doi: 10.1016/j.ijbiomac.2020.01.216
99. Zhu, K, Meng, Z, Tian, Y, Gu, R, Xu, Z, Fang, H, et al. Hypoglycemic and hypolipidemic effects of total glycosides of *Cistanche tubulosa* in diet/streptozotocin-induced diabetic rats. *J Ethnopharmacol.* (2021) 276:113991. doi: 10.1016/j.jep.2021.113991
100. Panel, EN, Turck, D, Castenmiller, J, de Henauw, S, Hirsch-Ernst, KI, Kearney, J, et al. Safety of water extract of *Cistanche tubulosa* stems as a novel food pursuant to regulation (EU) 2015/2283. *EFSA J.* (2021) 19:e06346:e06346. doi: 10.2903/j.efsa.2021.6346
101. Liao, PL, Li, CH, Tse, LS, Kang, JJ, and Cheng, YW. Safety assessment of the *Cistanche tubulosa* health food product Memoregain: genotoxicity and 28-day repeated dose toxicity test. *Food Chem Toxicol.* (2018) 118:581–8. doi: 10.1016/j.fct.2018.06.012



## OPEN ACCESS

## EDITED BY

Haining Zhuang,  
Shanghai Urban Construction  
Vocational College,  
China

## REVIEWED BY

Shuzhen Mu,  
Key Laboratory of Chemistry for Natural  
Products of Guizhou Province (CAS),  
China  
Zhang Qianjun,  
Guizhou University,  
China  
Yang Zhao,  
United States Food and Drug Administration,  
United States

## \*CORRESPONDENCE

Chao Zhao  
✉ chaozhao@126.com  
Xin Zhou  
✉ alic9800@sina.com

## SPECIALTY SECTION

This article was submitted to  
Food Chemistry,  
a section of the journal  
Frontiers in Nutrition

RECEIVED 22 December 2022

ACCEPTED 07 February 2023

PUBLISHED 13 April 2023

## CITATION

Mu Y, Cheng L, Gong X, Ma J, Zhang S, Mu Y,  
Liang K, Zhou X and Zhao C (2023)  
Simultaneous determination of nine phenolic  
compounds in imitation wild *Dendrobium  
officinale* samples using ultrahigh-performance  
liquid chromatography–tandem mass  
spectrometry.  
*Front. Nutr.* 10:1129953.  
doi: 10.3389/fnut.2023.1129953

## COPYRIGHT

© 2023 Mu, Cheng, Gong, Ma, Zhang, Mu,  
Liang, Zhou and Zhao. This is an open-access  
article distributed under the terms of the  
Creative Commons Attribution License (CC BY).  
The use, distribution or reproduction in other  
forums is permitted, provided the original  
author(s) and the copyright owner(s) are  
credited and that the original publication in this  
journal is cited, in accordance with accepted  
academic practice. No use, distribution or  
reproduction is permitted which does not  
comply with these terms.

# Simultaneous determination of nine phenolic compounds in imitation wild *Dendrobium officinale* samples using ultrahigh-performance liquid chromatography–tandem mass spectrometry

Yingsu Mu<sup>1,2</sup>, Li Cheng<sup>3</sup>, Xiaojian Gong<sup>1,2</sup>, Jiangxiong Ma<sup>1,2</sup>,  
Shiyu Zhang<sup>1,2</sup>, Yinghua Mu<sup>4</sup>, Kang Liang<sup>5</sup>, Xin Zhou<sup>1,2\*</sup> and  
Chao Zhao<sup>1,2\*</sup>

<sup>1</sup>Key Laboratory for Information System of Mountainous Areas and Protection of Ecological Environment, Guizhou Normal University, Guiyang, China, <sup>2</sup>Guizhou Engineering Laboratory for Quality Control and Evaluation Technology of Medicine, Guizhou Normal University, Guiyang, China, <sup>3</sup>Guizhou University of Traditional Chinese Medicine, Guiyang, China, <sup>4</sup>College of Food and Pharmaceutical Sciences, Ningbo University, Ningbo, China, <sup>5</sup>Guizhou Forestry Scientific Research Institute, Guiyang, China

*Dendrobium officinale* Kimura et Migo (*D. officinale*), one of the nine everlasting types of grass, has gained increasing attention owing to its important roles in alternative medicines and drug discovery. Due to its natural resources being in danger of being extinct, imitation wild planting is becoming increasingly common. To assess the product's quality completely, an efficient ultrahigh performance liquid chromatography–triple quadrupole tandem mass spectrometry (UHPLC–QQQ–MS/MS) method was established to simultaneously quantify nine phenolic compounds in *D. officinale* samples. The extraction parameters, including solvent, solvent concentration, solid–liquid ratio, and extraction time, were systematically optimized with the single-factor test. The results demonstrated that extraction with a 1:200 solid-to-liquid ratio of 80% methanol for 1.5h was the most efficient condition for the extraction of flavonoids. Satisfactory retention times and resolution of the nine analytes were acquired on the Thermo Scientific Hypersil GOLD column with multiple reaction monitoring in negative ion scanning mode. The method was validated to demonstrate its selectivity, linearity, precision, accuracy, and robustness. Thus, the verified UHPLC–QQQ–MS/MS method was successfully applied to the quantification of phenolic components present in *D. officinale* samples. The results indicated that the quantity and composition of phenolic components in *D. officinale* from various provenances were significantly different. This work provides a theoretical foundation for the cultivation and assessment of wild *D. officinale* quality.

## KEYWORDS

*Dendrobium officinale*, phenolic components, UHPLC–QQQ–MS/MS, provenance, method validation

## 1. Introduction

*Dendrobium officinale* Kimura et Migo (*D. officinale*), a perennial epiphytic member of the Orchidaceae, is considered to have the best medicinal properties in traditional Chinese medicine (1, 2). *Dendrobium officinale*, is a well-known medicinal and food homologous plant, that strengthens the stomach and promotes the production of body fluid, nourishing Yin and clearing heat (3, 4). It is known that *D. officinale* is primarily distributed in several nations, including the United States, Japan, and Australia, and is more broadly distributed in southern China, including the provinces of Zhejiang, Anhui, Fujian, Guangxi, Yunnan, and Guizhou (3, 5). However, *D. officinale* has strict requirements for habitat conditions, a slow growth rate, low yield, and excessive harvesting, which has led to a sharp decrease in the number of wild plants and has been included in the “China Plant Red Data Book” (6). Currently, the market for *D. officinale* mainly comes from greenhouse cultivation and imitation wild planting, among which imitation wild planting improves the quality of *D. officinale* while making full use of woodland resources, with low cultivation cost and a good ecological environment. However, the 2020 edition of the Chinese Pharmacopoeia only uses polysaccharide content as its quality evaluation index, which is contrary to the theory that complex components in Chinese medicine interact with each other and work synergistically. Therefore, we should comprehensively analyze the active ingredients of *D. officinale* and establish a more scientific quality control standard for *D. officinale* (7).

Phenolic compounds include flavonoids, simple phenols and quinones. Numerous natural phenols have attracted great interest from scientists around the world because they are considered safer and have a wide range of health-promoting properties. Flavonoids are a widespread group of secondary metabolites in plants that not only play a key role in the pharmaceutical industry but also serve as excellent chemical markers for quality control of medicinal plants (8). *Dendrobium officinale*'s active pharmaceutical ingredients include phenols, flavonoids, alkaloids, amino acids, coumarins, terpenes, benzylic compounds, and several trace minerals, in addition to polysaccharides (9–12), which have been widely used to treat hyperglycemia (13), hyperlipidemia (14), and immune enhancement (15) and to benefit the stomach (16). Polysaccharides are the predominant bioactive compounds in these substances. Of course, phenolic components are a group of compounds that are also prevalent in *D. officinale*. In recent years, interest has increased due to the potent antioxidant and protective effects of phenolic components against cell toxicity (17). Phenolic contents have been effectively isolated, and their structures have been validated. Unfortunately, the development of phenolic components from *D. officinale* has been hampered by the lack of a reliable method for quantitative determination. With the birth and development of large-scale instruments and equipment such as gas chromatographs (GC), liquid chromatography (LC), ultrahigh-performance liquid

chromatography (HPLC), and mass spectrometers (MS), instrumental analysis methods have become the most commonly used methods for quantitative analysis of secondary metabolites of plants (18–20). Zhu et al. (21) used an HPLC assay to simultaneously quantify 11 phenolics in four *Dendrobium* species. The contents of kaempferol, quercetin and myricetin in flavonoids are mainly determined based on the HPLC method (22). However, some phenolic components cannot be effectively identified and quantified using HPLC because of poor separation from more abundant components (23). Compared with ultrahigh-performance liquid chromatography (HPLC), ultrahigh-performance liquid chromatography–tandem mass spectrometry (UHPLC–MS/MS) has the characteristics of higher-resolution separation and better identification and quantification of individual components (19, 24–27).

To establish the method of UHPLC–QQQ–MS/MS for the first time for the simultaneous determination of various components of phenolic *D. officinale* for overall quality control. The extraction conditions were optimized, and the extraction method, extraction solvent, solvent concentration, extraction time, and material-to-liquid ratio were investigated. The contents of ferulic acid, chrysin, naringenin, luteolin, L-epicatechin, quercetin, isorhamnetin, cynaroside, and naringin in *D. officinale* from different provenances were determined, and the quality of nine phenolic compounds was comprehensively evaluated by the TOPSIS comprehensive evaluation method. This study may offer a workable and straightforward technique for quality control of imitation wild *D. officinale* as well as a theoretical framework for its development and cultivation.

## 2. Materials and methods

### 2.1. Instruments, reagents, and materials

The TSQ Quantum Liquid Chromatography–Mass Spectrometer (UHPLC–MS/MS) included a triple quadrupole mass analyzer, ESI ion source, and Xcalibur workstation. The liquid phase part was a Thermo Accela UHPLC, including an Accela PDA detector, Accela autosampler and Accela 1250 infusion pump, which were purchased from Thermo Fisher Scientific, Inc. XS-105DU 1/100000 and the AL204 1/10000 electronic analytical as well as the KQ-5200E type ultrasonic cleaner were both obtained from Kunshan Ultrasonic Instruments Co.

Quercetin was purchased from the China Institute of Food and Drug Control; Ferulic acid and L-epicatechin were purchased from the China Institute for Testing and Certification of Pharmaceutical and Biological Products. Chrysin, naringenin, luteolin, and cynaroside were acquired from Guizhou Dida Biotechnology Co., Ltd. Isorhamnetin was acquired from Chengdu Pfeiffer Biotechnology Co., Ltd. Quercetin was acquired from the China Institute of Food. Naringin was purchased from Chengdu Botanical Standard Pure Biotechnology Co., Ltd., Research Central Reference Materials Research Center. The purities of the 9 reference substances were all greater than 98%. The analytical purities of methanol (MeOH) and ethanol were purchased from Tianjin Comitry Co., Ltd. Acetonitrile (HPLC grade) was purchased from American TEDIA Company. Formic acid (LC/MS grade) was acquired by ROE SCIENTIFIC Corporation, United States.

Abbreviations: *D. officinale*, *Dendrobium officinale* Kimura et Migo; UHPLC–QQQ–MS/MS, ultrahigh performance liquid chromatography–triple quadrupole tandem mass spectrometry; TOPSIS, technique for order preference by similarity to ideal solution; LOD, limits of determination; LOQ, limits of quantification; D–, negative ideal solution distance; CI, composite score index.

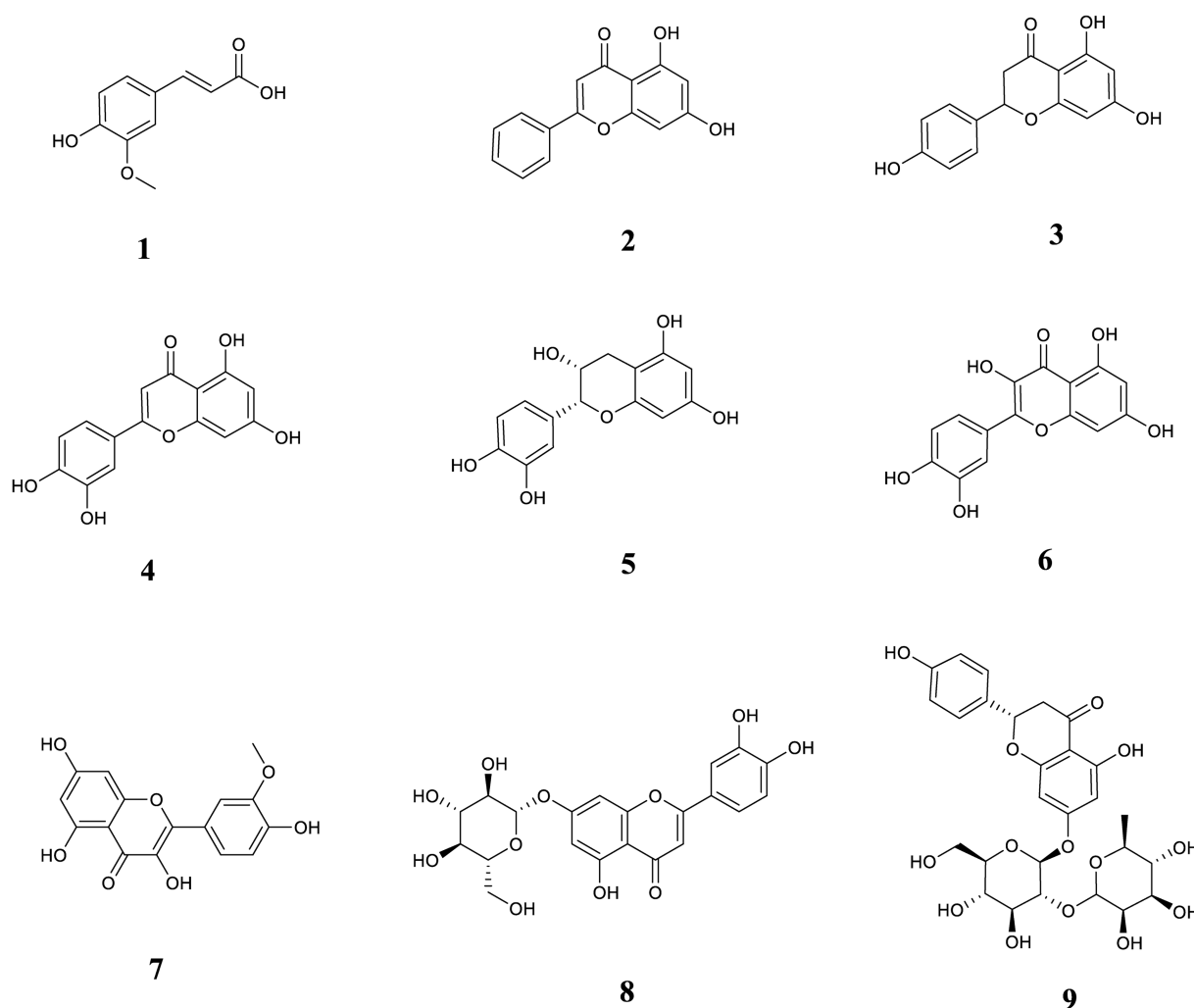


FIGURE 1

The chemical structures of nine phenolic components in this study. (1) ferulic acid; (2) chrysin; (3) naringenin; (4) luteolin; (5) L-epicatechin; (6) quercetin; (7) isorhamnetin; (8) cynaroside; (9) naringin.

Food-grade distilled water was purchased from Watson's Food and Beverage Guangzhou Co. The structural formulas of the 9 compounds are shown in Figure 1.

The majority of medicinal plants are harvested and grown in Yun Guan Shan, a state-owned forest farm in Guizhou Province, China, where they mimic wild *D. officinale* from *Pinus massoniana* Lamb. tree species.

## 2.2. Sample pretreatment and standard solution

All dry ingredients were ground up and put through a sieve with a mesh size of 60. As mentioned below, 0.1 g of samples were weighed exactly (within 0.00001), and they were then extracted once with 80% methanol (20 ml) by reflux for 1.5 h. The sample was meticulously weighed before extraction, and the weight loss was compensated once the sample solution was weighed and cooled to room temperature. All of the solutions were filtered through a 0.22  $\mu$ m microporous membrane before being put on the device.

Each standard was properly weighed. The reference standards' standard stock solutions were made by combining and evaporating in 80% methanol. The working standard solution was then made by gradient-diluting the standard stock solution with the same solvent, and both of these solutions were stored at 4°C for further analysis.

## 2.3. Instrumentation and chromatography

### 2.3.1. Ultrahigh-performance liquid chromatography conditions

The chromatographic separations were performed on a thermostat-controlled, 25°C, Thermo Scientific Hypersil GOLD column (50 mm  $\times$  2.1 mm, 5  $\mu$ m). The following procedure was used for the gradient elution of 0.1% formic acid acetonitrile (solvent A) and 0.1% formic acid aqueous solution (solvent B) at a flow rate of 200  $\mu$ l/min: 0–3 min, 5% A; 3–3.1 min, 5–80% A; 3.1–6 min, 80% A; 6.0–6.1 min, 80–5% A and 6.1–12 min, 5% A. The injection volume was 10  $\mu$ l.



### 2.3.2. Mass spectrometer conditions

Electrospray ionization in the negative ionization mode was used to obtain the mass spectra. The ESI source performed best under the following conditions: spray voltage of 2,500 V, the capillary temperature of 350°C, vaporizer temperature of 200°C, sheath gas pressure of 35 Arb, the auxiliary gas pressure of 15 Arb, and vaporizer temperature of 200°C. Multiple reaction monitoring (MRM) was used as the measurement technique, and 0.1 s was the scanning interval. [Table 1](#) displays the precise quantitative analysis. [Figure 2](#) displays 9 compounds' MRM diagrams.

### 2.4. Extraction optimization

Different extraction methods were investigated by a single-factor experiment: ultrasound (100 W, 90 kHz, 60 min), reflux (60 min, 67°C), and cold soaking (60 min); different solvents: ethanol, methanol, water, different concentrations: methanol (40, 60, 80, and 100%). Then the effects of different solid–liquid ratios of 1:200, 1:300, 1:400, and 1:500 (*m/v*), and reflux extraction times of 0.5, 1, 1.5, and 2 h on the extraction were studied. The supernatant was examined by “2.3” chromatography after being filtered using a 0.22 μm microporous organic membrane. Nine peaks' response values, peak areas, and peak forms were compared.

### 2.5. Method validation for quantitative analysis

#### 2.5.1. Linearity LOQ and LOD

The master batch of the control solution was aspirated and prepared into a mass concentration gradient solution. Following

“2.3”s chromatographic conditions, the mass concentration was employed as the horizontal coordinate (*X*), and the peak area as the vertical coordinate (*Y*). The standard curve's lowest concentration point is called the LOQ. Signal-to-noise ratios (*S/N*) of 3 were used to calculate the limits of detection (LOD).

#### 2.5.2. Precision, stability, repeatability, and recovery

The intraday and interday variations were used to investigate the accuracy of the suggested approach. The intraday precision was calculated by following the standard curve for three consecutive days, mixing 9 standards, injecting them six times, and calculating the concentration and relative standard deviation (RSD%) at each level. At various time intervals of 0, 2, 4, 8, 12, and 24 h, the sample was injected and examined. Six identical samples were prepared in parallel to test the repeatability of the process. Three different concentration levels of the standard solutions—50, 100, and 150%—were added to the sample powder for the recovery test to assess the method's accuracy. The sample powder was then extracted, and the results were examined. For each level, three parallel samples were taken.

### 2.6. The Technique for Order Preference by Similarity to Ideal Solution evaluation

The Technique for Order Preference by Similarity to Ideal Solution (TOPSIS) method is a multi-index decision analysis method, that calculates the multi-index as a comprehensive index, and transforms the multidimensional problem into a one-dimensional problem, which greatly reduces the interference of different types of indicators on decision-making in the analysis process, and significantly improves the scientificity and accuracy of multiobjective decision analysis (28).

TABLE 1 Mass spectral parameters of the nine components.

Compound	Molecular weight	Chemical formula	Parent mass (m/z)	Product mass (m/z)	T Lens (v)	Collision voltage (mTorr)	Collision energy (eV)
ferulic acid	194.18	C10H10O4	193.010	133.945	73	1.5	18
				177.897	73	1.5	14
Chrysin	254.24	C15H10O4	253.040	142.948	120	1.5	26
				185.062	120	1.5	21
Naringenin	272.25	C15H12O5	271.019	118.953	107	1.5	30
				150.880	107	1.5	21
Luteolin	286.05	C15H10O6	285.036	132.933	123	1.5	36
L-Epicatechin	290.27	C15H14O6	289.043	203.018	130	1.5	14
				244.948	130	1.5	12
Quercetin	302.24	C15H10O7	301.001	150.980	109	1.5	19
				178.864	109	1.5	12
Isorhamnetin	316.26	C16H12O7	315.006	150.884	116	1.5	20
				299.863	116	1.5	15
Cynaroside	448.38	C21H20O11	447.064	283.742	133	1.5	40
				284.859	133	1.5	29
Naringin	580.18	C27H32O14	579.135	270.784	182	1.5	33

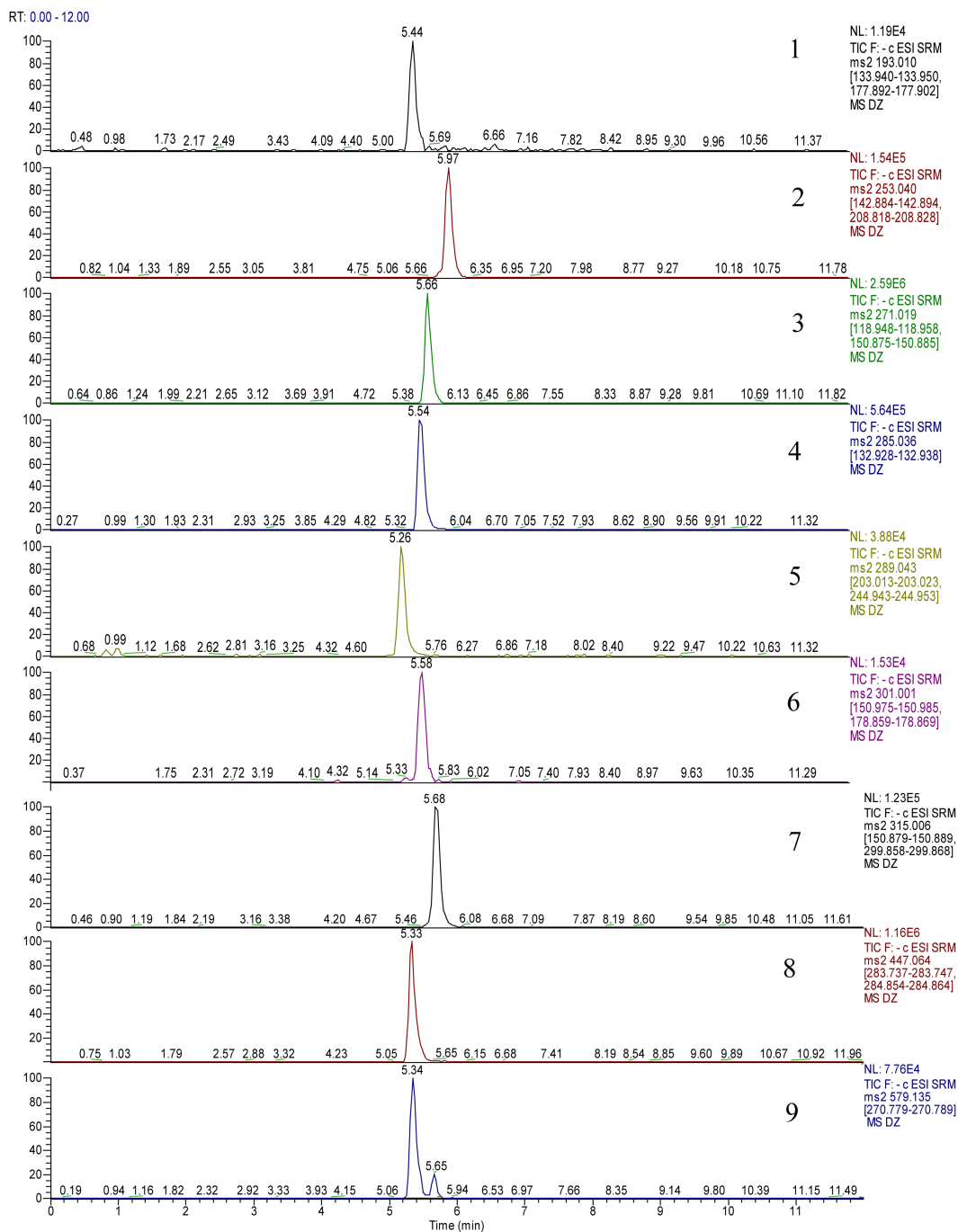


FIGURE 2  
Multiple reaction monitoring (MRM) chromatograms of 9 components.

It has been widely used in the quality evaluation of various Chinese medicinal materials.

### 3. Results and discussion

#### 3.1. Qualitative analysis

In this paper, 597 metabolites were detected based on the UHPLC-MS/MS detection platform and a self-built database,

and 185 flavonoids were screened through primary classification. This part of the experiment was performed by Wuhan Maitville Biotechnology Co., Ltd. Therefore, the UHPLC-ESI MS/MS method was established to compare the total ion current diagram and fragment ion diagram of the *D. officinale* extract and standard sample, and nine phenolic compounds were identified, ferulic acid (1), chrysin (2), naringenin (3), luteolin (4), L-epicatechin (5), quercetin (6), isorhamnetin (7), cynaroside (8), and naringin (9), as shown in Figure 3.

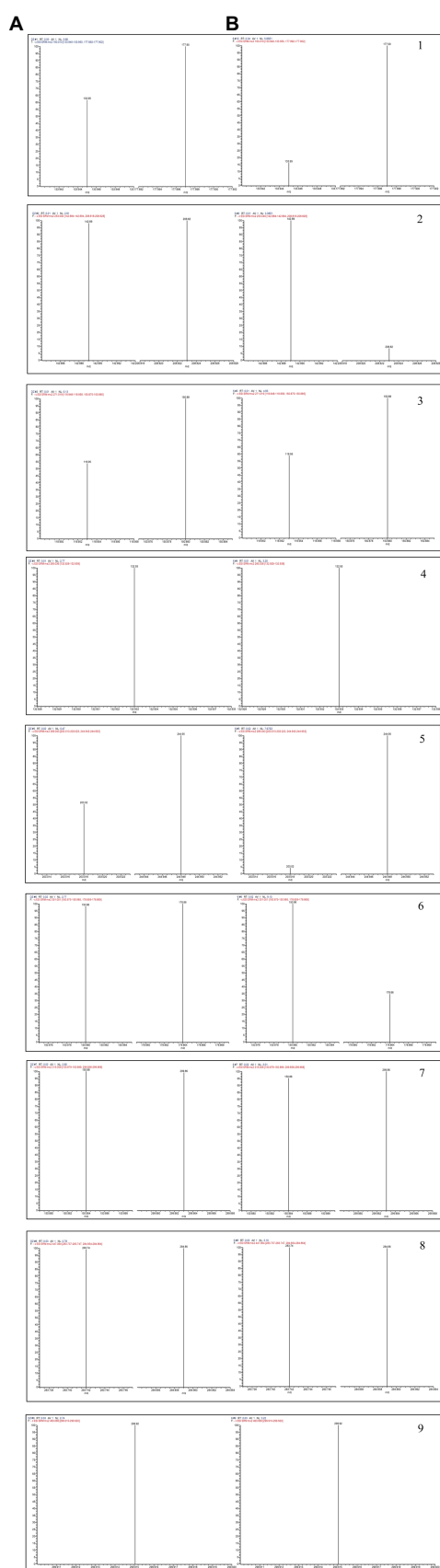


**FIGURE 3**  
The tandem mass spectrometry (MS/MS) spectra of the standards (A) and the phenolic components in the samples (B).

## 3.2. Extraction optimization

The following extraction methods (sonication, reflux, cold soak), extraction solvents (ethanol, methanol, water), solvent concentrations (40, 60, 80, 100% methanol), extraction stock ratios [1:200, 1:300, 1:400, 1:500 (m/v)], and extraction times (0.5, 1, 1.5, and 2 h) were optimized, as shown in Figure 4. Reflux extraction was chosen for the herb's extraction because it produced much more naringenin and cynaroside than the other two extraction techniques. More phenols were extracted from methanol, while more polysaccharides were extracted from aqueous extracts that were not well filtered. The longer the extraction time was, the greater the extracted phenol content increased, but when the time was 1.5 h after the slow growth. The extraction of phenolic compounds was not significantly impacted by the material-to-liquid ratio. The feed-to-liquid ratio of 1:200 and 1.5 h of refluxing 80% methanol resulted in the best extraction conditions.

## 3.3. Validation of the quantitative analysis method

The mass concentration was used as the horizontal coordinate (X), and the peak area was used as the vertical coordinate in the linear regression (Y). The regression equation and correlation coefficient ( $R^2$ ) were calculated, and the maximum LOD and LOQ of the 9 compounds were 16.89 and 15 ng/ml, respectively. The result shown in Table 2, show good linearity.

The within-day and between-day variations were used to evaluate the precision of this UHPLC–MS/MS method for measuring *D. officinale*. The relative standard deviation RSD for the intraday and interday precision ranged from 1.60 to 7.49% and from 5.89 to 9.99%, respectively. Then, the relative standard deviation for repeatability and stability varies from 1.49 to 12.50%. Table 3 presents the outcomes. According to Table 4, the average recoveries of the spiked trials ranged from 79.87 to 99.15%, with RSDs between 7.02 and 16.98%. The experimental outcomes further showed that the analytical approach is reliable and capable of fulfilling the assay's requirements.

## 3.4. *Dendrobium officinale* sample analysis

The validated method is used to analyze samples from different sources. Table 5 displays the quantitative results obtained from the calibration curve. Each sample was analyzed in triplicate. A total of 9 flavonoids were detected in the *D. officinale* samples. The ferulic acid, naringenin, and epicatechin contents were higher in each provenance than the other components, while the luteolin content was lower in each provenance. Of these, the Guangxi provenance had the highest levels of ferulic acid and L-epicatechin, at 88.27 and 109.68  $\mu\text{g/g}$ , respectively. Chrysin, naringenin, quercetin, and isorhamnetin were all much more abundant in ZJ origin than they were in other compounds, while luteolin and naringenin were the least abundant of all ZJ provenances. The impacts of geographical origins and storage conditions may account for the significant variations in flavonoid composition and content between batches of *D. officinale* samples.

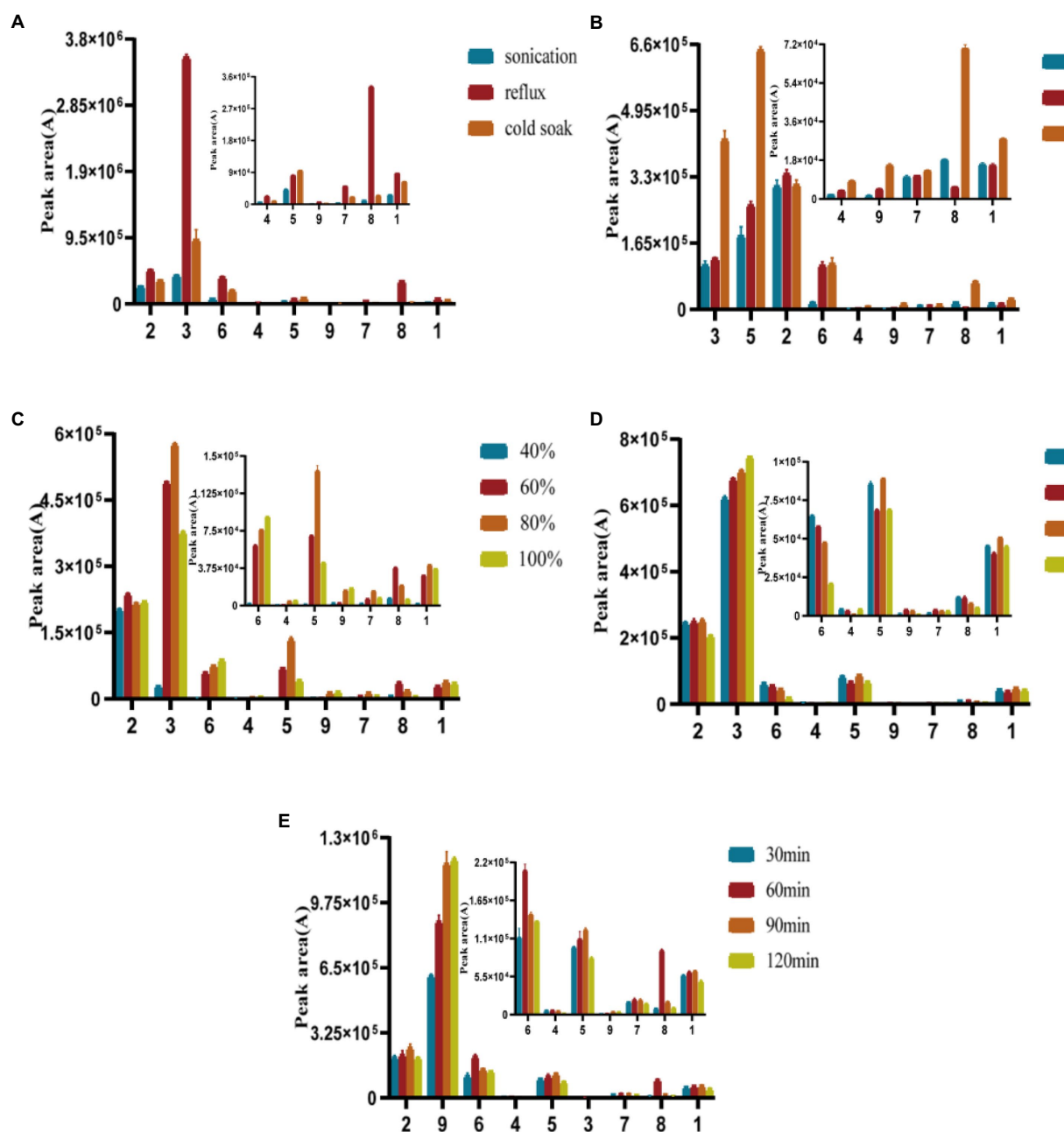


FIGURE 4 Optimization of extraction methods (A), extraction solvent (B), solvent concentrations (C), extraction stock ratios (D), and extraction times (E).

The quality of imitation wild *D. officinale* was properly evaluated by TOPSIS, and elevated provenances were selected based on their phenol content.  $D+$  is the distance between each treatment and the optimal index, and  $D-$  is the distance from the worst vector. The smaller the value is, the closer it is to the optimal index or the worst index.  $CI = D-/(D++D-)$ , the greater the value, the better the overall efficiency. According to the CI value of each index, the advantages and disadvantages of the 5 provenances were as follows: Zhejiang > Fujian > Guangxi > Anlong > Fanjingshan. Among them, the Anlong, Fanjingshan, and Guangxi CI values are close to the specific data shown in

Table 6. The maximum CI of the ZJ provenance is 0.7296, which can be further studied and developed as a superior quality provenance (Table 6).

## 4. Conclusion

In this study, an effective UHPLC-QQQ-MS/MS technique for the isolation and quantification of nine phenolic compounds in *D. officinale* was effectively established and verified. Following optimization, samples were extracted using reflux and an aqueous

TABLE 2 Linear regression date of nine components.

Compound	Regression equation	$R^2$	Linearity range (ng/mL)	LOD (ng/mL)	LOQ (ng/mL)
Ferulic acid	$Y = 208.33X + 1515.2$	0.9992	15 ~ 1,500	15	9.11
Chrysin	$Y = 6,986X + 106,987$	0.9992	5 ~ 500	5	1.77
Naringenin	$Y = 22,034X + 320,994$	0.9991	8 ~ 800	8	8.96
Luteolin	$Y = 18,117X + 14,977$	0.9993	1 ~ 100	1	0.27
L-Epicatechin	$Y = 1397.4X + 17,484$	0.999	14 ~ 1,400	14	16.89
Quercetin	$Y = 6877.6X + 1,084$	0.9992	3 ~ 300	3	3.96
Isorhamnetin	$Y = 26,369X + 12,225$	0.9994	1 ~ 100	1	0.49
Cynaroside	$Y = 28,092X - 7772.9$	0.9993	1 ~ 100	1	0.37
Naringin	$Y = 18,604X - 835.32$	0.9992	0.05 ~ 5	0.05	0.05

TABLE 3 Stability, repeatability, inter-day precision, and intra-day precision of nine components.

Compound	Stability		Repeatability		Precision			
					Intra-day		Inter-day	
	Mean	RSD (%)	Mean	RSD (%)	Mean	RSD (%)	Mean	RSD (%)
Ferulic Acid	380.18	1.49	46.60	7.21	47.77	4.61	417.29	9.99
Chrysin	19.43	5.65	42.51	7.36	48.90	2.16	14.79	7.11
Naringenin	115.94	4.23	49.82	6.42	57.48	4.31	114.45	7.83
Luteolin	0.41	9.83	11.84	4.04	7.37	1.60	0.58	7.82
L-Epicatechin	85.02	3.89	110.64	3.41	114.43	2.40	60.49	6.02
Quercetin	38.76	3.56	18.42	6.43	17.14	2.35	25.45	9.85
Isorhamnetin	2.54	8.49	6.46	2.92	6.45	4.87	0.36	8.21
Cynaroside	1.09	3.18	7.59	1.53	7.31	6.58	1.26	6.55
Naringin	0.49	7.14	0.78	12.50	0.66	5.17	20.49	6.35

TABLE 4 Results of *Dendrobium officinale* spiked sample recovery experiment.

Compound	Average recovery (%)	RSD (%)	Compound	Average recovery (%)	RSD (%)
Ferulic Acid	93.39	7.02	Quercetin	86.97	14.83
Chrysin	89.17	14.94	Isorhamnetin	89.43	12.07
Naringenin	87.25	11.68	Cynaroside	86.07	16.98
Luteolin	79.87	7.47	Naringin	86.79	14.80
L-Epicatechin	90.20	10.91			

solution of 80% methanol. The UHPLC-QQQ-MS/MS technology developed in the current study is precise and sensitive for quantifying the main phenolic components. Further analysis with TOPSIS using the contents of the nine phenolic compounds suggested that *D. officinale* should be screened for high-quality ZJ

seed sources. The validation data demonstrated satisfactory linearity, precision, accuracy, repeatability, and stability. According to the findings, the UHPLC-QQQ-MS/MS approach shows excellent potential for use in the investigation of bioactive substances in herbal medicines.



TABLE 5 The content of nine compounds in *Dendrobium officinale* samples (μg/g).

Compound	FJ	AL	FJS	GX	ZJ
Ferulic acid	77.85 ± 2.60	71.00 ± 5.68	31.06 ± 4.55	88.27 ± 1.96	55.36 ± 3.52
Chrysin	2.14 ± 0.73	2.56 ± 0.98	2.62 ± 0.62	2.33 ± 0.06	10.20 ± 0.46
Naringenin	60.18 ± 0.34	35.74 ± 1.28	67.07 ± 0.58	67.96 ± 0.09	76.56 ± 1.66
Luteolin	0.60 ± 0.46	0.12 ± 0.07	0.19 ± 0.04	0.30 ± 0.03	0.20 ± 0.10
L-Epicatechin	37.28 ± 1.07	101.09 ± 2.62	94.86 ± 9.55	109.68 ± 2.87	67.54 ± 4.52
Quercetin	3.16 ± 0.05	2.13 ± 0.32	2.31 ± 0.25	2.44 ± 0.24	4.84 ± 0.40
Isorhamnetin	0.32 ± 0.05	0.23 ± 0.02	0.30 ± 0.11	0.23 ± 0.02	0.80 ± 0.40
Cynaroside	0.39 ± 0.09	0.35 ± 0.04	0.31 ± 0.02	0.42 ± 0.08	0.42 ± 0.20
Naringin	0.11 ± 0.02	0.24 ± 0.00	0.21 ± 0.06	0.14 ± 0.06	0.20 ± 0.20

TABLE 6 The Technique for Order Preference by Similarity to Ideal Solution (TOPSIS) evaluation results (7).

Index value	(D+)	(D−)	CI	Rank
FJ	0.6964	0.3942	0.3614	2
AL	0.8111	0.2570	0.2406	4
FJS	0.7695	0.2248	0.2261	5
GX	0.7582	0.3174	0.2951	3
ZJ	0.2933	0.7914	0.7296	1

## Data availability statement

The original contributions presented in the study are included in the article/supplementary material, further inquiries can be directed to the corresponding authors.

## Author contributions

YsM, LC, and XG finished all the experiments. CZ and XZ contributed to the concept development and outline arrangement, and revised the work critically for important intellectual content. YhM and SZ contributed to relevant references by collecting and drawing pictures. JM and KL analyzed the data and participated in the discussion on views in the manuscript. All authors contributed to the article and approved the submitted version.

## References

1. Fu, Y, Wang, Q, Zhang, L, Ling, S, Jia, H, and Wu, Y. Dissipation, occurrence, and risk assessment of 12 pesticides in dendrobium Officinale Kimura et Migo. *Ecotoxicol Environ Saf.* (2021) 222:112487. Epub 2021/07/13. doi: 10.1016/j.ecoenv.2021.112487

2. Yu, ZM, Yang, ZY, da Silva, JAT, Luo, JP, and Duan, J. Influence of low temperature on physiology and bioactivity of postharvest dendrobium Officinale stems. *Postharvest Biol Technol.* (2019) 148:97–106. doi: 10.1016/j.postharvbio.2018.10.014

3. Chen, W, Lu, J, Zhang, J, Wu, J, Yu, L, Qin, L, et al. Traditional uses, phytochemistry, pharmacology, and quality control of *Dendrobium officinale* Kimura et Migo. *FPHAR.* (2021) 12:726528. doi: 10.3389/fphar.2021.726528

4. Wang, Y, Tong, Y, Adejobi, OI, Wang, Y, and Liu, A. Research advances in multi-omics on the traditional Chinese herb dendrobium Officinale. *Front Plant Sci.* (2021) 12:808228. doi: 10.3389/fpls.2021.808228

## Funding

This research was supported by Guizhou Forestry Scientific Research Project [Qianlin Kehe (202112)]; High level innovative talents training project of Guizhou Province (20154033); Guizhou Rural Industrial Revolution Dendrobium Industry Development Special Funds; He Chengyao National Medical Master Inheritance Studio.

## Conflict of interest

The authors declare that the research was conducted in the absence of any commercial or financial relationships that could be construed as a potential conflict of interest.

## Publisher’s note

All claims expressed in this article are solely those of the authors and do not necessarily represent those of their affiliated organizations, or those of the publisher, the editors and the reviewers. Any product that may be evaluated in this article, or claim that may be made by its manufacturer, is not guaranteed or endorsed by the publisher.

## Supplementary material

The Supplementary material for this article can be found online at: <https://www.frontiersin.org/articles/10.3389/fnut.2023.1129953/full#supplementary-material>

5. Chen, W-h, Wu, J-j, Li, X-f, Lu, J-m, Wu, W, Sun, Y-q, et al. Isolation, structural properties, bioactivities of polysaccharides from *Dendrobium officinale* Kimura et Migo: a review. *Int J Biol Macromol.* (2021) 184:1000–13. doi: 10.1016/j.ijbiomac.2021.06.156

6. Guo, FL. *China Plant Red Data Book: Rare and Endangered Plants.* Beijing: Science Press (1992).

7. Yang, L, Zhang, W, Deng, W, Wang, H, and Liu, H. Simultaneous quantification and evaluate the differences of two skeleton components in raw, salt and wine Angelicae Pubescentis radix by UPLC–MS/MS in negative/positive modes coupled with Chemometrics. *J Future Foods.* (2022) 2:82–90. doi: 10.1016/j.jfutfo.2022.03.020

8. Zhou, C, Xie, Z, Lei, Z, Huang, Y, and Wei, G. Simultaneous identification and determination of flavonoids in dendrobium Officinale. *BMC Chem.* (2018) 12:40. doi: 10.1186/s13065-018-0403-8

9. Yuan, Y, Zhang, J, Liu, X, Meng, M, Wang, J, and Lin, J. Tissue-specific transcriptome for *Dendrobium Officinale* reveals genes involved in flavonoid biosynthesis. *Genomics*. (2020) 112:1781–94. doi: 10.1016/j.ygeno.2019.10.010
10. Li, M, Yue, H, Wang, Y, Guo, C, Du, Z, Jin, C, et al. Intestinal microbes derived butyrate is related to the immunomodulatory activities of *Dendrobium Officinale* polysaccharide. *Int J Biol Macromol*. (2020) 149:717–23. doi: 10.1016/j.ijbiomac.2020.01.305
11. Tang, FPS, Zhao, T, Sheng, Y, Zheng, T, Fu, L, and Zhang, Y. *Dendrobium officinale* Kimura et Migo: a review on its ethnopharmacology, phytochemistry, pharmacology, and industrialization. *Evid Based Complement Alternat Med*. (2017) 2017:7436259:1–19. doi: 10.1155/2017/7436259
12. Yang, J, Kuang, M-t, Yang, L, Huang, W, and Hu, J-m. Modern interpretation of the traditional application of Shihu—a comprehensive review on Phytochemistry and pharmacology Progress of *Dendrobium Officinale*. *J Ethnopharmacol*. (2023) 302:115912. doi: 10.1016/j.jep.2022.115912
13. Xu, X, Zhang, C, Wang, N, Xu, Y, Tang, G, Xu, L, et al. Bioactivities and mechanism of actions of *Dendrobium Officinale*: a comprehensive review. *Oxidative Med Cell Longev*. (2022) 2022:1–21. doi: 10.1155/2022/6293355
14. Ye, Z, Dai, JR, Zhang, CG, Lu, Y, and Wang, ZT. Chemical differentiation of *Dendrobium officinale* and *Dendrobium devonianum* by using HPLC fingerprints, HPLC-Esi-MS, and HPTLC analyses. *Evid Based Complement Alternat Med*. (2017) 2017:8647212:1–9. doi: 10.1155/2017/8647212
15. Xu, Z, Li, L, Xu, Y, Wang, S, and Zhao, X. Pesticide multi-residues in *Dendrobium Officinale* Kimura et Migo: method validation, residue levels and dietary exposure risk assessment. *Food Chem*. (2021) 343:128490. doi: 10.1016/j.foodchem.2020.128490
16. He, T-B, Huang, Y-P, Yang, L, Liu, T-T, Gong, W-Y, Wang, X-J, et al. Structural characterization and immunomodulating activity of polysaccharide from *Dendrobium officinale*. *Int J Biol Macromol*. (2016) 83:34–41. doi: 10.1016/j.ijbiomac.2015.11.038
17. Li, J, Huang, H-Y, and Wang, Y-Z. Optimized determination of phenolic compounds in *Dendrobium officinale* stems by reverse-phase high performance liquid chromatography. *J Liq Chromatogr Relat Technol*. (2018) 41:508–16. doi: 10.1080/10826076.2018.1470983
18. Kalogiouri, NP, and Samanidou, VF. HPLC fingerprints for the characterization of walnuts and the detection of fraudulent incidents. *Foods*. (2021) 10:2145. doi: 10.3390/foods10092145
19. Biao, H, Wei, H, Jianhong, W, Hongmei, W, and Wei, L. Simultaneous determination of phenolic components in *Dendrobium officinale* stems, leaves and flowers of by UPLC–MS/MS. *J Food Sci*. (2021) 42:2145:7. doi: 10.7506/spkx1002-6630-20200529-363
20. Wang, J, Peng, L, Shi, M, Li, C, Zhang, Y, and Kang, W. Spectrum effect relationship and component knock-out in *Angelica dahurica* radix by high performance liquid chromatography–Q exactive hybrid quadrupole–Orbitrap mass spectrometer. *Molecules*. (2017) 22:1231. doi: 10.3390/molecules22071231
21. Zhu, A-L, Hao, J-W, Liu, L, Wang, Q, Chen, N-D, Wang, G-L, et al. Simultaneous quantification of 11 phenolic compounds and consistency evaluation in four *Dendrobium* species used as ingredients of the traditional Chinese medicine Shihu. *Front Nutr*. (2021) 8:771078. doi: 10.3389/fnut.2021.771078
22. Toth, A, Riethmuller, E, Vegh, K, Alberti, A, Beni, S, and Kery, A. Contribution of individual flavonoids in *Lysimachia* species to the antioxidant capacity based on HPLC–DPPH assay. *Nat Prod Res*. (2018) 32:2058–61. doi: 10.1080/14786419.2017.1359176
23. Fei, S, Minmin, T, Hui, W, Yufeng, Z, Kexue, Z, Xiaoi, C, et al. UHPLC–MS/MS identification, quantification of flavonoid compounds from *Areca catechu* L. extracts and *in vitro* evaluation of antioxidant and key enzyme inhibition properties involved in hyperglycemia and hypertension. *Ind Crop Prod*. (2022) 189:115787. doi: 10.1016/j.indcrop.2022.115787
24. Zhang, Z, Li, Q, Li, Q, Du, S, Zhou, Y, Lv, C, et al. Simultaneous determination of nineteen major components in qi she pill by ultra-high-performance liquid chromatography–tandem mass spectrometry. *Acta Pharm Sin B*. (2014) 4:384–93. doi: 10.1016/j.apsb.2014.05.003
25. Luo, D, Mu, T, and Sun, H. Profiling of phenolic acids and flavonoids in sweet potato (*Ipomoea Batatas* L.) leaves and evaluation of their anti-oxidant and hypoglycemic activities. *Food Biosci*. (2021) 39:100801. doi: 10.1016/j.fbio.2020.100801
26. Li, C, Cui, Y, Lu, J, Meng, L, Ma, C, Liu, Z, et al. Spectrum-effect relationship of immunologic activity of *Ganoderma lucidum* by UPLC–MS/MS and component knock-out method. *Food Sci Human Wellness*. (2021) 10:278–88. doi: 10.1016/j.fshw.2021.02.019
27. Li, W, Zhang, Y, Shi, S, Yang, G, Liu, Z, Wang, J, et al. Spectrum-effect relationship of antioxidant and tyrosinase activity with *malus Pumila* flowers by UPLC–MS/MS and component knock-out method. *Food Chem Toxicol*. (2019) 133:110754. doi: 10.1016/j.fct.2019.110754
28. Yun, LI. Multiple attribute decision making analysis Topsis on quality evaluation study of *Panax notoginseng*. *Tradit Herbal Drugs*. (2017) 48:4764–71. doi: 10.7501/j.issn.0253-2670.2017.22.027



## OPEN ACCESS

## EDITED BY

Haining Zhuang,  
Shanghai Urban Construction Vocational  
College, China

## REVIEWED BY

Guitang Chen Chen,  
China Pharmaceutical University, China  
Shaodan Chen,  
Guangdong Academy of Science, China  
Yuanda Song,  
Shandong University of Technology, China

## \*CORRESPONDENCE

Xuefeng Xi  
✉ xuefeng350286@sina.com  
Zhenhua Liu  
✉ liuzhenhua623@163.com

<sup>†</sup>These authors have contributed equally to this work and share first authorship

RECEIVED 04 November 2022

ACCEPTED 11 July 2023

PUBLISHED 10 August 2023

## CITATION

Ma C, Lu J, Ren M, Wang Q, Li C, Xi X and Liu Z (2023) Rapid identification of  $\alpha$ -glucosidase inhibitors from *Poria* using spectrum-effect, component knock-out, and molecular docking technique. *Front. Nutr.* 10:1089829. doi: 10.3389/fnut.2023.1089829

## COPYRIGHT

© 2023 Ma, Lu, Ren, Wang, Li, Xi and Liu. This is an open-access article distributed under the terms of the [Creative Commons Attribution License \(CC BY\)](#). The use, distribution or reproduction in other forums is permitted, provided the original author(s) and the copyright owner(s) are credited and that the original publication in this journal is cited, in accordance with accepted academic practice. No use, distribution or reproduction is permitted which does not comply with these terms.

# Rapid identification of $\alpha$ -glucosidase inhibitors from *Poria* using spectrum-effect, component knock-out, and molecular docking technique

Changyang Ma<sup>1,2,3,4†</sup>, Jie Lu<sup>1,3†</sup>, Mengjie Ren<sup>1,4</sup>, Qiuyi Wang<sup>1,4</sup>, Changqin Li<sup>1</sup>, Xuefeng Xi<sup>1,5,6\*</sup> and Zhenhua Liu<sup>1,2,3\*</sup>

<sup>1</sup>National R&D Center for Edible Fungus Processing Technology, Henan University, Kaifeng, China,

<sup>2</sup>Shenzhen Research Institute of Henan University, Shenzhen, China, <sup>3</sup>Joint International Research

Laboratory of Food and Medicine Resource Function, Kaifeng, Henan, China, <sup>4</sup>Henan Province

Functional Food Engineering Technology Research Center, Kaifeng, Henan, China, <sup>5</sup>College of Physical Education, Henan University, Kaifeng, Henan, China, <sup>6</sup>Kaifeng Key Laboratory of Functional Components in Health Food, Kaifeng, China

**Instruction:** *Poria* (*Poria cocos*) is known for its health-promoting effects and is consumed as a food due to its potential hypoglycemic activity. However, the composition of *Poria* is complex, and the bioactive compounds that inhibit  $\alpha$ -glucosidase are not clear.

**Methods:** In this study, the fingerprint of the *Poria* methanol extract characterized by high-performance liquid chromatography (HPLC) and the model of the corresponding spectrum-effect relationship for  $\alpha$ -glucosidase was first established to screen the active compounds from *Poria*. Then, the predicted bioactive compounds were knocked out and identified using mass spectrometry. Finally, the potential binding sites and main bonds of each compound with  $\alpha$ -glucosidase were studied using molecular docking.

**Results:** The results have shown that at least 11 compounds from *Poria* could inhibit  $\alpha$ -glucosidase effectively. Moreover, eight individual compounds, i.e., poricoic acid B (**P8**), dehydrotumulosic acid (**P9**), poricoic acid A (**P10**), polyporenic acid C (**P12**), 3-epidehydrotumulosic acid (**P13**), dehydropachymic acid (**P14**), 3-O-acetyl-16 $\alpha$ -hydroxytrametenolic acid (**P21**), and pachymic acid (**P22**), were identified, and they exhibited effective inhibitory activity against  $\alpha$ -glucosidase.

**Discussion:** The possible inhibitory mechanism of them based on molecular docking showed that the binding sites are mainly found in the rings A, B, and C of these compounds, and C-3 C-16 and side chains of C-17, with the phenylalanine, arginine, tyrosine, histidine, and valine of  $\alpha$ -glucosidase. The main interactions among them might be alkyl and hydrogen bonds, which theoretically verified the inhibitory activity of these compounds on  $\alpha$ -glucosidase. The achievements of this study provided useful references for discovering bioactive compounds with hypoglycemic effects from *Poria*.

## KEYWORDS

*Poria*, spectrum-effect relationships,  $\alpha$ -glucosidase, molecular docking, rapid identification

## 1. Introduction

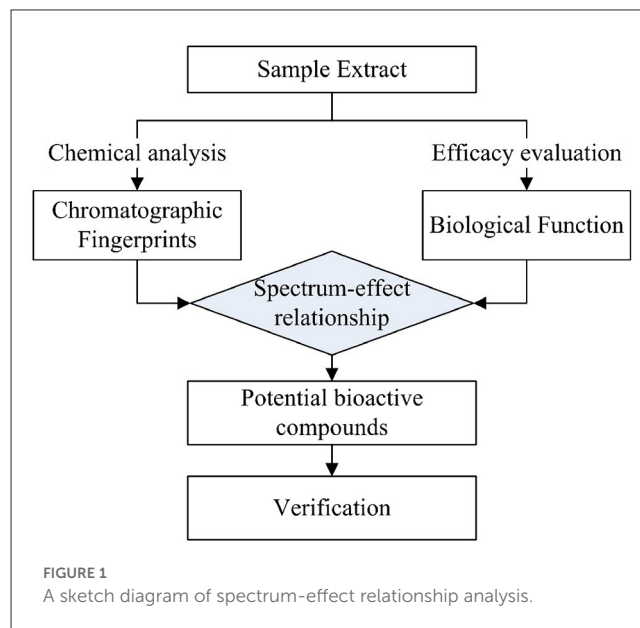
Over the past several decades, the number of people with diabetes has increased annually and is expected to reach 693 million by 2,045 (1).  $\alpha$ -glucosidase inhibitors, such as acarbose, voglibose, and miglitol, have been recommended as first-line hypoglycemic agents in the Asia-Pacific Diabetes Treatment Drug Guide (3rd Edition). The inhibitors can treat diabetes

by inhibiting glucosidase activity in the epithelial villi of the small intestine and reducing the peak postprandial blood glucose concentration in patients (2, 3). Meanwhile, these inhibitors cause many gastrointestinal adverse effects during clinical application, such as gastric distension, diarrhea, and gastrointestinal cramping pain (4). Therefore, it is necessary to find  $\alpha$ -glucosidase inhibitors with fewer side effects.

Many food materials with antidiabetic functions are important resources for medicine development, especially many edible fungi (5–7). According to previous research, *Poria*, a popular edible fungus, has been proven to have significant hypoglycemic activity (8–10) and documented in Traditional Chinese Medicine (TCM) as having clinical effectiveness in treating sugar imbalances in diabetes mellitus (11). The crude extract of *Poria* and its phytochemicals, such as dehydrotumulosic acid, dehydrotrametenolic acid, and pachymic acid, were proven to have insulin sensitizer activity and decrease postprandial blood glucose levels in db/db mice (12). There were a number of mechanisms explored in *Poria* bioactive. Dehydrotrametenolic acid could activate peroxisome proliferator-activated receptor  $\gamma$  (PPAR  $\gamma$ ), which was involved with insulin resistance (13). Pachymic acid, polyporenic acid C, dehydropachymic acid, tumulosic acid, and 3-epidehydrotumulosic acid could also promote glucose uptake in 3T3-L1 adipocytes and exhibit hypoglycemic activity (14). The inhibitory effect of *Poria* extracts on  $\alpha$ -glucosidase was verified in our pre-experiments. However, the composition of *Poria* is complex, and the corresponding bioactive compounds with inhibitive activity on  $\alpha$ -glucosidase are still not clear.

Spectrum-effect studies are currently used as a rapid method to determine the main components with specific efficacy. In the process, the fingerprint of samples, which could reflect the type and relative contents of chemical composition in the samples, is studied using spectrum technology, while corresponding bioactivities of given samples are carried out using rapid evaluation methods. Spectrum-effect analysis can link the information of the fingerprint and biological activity through statistical methods, establish the relationship between chemical composition and the corresponding activity of the research object, identify activity-related peaks from the fingerprint, and determine the active compounds after the structure identification. The spectrum-effect relationship method has successfully been used in *Ganoderma lucidum*, *Malus pumila* flowers, and *Schefflera heptaphylla* for the active compounds of immunomodulation, tyrosinase inhibition, and anti-hepatoma, respectively (15–17).

Spectrum-effect relationship studies usually involve three steps (see Figure 1): First, the chromatographic fingerprints of the given samples with chemical composition information were obtained using analytical methods, and the specific efficacy of the corresponding samples was determined in *in vitro* or *in vivo* experiments (16). Then, the data on fingerprints and effects were integrated using chemometric methods to reveal the correlation between chemical composition and efficacy, thus identifying the key active substances (18). In terms of the data analysis of spectrum-effect relationships, gray correlation analysis (GRDA), partial least squares analysis (PLSR), and principal component analysis (PCA) are useful data processing methods (15, 19, 20). Among them, PLSR was more frequently used during the



mechanism elucidation of TCM compared with the others, and better results were obtained (21, 22). Afterward, the predicted bioactive compounds were knocked out to verify their activities, and the actual efficacy compounds were finalized.

In this study, the spectrum-effect relationship between the chemical composition of *Poria* samples from different origins and their  $\alpha$ -glucosidase inhibitory activity was carried out, and the compounds with hypoglycemic effects were identified using the knock-out technique.

## 2. Materials and methods

### 2.1. Materials

The samples of *Poria* were selected from seven provinces of China (Yunnan, Sichuan, Hubei, Hunan, Henan, Zhejiang, and Jiangxi). The sample authentication was performed by Professor Changqin Li at Henan University. A total of 12 batches of *Poria* samples were collected from different origins in 2019 without obvious different sensory characteristics, and the origin information is shown in Table 1.

4-Nitrophenyl- $\alpha$ -D-glucopyranoside (Lot: 2875129) and  $\alpha$ -glucosidase (Lot: G5003, activity: 1 KU) were purchased from Sigma-Aldrich (Darmstadt, Germany).

An LC-20AT HPLC system (Shimadzu, Kyoto, Japan) equipped with an LC solution chromatography workstation and a Thermo BDS HYPERSIL C18 column (4.6 mm  $\times$  250 mm, 5  $\mu$ m) was used for the chromatographic analysis of *Poria* composition. A microplate reader (Multiskan MK3) was purchased from Thermo Electron (New York, USA). A UPLC-MS/MS system equipped with a Thermo Ultimate 3000 UHPLC system and a quadrupole-exactive-orbitrap mass spectrometer was purchased from Thermo Fisher Scientific (Waltham, USA).

TABLE 1 Different batches of Poria.

No.	Origin (Province in China)
S1	Yunnan
S2	Hubei
S3	Henan
S4	Yunnan
S5	Hunan
S6	Hunan
S7	Jiangxi
S8	Zhejiang
S9	Zhejiang
S10	Hubei
S11	Sichuan
S12	Hubei

TABLE 2 Elution program for the fingerprint of Poria.

t/min	A/% (acetonitrile)	B/% (0.1% phosphoric acid aqueous solution)
0	50	50
5	55	45
12	60	40
15	65	35
19	70	30
25	75	25
30	75	25
35	100	0

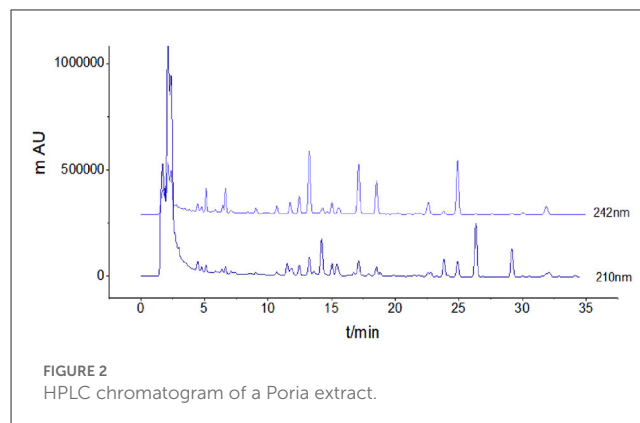
## 2.2. Methods

### 2.2.1. Extraction

Each Poria sample was crushed into 80-mesh powder, and exactly 5.00 g of powder was taken for the next step. Afterward, 50 mL of methanol was added to the powder and mixed well, and then the resulting mixture was settled for 3 days with occasional shaking. The mixture was filtered, and the solid residue was extracted again two more times with the same procedure. The filtrate of three extractions was combined and concentrated in vacuo. Methanol was added to the residue to make a 1 g/mL solution, which was filtered with a 0.22  $\mu$ m filter membrane prior to HPLC analysis.

### 2.2.2. HPLC analysis

In this study, the fingerprint of Poria extract was profiled under optimized HPLC conditions by Wang (23) and Song et al. (24) as follows: flow rate was 1.4 mL/min; column temperature, 30°C; injection volume, 20  $\mu$ L; and UV detection wavelength, 242 and 210 nm. The HPLC elution program was as shown in Table 2.



### 2.2.3. Determination method of $\alpha$ -glucosidase activity

According to the literature, the activity assays were performed on 96-well microtiter plates (25). The basic principle of this method was the enzymatic reaction of  $\alpha$ -glucosidase with PNPG (4-Nitrophenyl- $\alpha$ -D-glucopyranoside) as substrate in the potassium phosphate buffer (PBS, pH 6.8) system. During the spectrum-effect relationship analysis, a series of concentrations of extract solution, including 1.00, 0.50, 0.25, 0.125, and 0.0625 g/mL (equivalent to the Poria sample concentration), were adopted, while 1 g/mL (Poria sample concentration) was used for evaluating the inhibitory effect of target compounds and corresponding negative solutions.

### 2.2.4. Spectrum-effect relationship analysis

The retention time of each common peak of Poria was calibrated according to the “Chinese traditional medicine chromatographic fingerprint similarity evaluation system (2012 Edition).” Then, the peak area after equalization was taken as the independent variable (X),  $\alpha$ -glucosidase activity rate was taken as the dependent variable (Y), and the corresponding PLSR equation was established using the analysis software DPS 7.05.

### 2.2.5. Knock-out method for the target compounds

To obtain each compound with potential bioactivity and a corresponding negative sample, the potential target compounds predicted from 2.2.4 and the rest of the negative solution without the target fraction were collected separately according to the peak retention time of the target fraction. The details were that, after each injection of 20  $\mu$ L Poria extract, all the eluate would be collected in one container after the detector except the target fractions appeared. The eluate right after the detection was collected in one container marked with the sequence number of the target fraction. For the purity of the target compound and the rest of the negative solution, only the top of the fraction peak was collected as the target compound, and the solution at the bottom of the target fraction was discarded.

After the collection of target compounds, 2.2.3 would be carried out to examine the  $\alpha$ -glucosidase activity inhibitory rate of these



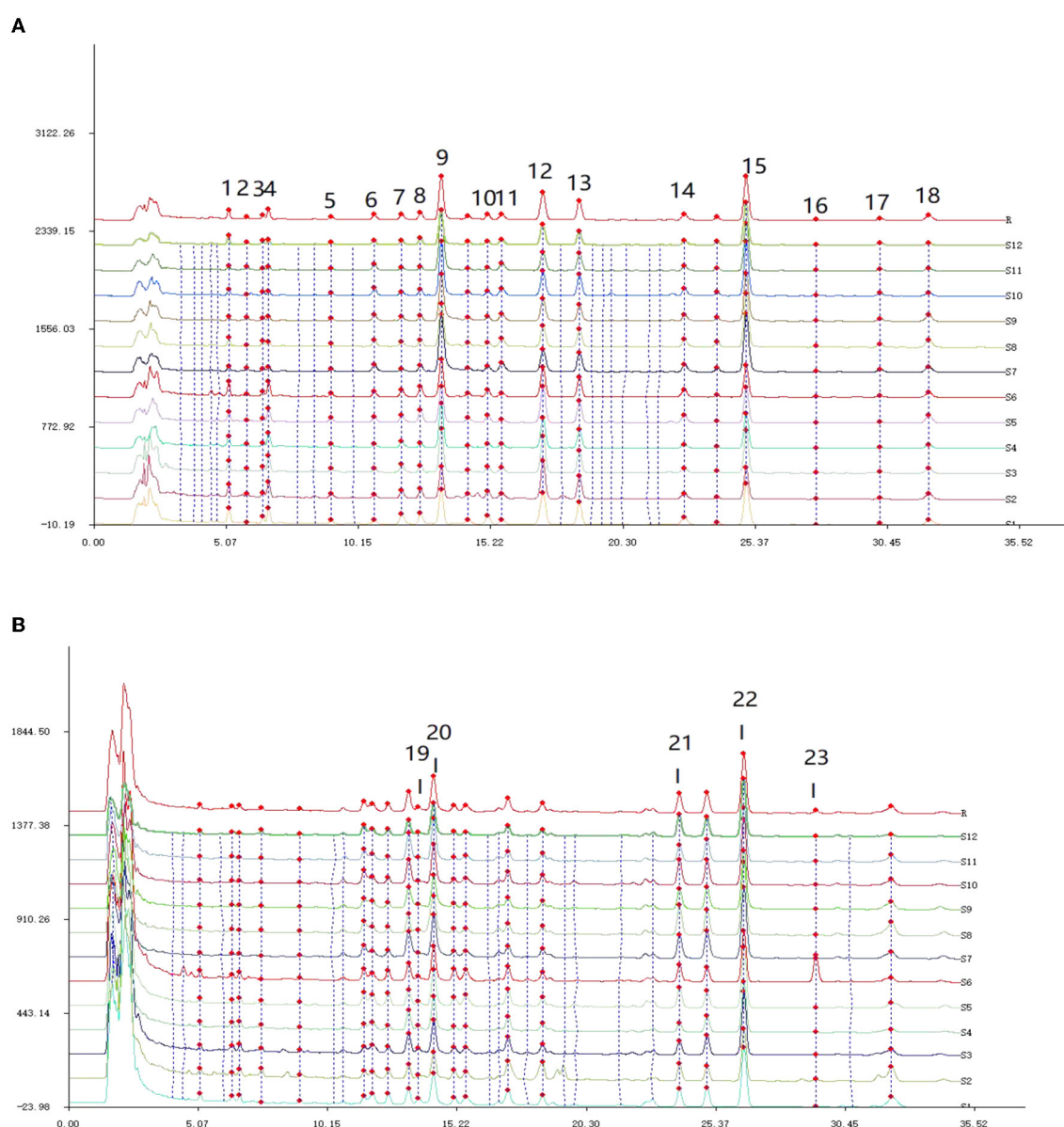


**FIGURE 3**  
HPLC feature peak matching map of 12 batches of Poria. (A) The fingerprint of Poria detected at 242 nm; (B) the fingerprint of Poria detected at 210 nm.

target compounds and corresponding negative solutions, and the target compounds with exact bioactivity would be identified.

### 2.2.6. Mass spectrometry analysis

Mass spectrometry is an effective method for the identification of phytochemicals (26). The compounds in the target fractions were identified using mass spectrometry analysis. The chromatographic column was a Thermo Hypersil GOLD C18 column (100 mm × 2.1 mm, 1.9 μm) with a flow rate of 0.3 mL/min. The mobile phases were 0.1% formic acid-water (A) and acetonitrile (B) with gradient elution mode as 0–2 min: 90% (A), 2–10 min: 90–95% (A), 10–13 min: 20–15% (A), 13–14 min: 5% (A), and 14–18 min: 90% (A). The injection volume was 2 μL, and the column temperature was 25°C.

### 2.2.7. Molecular docking analysis

The protein crystal structure of α-glucosidase was obtained from the RCSB PDB protein database. According to a previous study, the protein 3D structure with high sequence similarity with α-glucosidase (α-1,4-glucosidase) from *S. cerevisiae* (PDB code 3A4A) was taken for molecular docking analysis (27, 28). In addition, the α-glucosidase used for experimental research in this paper was also the enzyme extracted from *S. cerevisiae*. The α-glucosidase macromolecule (receptor) was processed (dehydrated, hydrogenated, and charged) using Auto-Dock software (29). The npts in XYZ were set as 126, 126, and 126, the spacing value was 0.458, and the grid center was located at the XYZ coordinates (24.473, −3.89, and 16.514). Compound molecules were optimized using Chem3D 18.0 software to generate Mol2 format files.

TABLE 3 Inhibitory rate of  $\alpha$ -glucosidase from 12 batches of Poria extracts ( $\bar{x} \pm s$ ,  $n = 3$ ).

No.	The concentration of Poria exact (%)				
	1 g/mL	0.5 g/mL	0.25 g/mL	0.125 g/mL	0.0625 g/mL
S1	46.05 $\pm$ 0.60 <sup>aaa</sup>	46.13 $\pm$ 1.22 <sup>bbb</sup>	49.67 $\pm$ 1.33	29.49 $\pm$ 1.83 <sup>ddd</sup>	23.08 $\pm$ 1.61 <sup>eee</sup>
S2	34.53 $\pm$ 1.61 <sup>aaa</sup>	38.34 $\pm$ 1.53 <sup>bbb</sup>	37.55 $\pm$ 2.39 <sup>ccc</sup>	25.35 $\pm$ 0.98 <sup>ddd</sup>	12.54 $\pm$ 1.73 <sup>eee</sup>
S3	41.72 $\pm$ 0.43 <sup>aaa</sup>	30.57 $\pm$ 1.47 <sup>bbb</sup>	29.47 $\pm$ 2.51 <sup>ccc</sup>	23.55 $\pm$ 1.75 <sup>ddd</sup>	5.19 $\pm$ 1.45 <sup>eee</sup>
S4	13.65 $\pm$ 0.93 <sup>aaa</sup>	21.98 $\pm$ 1.79 <sup>bbb</sup>	38.02 $\pm$ 0.33 <sup>ccc</sup>	36.49 $\pm$ 2.19 <sup>ddd</sup>	28.02 $\pm$ 0.08
S5	37.99 $\pm$ 1.42 <sup>aaa</sup>	43.79 $\pm$ 0.94 <sup>bbb</sup>	31.53 $\pm$ 2.41 <sup>ccc</sup>	26.4 $\pm$ 1.75 <sup>ddd</sup>	24.22 $\pm$ 1.52 <sup>eee</sup>
S6	81.71 $\pm$ 1.45	56.21 $\pm$ 2.37	32.27 $\pm$ 1.5 <sup>ccc</sup>	23.47 $\pm$ 1.16 <sup>ddd</sup>	19.4 $\pm$ 1.78 <sup>eee</sup>
S7	48.99 $\pm$ 2.74 <sup>aaa</sup>	32.53 $\pm$ 0.89 <sup>bbb</sup>	33.71 $\pm$ 1.92 <sup>ccc</sup>	26.74 $\pm$ 1.9 <sup>ddd</sup>	8.55 $\pm$ 1.36 <sup>eee</sup>
S8	29.33 $\pm$ 2.4 <sup>aaa</sup>	27.53 $\pm$ 2.63 <sup>bbb</sup>	18.7 $\pm$ 1.8 <sup>ccc</sup>	15.85 $\pm$ 2.3 <sup>ddd</sup>	10.68 $\pm$ 2.48 <sup>eee</sup>
S9	15.64 $\pm$ 1.04 <sup>aaa</sup>	17.28 $\pm$ 1.37 <sup>bbb</sup>	28.49 $\pm$ 1.2 <sup>ccc</sup>	31.19 $\pm$ 1.1 <sup>ddd</sup>	15.47 $\pm$ 2.87 <sup>eee</sup>
S10	58.47 $\pm$ 0.39 <sup>aaa</sup>	37.64 $\pm$ 2.54 <sup>bbb</sup>	34.5 $\pm$ 1.73 <sup>ccc</sup>	21.94 $\pm$ 1.59 <sup>ddd</sup>	29.33 $\pm$ 1.78
S11	42.37 $\pm$ 0.87 <sup>aaa</sup>	48.36 $\pm$ 0.89 <sup>bbb</sup>	31.56 $\pm$ 1.85 <sup>ccc</sup>	49.52 $\pm$ 2.21	26.35 $\pm$ 1.85
S12	55.37 $\pm$ 2.11 <sup>aaa</sup>	48.36 $\pm$ 0.69 <sup>bbb</sup>	44.2 $\pm$ 1.37 <sup>ccc</sup>	38.24 $\pm$ 1.56 <sup>ddd</sup>	9.32 $\pm$ 1.95 <sup>eee</sup>

Compared at 1 g/mL with S6, <sup>aaa</sup> $P < 0.001$ ; Compared at 0.5 g/mL with S6, <sup>bbb</sup> $P < 0.001$ ; Compared at 0.25 g/mL with S1, <sup>ccc</sup> $P < 0.001$ ; Compared at 0.125 g/mL with S11, <sup>ddd</sup> $P < 0.001$ ; Compared at 0.0625 g/mL with S10, <sup>eee</sup> $P < 0.001$ .

Molecular docking of the target compounds with  $\alpha$ -glucosidase was performed using Sybyl X2.1.1 software to assess their chemical bonding ability. The ligand molecules were mapped using the Sketch module of Sybyl X2.1.1, and the Tripos force field molecular mechanics program Minimize was used for structure optimization.

## 2.2.8. Statistical analysis

The inhibitory bioactivity of each Poria exact and knock-out component on  $\alpha$ -glucosidase was determined in triplicates and reported as means  $\pm$  standard deviation. For multiple comparisons, a two-sided analysis of variance and a  $T$ -test were performed using DPS 7.05.

## 3. Results

### 3.1. The spectrum-effect analysis of Poria on $\alpha$ -glucosidase inhibition

#### 3.1.1. HPLC fingerprint of Poria extract

The HPLC chromatogram of Poria extracts at two detection wavelengths was recorded (Figure 2).

The HPLC chromatogram of all batches of Poria was imported into the software “Chinese traditional medicine chromatographic fingerprint similarity evaluation system (2012 Edition)”, and the 23 common peaks with two detection wavelengths were matched in Figure 3.

From Figure 3A, it can be observed that there were a total of 18 common peaks at the detection wavelength of 242 nm, and the detection signals of P9, P15, P12, and P13 were relatively high. In Figure 3B, according to corresponding retention times, five new common peaks were identified at the wavelength of 210 nm, and the detection signals of P19, P20, P21, and P22 were relatively strong.

Based on the 2-wavelength detection systems, a total of 23 common peaks were identified from the fingerprints of Poria.

#### 3.1.2. The $\alpha$ -glucosidase inhibitory effect of Poria extract

The *in vitro*  $\alpha$ -glucosidase inhibition rates of different batches of Poria extract are shown in Table 3. The results showed that the inhibition rates of most samples at a concentration of 1 g/mL (equivalent to the raw material of Poria) ranged from 13.65 to 81.71%. Along with the decreasing concentration of Poria exacta, the corresponding inhibitory rate became weak. For multiple comparisons of the samples, the significant difference was determined with the highest inhibitory rate as the reference. For example, S6 had the strongest inhibition (81.71%) at a concentration of 1 g/mL and was significantly higher than the others ( $P < 0.001$ ). In general, 12 batches of Poria samples varied greatly in the degree of inhibition of  $\alpha$ -glucosidase.

#### 3.1.3. Spectrum-effect analysis based on PLSR

Using DPS software, the PLSR equation was developed and listed as follows:

$$Y = 0.000002 - 0.074383x_1 + 0.165853x_2 - 0.158367x_3 + 0.110130x_4 - 0.268134x_5 + 0.007144x_6 + 0.335275x_7 + 0.592098x_8 - 0.225877x_9 + 0.076574x_{10} - 0.181819x_{11} - 0.011150x_{12} + 0.272292x_{13} - 0.011564x_{14} - 0.137367x_{15} + 0.360107x_{16} + 0.286721x_{17} - 0.675986x_{18} - 0.139855x_{19} + 0.198398x_{20} - 0.029304x_{21} + 0.103270x_{22} + 0.318297x_{23}.$$

The goodness of fit ( $R^2 = 0.8954$ ) was high enough to analyze the possible effect of the 23 common compounds on the  $\alpha$ -glucosidase. All the regression coefficients of the 23 common compounds are represented in Figure 4. The results showed that P2, P4, P7, P8, P10, P13, P16, P17, P20, P22, and P23 were positively effective in inhibiting  $\alpha$ -glucosidase, while P1, P3, P5, P9, P11, P12,

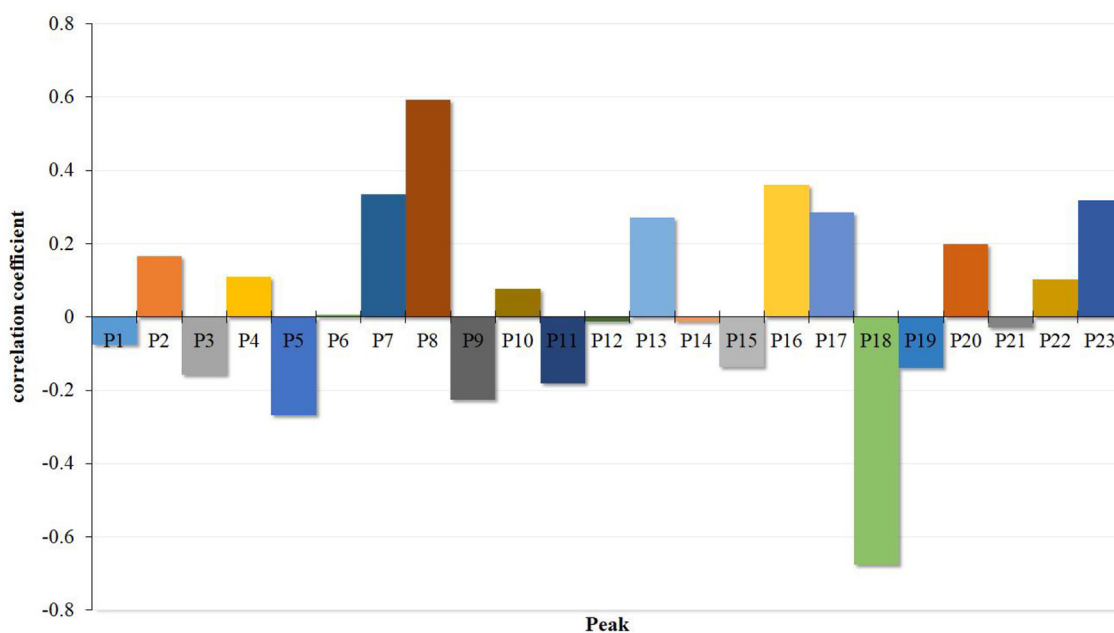


FIGURE 4  
PLSR coefficient diagram of Poria.

P14, P15, P18, P19, and P21 were negatively effective, which means that increasing the proportion of the compounds with positive effects would enhance the  $\alpha$ -glucosidase inhibitory ability of Poria.

## 3.2. Identification of the compounds with the activity of inhibiting $\alpha$ -glucosidase

### 3.2.1. The effect of knock-out compounds and negative samples on $\alpha$ -glucosidase

For further confirmation of the potential inhibition activity, the target compounds, P1, P5, P6, P7, P8, P9, P10, P12, P13, P14, P15, P21, P22, and P23, as well as corresponding negative samples, were used to test the inhibitory effect on  $\alpha$ -glucosidase. However, these compounds with lower concentrations or poor resolution were not collected for further research. The results are shown in Figure 5.

In General, all the compounds and negative solutions showed some inhibitory effect on  $\alpha$ -glucosidase. Among them, the target compounds including P1, P5, P6, P7, P9, P12, P14, P15, P21, P22, and P23 exhibited strong inhibitory effect on  $\alpha$ -glucosidase, while P8, P10, and P13 showed weak inhibitory effect. Compared with the full extracts, the target compound P9 and the corresponding negative solution would exhibit a lower effect on the  $\alpha$ -glucosidase, while P1, P5, P6, P7, P8, P10, P12, P14, P15, P21, P22 and their negative solutions showed stronger inhibitory effects, respectively. The sum effects of compounds P23 and P13 with their negative solutions were not significantly different from the full extracts. It can be observed that, for most compounds, separation was one effective way to alter their inhibitory effect on  $\alpha$ -glucosidase (30).

Based on the comparison among these columns, it could be found that the inhibitory activity of each target compound and the negative solution was different. Taking P22 as an example, although

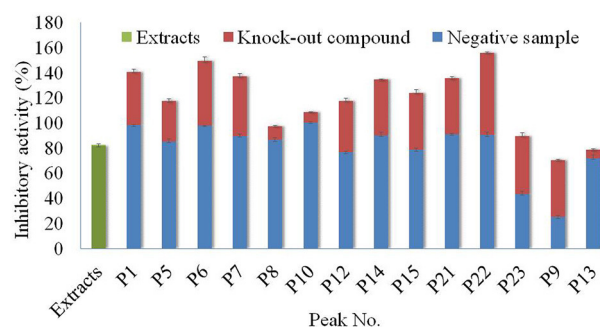


FIGURE 5  
Analysis of antagonistic and synergistic effects between knock-out compounds of Poria extract and negative samples.

the inhibitory activity of the full extracts was ~80%, the inhibitory activities of the compound and corresponding negative solution were almost 60 and 100%, respectively. The results also showed that separation was essential for using the specific function of the resource, or the function would not be demonstrated if the whole extract was used directly.

### 3.2.2. Identification of target compounds

The relative molecular masses of these target compounds were detected by positive ion modes under the mass spectrometry conditions of 2.2.6. Then, the possible molecular structure of the compounds was inferred from the secondary cleavage fragments by positive ion mode and from many relevant studies. After that, the compounds' structure was initially

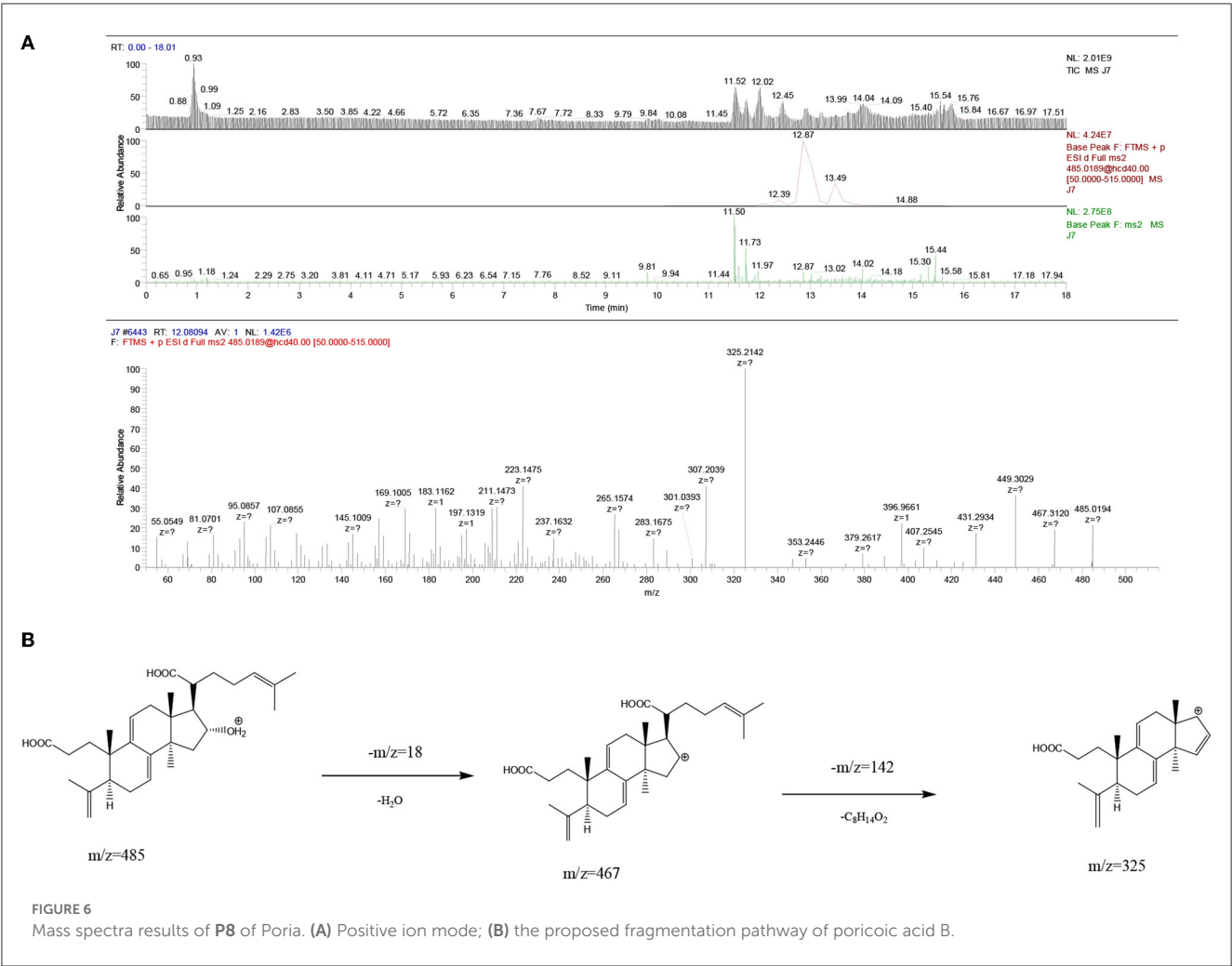


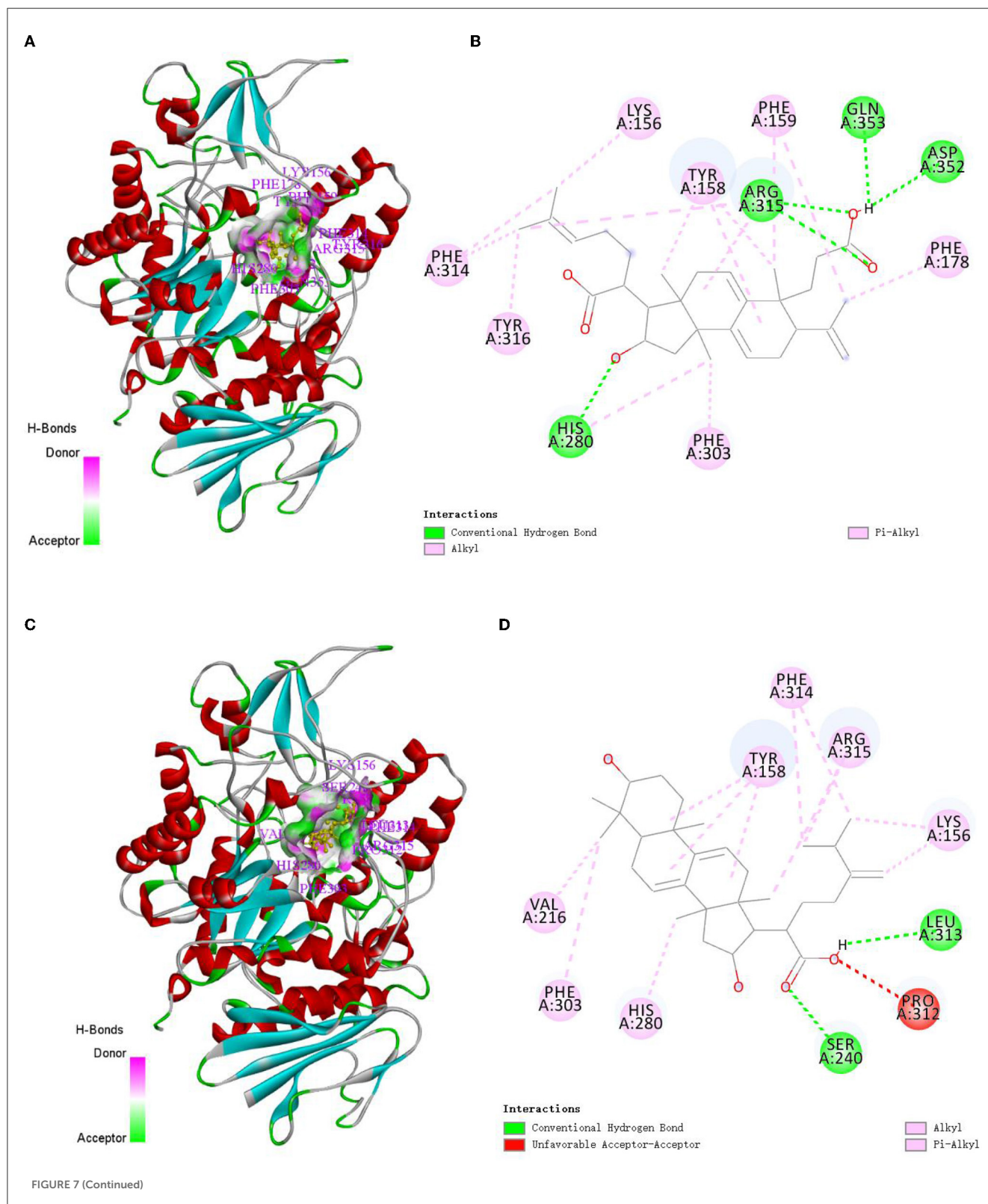
TABLE 4 Identification of chemical compounds in *Poria*.

Peak No.	T <sub>R</sub> (min)	[M + H] <sup>+</sup> (m/z)	Secondary ionic debris	Compound	Analytic diagram
P8	12.08094	485.0194	467.3120, 325.2142	Poricoic acid B (C <sub>30</sub> H <sub>44</sub> O <sub>5</sub> )	Figure 6
P9	12.11050	485.0197	467.3505, 311.2349	Dehydrotumulosic acid (C <sub>31</sub> H <sub>48</sub> O <sub>4</sub> )	Supplementary Figure 1
P10	12.11223	499.4323	481.3296, 325.2140	Poricoic acid A (C <sub>31</sub> H <sub>46</sub> O <sub>5</sub> )	Supplementary Figure 2
P12	12.42158	483.0211	465.3350, 447.3237, 309.2191	Polyporenic acid C (C <sub>31</sub> H <sub>46</sub> O <sub>4</sub> )	Supplementary Figure 3
P13	12.60692	485.0191	467.3503, 449.3398, 311.2350	3-epidehydrotumulosic acid (C <sub>31</sub> H <sub>48</sub> O <sub>4</sub> )	Supplementary Figure 4
P14	12.67910	527.4883	509.3608, 353.2455, 449.3399	Dehydropachymic acid (C <sub>33</sub> H <sub>50</sub> O <sub>5</sub> )	Supplementary Figure 5
P21	12.74769	515.3712	497.3600, 479.3502, 437.3400, 293.2244	3-O-Acetyl-16 $\alpha$ -hydroxytrametenolic acid (C <sub>32</sub> H <sub>50</sub> O <sub>5</sub> )	Supplementary Figure 6
P22	12.92147	529.3864	511.3762, 451.3554, 429.3864	Pachymic acid (C <sub>33</sub> H <sub>52</sub> O <sub>5</sub> )	Supplementary Figure 7

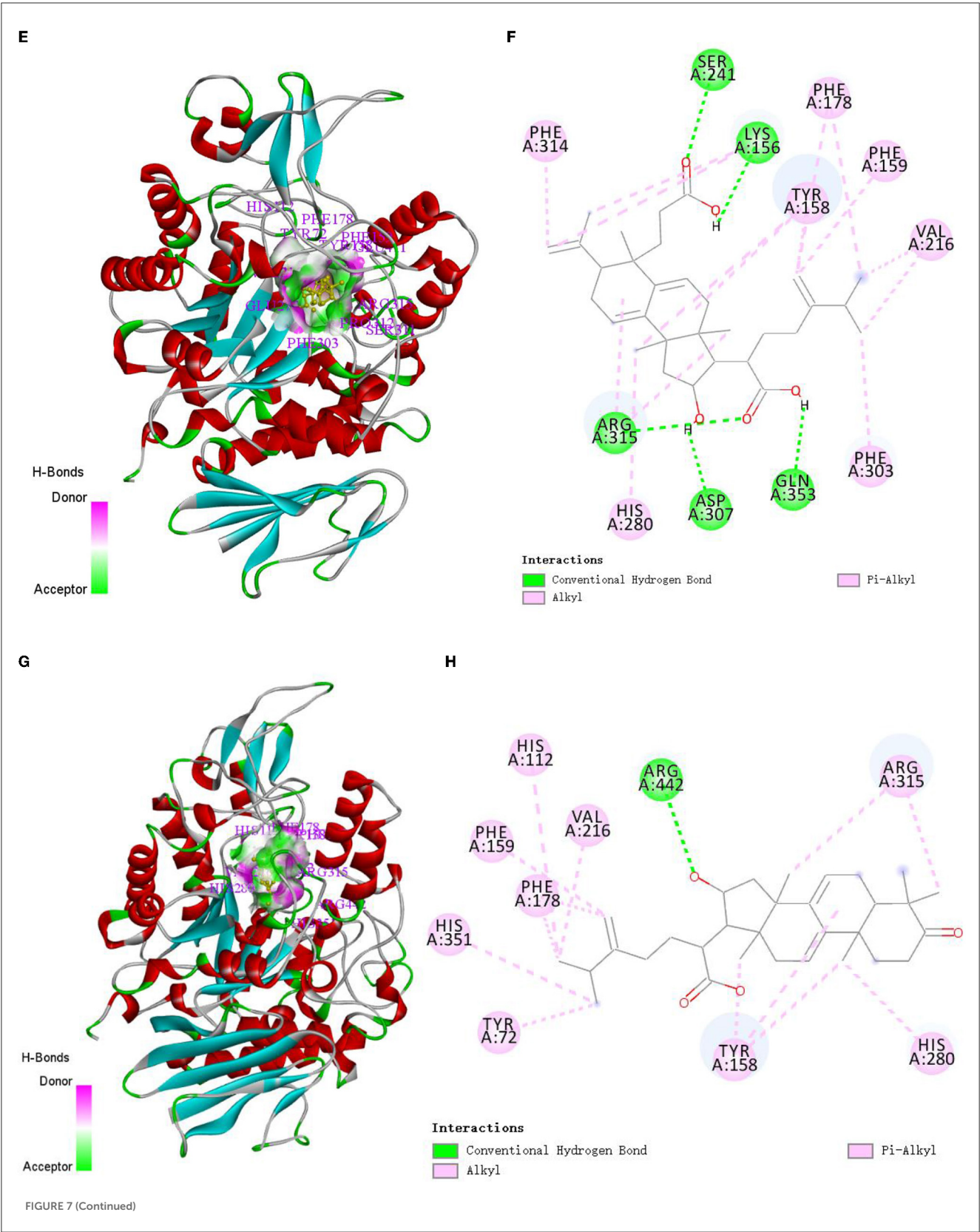


identified by the literature contrast of the polar order and UV absorption spectra with reported molecules (31–35). Finally, eight compounds, namely, **P8**, **P9**, **P10**, **P12**, **P13**, **P14**, **P21**, and **P22**, knocked out of Poria, were identified as follows:

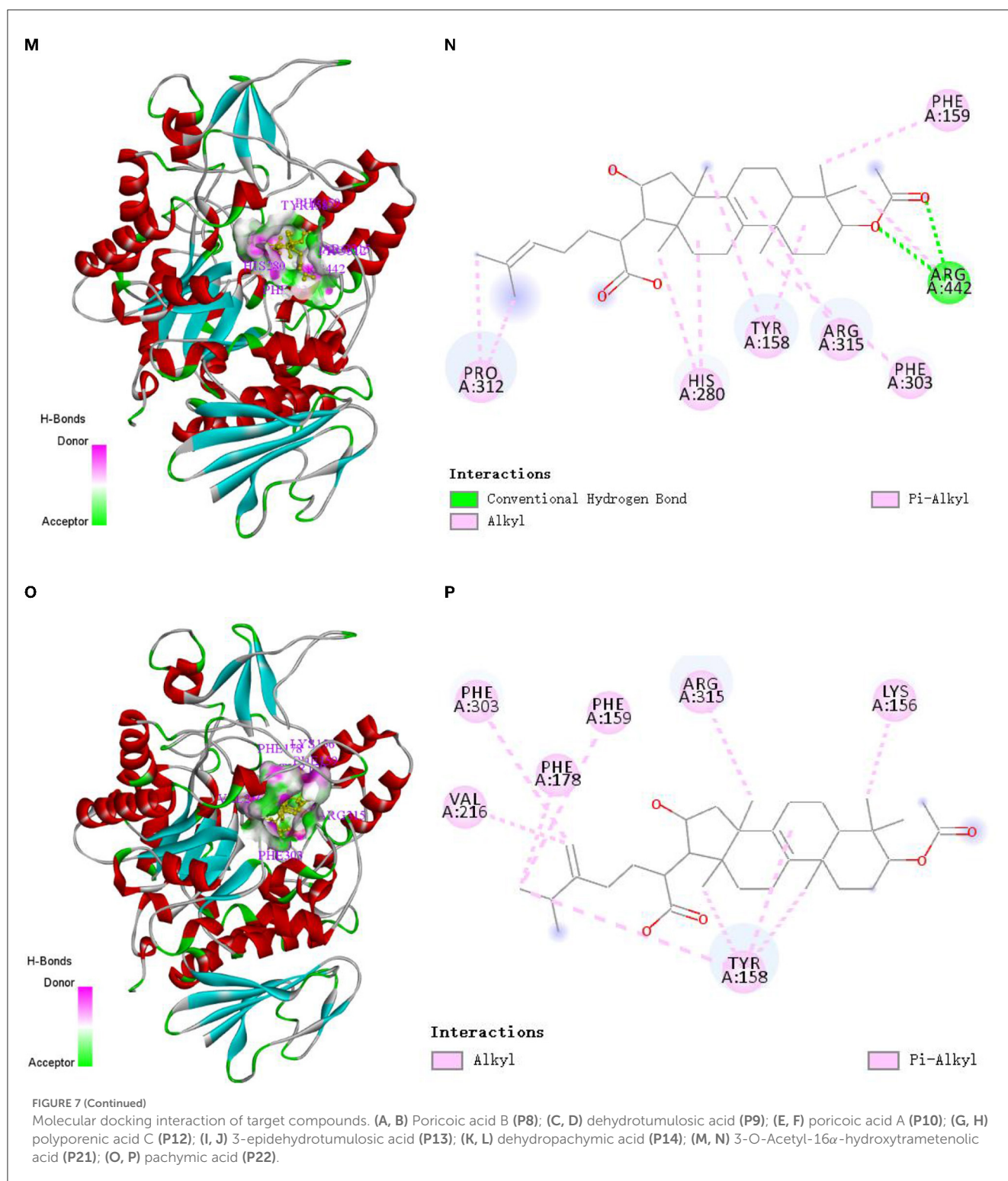
The UPLC-MS<sup>2</sup> result of **P8** (retention time of 12.08094 min) was shown in Figure 6, and a primary ion peak  $m/z$  485.0189  $[M + H]^+$  was yielded in positive ion mode, which revealed the presumed molecular weight of 484 and a possible molecular formula of  $C_{30}H_{44}O_5$ . The secondary mass spectral fragmentation











and cleavage pathway of the compound were shown in Figure 6B, indicating that it would be poricoic acid B.

By analogy, the UPLC-MS<sup>2</sup> results of P9, P10, P12, P13, P14, P21, and P22 were listed as Supplementary Figures S1–S7, respectively, and they were presumed to be dehydrotumulosic acid, poricoic acid A, polyporenic acid C, 3-epidehydrotumulosic acid, dehydropachymic acid, 3-O-Acetyl-16 $\alpha$ -hydroxytrametenolic acid, and pachymic acid, respectively. The molecular details of them are listed in Table 4.

### 3.3. Molecular docking of target compounds with $\alpha$ -glucosidase

The molecular docking technique is a theoretical simulation method for predicting intermolecular binding sites and forces, which can provide further insight into the interaction mechanism of compounds with  $\alpha$ -glucosidase (36, 37). In this study, molecular docking technique was used to simulate the binding sites and power of poricoic acid B (P8), dehydrotumulosic



TABLE 5 The interaction site of  $\alpha$ -glucosidase with active compounds.

Interaction site	PHE	TYR	VAL	ARG	HIS	LYS	PRO	GLN	ASP	SER	GLU	LEU
Poricoic acid B	4 $\times$ Alk	2 $\times$ Alk		1 $\times$ Hyd	1*Hyd	1*Alk		1*Hyd	1*Hyd			
Dehydrotumulosic acid	2 $\times$ Alk	1 $\times$ Alk	1 $\times$ Alk	1 $\times$ Alk	1*Alk	1*Alk	1*UAA			1*Hyd		1*Hyd
Poricoic acid A	4 $\times$ Alk	1 $\times$ Alk	1 $\times$ Alk	1 $\times$ Hyd	1*Alk				1*Hyd	1*Hyd	1*Hyd	
Polyporenic acid C	2 $\times$ Alk	2 $\times$ Alk	1 $\times$ Alk	1 $\times$ Alk 1 $\times$ Hyd	3*Alk							
3-epidehydrotumulosic acid	1 $\times$ Alk 1 $\times$ PHB 1 $\times$ PSi	1 $\times$ Alk 1 $\times$ PSi	1 $\times$ Alk	1 $\times$ Hyd	1*Alk		1*Hyd			1*Hyd	2*Hyd	
Dehydropachymic acid	3 $\times$ Alk	1 $\times$ Alk	1 $\times$ Alk	1 $\times$ Alk		1*Alk				1*Hyd		
3-O-Acetyl-16 $\alpha$ -hydroxytrametenolic acid	2 $\times$ Alk	1 $\times$ Alk		1 $\times$ Alk 1 $\times$ Hyd	1*Alk		1*Alk					
Pachymic acid	3 $\times$ Alk	1 $\times$ Alk	1 $\times$ Alk	1 $\times$ Alk		1*Alk						

Alk, Alkyl (including Pi-Alkyl); Hyd, conventional Hydrogen Bond; PSi, Pi-Sigma; UAA, unfavorable acceptor-acceptor; PHE, phenylalanine; TYR, tyrosine; VAL, valine; ARG, arginine; HIS, histidine; LYS, lysine; PRO, proline; GLN, glutamine; ASP, aspartic acid; SER, serine; GLU, glutamic acid; LEU, leucine.

acid (P9), poricoic acid A (P10), polyporenic acid C (P12), 3-epidehydrotumulosic acid (P13), dehydropachymic acid (P14), 3-O-Acetyl-16 $\alpha$ -hydroxytrametenolic acid (P21) and pachymic acid (P22) with  $\alpha$ -glucosidase, and the result are shown in Figure 7.

The binding energy of poricoic acid B (P8), dehydrotumulosic acid (P9), poricoic acid A (P10), polyporenic acid C (P12), 3-epidehydrotumulosic acid (P13), dehydropachymic acid (P14), 3-O-Acetyl-16 $\alpha$ -hydroxytrametenolic acid (P21), and pachymic acid (P22) with  $\alpha$ -glucosidase were  $-8.9$ ,  $-10.6$ ,  $-9.2$ ,  $-9.7$ ,  $-9.9$ ,  $-9.3$ ,  $-9.3$  and  $-9.3$  kcal/mol, respectively. Their energy values were lower than  $-5.0$  kcal/mol, which means that all eight compounds could bind with  $\alpha$ -glucosidase steadily. It could be observed that the interaction between these compounds and  $\alpha$ -glucosidase was mostly through alkyl and pi-alkyl with methyl groups and double bonds of C-17 side chain, A-ring, B-ring, or C-ring, followed by a conventional hydrogen bond with hydroxyl, carboxyl or acetoxy groups of C-3 and C-16. In addition, these compounds could also sometimes combine with the rings of  $\alpha$ -glucosidase directly.

Specifically, if we take poricoic acid B (Figures 7A, B) as an example, poricoic acid B could form hydrogen bonds with amino acid residues of ARG: 315, ASP: 352, GLN: 353, and HIS: 280, as well as alkyl forces with PHE: 159, PHE: 178, PHE: 303, PHE: 314, TYR: 158, TYR: 316, and LYS: 156. The other compounds have similar interaction relationships with many amino acid residues of  $\alpha$ -glucosidase. Therefore, it could be observed that the inhibitory ability of the compound on  $\alpha$ -glucosidase was positively correlated with the ability of the compound to bind  $\alpha$ -glucosidase, which indicated that the results of molecular docking were consistent with the results of compound activity screening, which might depend on the main forces of hydrogen bonds and alkyl bonds including Pi-Alkyl.

To elucidate interaction relationships clearly, the interaction relationships of the compounds with  $\alpha$ -glucosidase were collected in Table 5. From the summarized results, it could be concluded that the main potential interaction sites of  $\alpha$ -glucosidase were phenylalanine (PHE), tyrosine (TYR), arginine (ARG), valine (VAL), histidine (HIS), and others by the alkyl and conventional hydrogen bond, which was the possible working mechanism of Poria in inhibiting the activity of  $\alpha$ -glucosidase.

## 4. Discussion

The study of the spectrum-effect relationship method has gradually attracted broad attention. Combined with the “component knock-out” technique, the spectrum-effect relationship method could discover the active substances from a complex system of samples such as Traditional Chinese Medicine (TCM), benefiting product development and quality control (38). The PLSR method was frequently used to establish a quantitative model of the spectrum-effect relationship to explore the information from the relationship (39, 40). In previous research, the spectrum-effect relationship method with PLSR successfully identified oxypeucedanin hydrate, imperatorin, cnidilin, isoimperatorin, byakangelicin, and bergapten from *Angelica dahurica*. The former four compounds were the main components with inhibitory effects on tyrosinase activity, while the latter two compounds had activating effects (21). In this study, 23 common spectrum peaks were matched from different batches of Poria samples according to HPLC fingerprints, and the PLSR method was used to establish the correlation between the peaks and  $\alpha$ -glucosidase inhibitory activity. The results revealed that peaks P2, P4, P6, P7, P8, P10, P13, P16, P17, P20, P22, and P23 were positively correlated with the inhibition of  $\alpha$ -glucosidase activity, while peaks P1, P3, P5, P9, P11, P12, P14, P15, P18, P19, and P21 were negatively correlated with the inhibitory ability.

The “component knock-out” technique was usually used to obtain the active target compounds from natural products and assist the spectrum-effect relationship analysis to test the structure and the activity of target compounds separately. For example, Liu et al. knocked out a series of compounds from the alcoholic extracts of *Begonia angustifolia* under the guidance of the spectrum-effect relationship and successfully found four compounds with a positive or negative effect on the tyrosinase, which were isochlorogenic acid B, isochlorogenic acid C, isochlorogenic acid A, and cymaroside (19). Shi et al. (41) successfully screened the main  $\alpha$ -glucosidase inhibitor in pomegranate peel under the guidance of the spectrum-effect relationship and further confirmed that the inhibitor could significantly reduce postprandial blood sugar *in vivo*. The present study isolated 14 targeted compounds from Poria with potential

inhibition effects using the “component knock-out” technique and tested their effect on the  $\alpha$ -glucosidase activity, and the results showed that **P1, P5, P6, P7, P9, P12, P14, P15, P21, P22, and P23** had an inhibitory effect on  $\alpha$ -glucosidase activity. Among them, the structures of eight compounds were determined using UPLC-MS<sup>2</sup> and references as poricoic acid B, dehydrotumulosic acid, poricoic acid A, polyporenic acid C, 3-epidehydrotumulosic acid, dehydropachymic acid, 3-O-acetyl-16 $\alpha$ -hydroxytrametenolic acid, and pachymic acid, respectively. According to many types of research, most of them, including dehydrotumulosic acid, polyporenic acid C, pachymic acid, dehydrotrametenolic acid, and dehydroeburicoic acid, could act as an insulin sensitizer in glucose tolerance tests and reduce hyperglycemia (42, 43). Xie et al. extracted poricoic acid A from *Sargassum pallidum* and also found the inhibitory effect of poricoic acid A on  $\alpha$ -glucosidase (44). In addition, Xie also found that poricoic acid A could inhibit the formation of advanced glycation end products (AGEs) and fructosamine and have great potential as antiglycation inhibitors to treat diabetes (45). The mechanism in antidiabetics or the effect on  $\alpha$ -glucosidase of the other bioactive compounds were not mentioned by scholars.

In recent years, the molecular docking technique has been widely used for the working mechanism of  $\alpha$ -glucosidase inhibitors. Rahman et al. (46) studied the binding potential of 32 alkaloids with  $\alpha$ -glucosidase using molecular docking techniques and found that nummular-R and vindoline had significant interaction with the enzyme; Ur-Rehman et al. (47) used molecular docking technique to study the connection of triterpenic acids isolated from *Boswellia elongata* with  $\alpha$ -glucosidase and the results explored the inhibitory ability of these isolated compounds on  $\alpha$ -glucosidase. In the research by Xie et al. (44), it was found that there were Four hydrogen bonds, alkyl and pi-alkyl, between poricoic acid A and  $\alpha$ -glucosidase. This research identified 4 alkyl and four conventional hydrogen bonds between them. Similarly, the other seven compounds were docked with the residents of  $\alpha$ -glucosidase, i.e., phenylalanine, tyrosine, arginine, valine, histidine, etc., via alkyl and hydrogen bonds, which were not reported before. The results showed that the alkyl and hydrogen bond between the compounds of *Poria* and the  $\alpha$ -glucosidase lead to the inhibition of this enzyme, which would help to elucidate the mechanism of *Poria* treating diabetes.

## 5. Conclusion

In this research, the fingerprint of *Poria* was studied using HPLC analysis, and 23 common peaks were identified. Additionally, the inhibitory effect on the  $\alpha$ -glucosidase of the 23 compounds of *Poria* was predicted using spectrum-effect relationship analysis and PLSR analysis. Combined with the “component knock-out” technique, LC-MS<sup>2</sup>, and molecular docking technique, 14 common compounds were knocked out, and the molecule structure of eight active compounds was identified for further analysis. Based on the analysis, it was concluded that Poricoic acid B, dehydrotumulosic acid, poricoic acid A, polyporenic acid C, 3-epidehydrotumulosic acid, dehydropachymic acid, 3-O-acetyl-16 $\alpha$ -hydroxytrametenolic acid, and pachymic acid exhibited a significantly inhibitory effect on the  $\alpha$ -glucosidase, and

their inhibitory effect might be related to the interaction with  $\alpha$ -glucosidase mainly through alkyl and hydrogen bonds. These results, including the HPLC fingerprint and bioactive compound of *Poria*, can be used for the quality evaluation and control of *Poria* and the development of effective medicines for the treatment of diabetes.

## Data availability statement

The original contributions presented in the study are included in the article/Supplementary material, further inquiries can be directed to the corresponding authors.

## Author contributions

CM and JL designed the study and performed experiments, writing, and original draft preparation. MR and QW analyzed the summarized data and verified it. CL and XX contributed to the data acquisition, project administration, and critically reviewed the manuscript. ZL provided resources and funding and reviewed the manuscript. All authors contributed to the article and approved the submitted version.

## Funding

This study was supported by Major Public Welfare Projects in Henan Province (201300110200), Research on Precision Nutrition and Health Food, the Department of Science and Technology of Henan Province (CXJD2021006), and The Key Project in the Science and Technology Agency of Henan Province (221111110600 and 232102110156).

## Conflict of interest

The authors declare that the research was conducted in the absence of any commercial or financial relationships that could be construed as a potential conflict of interest.

## Publisher's note

All claims expressed in this article are solely those of the authors and do not necessarily represent those of their affiliated organizations, or those of the publisher, the editors and the reviewers. Any product that may be evaluated in this article, or claim that may be made by its manufacturer, is not guaranteed or endorsed by the publisher.

## Supplementary material

The Supplementary Material for this article can be found online at: <https://www.frontiersin.org/articles/10.3389/fnut.2023.1089829/full#supplementary-material>



## References

- Artasensi A, Pedretti A, Vistoli G, Fumagalli L. Type 2 diabetes mellitus: a review of multi-target drugs. *Molecules*. (2020) 25:1987. doi: 10.3390/molecules2501031414
- Cheng AYY, Fantus IG. Oral antihyperglycemic therapy for type 2 diabetes mellitus. *Can Med Assoc J*. (2005) 172:231–226. doi: 10.1503/cmaj.1031414
- Yin Z, Sun-Waterhouse D, Wang J, Ma C, Waterhouse G, Kang W. Polysaccharides from edible fungi *Pleurotus* spp: advances and perspectives. *J Fut Foods*. (2021) 1:128–40. doi: 10.1016/j.jfutfo.2022.01.002
- Van De Laar FA, Lucassen P, Akkermans RP, Van de Lisdonk EH, Rutten GE, Van Weel C. Alpha-glucosidase inhibitors for type 2 diabetes mellitus: a systematic review. *Cochr Database Syst Rev*. (2005) 2005:CD003639. doi: 10.1002/14651858.CD003639.pub2
- Zhang Y, Wang D, Chen Y, Liu T, Zhang S, Fan H, et al. Healthy function and high valued utilization of edible fungi. *Food Sci Human Wellness*. (2021) 10:408–20. doi: 10.1016/j.fshw.2021.04.003
- Yin Z, Liang Z, Li C, Wang J, Ma C, Kang W. Immunomodulatory effects of polysaccharides from edible fungus: a review. *Food Sci Human Wellness*. (2021) 10:393–400. doi: 10.1016/j.fshw.2021.04.001
- Barzee TJ, Cao L, Pan Z, Zhang R. Fungi for future foods. *J Fut Foods*. (2021) 1:25–37. doi: 10.1016/j.jfutfo.2021.09.002
- Ning C, Jiao Y, Wang J, Li W, Zhou J, Lee Y, et al. Recent advances in the managements of type 2 diabetes mellitus and natural hypoglycemic substances. *Food Sci Human Wellness*. (2022) 11:1121–33. doi: 10.1016/j.fshw.2022.04.004
- Saadelddeen FSA, Niu Y, Wang H, Zhou L, Meng L, Chen S, et al. Natural products: regulating glucose metabolism and improving insulin resistance. *Food Sci Human Wellness*. (2020) 9:214–28. doi: 10.1016/j.fshw.2020.04.005
- Lu J, Tian J, Zhou L, Meng L, Chen S, Ma C, et al. Phytochemistry and biological activities of *poria*. *J Chem*. (2021) 2021:6659775. doi: 10.1155/2021/6659775
- Jia W, Gao W, Tang L. Antidiabetic herbal drugs officially approved in China. *Phytother Res*. (2003) 17:1127–34. doi: 10.1002/ptr.1398
- Li T-H, Hou C-C, Chang CL-T, Yang W-C. Anti-hyperglycemic properties of crude extract and triterpenes from *Poria cocos*. *Evid Based Comp Altern Med*. (2011) 2011:128402. doi: 10.1155/2011/128402
- Sato M, Tai T, Nunoura Y, Yajima Y, Kawashima S, Tanaka K. Dehydrotrametenolic acid induces preadipocyte differentiation and sensitizes animal models of noninsulin-dependent diabetes mellitus to insulin. *Biol Pharm Bull*. (2002) 25:81–6. doi: 10.1248/bpb.25.81
- Huang Y-C, Chang W-L, Huang S-F, Lin C-Y, Lin H-C, Chang T-C. Pachymic acid stimulates glucose uptake through enhanced GLUT4 expression and translocation. *Eur J Pharmacol*. (2010) 648:39–49. doi: 10.1016/j.ejphar.2010.08.021
- Li C, Cui Y, Lu J, Meng L, Ma C, Liu Z, et al. Spectrum-effect relationship of immunologic activity of *Ganoderma lucidum* by UPLC-MS/MS and component knock-out method. *Food Sci Human Wellness*. (2021) 10:278–88. doi: 10.1016/j.fshw.2021.02.019
- Li W, Zhang Y, Shi S, Yang G, Liu Z, Wang J, et al. Spectrum-effect relationship of antioxidant and tyrosinase activity with *Malus pumila* flowers by UPLC-MS/MS and component knock-out method. *Food Chem Toxicol*. (2019) 133:110754. doi: 10.1016/j.fct.2019.110754
- Liu X, Jiang N, Xu X, Liu C, Liu Z, Zhang Y, et al. Anti-hepatoma compound determination by the method of spectrum-effect relationship, component knock-out, and UPLC-MS2 in *Schefflera heptaphylla* (L.)Frodin Harms and its mechanism. *Front Pharmacol*. (2020) 11:1342. doi: 10.3389/fphar.2020.01342
- Shi M, Zhang Y, Song M, Sun Y, Li C, Kang W. Screening the marker components in *Psoralea corylifolia* L. with the aids of spectrum-effect relationship and component knock-out by UPLC-MS<sup>2</sup>. *Int J Mol Sci*. (2018) 19:3439. doi: 10.3390/ijms19113439
- Liu H, Zhu S, Liu Q, Zhang Y. Spectrum-effect relationship study between HPLC fingerprints and anti-oxidant of honeysuckle extract. *Biomed Chromatogr*. (2019) 33:e4583. doi: 10.1002/bmc.4583
- Chen Y, Pan G, Xu W, Sun Q, Wang B, Zhang Y, et al. Spectrum-effect relationship study between HPLC fingerprints and antioxidant activity of *Sabia parviflora*. *J Chromatogr B*. (2020) 1140:121970. doi: 10.1016/j.jchromb.2020.121970
- Wang J, Peng L, Shi M, Li C, Zhang Y, Kang W. Spectrum effect relationship and component knock-out in *Angelica dahurica* radix by high performance liquid chromatography-q exactive hybrid quadrupole-orbitrap mass spectrometer. *Molecules*. (2017) 22:1231. doi: 10.3390/molecules22071231
- Li C-Q, Yao C, Zhu R-Y, Huang Y-X, Kang W-Y, Wang J-M. Spectrum-effect relationship in antioxidant activity of *Ligustri lucidi* Fructus based on DPPH, ABTS and FRAP assays. *China J Chin Mater Med*. (2016) 41:1670–7. doi: 10.4268/cjcm20160917
- Wang KF. *Study on Chemical Constituents and Quality Control methods of Poria cocos*. Beijing: Beijing University of Chinese Medicine (2014) .
- Song X, Xie Z, Huang D, Liu T, Deng F, Shu Z, et al. HPLC fingerprint and chemical pattern recognition of *Poria*. *Chin J Exp Trad Med Form*. (2015) 21:36–9. doi: 10.13422/j.cnki.syfx.2015170036
- Cui L, He N, Zhang X, Li S, Zhang Y, Kang W. Dynamic change of secondary metabolites and spectrum-effect relationship of *Malus halliana* Koehne flowers during blooming. *Open Chem*. (2018) 16:362–70. doi: 10.1515/chem-2018-0043
- Cui L, Liu Y, Liu M, Ren M, Ahmed A, Kang W, et al. Identification of phytochemicals from *Letinus edodes* and *Auricularia auricula* with UPLC-Q-Exactive Orbitrap MS. *J Fut Foods*. (2022) 2:253–60. doi: 10.1016/j.jfutfo.2022.06.006
- Azizian H, Pedrood K, Moazzam A, Valizadeh Y, Khavaninzadeh K, Zamani A, et al. Docking study, molecular dynamic, synthesis, anti- $\alpha$ -glucosidase assessment, and ADMET prediction of new benzimidazole-Schiff base derivatives. *Sci Rep*. (2022) 12:14870. doi: 10.1038/s41598-022-18896-0
- Sakulkeo O, Wattanapiromsakul C, Pitakbut T, Dej-Adisai S. Alpha-glucosidase inhibition and molecular docking of isolated compounds from traditional thai medicinal plant, *Neuropeltis racemosa* Wall. *Molecules*. (2022) 27:639. doi: 10.3390/molecules27030639
- Trott O, Olson AJ. AutoDock Vina: improving the speed and accuracy of docking with a new scoring function, efficient optimization and multithreading. *J Comput Chem*. (2010) 31:455–61. doi: 10.1002/jcc.21334
- Ning ZW, Zhai LX, Huang T, Pen J, Hu D, Xiao H, et al. Identification of  $\alpha$ -glucosidase inhibitors from cyclocarya paliurus tea leaves using UF-UPLC-Q/TOF-MS/MS and molecular docking. *Food Funct*. (2019) 10:1893–902. doi: 10.1039/C8FO01845F
- Wang HX. *Qualitative and Quantitative Analysis of Components in Different Medicinal Parts of Poria and Study on Quality Standard of Rubra Poria*. Shijiazhuang: Hebei Medical University (2016).
- Shu T, Ding LN, Wang Q, Jia C, Qiu Y, Ruan H. Structural elucidation of flavonoids in the supercritical CO<sub>2</sub> extract of black goji fruit by using ultra-high performance liquid chromatography coupled with tandem mass spectrometry. *Food Sci*. (2020) 41:206–12. doi: 10.7506/spkx1002-6630-20190505-033
- Luo XY. *Study on the Material Basis of Poria cocos Spleen Strengthening Effect Based on Spectrum Effect Relationship*. Wuhan: University of Chinese Medicine (2020).
- Ma Y, Zheng W, Wang Z, Xiao W, Huang W, Zhang Y. Establishment of UPLC/Q-TOF-MS chromatographic fingerprint of triterpenic acids in Guizhi Fuling Capsule. *Chin Trad Herbal Drugs*. (2019) 50:626–31. doi: 10.7501/j.issn.0253-2670.2019.03.014
- Ding G, Wang ZZ, Zhang CF, Sheng L. Study on HPLC fingerprint of the triterpene acids in *Poria cocos*. *China J Chin Mater Med*. (2002) 27:756–8. doi: 10.3321/j.issn:1001-5302.2002.10.014
- Dong D, Xu ZJ, Wu Z, Peng S. Parallelization of molecular docking: a review. *Curr Top Med Chem*. (2018) 18:1015–28. doi: 10.2174/1568026618666180821145215
- Han L, Wang H, Cao J, Li Y, Jin X, He C, et al. Inhibition mechanism of  $\alpha$ -glucosidase inhibitors screened from Tartary buckwheat and synergistic effect with acarbose. *Food Chem*. (2023) 420:136102. doi: 10.1016/j.foodchem.2023.136102
- Yang L, Jiang H, Wang S, Hou A, Man W, Zhang J, et al. Discovering the major antitussive, expectorant, and anti-inflammatory bioactive constituents in *Tussilago Farfara* L. based on the spectrum-effect relationship combined with chemometrics. *Molecules*. (2020) 25:620. doi: 10.3390/molecules25030620
- Zhu CS, Lin ZJ, Xiao ML, Niu H, Zhang B. The spectrum-effect relationship-a rational approach to screening effective compounds, reflecting the internal quality of Chinese herbal medicine. *Chin J Nat Med*. (2016) 14:177–84. doi: 10.1016/S1875-5364(16)30014-0
- Chang WQ, Zhou JL Li Y, Shi Z, Wang L, Yang J, et al. An *in vitro* approach for lipolysis measurement using high-resolution mass spectrometry and partial least squares-based analysis. *Anal Chim Acta*. (2017) 950:138–46. doi: 10.1016/j.aca.2016.10.043
- Shi R, Zhou N, Zhang H, Gong M, Han L. Bioaffinity ultrafiltration coupled with HPLC-ESI-MS/MS for screening potential  $\alpha$ -glucosidase inhibitors from pomegranate peel. *Front Nutr*. (2022) 9:1014862. doi: 10.3389/fnut.2022.1014862
- Gulati V, Singh MD, Gulati P. Role of mushrooms in gestational diabetes mellitus. *AIMS Med Sci*. (2019) 6:49–66. doi: 10.3934/medsci.2019.1.49
- Fu M, Wang L, Wang X, Deng B, Hu X, Zou J. Determination of the five main terpenoids in different tissues of *Wolfiporia cocos*. *Molecules*. (2018) 23:1839. doi: 10.3390/molecules23081839

44. Xie X, Chen C, Fu X. Screening  $\alpha$ -glucosidase inhibitors from four edible brown seaweed extracts by ultra-filtration and molecular docking. *LWT*. (2021) 138:110654. doi: 10.1016/j.lwt.2020.110654
45. Xing X, Chun C, Xiong F, Rui-Hai L. Influence of *Sargassum pallidum* and the synergistic interaction mechanism of 6-gingerol and pericoic acid A on inhibiting ovalbumin glycation. *Food Funct*. (2021) 12:9315–26. doi: 10.1039/D1FO01886H
46. Rahman N, Muhammad I, Gul-E-Nayab, Khan H, Aschner M, Filosa R, et al. Molecular docking of isolated alkaloids for possible  $\alpha$ -glucosidase inhibition. *Biomolecules*. (2019) 9:544. doi: 10.3390/biom9100544
47. Ur-Rehman N, Halim SA, Al-Azri MH, Khan M, Khan A, Rafiq K, et al. Triterpenic acids as non-competitive  $\alpha$ -glucosidase inhibitors from *Boswellia elongata* with structure-activity relationship: *in vitro* and *in silico* studies. *Biomolecules*. (2020) 10:751. doi: 10.3390/biom10050751



## OPEN ACCESS

## EDITED BY

Yisheng Chen,  
Shanxi Agricultural University, China

## REVIEWED BY

Zhenfeng Wu,  
Jiangxi University of Traditional Chinese  
Medicine, China  
Petar Ristivojevic,  
University of Belgrade, Serbia  
Laura Barp,  
University of Udine, Italy

## \*CORRESPONDENCE

Gertrud E. Morlock  
✉ gertrud.morlock@uni-giessen.de

<sup>†</sup>Member of the More than One Constituent  
Substances (MOCS)  
Initiative, [www.vielstoffgemische.de](http://www.vielstoffgemische.de)

RECEIVED 23 May 2023

ACCEPTED 04 August 2023

PUBLISHED 22 September 2023

## CITATION

Müller I, Gulde A and Morlock GE (2023)  
Bioactive profiles of edible vegetable oils  
determined using 10D hyphenated  
comprehensive high-performance thin-layer  
chromatography (HPTLC×HPTLC) with  
on-surface metabolism (nanoGIT) and planar  
bioassays. *Front. Nutr.* 10:1227546.  
doi: 10.3389/fnut.2023.1227546

## COPYRIGHT

© 2023 Müller, Gulde and Morlock. This is an  
open-access article distributed under the terms  
of the [Creative Commons Attribution License](https://creativecommons.org/licenses/by/4.0/)  
(CC BY). The use, distribution or reproduction  
in other forums is permitted, provided the  
original author(s) and the copyright owner(s)  
are credited and that the original publication in  
this journal is cited, in accordance with  
accepted academic practice. No use,  
distribution or reproduction is permitted which  
does not comply with these terms.

# Bioactive profiles of edible vegetable oils determined using 10D hyphenated comprehensive high-performance thin-layer chromatography (HPTLC×HPTLC) with on-surface metabolism (nanoGIT) and planar bioassays

Isabel Müller <sup>1</sup>, Alexander Gulde<sup>1</sup> and Gertrud E. Morlock <sup>1,2\*†</sup>

<sup>1</sup>Institute of Nutritional Science, Chair of Food Science, as well as Interdisciplinary Research Centre for Biosystems, Land Use and Nutrition, Justus Liebig University Giessen, Giessen, Germany, <sup>2</sup>Center for Sustainable Food Systems, Justus Liebig University Giessen, Giessen, Germany

**Introduction:** Vegetable oils rich in unsaturated fatty acids are assumed to be safe and even healthy for consumers though lipid compositions of foods vary naturally and are complex considering the wealth of minor compounds down to the trace level.

**Methods:** The developed comprehensive high-performance thin-layer chromatography (HPTLC×HPTLC) method including the on-surface metabolization (nanoGIT) and bioassay detection combined all steps on the same planar surface. The pancreatic lipolysis (intestinal phase) experiment and the subsequent analysis of the fatty acid composition including its effect-directed detection using a planar bioassay was performed without elaborate sample preparation or fractionation to ensure sample integrity. Thus, no sample part was lost, and the whole sample was studied on a single surface regarding all aspects. This made the methodology as well as technology miniaturized, lean, all-in-one, and very sustainable.

**Results and discussion:** To prioritize important active compounds including their metabolism products in the complex oil samples, the nanoGIT method was used to examine the pancreatic lipolysis of nine different vegetable oils commonly used in the kitchen and food industry, e.g., canola oil, flaxseed oil, hemp oil, walnut oil, soybean oil, sunflower oil, olive oil, coconut oil, and palm oil. The digested oils revealed antibacterial and genotoxic effects, which were assigned to fatty acids and oxidized species via high-resolution tandem mass spectrometry (HRMS/MS). This finding reinforces the importance of adding powerful techniques to current analytical tools. The 10D hyphenated nanoGIT-HPTLC×HPTLC-Vis/FLD-bioassay-heart cut-RP-HPLC-DAD-HESI-HRMS/MS has the potential to detect any potential hazard due to digestion/metabolism, improving food safety and understanding on the impact of complex samples.

## KEYWORDS

all-in-one digestion analysis system, on-surface metabolization, lipolysis, effect-directed analysis, intestinal phase, comprehensive high-performance thin-layer chromatography, plant oils, sustainability transition

## 1. Introduction

Lipids are one of the three important macronutrients in the human diet, and fat has the highest energy density of all nutrients. It is recommended that not more than 30%–35% of the energy intake should be in the form of fat (1, 2). The fatty acid (FA) composition of dietary fats can influence body weight (3, 4). High intake of saturated or monounsaturated fats causes an increase in weight gain and waist circumference, a factor for adiposity, whereas polyunsaturated fatty acids (PUFAs) show no increase. Among other aspects, saturated fatty acids (SFAs) such as lauric acid (C12:0), myristic acid (C14:0), and palmitic acid (C16:0) are associated with a higher risk of cardiovascular disease (5, 6). Replacing SFA-rich fats with PUFA-rich oils showed a lower risk of cardiovascular disease but no effect on adiposity (7), as mentioned earlier. Therefore, a deeper knowledge of the FA composition of food and its impact is of the utmost interest since the biological activity of FAs may influence not only cell and tissue metabolism and signaling pathways (8) but also our microbiome (9) and health (10). To achieve a low-fat diet, foods of plant origin are preferred to those of animal origin (1). Such plant-based foods contain less total fat and a more favorable FA composition, such as more essential FAs, namely  $\alpha$ -linolenic acid (C18:3, *n*-3) and linoleic acid (C18:2, *n*-6), whereby *n*-6 to *n*-3 FA ratios of 1–5:1 are preferred (4, 11, 12); however, the ratio alone is not decisive for a diet recommendation (13, 14). Therefore, edible vegetable oils are the most commonly used fats in the kitchen and for the preparation and processing of foods (15, 16). They mainly consist of triacylglycerols (TAGs), in addition to a few percent of diacylglycerols (DAGs), monoacylglycerols (MAGs), and free FAs, as well as further lipophilic minor compounds in the per mille range down to the trace level (17–19).

The simulation of *in vitro* digestion is important to provide insights into the digestion mechanisms of fats and oils. After partial hydrolysis of TAGs by gastric lipases, the nutrients entering the small intestine are emulsified by bile salts and further digested enzymatically by pancreatic lipases in the intestinal phase (20). Both lipases cleave TAGs mainly into 2-MAGs and free FAs. However, while the main hydrolysis takes place in the intestine, it should not be neglected that gastric and pancreatic lipases act as complementary enzymes (21). The rate of lipolysis of TAGs is dependent on the FA chain length and degree of saturation (22–24). Research is currently being conducted on various simulated digestion models to study the digestibility of isolated nutrients in foods or the food itself, not ignoring the influence of the food matrix (25, 26). Due to the sensitivity of simulated digestion systems to altering enzymatic parameters and environmental conditions, Minekus et al. (27) designed an internationally harmonized protocol for static *in vitro* digestion via oral, gastric, and intestinal phases. Morlock et al. (28) showed the successful transfer of the internationally harmonized protocol for *in vitro* assays to high-performance thin-layer chromatography (HPTLC–UV/Vis/FLD), and moreover, they created an all-in-one digestion and analysis system for on-surface digestion at the nanomolar level (nanoGIT), followed by the analysis of the food samples, including the resulting metabolism products, all on the same surface. The optional hyphenation with post-chromatographic derivatization

reagents, planar bioassays, and high-resolution tandem mass spectrometry (HRMS/MS) makes the lean all-in-one methodology very flexible, fast, and sustainable. In contrast, all current methods require elaborate sample preparation after the simulated lipolysis and the subsequent analysis of the metabolized food samples. Mostly, spectrophotometric assay kits or titration methods, such as the pH-stat method, are used for the determination of the sum of hydrolyzed FAs and thus lipolysis rate (26, 29, 30). Gas chromatography and high-performance liquid chromatography methods are performed rarely (23, 31), although Helbig et al. (29) showed the necessity of examining the detailed FA composition.

In this study, an all-in-one 10D hyphenated nanoGIT–HPTLC×HPTLC–Vis/FLD–bioassay–heart cut–RP–HPLC–DAD–HESI–HRMS/MS methodology was created and studied for the first time. The nanoGIT system was used to examine the pancreatic lipolysis of nine different vegetable oils commonly used in the kitchen and food industry, i.e., canola oil, flaxseed oil, hemp oil, walnut oil, soybean oil, sunflower oil, olive oil, coconut oil, and palm oil. A two-dimensional (2D) separation with orthogonal selectivity was developed for the differentiation of the lipids, resulting in a comprehensive HPTLC×HPTLC method. The entire sample separated in the first dimension was transferred to the second orthogonal separation dimension by a simple 90° plate turn. After the on-surface nanoGIT digestion, the first dimension was separated based on functional groups such as TAGs, DAGs, MAGs, and FAs. In the second separation dimension, the FAs were separated according to lipophilicity, and the approximate FA composition was determined. Antibacterial and genotoxic properties of the lipids were detected via respective bioassays and assigned to molecules via automated heart cuts of the active zones of interest to RP–HPLC–DAD–HESI–HRMS/MS. No information or sample part was lost since the whole workflow was performed on the same planar surface.

## 2. Materials and methods

### 2.1. Chemicals and materials

3-(4,5-Dimethylthiazol-2-yl)-2,5-diphenyltetrazolium bromide (MTT,  $\geq 98\%$ ), acetone ( $\geq 99.9\%$ ), formic acid ( $\geq 99.9\%$ ), acetic acid (100%), dipotassium phosphate trihydrate ( $\geq 99.9\%$ ), glycerol (86%), monopotassium phosphate ( $\geq 99\%$ ), magnesium chloride ( $\geq 98.5\%$ ), sodium chloride ( $\geq 99.8\%$ ), monosodium phosphate monohydrate ( $\geq 98\%$ ), *n*-hexane ( $\geq 98\%$ ), sulfuric acid (96%, *p. a.*), decanoic acid (C10:0,  $> 98\%$ ), octanoic acid (C8:0,  $> 99\%$ ), oleic acid (C18:1,  $> 99\%$ ), stearic acid (C18:0,  $> 98\%$ ), sodium hydroxide ( $\geq 98\%$ ), 4-methylumbelliferyl- $\beta$ -D-galactopyranoside ( $\geq 99\%$ , for biochemistry), dimethylsulfoxide ( $\geq 99.8\%$ ), and molecular sieve 3 Å (0.3 nm, type 564, beads) were purchased from Carl Roth (Karlsruhe, Germany). Acetonitrile ( $\geq 99.9\%$ ), disodium phosphate ( $\geq 99\%$ ), sodium bicarbonate ( $\geq 99.7\%$ ), pancreatin from porcine pancreas (8 × USP specifications), bile extract porcine, dioleoylglycerol (diolein,  $> 99\%$ , mixture of 1,3- and 1,2-isomers), glyceryl trioleate (triolein,  $\geq 99\%$ ), 1-oleoyl-*rac*-glycerol (monoolein,  $> 99\%$ ; 2-monoolein was rarely available and six times more expensive), caffeine ( $> 99\%$ ),

linoleic acid (C18:2, 60%–74%), myristic acid (C14:0, >99%), palmitic acid (C16:0, >99%), dodecanoic acid (C12:0, 98%), peptone from casein (for microbiology), Müller-Hinton broth (for microbiology), D-(+)-glucose (99.5%), ampicillin sodium salt, and lysogeny broth (LB) powder (including 5 g/L of sodium chloride) were purchased from Fluka-Sigma-Aldrich (Steinheim, Germany). Methanol (99.9%) was supplied by VWR International (Darmstadt, Germany). Magnesium sulfate heptahydrate (99.5%), potassium chloride ( $\geq 99.5\%$ ), citric acid monohydrate ( $\geq 99.5\%$ ), HPTLC plates silica gel 60 RP-18 W, HPTLC plates silica gel 60 RP-18, and HPTLC plates silica gel 60 as cover plates (all 20 cm  $\times$  10 cm), and *Bacillus subtilis* subsp. *spizizenii* spore suspension (DSM 618) were purchased from Merck (Darmstadt, Germany). Diammonium phosphate ( $\geq 99\%$ ), diethyl ether ( $\geq 99\%$ ), and linolenic acid (C18:3, 99%) were purchased from Acros Organics (Morris Plains, NJ, USA). Yeast extract powder (for microbiology), ethyl acetate ( $\geq 99.8\%$ ), *o*-phosphoric acid (85%), ethanol ( $\geq 99.9\%$ ), and dichloromethane ( $\geq 99.9\%$ , stabilized with amylene) were purchased from Th. Geyer (Renningen, Germany). Copper(II) sulfate pentahydrate (p. a.) was purchased from Honeywell International (Morristown, NJ, USA). Calcium chloride dihydrate ( $\geq 99.9\%$ ) was supplied by Bernd Kraft (Duisburg, Germany). The luminescent marine *Aliivibrio fischeri* (DSM 7151) bacteria were purchased from the DSMZ Leibnitz Institut (Berlin, Germany). Tetracycline hydrochloride (research grade, USP) was purchased from Serva Electrophoresis (Heidelberg, Germany). Bidistilled water was produced by a Heraeus Destamat B-18E (Thermo Fisher Scientific, Dreieich, Germany). Rhodamine 6G (100%  $\pm$  3%) was purchased from Alfa Aesar (Kandel, Germany). *Salmonella typhimurium* bacteria strain TA1535, modified to contain the plasmid pSK1002 (PTM *S. typhimurium* TA1535/pSK1002, cryostock), was purchased from Trinova Biochem (Giessen, Germany). 4-Nitroquinoline-1-oxide (98%) was purchased from TCI (Eschborn, Germany). Edible vegetable oils ([Supplementary Table S1](#)) were purchased from local supermarkets.

## 2.2. Pre-treatment of the HPTLC RP-18 W plate

For on-surface metabolic reactions, the HPTLC RP-18 W plate was pre-treated as follows. The plate was heated at 120°C for 60 min (TLC Plate Heater III, CAMAG, Muttens, Switzerland; to fix the binder for the current plate batches used) and pre-washed by development first with methanol and then, after plate drying, with ethyl acetate, both up to 90 mm in a twin-trough chamber. To ensure the pancreatin reaction in the application zone, the acidic plate pH (ca. pH 4.2) was neutralized via piezoelectrical spraying (2.8 ml, ultra-yellow nozzle, level 3, Derivatizer, CAMAG) with phosphate-citrate buffer (6 g/L of citric acid and 10 g/L of disodium hydrogen phosphate, adjusted to pH 12 by sodium hydroxide). Therefore, except for the application zone, the plate was covered by a cut HPTLC plate silica gel 60, with the layer facing upward ([Supplementary Figure S1](#)). Then, the plates were dried at 120°C for 10 min.

## 2.3. Preparation of solutions for the enzyme, calcium chloride, standards, and samples

The digestion fluid stock solution was prepared as described by Minekus et al. (27). The pancreatin solution (200 TAME mU/ $\mu$ l) and the corresponding calcium chloride solution (6 pmol/ $\mu$ l) were prepared according to Morlock et al. (28). Monoolein, diolein, triolein, fatty acids (reference compounds were applied via overspraying to obtain the mixture on the start zone), and samples were weighed via a pipette and dissolved in *n*-hexane (all 1 mg/ml each), whereby solid fats (i.e., palm oil and coconut oil) were slightly warmed to the melting point before pipetting. All solutions were stored in solvent-tight vials in the dark at 4°C.

## 2.4. Initial triacylglycerol separation on HPTLC plate RP-18

Oil sample and FA standard solutions (10  $\mu$ l/band each; 1 mg/ml) were applied as 8-mm bands, unless stated otherwise, as follows: a track distance of 10 mm, distance from the lower edge of 10 mm and left edge of 10 mm, dosage speed of 150 nl/s, filling speed of 15  $\mu$ l/s, filling vacuum time of 0 s, and syringe volume of 25  $\mu$ l (Automatic TLC Sampler ATS 4, CAMAG). The plate was developed with dichloromethane/acetic acid/acetone 2:4:5 (V/V/V) (32) in a twin-trough chamber (20 cm  $\times$  10 cm) up to 80 mm. The plate was subjected to a derivatization reagent sequence performed via dipping (immersion time 8 s, immersion speed 3 cm/s, Chromatogram Immersion Device 3, CAMAG), i.e., first in rhodamine 6G reagent solution (0.1% in ethanol) and, after plate drying and detection at FLD 366 nm (TLC Visualizer 2, CAMAG), then in copper sulfate phosphoric acid reagent (25 g copper sulfate pentahydrate in 250 ml *o*-phosphoric acid/water 4:41, V/V), followed by heating at 150°C for 20 min (TLC Plate Heater III, CAMAG) and detection at FLD 366 nm and white light illumination.

## 2.5. On-surface lipolysis and separation systems on HPTLC plate RP-18 W

The following workflow was adapted from the nanoGIT<sup>+</sup> active methodology (28, 33). The application was performed as mentioned, except for a band length of 6 mm, a track distance of 9 mm, and a distance from the left edge of 14.5 mm. Reference standard mixtures were applied via overspraying. Since the previous solutions were in *n*-hexane, the cleaning unit of the ATS 4 had to be rinsed with bi-distilled water once and the syringe twice before pancreatin application. The applied sample bands were first oversprayed with pancreatin solution (5  $\mu$ l/band, 200 TAME mU/ $\mu$ l) and then with calcium chloride solution (1  $\mu$ l/band, 6 pmol/ $\mu$ l) using a dosage speed of 50 nl/s and a filling speed of 8  $\mu$ l/s. The application zone of the plate was wetted with 2.5 ml of 0.1 M sodium chloride solution by piezoelectrical spraying (yellow nozzle, level 6, Derivatizer), whereby the plate area for chromatographic separation was covered with a cut HPTLC plate



silica gel 60 (Supplementary Figure S2A) (33) to avoid the salt load on this adsorbent area and ensure good zone resolution during the later separation. This plate package was incubated at 37°C in a humid plastic box (26.5 × 16 × 10 cm, ABM, Wolframs-Eschenbach, Germany) for 60 min. After plate drying (120°C, 10 min), the lipids were focused twice by front elution with acetone up to 25 mm in a twin-trough chamber (10 min before, the second trough of the twin-trough chamber was filled up to half with molecular sieve 0.3 nm), and the lower part of the plate was cut off at 15 mm (Supplementary Figure S3) to reduce the influence of the pancreatin matrix on the chromatographic separation. The plate was developed from the cut edge side with either *n*-hexane/diethyl ether/formic acid 90:25:2 (V/V/V) (34) up to 60 mm for the separation of acylglycerols or acetonitrile/water 4:1 (V/V) up to 50 mm for the separation of FAs in the twin-trough chamber filled with molecular sieve as mentioned. Chromatograms were derivatized via the reagent sequence, whereby the cut 15-mm plate strip was stuck together with adhesive tape on the glass side of the HPTLC plate and detected as mentioned.

## 2.6. On-surface lipolysis and HPTLC×HPTLC analysis on HPTLC plate RP-18 W

As mentioned in the previous subsection, one oil sample per plate (10 cm × 10 cm) was applied as a 3-mm band, except for setting the distance from the left edge to 9 mm and using cover plates that covered everything but the applied sample band (Supplementary Figures S1B, S2B). The applied sample was treated with pancreatin and calcium chloride, wetted, incubated, focused (but no plate cut), developed two-dimensionally, detected via a bioassay as follows, or derivatized optionally via the reagent sequence, and detected as mentioned. For 2D development, the apolar mobile phase for acylglycerol separation was chosen as the first dimension, and the polar mobile phase for FAs separation as the second dimension. In between, the plate was dried at 120°C (TLC Plate Heater III) for 10 min and rotated by 90° (Supplementary Figure S4). Before the bioassay application, the plate was freed from residuals of the mobile phase via heating at 120°C for 10 min (TLC Plate Heater III) and neutralization with 2.5% sodium bicarbonate solution (2.8 ml, yellow nozzle, level 3, Derivatizer) followed by drying at 120°C for 10 min.

### 2.6.1. Gram-negative *Aliivibrio fischeri* bioassay

The bacterial cryostock solution (200 µl) was suspended in 20 ml of medium according to DIN EN ISO 11348-1, Section 5 (35), and the cultivation was performed overnight (18–24 h) in a 100-ml baffled flask in room temperature by shaking at 120 rpm (KMCO2, Edmund Bühler, Hechingen, Germany). As soon as the culture showed brilliant turquoise bioluminescence when shaken in the dark, it was ready for use. The bacterial suspension was piezoelectrically sprayed onto the plate (3.5 ml, blue nozzle, level 6, Derivatizer) (36, 37), and the instant bioluminescence was recorded from the wet plate over a 30-min period (time interval 3 min, exposure time 100 s, BioLuminizer 2, CAMAG).

Antibacterials and cytotoxins were detected as dark zones, whereas metabolism-enhancing substances appeared as bright zones on the bioluminescent background, depicted as a grayscale image. The positive control was caffeine (1–7 µl/band, 1 mg/ml in methanol).

### 2.6.2. Gram-positive *Bacillus subtilis* bioassay

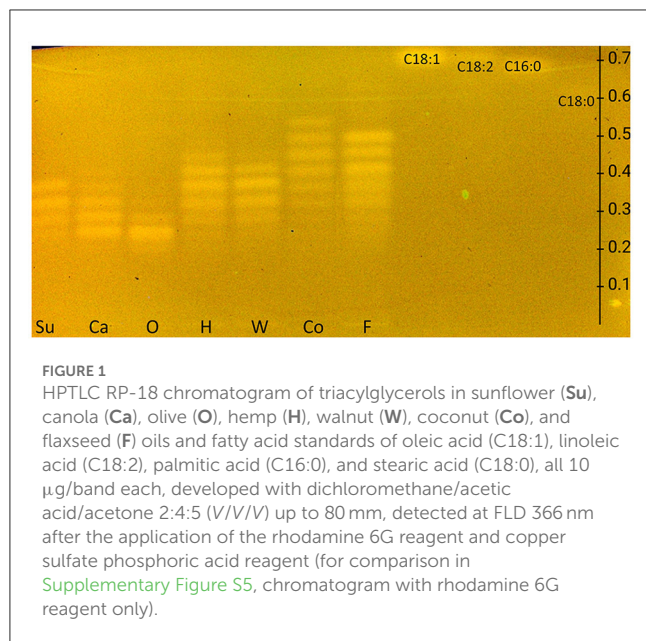
The bacterial stock solution (80 µl) was suspended in 20 ml of Müller–Hinton broth and incubated overnight at 37°C and 120 rpm. The culture was ready to use at an optical density measured at 600 nm (OD<sub>600</sub>) between 0.7 and 1.1 (Spectrophotometer M501, CamSpec, Garforth, UK). The bacterial suspension was piezoelectrically sprayed onto the plate (3.0 ml, red nozzle, level 6, Derivatizer) and incubated at 37°C for 2 h in a humid plastic box (38). Subsequently, the plate was sprayed with a 0.2% phosphate-buffered saline MTT solution (0.75 ml, blue nozzle, level 6, Derivatizer), incubated for 5 h (until an appropriate purple plate background coloring was achieved), and heated at 50°C for 10 min (TLC Plate Heater III). The positive control was tetracycline (1–7 µl/band, 10 ng/µl in ethanol). Antibacterials and cytotoxins appeared colorless (i.e., white) on a formazan-purple plate background under white light illumination.

### 2.6.3. Planar SOS-Umu-C genotoxicity bioassay

The *S. typhimurium* TA1535/pSK1002 bacterial cryostock (25 µl) was suspended in 35 ml of LB medium (20 g/L), containing 0.1063 mg/ml of ampicillin sodium salt and 1 mg/ml of glucose, and cultivated at 37°C in a 125-ml plastic baffled flask with an aeration filter at 120 rpm for 16 h. The culture was 1:10 diluted to adjust to an OD<sub>660</sub> of 0.2. The bacterial suspension was piezoelectrically sprayed onto the plate (2.8 ml, red nozzle, level 6, Derivatizer). After incubation at 37°C in a humid plastic box for 3 h, the plate was dried for 4 min in a cold air stream. The 4-methylumbelliferyl-β-D-galactopyranoside substrate (2 mg in 100 µl of dimethylsulfoxide added to 3 ml of phosphate-citrate buffer of pH 12) was piezoelectrically sprayed onto the plate (2.5 ml yellow nozzle, level 3, Derivatizer), followed by incubation at 37°C for 1 h. 4-Nitroquinoline-1-oxide (0.2–1.0 µl/band, 1 µg/ml in methanol) was used as a positive control. Genotoxins appeared as 4-methylumbelliferone-blue fluorescent zones on a dark bluish background at FLD 366 nm.

### 2.6.4. HRMS/MS recording of active substance zones

After the bioassay, HPTLC–UV/Vis/FLD–bioassay–heart cut–RP–HPLC–DAD–HESI–HRMS/MS (39) equipped with an autoTLC interface (40) was used to analyze zones of interest directly from the bioautogram. HRMS/MS signals were recorded via the polarity switching full-scan data-dependent MS2 (ddMS2) mode. Ionization settings were equal for all MS acquisition methods: sheath gas of 20 AU, aux gas of 10 AU, a spray voltage of 3.5 kV, capillary temperature of 320°C, probe heater temperature of 350°C, and S-lens RF level 50 AU. The full-scan settings were a mass range of *m/z* 100–1,100, a resolving power of 70,000 (at *m/z* 200, full width at half-maximum, FWHM), and automatic gain control (AGC) target 3e6. Fragmentation scans followed



in Top5 ddMS2 acquisition mode at a mass range of  $m/z$  80–1,000, resolution of 17,500 FWHM, AGC target  $1e6$ , and stepped normalized collision energies of 20, 40, and 60 eV. The HRMS/MS fragmentation data were optionally evaluated. Substances were eluted from the plate using methanol/water 1:1 (V/V). During the study, the binary pump (HPG-3200SD) of the Dionex Ultimate HPLC system (Dionex Softron, Germering, Germany) was changed to a quaternary pump (LPG-3400RS), which caused a retention time shift.

### 3. Results and discussion

#### 3.1. Development of the on-surface lipolysis and both orthogonal one-dimensional separations

The European Pharmacopeia Chapter 2.3.2 method on HPTLC RP-18 plates (32) was tested first and extended to include FAs. Differently, the plate was derivatized with the rhodamine 6G reagent. The resulting FLD 366 nm chromatogram showed bands, although weak, only for FAs but not for TAGs ([Supplementary Figure S5](#)). Therefore, by exploiting the reagent sequence technique, the plate was subsequently derivatized with copper sulfate phosphoric acid reagent, and in the study, both TAG and FA zones appeared in the HPTLC RP-18 chromatogram at FLD 366 nm ([Figure 1](#)), but no charring reaction could be observed on the HPTLC RP-18 plate at white light illumination as intended for this reagent. The currently revealed fluorescence of the rhodamine 6G reagent was explained by the pH dependence of the rhodamine 6G fluorescence and the needed acidic pH for proper visualization, here provided via the copper sulfate phosphoric acid reagent (36).

Next, the plate type had to be changed from RP-18 to a wettable reversed-phase (RP-18 W), and thus, the mobile phase system had to be changed as well since the desired aim for

this study was on-surface digestion via the nanoGIT method (28). Before on-surface digestion, the intrinsic acidic pH of the RP-18 W plate (ca. pH 4.2) needed to be neutralized in the application zone with a phosphate-citrate buffer of pH 12. Unfortunately, the buffer salts interfered with derivatization via the rhodamine 6G reagent ([Supplementary Figure S6](#)); therefore, everything except the application zone had to be covered as narrowly as possible ([Supplementary Figure S1](#)). Unification of the wetting and neutralization processes (after the application) to only one neutralizing wetting step is recommended, as we established in another study. The pancreatin matrix interfered during development by causing a retardation shift in contrast to the reference standards. Thus, it had to be removed by focusing the lipids twice by front-elution with acetone after the lipolysis and cutting off the lower plate part containing the remaining pancreatin matrix. Since the focusing result with acetone was strongly dependent on the relative humidity of the laboratory environment, the second trough was half-filled with a molecular sieve of 0.3 nm within 10 min prior to focusing. When a dry environment (<15% relative humidity) in the twin-trough chamber was reached, acetone was filled in the opposite trough, and the plate was placed inside as fast as possible for development. The dry conditions during focusing as well as the (second) polar mobile phase development showed reproducibly good zone resolutions.

Due to the amphiphilic properties of the RP-18 W phase (apolar C18 chains and residual silanol groups), two orthogonal mobile phase systems were developed, i.e., one apolar to separate acylglycerols and one polar to separate FAs. Both resulting nanoGIT-HPTLC RP-18 W chromatograms ([Figures 2A, C](#)) proved the orthogonality of the mobile phases. Surprisingly, the derivatization with rhodamine 6G directly showed all lipophilic compounds. This variation in the fluorescence response was explained by different initial plate pHs and proven by additional experiments, in which the rhodamine 6G fluorescence showed a strong plate batch dependence due to different plate pHs. Fortunately, the current plate batch pH supported the required acidic milieu for the rhodamine 6G fluorescence (41). To exploit a reagent sequence, the subsequent derivatization of the same plate with copper sulfate phosphoric acid reagent ([Figures 2B, D](#)) led to a charring reaction of all unsaturated lipophilic compounds detected as black zones. The combination of both derivatization reagents on the same plate surface made it possible to first visualize all lipophilic compounds and then differentiate saturated and unsaturated zones.

As observed for the standard mixture ([Figures 2A, B, St](#)), the separation of acylglycerols according to polarity in TAGs, DAGs, and MAGs was successful, but all the reference FAs were eluting as one unseparated diffuse zone ( $hR_F$  37–57). This system also allowed the separation of both DAG isomers ( $hR_F$  19 and 26) and TAG isomers, as observed for flaxseed oil (F,  $hR_F$  80 and 86). Comparing the side-by-side separated undigested and digested (+) samples, a massive increase in the FAs and decrease in the TAGs amount/signal was observed, indicating the successful simulation of the lipolysis. The undigested samples showed two bands at the DAG zone; however, after the lipolysis, only one band remained, which was caused by the pancreatin enzyme blank (EB). Two further interferences were observed from the pancreatin blank, one intense zone was just below the MAGs, and another weaker

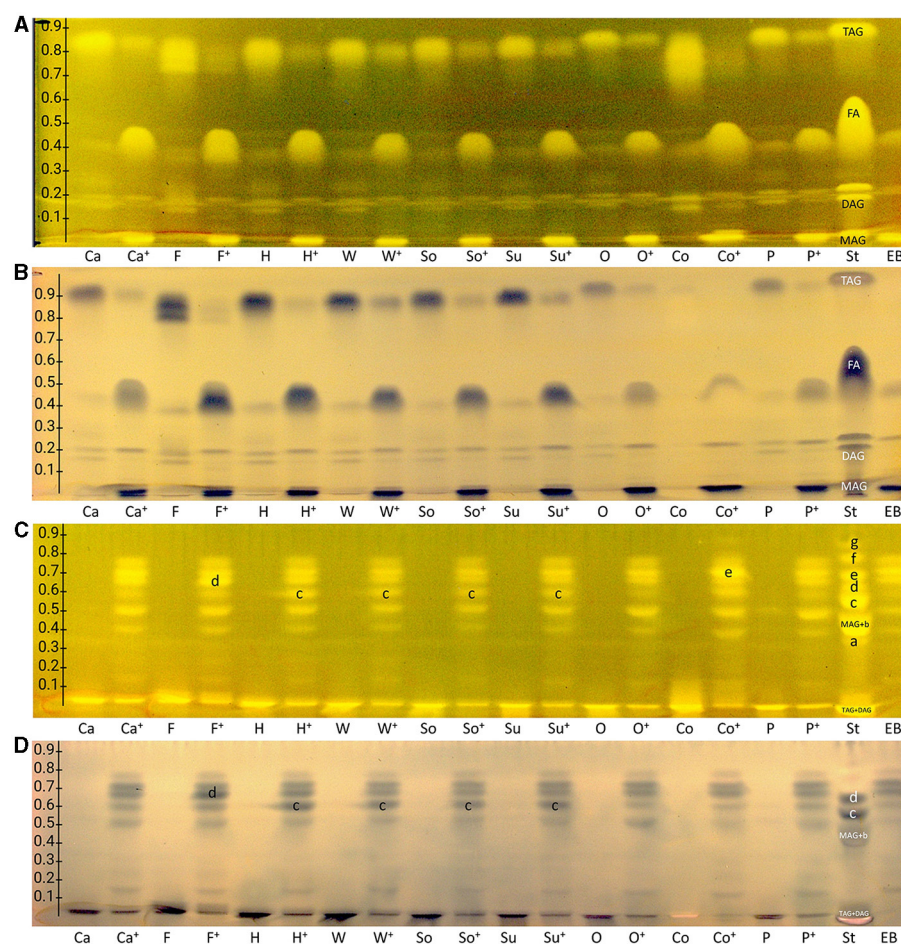


FIGURE 2

nanoGIT-HPTLC RP-18 W chromatograms of (A, B) acylglycerols and (C, D) fatty acids (FAs) in canola (Ca), flaxseed (F), hemp (H), walnut (W), soybean (So), sunflower (Su), olive (O), coconut (Co), and palm (P) oil (all 10  $\mu$ g/band each) before and after (+) lipolysis via overspraying of pancreatin (each 1 TAME U/band), focused twice with acetone and, after plate cut off at 15 mm, developed (from the cut edge) with (A, B) *n*-hexane/diethyl ether/formic acid 90:25:2 (V/V/V) up to 60 mm, or (C, D) acetonitrile/water 4:1 (V/V, with molecular sieve) up to 50 mm, derivatized as reagent sequence on the same plate (A, C) first with rhodamine 6G reagent detected at FLD 366 nm, (B, D) followed by copper sulfate phosphoric acid reagent detected at white light illumination (in remission); for comparison, standards (St) triolein (TAG), diolein (DAG), monoolein (MAG), stearic acid (C18:0, a), palmitic acid (C16:0, b), oleic acid (C18:1, c), linoleic acid (C18:2, d), myristic acid (C14:0, e), linolenic acid (C18:3, f), lauric acid (C12:0, g), capric acid (C10:0, f), and caprylic acid (C8:0, g) and enzyme blank (EB, 1 TAME U/band of pancreatin).

zone was at the FAs position (assigned to triterpenoid acids as discussed later), which complicated the evaluation of those in the sample. Nevertheless, the comparison of both derivatization reagents supported the literature-known oil composition of all samples. Oils with a variety of FAs, such as flaxseed, hemp, and coconut oils, showed broader TAG and FA zones, whereas olive oil (mainly containing C18:1) showed comparatively compact zones. Concentrating on the unsaturated FAs in the copper sulfate phosphoric acid chromatogram (Figure 2B), the most intense zones for flaxseed oil (mainly PUFAs) and, in contrast, almost no zones for coconut oil (containing comparatively much more SFAs) confirmed the oil compositions as well.

The orthogonal selectivity selected for the separation of FAs according to lipophilicity showed a successful qualitative separation of nearly all FA reference standards (Figures 2C, D, St). In this system, TAGs and DAGs were retained at the application zone, whereas the MAGs were eluted. Due to their similar lipophilicity,

C18:1, C16:0, and MAGs co-eluted as well as C18:2 and C14:0, which was proven in another experiment (Figure 3, framed). In the nanoGIT-HPTLC RP-18 W chromatogram (Figures 2C, D), the undigested samples did not show any noticeable FA zones, but the digested samples did. Thus, the lipolysis of TAGs into FAs was successful. High FA amounts as in the reference track (Figures 2C, D, St) and pancreatin matrix effects on the sample tracks led to a retardation shift; thus, the zone matching between the samples and reference compounds was challenging but nevertheless possible. With the aid of the copper sulfate phosphoric acid reagent chromatogram, C18:2 and C18:3 could be identified as intense black zones. The rhodamine 6G reagent chromatogram helped identify C8:0, C10:0, and C12:0. Due to this assigned pattern of the FAs and the literature data (37, 38), the FAs in the samples could be identified successfully via pattern recognition based on their main components. Intense zones for C18:3 (zone d) in flaxseed oil, C18:2 (zone c) in hemp, walnut, soybean, and



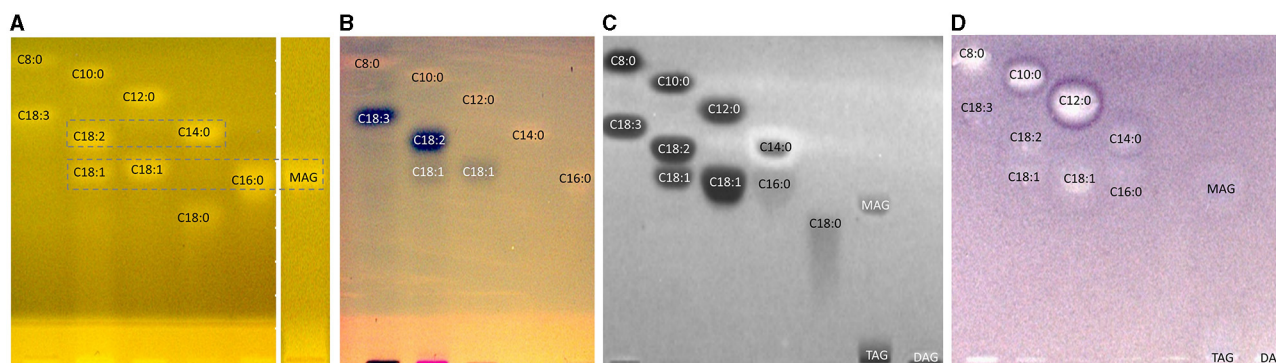


**FIGURE 3**  
HPTLC RP-18 W chromatograms (A, B) and bioautograms (C, D) of fatty acids (C8:0–C18:3) and acylglycerols (MAG, TAG, and DAG), 10  $\mu$ g/band each, separated with acetonitrile/water 4:1 (V/V, with molecular sieve) up to 50 mm, detected (A) at FLD 366 nm after derivatization with rhodamine 6G reagent, and a white light illumination (in remission) after (B) derivatization as reagent sequence first with rhodamine 6G reagent followed by copper sulfate phosphoric acid reagent, (C) Gram-negative *Aliivibrio fischeri* bioassay (bioluminescence depicted as a greyscale image), and (D) Gram-positive *Bacillus subtilis* bioassay.

sunflower oils, and C14:0 (zone e) in coconut oil were determined after digestion via pancreatin (Figures 2C, D).

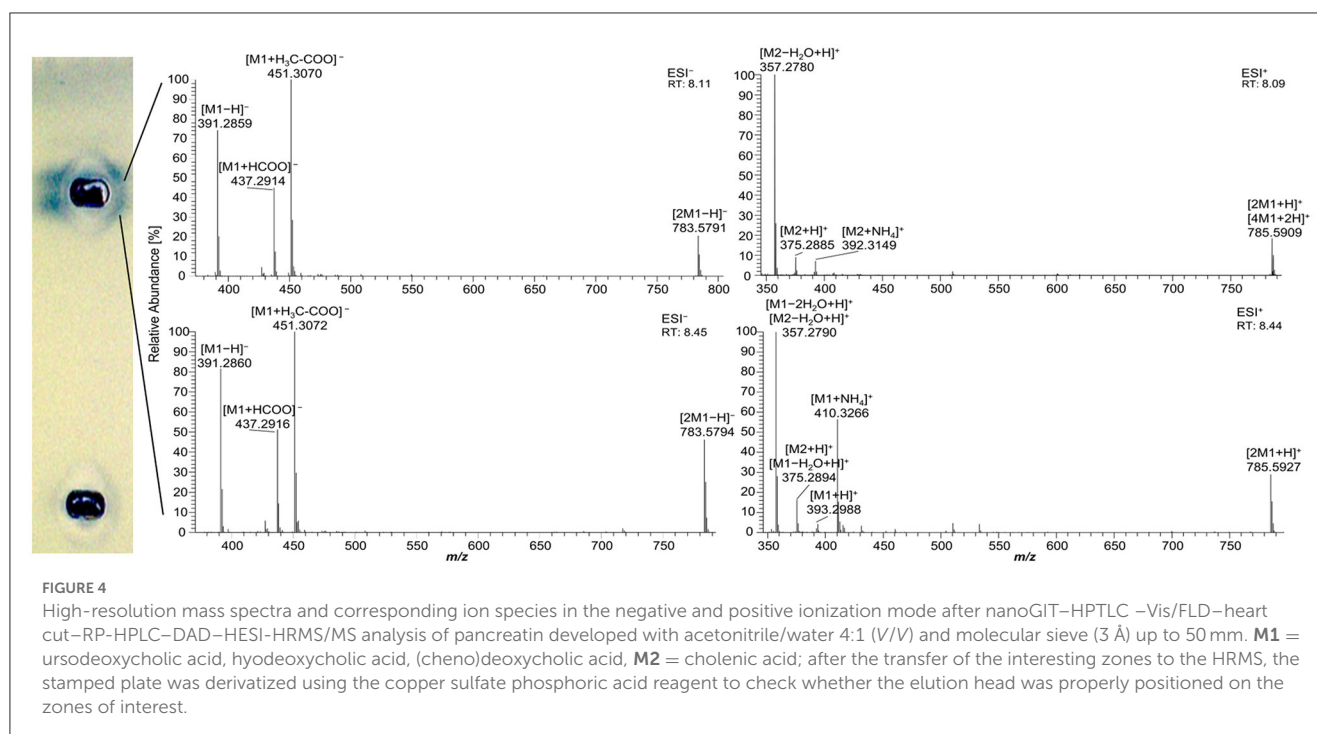
As mentioned for the separation of acylglycerols, polar impurities of the pancreatin co-eluting with the FAs hindered their assignment and could also lead to false-positive interpretations. Using automated heart-cut elution of the interesting zones to RP-HPLC–DAD–HESI–HRMS/MS (39), these impurities were assigned as the bile acids ursodeoxycholic acid (UDCA), hyodeoxycholic acid (HDCA), (cheno)deoxycholic acid (CDCA/DCA), and cholenic acid (Figure 4 and Supplementary Table S2). The isomers UDCA, HDCA, and (C)DCA were identified in the negative ionization mode (HESI<sup>−</sup>) in two separate peaks at retention times of 8.11 min and 8.45 min with  $[M-H]^{-}$  at  $m/z$  391.2858 and 391.2860, respectively. The HESI<sup>−</sup> and respective positive ionization mode (HESI<sup>+</sup>) revealed the presence of their dimers ( $[2M-H]^{-}$  at  $m/z$  783.5791 and  $[2M+H]^{+}$  at  $m/z$  785.5927, Figure 4), identified via fragmentation (Supplementary Figure S7), as well as their tetramer ( $[4M+2H]^{+}$  at  $m/z$  785.5909 with its corresponding isotopic pattern, Supplementary Figure S8). Cholenic acid could only be assigned via HESI<sup>+</sup> as  $[M+H]^{+}$  at  $m/z$  375.2885. Since bile acids also show antibacterial properties (40), false-positive results should be considered and, when necessary, confirmed/excluded via HRMS. Fortunately, the following comprehensive separation system solved this coelution issue.

### 3.2. Development and proof of the nanoGIT–HPTLC×HPTLC–FLD on RP-18 W plates

The one-dimensional separation systems showed some limits, such as interferences with the pancreatin used and no separation of acylglycerols and FAs at once, which could not be overcome by method optimization or modification. Hence, the combination of both orthogonal separation systems into a comprehensive HPTLC method (HPTLC×HPTLC) was evaluated (Figure 5). The

normal phase separation mechanism separating according to polarity (apolar acylglycerol-separating mobile phase) was chosen to be the first dimension, whereas the reversed-phase separation mechanism separating according to lipophilicity (polar FA-separating mobile phase) was selected as the second dimension. The orthogonality was given by the very different selectivity of the first dimension in contrast to the second dimension. The orthogonal separation was first tested with reference standards (Figure 6A), and successful separation of acylglycerols and FAs could be achieved, in particular the separation of the previously co-eluted MAGs and FAs. The zone assignment of the FAs in the nanoGIT–HPTLC×HPTLC–FLD chromatogram was more difficult than via one-dimensional separation. Using the co-development of reference standards for each dimension on a separate plate (Supplementary Figure S4), a retardation shift could be observed for the FA zones. Since both mobile phases were prone to changes in relative humidity, the co-development of reference standards on the same plate was recommended to verify a retardation shift and proper assignment. The dominance of the C18:2 and C18:3 fatty acids (zones c and d, respectively) was also helpful for proper assignment.

Next, the on-surface digestion of an oil sample and the subsequent lipid separation of its lipolysis products on the same surface were demonstrated (Figure 6B). Therefore, flaxseed oil rich in C18:3 and C18:2 was selected for the proof of principle. A retardation shift was observed between reference standards (Figure 6A) and samples (Figure 6B). Using automated heart cuts to RP-HPLC–DAD–HESI–HRMS/MS (39), the highest eluting FAs (Figure 6B, zone d) were identified as C18:3, C18:2, C16:0, and C18:1 (Supplementary Figure S9, zone d, Supplementary Table S3). The most intense signal for this zone was from C18:3. Since it was stamped perpendicular to the band due to an accidentally 90°-rotated plate (positioned incorrectly) in the autoTLC interface (42), several FA signals were derived from and assigned to the neighboring bands. Some additional FAs were identified that could not be associated with the flaxseed oil sample: in zones c and d, oxidized C9:0 and oxidized C12:1 were identified, which could be explained as degradation products of linoleic acid and linolenic



acid, respectively. In zone **d**, C14:0, and zone **e**, C10:0, C11:0, and C12:0 were found. No fragmentation pattern was evident via HRMS/MS recording. The previously interfering pancreatin matrix was presently successfully separated from the FAs since most pancreatin impurities did not elute in the first dimension (in contrast, the FAs did) but did elute first in the second dimension. Thus, the FAs could be identified easily, in contrast to the one-dimensional separation of the reference standards (Figure 6B). Additionally, the eluted FA zones were fully separated from the bile acids, and their mass signals were not detected in the HRMS spectra anymore. By doing so, the nanoGIT–HPTLC×HPTLC–FLD method was proven to be successful in its application to real-life samples and in the detailed study of the lipolysis of complex samples. The whole sample was studied in all aspects on the same surface, and no sample part was lost.

### 3.3. Antibacterial profiles via nanoGIT–HPTLC×HPTLC–vis/FLD–bioassay–heart cut–RP–HPLC–DAD–HESI–HRMS/MS

After a successful proof of principle and implementation of the nanoGIT–HPTLC×HPTLC–FLD hyphenation, it was extended to bioassays to evaluate the antibacterial activity of the lipolysis products of digested flaxseed oil (Figures 7A, B) and coconut oil (Figure 7C) against Gram-negative *A. fischeri* and Gram-positive *B. subtilis* bacteria. The *A. fischeri* bioautogram revealed antibacterial effects for all seven FA reference standard zones as well as for the MAG, DAG (both isomers of diolein), and TAG reference standard zones (Figure 7A). In the *B. subtilis* bioautogram, the antibacterial detection was comparable, apart from the weaker response for

two FA reference zones (**d** and **g**, Figure 7B), which was proven and confirmed in another experiment (Figure 5). These findings of antibacterial activity were consistent with the literature, which confirmed the antibacterial effect of FAs and MAGs (8, 41, 43, 44) and DAGs (9) against Gram-negative and Gram-positive bacteria. Usually, no antibacterial effect for TAGs (three ester groups but optionally double bonds) would be expected due to the lack of reactive functional groups (41, 45). However, the studied TAG, DAG, and MAG had one double bond in each acyl chain, which could induce a genotoxic or cytotoxic effect, as discussed later.

A separate study of all reference standards (Figure 3) showed in more detail the differences in their antibacterial effects against both Gram-negative and Gram-positive bacteria. The FAs C18:0 and C16:0 showed only a very light antibacterial response, whereas a metabolism-enhancing effect (detected as a halo surrounding an antibacterial effect in the center) was detected for C14:0. If co-eluted with C18:2 as in the standard track, this enhancing effect was weakened since the antibacterial effect of C18:2 was stronger (Figure 7, zone **c**). Compared to previous bioautograms on HPTLC plates silica gel 60 (39, 46), C16:0 showed no metabolism-enhancing effect on RP-18 W plates, which was explained by the doubled amount (10 µg/band vs. 5 µg/band) since such enhancing effects are dose-dependent and, in addition, also time-dependent (bioluminescence images monitored for 30 min). The antibacterial response for C8:0–12:0 was very intense against both Gram-negative *A. fischeri* and Gram-positive *B. subtilis* bacteria (Figure 3). In the *A. fischeri* bioautogram, a strong antibacterial effect of unsaturated FAs (C18:1–C18:3) against *A. fischeri* was observed, whereas an increase in the antibacterial effect with increasing double bonds was not observed. In the *B. subtilis* bioautogram, the antibacterial effect of unsaturated FAs against Gram-positive bacteria was weaker, which was directly evident since the same



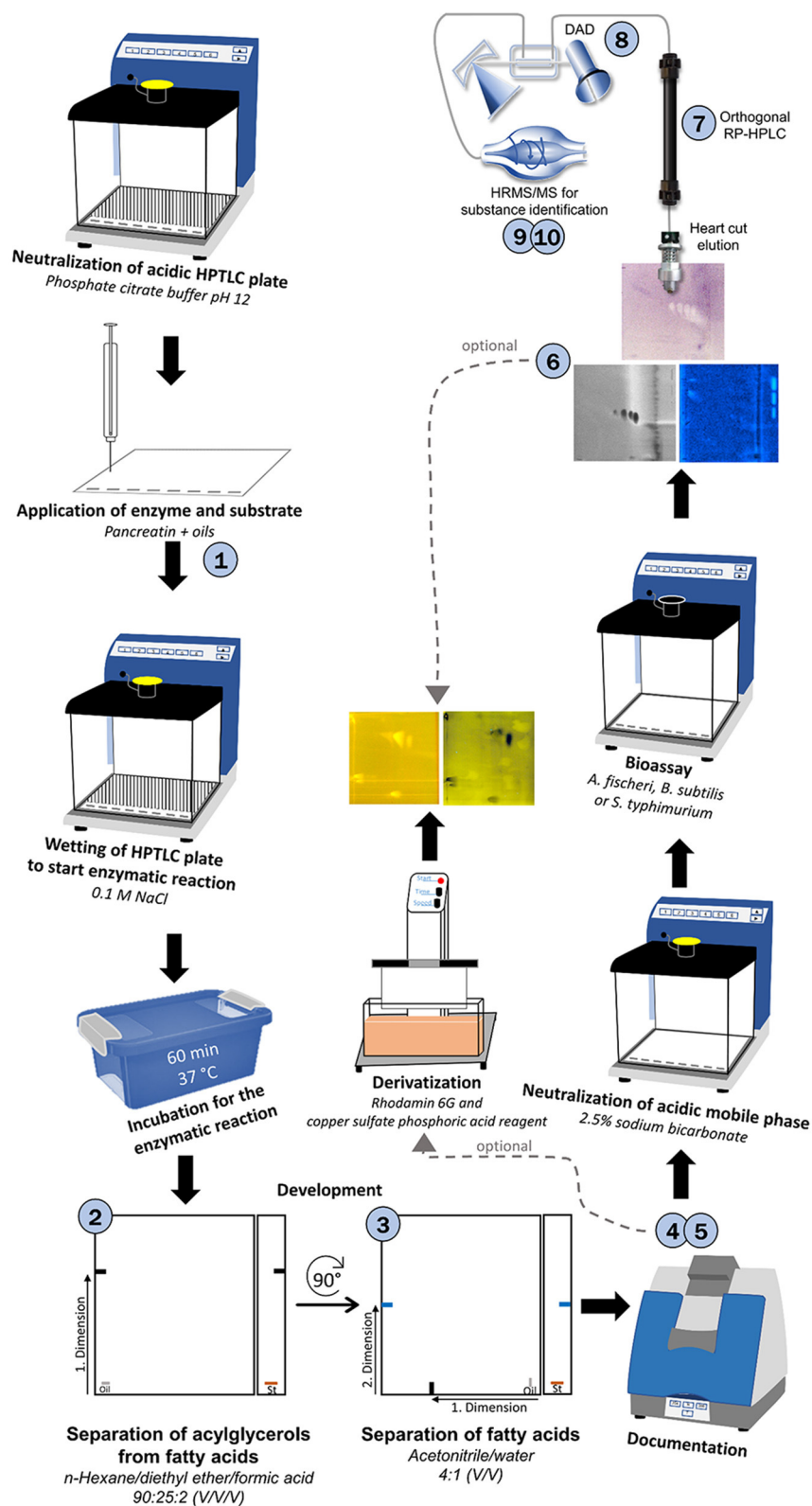


FIGURE 5

Schematic workflow of the developed 10D hyphenation, combining lipolysis with analysis and effect-detection on the same surface: nanoGIT-HPTLC x HPTLC-Vis/FLD-bioassay-heart cut-RP-HPLC-DAD-HESI-HRMS/MS.

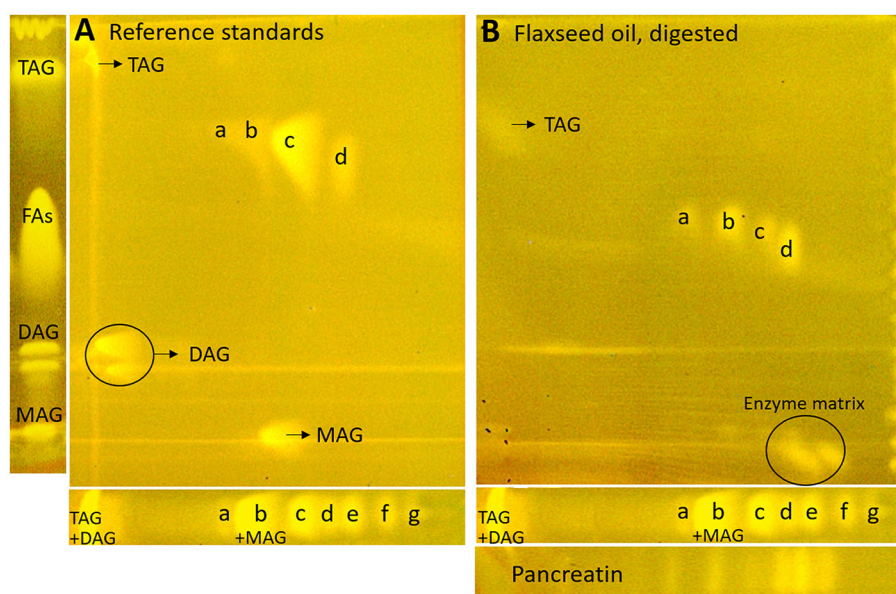


FIGURE 6

nanoGIT-HPTLCxHPTLC-FLD chromatograms of (A) the reference sample mixture (undigested) and (B) flaxseed oil (all 10  $\mu\text{g}/\text{band}$  each) after lipolysis via overspraying of pancreatin (1 TAME U/band) on HPTLC RP-18 W plate, focused twice with acetone and, after a plate cut off at 15 mm, developed (from the cut edge) first with *n*-hexane/diethyl ether/formic acid 90:25:2 (V/V/V) up to 60 mm and, after 90°-plate turn, then with acetonitrile/water 4:1 (V/V, with a molecular sieve) up to 50 mm, derivatized with rhodamine 6G reagent, and detected at FLD 366 nm; for comparison respective one-dimensionally separated references, i.e., acylglycerols (MAG, TAG, and DAG) and fatty acids (FAs) such as stearic acid (C18:0, a), palmitic acid (C16:0, b), oleic acid (C18:1, c), linoleic acid (C18:2, d), myristic acid (C14:0, e), linolenic acid (C18:3, f), lauric acid (C12:0, g), capric acid (C10:0, f), and caprylic acid (C8:0, g), all 10  $\mu\text{g}/\text{band}$  each.

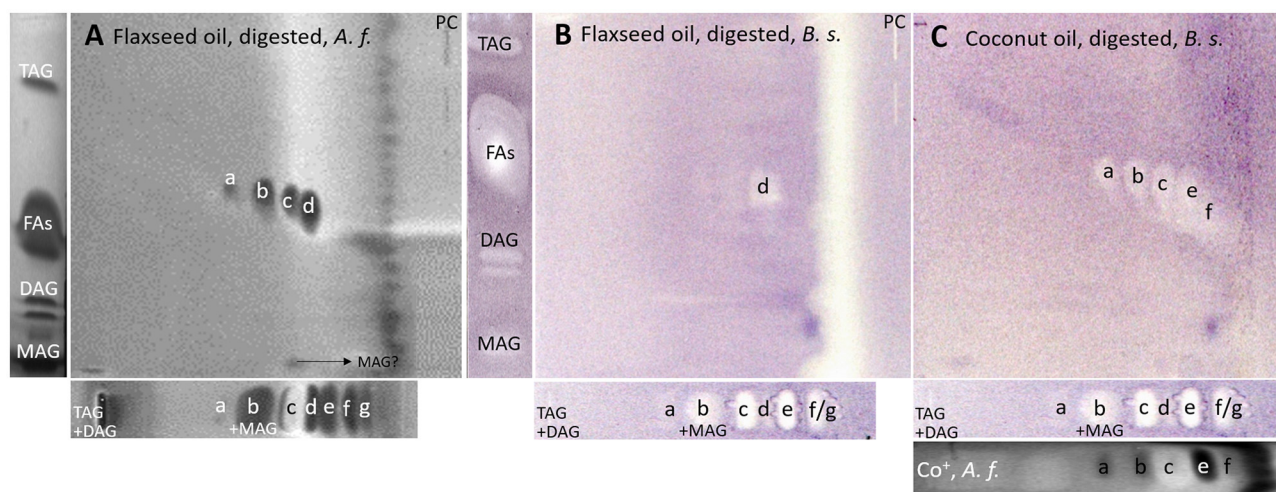


FIGURE 7

nanoGIT-HPTLCxHPTLC-bacterial bioassay-FLD/bioluminescence: Gram-negative *Aliivibrio fischeri* and Gram-positive *Bacillus subtilis* bioautograms showing the antibacterial activity (dark or colorless zones, respectively) of (A, B) digested flaxseed oil and (C) digested coconut oil (10  $\mu\text{g}/\text{band}$  each) analyzed as in Figure 5, detected (A) via the bioluminescence (depicted as a grayscale image) after the *A. fischeri* bioassay and (B, C) at white light illumination (in remission) after the *B. subtilis* bioassay; positive controls (PCs) were 10–70  $\mu\text{g}/\text{band}$  caffeine for *A. fischeri* bioassay or 10–70 ng/band tetracycline for *Bacillus subtilis* bioassay.

reference standard amounts were applied. Further research is needed to understand the mechanism of the observed biological responses of the FAs and acylglycerols. On the one hand, the biological response may derive from the acid head group and/or altered membrane permeability and thus be an antibacterial effect

(as one example of the many different antibacterial mechanisms). On the other hand, the biological effect may derive from trace impurities (e.g., co-eluting epoxidized longer-chain fatty acids, Figure 3) in the reference standards (only up to 99% pure) or oxidative degradation and thus be a cytotoxic effect.

Unfortunately, the separation power of HPTLC is too weak to chromatographically differentiate all of them. Nevertheless, the powerful hyphenation with the bioassay provides the first evidence of harmful compounds present.

Using automated heart cuts of the interesting zones to RP-HPLC–DAD–HESI–HRMS/MS, the Gram-positive antibacterial zones of the reference standard track (Figure 7B) could be identified as the corresponding FAs (Figure 8, Supplementary Table S4). The assignments for zones **a** (C18:0) and **b** (C16:0/C18:1) were reached through pattern recognition. The latter assignments were more challenging since these FAs can also be HRMS system signals, which must be excluded first. Zones **c** and **e** were the most intense, containing co-eluting C14:0/C18:2 and C12:0/C18:3 (from adjacent zone **d**), respectively. Zone **d** (C18:3) was too close to the surrounding zones for an elution head-based analysis (too narrow for an additional elution head imprint). The C8:0 (zone **g**) was not separated in the 2D bioautogram but co-eluted with the C10:0 (zone **f**).

Considering the information obtained about the antibacterial behavior of the reference standards, the assignment of the lipolysis products of flaxseed oil was possible. Flaxseed oil, which mainly consists of C18:3, C18:1, and C18:2 and small amounts of C16:0 and C18:0 (38), showed after on-surface digestion and effect-directed analysis of four zones in the 2D *A. fischeri* bioautogram but only one zone in the 2D *B. subtilis* bioautogram (Figures 7A, B). The four zones in the 2D *A. fischeri* bioautogram were identified as C18:0 (zone **a**), C18:1/C16:0 (zone **b**), C18:2 (zone **c**), and C18:3 (zone **d**) in comparison to corresponding reference standards. No metabolism-enhancing effect was detected, and thus, the presence of C14:0 was excluded, which could have co-eluted with C18:2. The antibacterial zone **d** in the *B. subtilis* bioautogram (Figure 7B) was not so clear in the assignment, and thus identified via HRMS as C18:3 ( $[M-H]^-$ ,  $m/z$  277.2175,  $\Delta$  ppm  $-0.71$ ) and *trans*-4,5-epoxy-(*E*)-2-decenal ( $C_{10}H_{16}O_2$ ,  $[M-H]^-$ ,  $m/z$  167.1078,  $\Delta$  ppm  $-0.28$ ). The latter is a typical genotoxic marker of linoleic acid oxidation (47–49).

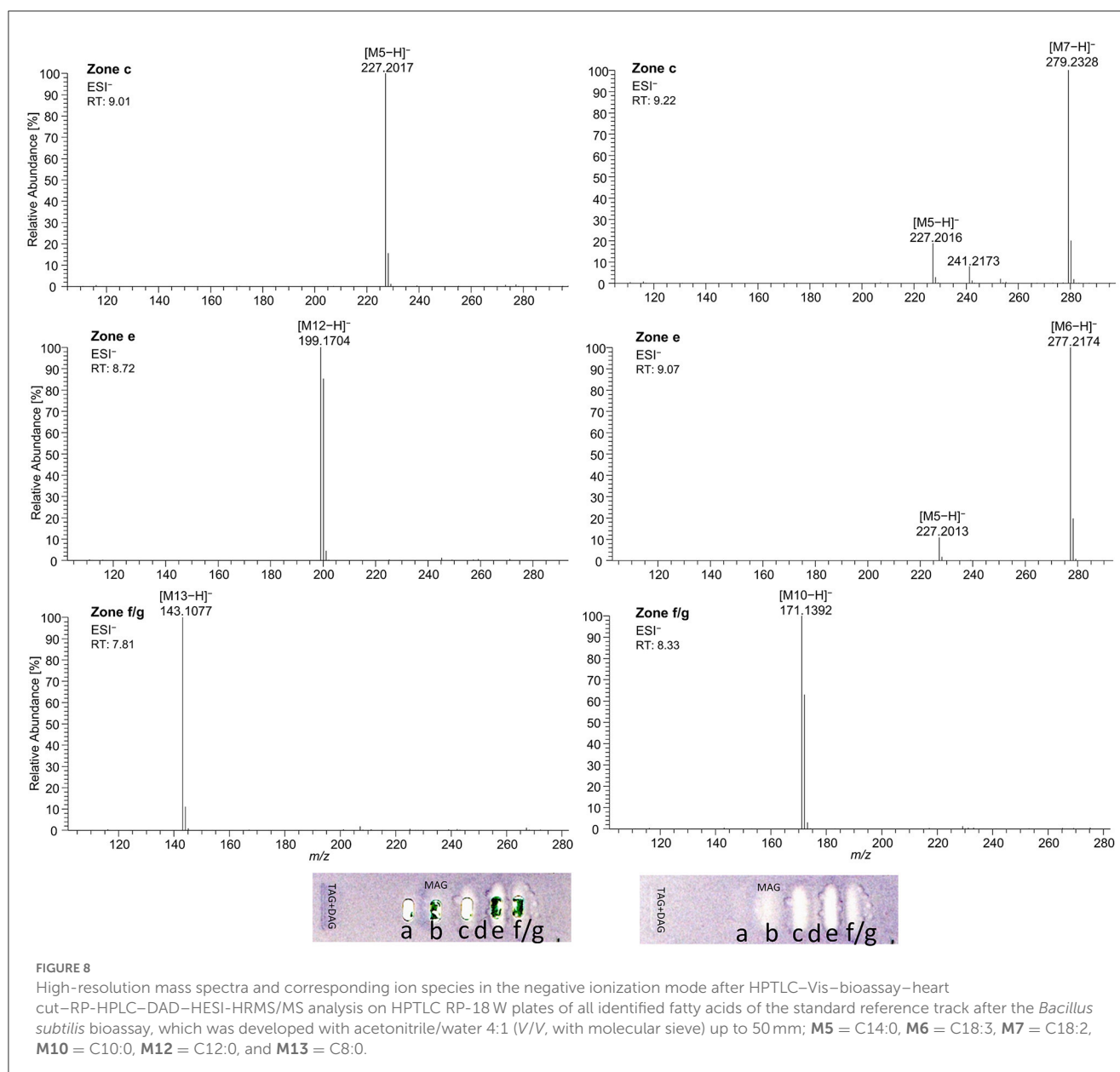
As a further example, coconut oil was digested on-surface and analyzed for any antibacterial effects (Figure 7B). Coconut oil was selected as a quite different oil sample compared to flaxseed oil since it consists of comparatively much more SFAs of shorter chain lengths (C8:0–14:0, mostly C12:0 and C14:0) (37, 45). In contrast to the flaxseed oil (one antibacterial zone), the 2D *B. subtilis* bioautogram showed five antibacterial zones. Using the standard track, the FAs were identified as C18:0 (zone **a**), C18:1/C16:0 (zone **b**), C18:2/C14:0 (zone **c**), C12:0 (zone **e**), and C10:0 (zone **f**); however, C18:3 (zone **d**) was not present. The zone was heart-cut eluted to RP-HPLC–DAD–HESI–HRMS/MS (Figure 9, Supplementary Table S5) and revealed C14:0, C12:0, and C10:0 signals for the zones **c**, **e**, and **f**, respectively, but no significant signals for C18:0 and C18:1/C16:0. The *A. fischeri* bioautogram of the on-surface digested coconut oil (Figure 7C, Co<sup>+</sup>) was used to confirm zone **c** to be C14:0 via its metabolism-enhancing effect as further proof.

### 3.4. Genotoxicity profiles via nanoGIT–HPTLC×HPTLC–vis/FLD–bioassay–heart cut–RP–HPLC–DAD–HESI–HRMS/MS

On-surface digested flaxseed oil revealed four genotoxic substance zones in the 2D bioautogram after the genotoxicity bioassay using the *S. typhimurium* TA1535/pSK1002 strain (Figure 10A). Two genotoxic substance zones did not migrate/elute at all in the second dimension, indicating apolar substances. One zone was assigned as TAGs via comparison with the standard track, and the second more apolar compound (marked\* close to the solvent front of the first dimension) could be a genotoxic aromatic mineral oil contaminant; however, the latter assumption still needs proof. The genotoxic effect of TAGs was explained by the epoxidized fatty acid bond in the TAG molecule. Only two weak signals for the FAs were detected in the flaxseed oil and reference standard mixture (second dimension), which were assigned to C18:2/C14:0 and C18:3/C12:0 or C10:0. The digestion of the TAGs did not eliminate genotoxicity but showed that the FAs produced have strongly different genotoxic potentials. Both FAs were not natively fluorescent, which was expected (Figure 10B); however, native blue fluorescence was observed for the genotoxic TAGs zone of flaxseed oil, which indicated any impurities, e.g., of aromatic structure, as mentioned.

For adequate signal intensity via the genotoxicity bioassay, the amount of flaxseed oil was doubled (20 µg/band). In contrast to our previous very sensitive screening method (10), the amount of oil needed to be increased 200-fold due to the (I) enzymatic metabolism with a 60-min on-surface incubation known to lead to diffusion at the application zone (33), (II) interference by the buffer salts (Supplementary Figure S6), (III) 2D separation known to cause signal loss (50) by the 2-fold diffusion of the substances (as for C18:0, Figure 3), (IV) usage of RP-18 W plates known to be possibly less sensitive in the response, though dependent on the molecule, compared to silica gel 60 plates (51, 52), and (V) purchased oils opened just before analysis (assumedly, comparatively fewer oxidized degradation products). These reasons also explained why HRMS analysis was challenging since oxidized species present at the trace level were not found. In contrast to Morlock and Meyer (19), in which a six-fold concentrated genotoxic compound zone was directly transferred to the HRMS, only one weaker genotoxic compound zone was eluted from the 2D bioautogram, passed through an HPLC column via a prior desalting unit and diode-array detector, and finally reached the HRMS. The presence of highly potent genotoxic FA in oxidized and epoxidized forms at the trace level in various plant oils (10, 49, 53), and its potential sources, such as the unsaturated FAs C18:2 (54) and C18:3 (54, 55), were already reported. If safely delivered to a healthy liver, detoxification may be expected, as was recently shown via simulated on-surface S9 liver metabolism (10, 56). Furthermore, synergistic effects can occur (57), which can be detected and studied via the latest multiplex planar assays (51).



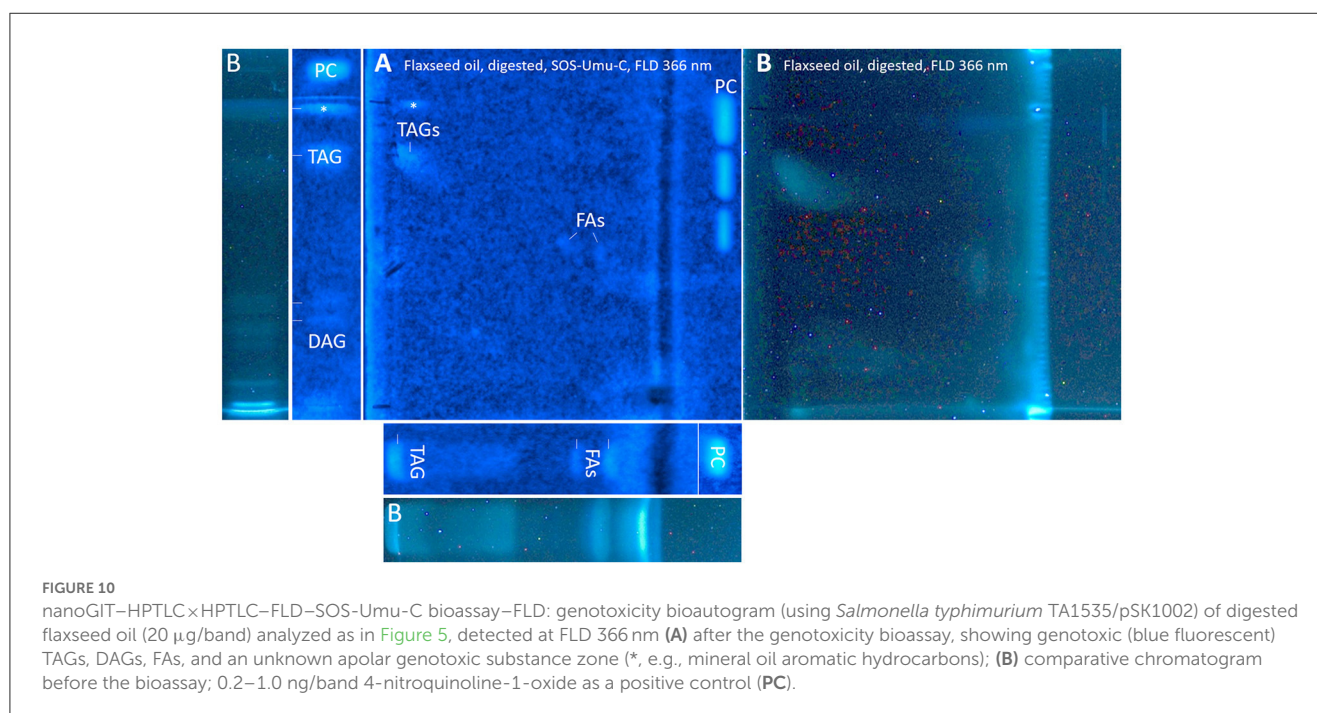
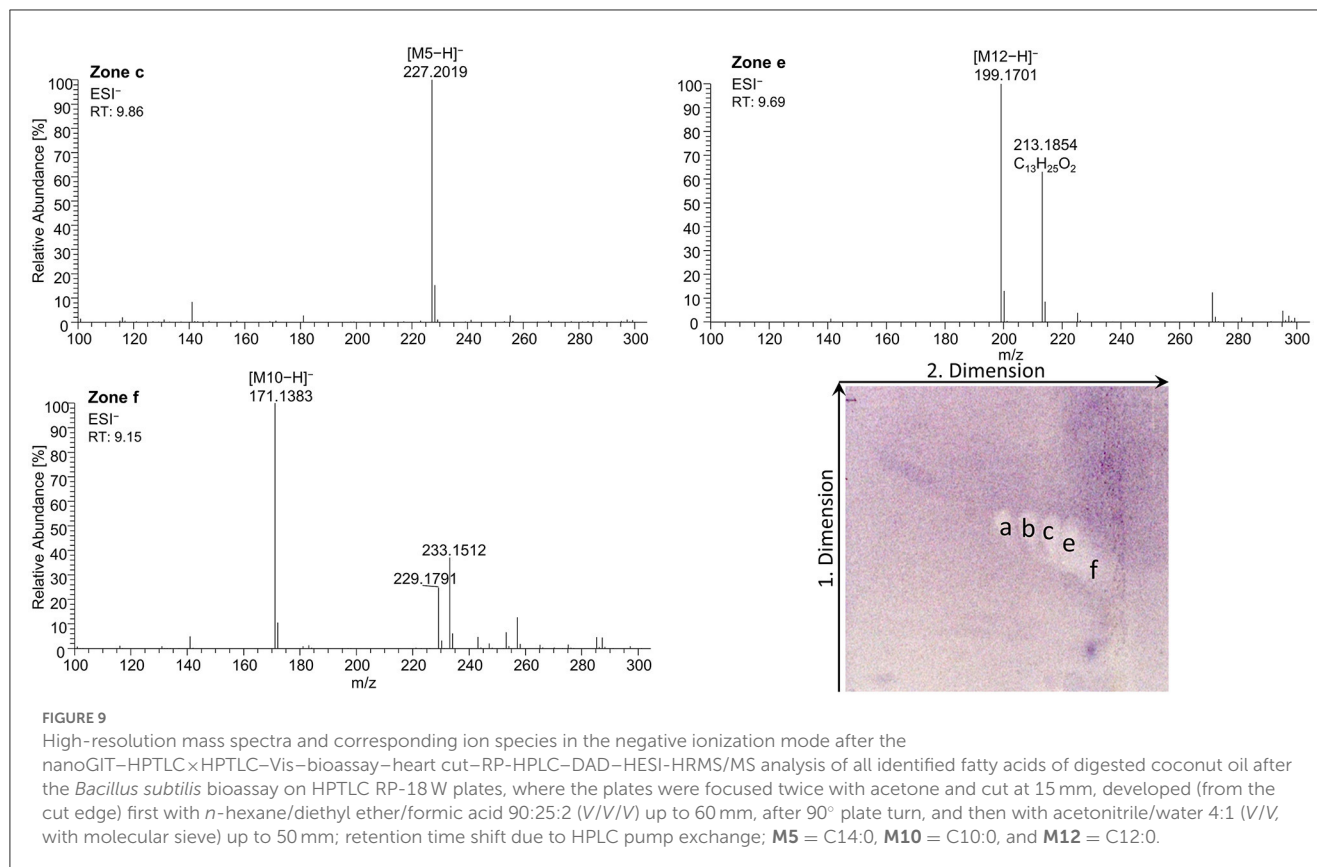


The advantages and disadvantages of this quite new methodology against reported conventional methods (Supplementary Table S6) (58, 59), including the further ability of an effect-directed analysis after separation, strongly highlight the ability to illuminate every facet of the sample.

## 4. Conclusion

The on-surface simulated digestion on the RP-18 W plate, followed by comprehensive orthogonal HPTLC×HPTLC separation and effect-directed bioassay detection, successfully demonstrated a sustainable all-in-one digestion and analysis system. It allowed the analysis of the digestion during the intestinal phase itself and the resulting products as well as their biological effects via antibacterial and genotoxic bioassays. Since the developed method included a 2D

development, the sample throughput was limited to only one sample per plate, but two sample plates could be processed at the same time with the HPTLC system used. The low solvent consumption (max. 16 ml per analysis/two plates) and rather short analysis time (5 h per analysis/two plates including bioassay and MS) endorsed the application as a multi-faceted analysis system. The developed 10D hyphenated nanoGIT-HPTLC×HPTLC-Vis/FLD-bioassay-heart cut-RP-HPLC-DAD-HESI-HRMS/MS methodology is a new tool that contributes to the understanding of complex samples and their harmful or beneficial metabolism/digestion products. Advantageously, no sample part was lost, and the whole sample was studied without any elaborate sample preparation. Digestion of the oils did not eliminate antibacterial effects or genotoxicity but showed that the metabolism products as well as a genotoxic contaminant may have harmful potential, which requires further investigation and consideration, or even reconsideration of



the current risk assessment. Literature about the potential of edible vegetable oils as next-generation antimicrobial agents was confirmed, whereas the observed genotoxic potential remaining after metabolic digestion needs further attention regarding food safety.

## Data availability statement

The original contributions presented in the study are included in the article/Supplementary material, further inquiries can be directed to the corresponding author.



## Author contributions

IM: conceptualization, methodology, experimental analysis, data analysis, and writing—original draft. AG: experimental analysis and data analysis. GM: conceptualization, methodology, supervision, and writing—review and editing. All authors contributed to the article and approved the submitted version.

## Funding

Instrumentation was partially funded by the Deutsche Forschungsgemeinschaft (DFG, German Research Foundation) —INST 162/536-1 FUGG and INST 162/471-1 FUGG.

## Acknowledgments

The authors would like to thank Lisa-Marie Niemeier for support.

## Dedication

Dedicated to the lifework of Prof. Dr. Colin Poole, Wayne State University, Detroit, USA.

## References

- Wolfram G, Bechthold A, Boeing H, Ellinger S, Hauner H, Kroke A, et al. Evidence-based guideline of the German Nutrition Society: fat intake and prevention of selected nutrition-related diseases. *Ann Nutr Metab.* (2015) 67:141–204. doi: 10.1159/000437243
- Deutsche Gesellschaft für Ernährung, Österreichische Gesellschaft für Ernährung, Schweizerische Gesellschaft für Ernährung. D-A-CH-Referenzwerte für die Nährstoffzufuhr. Bonn (2018).
- Doucet E, Alméras N, White MD, Després JP, Bouchard C, Tremblay A. Dietary fat composition and human adiposity. *Eur J Clin Nutr.* (1998) 52:2–6. doi: 10.1038/sj.ejcn.1600500
- Simopoulos AP. An increase in the omega-6/omega-3 fatty acid ratio increases the risk for obesity. *Nutrients.* (2016) 8:128. doi: 10.3390/nu8030128
- Keys A, Mickelsen O, Miller EVO, Chapman CB. The relation in man between cholesterol levels in the diet and in the blood. *Science.* (1950) 112:79–81. doi: 10.1126/science.112.2899.79
- Hooper L, Martin N, Jimoh OF, Kirk C, Foster E, Abdelhamid AS. Reduction in saturated fat intake for cardiovascular disease. *Cochrane Database Syst Rev.* (2020) 5:CD011737. doi: 10.1002/14651858.CD011737.pub2
- Abdelhamid AS, Martin N, Bridges C, Brainard JS, Wang X, Brown TJ, et al. Polyunsaturated fatty acids for the primary and secondary prevention of cardiovascular disease. *Cochrane Database Syst Rev.* (2018) 11:CD012345. doi: 10.1002/14651858.CD012345.pub3
- Casillas-Vargas G, Ocasio-Malavé C, Medina S, Morales-Guzmán C, Del Valle RG, Carballeira NM, et al. Antibacterial fatty acids: an update of possible mechanisms of action and implications in the development of the next-generation of antibacterial agents. *Prog Lipid Res.* (2021) 82:101093. doi: 10.1016/j.plipres.2021.101093
- Mehl A, Morlock GE. Strong antibacterial effects in animal-derived food detected via non-target planar bioassays. *Food Chem Adv.* (2023). doi: 10.1016/j.focha.2023.100283
- Morlock GE, Meyer D. Designed genotoxicity profiling detects genotoxic compounds in staple food such as healthy oils. *Food Chem.* (2023) 408:135253. doi: 10.1016/j.foodchem.2022.135253
- Russo GL. Dietary n-6 and n-3 polyunsaturated fatty acids: from biochemistry to clinical implications in cardiovascular prevention. *Biochem Pharmacol.* (2009) 77:937–46. doi: 10.1016/j.bcp.2008.10.020
- Simopoulos AP. The importance of the ratio of omega-6/omega-3 essential fatty acids. *Biomed Pharmacother.* (2002) 56:365–79. doi: 10.1016/S0753-3322(02)00253-6
- Czernichow S, Thomas D, Bruckert E. n-6 Fatty acids and cardiovascular health: a review of the evidence for dietary intake recommendations. *Br J Nutr.* (2010) 104:788–96. doi: 10.1017/S0007114510002096
- Salter AM. Dietary fatty acids and cardiovascular disease. *Animal.* (2013) 7(Suppl 1):163–71. doi: 10.1017/S1751731111002023
- Bundesministerium für Ernährung und Landwirtschaft. Konsum von Ölen und Fetten in Deutschland in den Jahren 2008 bis 2019 (in 1.000 Tonnen Reinfett): [Graph]. Deutschland (2021).
- Bundesministerium für Ernährung und Landwirtschaft. Konsum von pflanzlichen Ölen und Fetten in Deutschland nach Art in den Jahren 2007 bis 2019 (in 1.000 Tonnen Reinfett): [Graph]. Deutschland (2021).
- Fedeli E, Jacini G. Lipid composition of vegetable oils. *Adv Lipid Res.* (1971) 9:335–82. doi: 10.1016/B978-0-12-024909-1.50014-4
- Fronimaki P, Spyros A, Christophoridou S, Dais P. Determination of the diglyceride content in greek virgin olive oils and some commercial olive oils by employing (31)P NMR spectroscopy. *J Agric Food Chem.* (2002) 50:2207–13. doi: 10.1021/jf011380q
- Bosque-Sendra JM, Cuadros-Rodríguez L, Ruiz-Samblás C, de La Mata AP. Combining chromatography and chemometrics for the characterization and authentication of fats and oils from triacylglycerol compositional data—a review. *Anal Chim Acta.* (2012) 724:1–11. doi: 10.1016/j.aca.2012.02.041
- Carlier H, Bernard A, Caselli C. Digestion and absorption of polyunsaturated fatty acids. *Reprod Nutr Dev.* (1991) 31:475–500. doi: 10.1051/rnd:19910501
- Carriere F, Barrowman JA, Verger R, René L. Secretion and contribution to lipolysis of gastric and pancreatic lipases during a test meal in humans. *Gastroenterology.* (1993) 105:876–88. doi: 10.1016/0016-5085(93)90908-U
- Desnuelle P, Savary P. Specificities of lipases. *J Lipid Res.* (1963) 4:369–84. doi: 10.1016/S0022-2275(20)40278-0
- Giang TM, Gaucel S, Brestaz P, Anton M, Meynier A, Trelea IC, et al. Dynamic modeling of *in vitro* lipid digestion: individual fatty acid release and bioaccessibility kinetics. *Food Chem.* (2016) 194:1180–8. doi: 10.1016/j.foodchem.2015.08.125

## Conflict of interest

The authors declare that the research was conducted in the absence of any commercial or financial relationships that could be construed as a potential conflict of interest.

The reviewer PR declared a past co-authorship with the author GM to the handling editor.

## Publisher's note

All claims expressed in this article are solely those of the authors and do not necessarily represent those of their affiliated organizations, or those of the publisher, the editors and the reviewers. Any product that may be evaluated in this article, or claim that may be made by its manufacturer, is not guaranteed or endorsed by the publisher.

## Supplementary material

The Supplementary Material for this article can be found online at: <https://www.frontiersin.org/articles/10.3389/fnut.2023.1227546/full#supplementary-material>

24. Yang LY, Kuksis A, Myher JJ. Lipolysis of menhaden oil triacylglycerols and the corresponding fatty acid alkyl esters by pancreatic lipase *in vitro*: a reexamination. *J Lipid Res.* (1990) 31:137–47. doi: 10.1016/S0022-2275(20)42768-3
25. McClements DJ, Li Y. Review of *in vitro* digestion models for rapid screening of emulsion-based systems. *Food Funct.* (2010) 1:32–59. doi: 10.1039/c0fo00111b
26. Calvo-Lerma J, Fornés-Ferrer V, Heredia A, Andrés A. *In vitro* digestion of lipids in real foods: influence of lipid organization within the food matrix and interactions with nonlipid components. *J Food Sci.* (2018) 83:2629–37. doi: 10.1111/1750-3841.14343
27. Minekus M, Alminger M, Alvito P, Ballance S, Bohn T, Bourlieu C, et al. A standardised static *in vitro* digestion method suitable for food - an international consensus. *Food Funct.* (2014) 5:1113–24. doi: 10.1039/C3FO60702J
28. Morlock GE, Drotleff L, Brinkmann S. Miniaturized all-in-one nanoGIT+active system for on-surface metabolism, separation and effect imaging. *Anal Chim Acta.* (2021) 1154:338307. doi: 10.1016/j.aca.2021.338307
29. Helbig A, Silletti E, Timmerman E, Hamer RJ, Gruppen H. *In vitro* study of intestinal lipolysis using pH-stat and gas chromatography. *Food Hydrocoll.* (2012) 28:10–9. doi: 10.1016/j.foodhyd.2011.11.007
30. Mat DJ, Le Feunteun S, Michon C, Souchon I. *In vitro* digestion of foods using pH-stat and the INFOGEST protocol: impact of matrix structure on digestion kinetics of macronutrients, proteins and lipids. *Food Res Int.* (2016) 88:226–33. doi: 10.1016/j.foodres.2015.12.002
31. Janssen H-G, Hrnčíř K, Szórádi A, Leijten M. An improved method for sn-2 position analysis of triacylglycerols in edible oils and fats based on immobilised lipase D (*Rhizopus delemar*). *J Chromatogr A.* (2006) 1112:141–7. doi: 10.1016/j.chroma.2005.11.097
32. *European Pharmacopoeia: Amtliche deutsche Ausgabe.* Stuttgart: Deutscher Apotheker Verlag (2017), p. 5858.
33. Müller I, Morlock GE. Quantitative saccharide release of hydrothermally treated flours by validated salivary/pancreatic on-surface amylolysis (nanoGIT) and high-performance thin-layer chromatography. *Food Chem.* (2023) (in press). doi: 10.1016/j.foodchem.2023.137145
34. Schwertner HA, Mosser EL. Comparison of lipid fatty acids on a concentration basis vs weight percentage basis in patients with and without coronary artery disease or diabetes. *Clin Chem.* (1993) 39:659–63. doi: 10.1093/clinchem/39.4.659
35. European Committee for Standardization. *Water Quality - Determination of the Inhibitory Effect of Water Samples on the Light Emission of Vibrio Fischeri (Luminescent Bacteria Test): Part 1: Method Using Freshly Prepared Bacteria* (2009).
36. Vult von Steyern F, Josefsson JO, Tägerud S. Rhodamine B, a fluorescent probe for acidic organelles in denervated skeletal muscle. *J Histochem Cytochem.* (1996) 44:267–74. doi: 10.1177/44.3.8648087
37. Orsavova J, Misurcova L, Ambrozova JV, Vicha R, Mlcek J. Fatty acids composition of vegetable oils and its contribution to dietary energy intake and dependence of cardiovascular mortality on dietary intake of fatty acids. *Int J Mol Sci.* (2015) 16:12871–90. doi: 10.3390/ijms160612871
38. Silska G, Walkowiak M. Comparative analysis of fatty acid composition in 84 accessions of flax (*Linum usitatissimum* L.). *J Pre Clin Clin Res.* (2019) 13:118–29. doi: 10.26444/jpcr/111889
39. Schreiner T, Eggerstorfer NM, Morlock GE. Ten-dimensional hyphenation including simulated static gastro-intestinal digestion on the adsorbent surface, planar assays, and bioactivity evaluation for meal replacement products. *Food Funct.* (2023) 14:344–53. doi: 10.1039/D2FO02610D
40. Urdaneta V, Casadesús J. Interactions between bacteria and bile salts in the gastrointestinal and hepatobiliary tracts. *Front Med.* (2017) 4:163. doi: 10.3389/fmed.2017.00163
41. Desbois AP, Smith VJ. Antibacterial free fatty acids: activities, mechanisms of action and biotechnological potential. *Appl Microbiol Biotechnol.* (2010) 85:1629–42. doi: 10.1007/s00253-009-2355-3
42. Mehl A, Schwack W, Morlock GE. On-surface autosampling for liquid chromatography-mass spectrometry. *J Chromatogr A.* (2021) 1651:462334. doi: 10.1016/j.chroma.2021.462334
43. Kabara JJ, Swieczkowski DM, Conley AJ, Truant JP. Fatty acids and derivatives as antimicrobial agents. *Antimicrob Agents Chemother.* (1972) 2:23–8. doi: 10.1128/AAC.2.1.23
44. Churchward CP, Alany RG, Snyder LAS. Alternative antimicrobials: the properties of fatty acids and monoglycerides. *Crit Rev Microbiol.* (2018) 44:561–70. doi: 10.1080/1040841X.2018.1467875
45. Silalahi J, Permata YM, de lux putra E. Antibacterial activity of hydrolyzed virgin coconut oil. *Asian J Pharm Clin Res.* (2014) 7:90–4. Available online at: <https://journals.innovareacademics.in/index.php/ajpcr/article/view/1042>
46. Chandana NGASS, Morlock GE. Eight different bioactivity profiles of 40 cinnamons by multi-imaging planar chromatography hyphenated with effect-directed assays and high-resolution mass spectrometry. *Food Chem.* (2021) 357:129135. doi: 10.1016/j.foodchem.2021.129135
47. Gassenmeier K, Schieberle P. Formation of the intense flavor compound trans-4,5-epoxy-(E)-2-decenal in thermally treated fats. *J Am Oil Chem Soc.* (1994) 71:1315–9. doi: 10.1007/BF02541347
48. Nieva-Echevarría B, Goicoechea E, Guillén MD. Effect of adding alpha-tocopherol on the oxidation advance during *in vitro* gastrointestinal digestion of sunflower and flaxseed oils. *Food Res Int.* (2019) 125:108558. doi: 10.1016/j.foodres.2019.108558
49. Silano V, Bolognesi C, Castle L, Cravedi J-P, Engel K-H, Fowler P, et al. Scientific Opinion on Flavouring Group Evaluation 226 Revision 1 (FGE226Rev1): consideration of genotoxicity data on one  $\alpha,\beta$ -unsaturated aldehyde from chemical subgroup 111(b) of FGE19. *EFSA J.* (2017) 15:e04847. doi: 10.2903/j.efsa.2017.4847
50. Stütz L, Schulz W, Winzenbacher R. Identification of acetylcholinesterase inhibitors in water by combining two-dimensional thin-layer chromatography and high-resolution mass spectrometry. *J Chromatogr A.* (2020) 1624:461239. doi: 10.1016/j.chroma.2020.461239
51. Ronzheimer A, Schreiner T, Morlock GE. Multiplex planar bioassay detecting estrogens, antiestrogens, false-positives and synergists as sharp zones on normal phase. *Phytomedicine.* (2022) 103:154230. doi: 10.1016/j.phymed.2022.154230
52. Klingelhöfer I, Morlock GE. Sharp-bounded zones link to the effect in planar chromatography-bioassay-mass spectrometry. *J Chromatogr A.* (2014) 1360:288–95. doi: 10.1016/j.chroma.2014.07.083
53. Guillén MD, Goicoechea E. Formation of oxygenated  $\alpha,\beta$ -unsaturated aldehydes and other toxic compounds in sunflower oil oxidation at room temperature in closed receptacles. *Food Chem.* (2008) 111:157–64. doi: 10.1016/j.foodchem.2008.03.052
54. Rojas-Molina M, Campos-Sánchez J, Analla M, Muñoz-Serrano A, Alonso-Moraga A. Genotoxicity of vegetable cooking oils in the *Drosophila* wing spot test. *Environ Mol Mutagen.* (2005) 45:90–5. doi: 10.1002/em.20078
55. Anter J, Campos-Sánchez J, Hamss RE, Rojas-Molina M, Muñoz-Serrano A, Analla M, et al. Modulation of genotoxicity by extra-virgin olive oil and some of its distinctive components assessed by use of the *Drosophila* wing-spot test. *Mutat Res.* (2010) 703:137–42. doi: 10.1016/j.mrgentox.2010.08.012
56. Kiwamoto R, Spenkelink A, Rietjens IMCM, Punt A. A physiologically based in silico model for trans-2-hexenal detoxification and DNA adduct formation in human including interindividual variation indicates efficient detoxification and a negligible genotoxicity risk. *Arch Toxicol.* (2013) 87:1725–37. doi: 10.1007/s00204-013-1091-8
57. Beeharry N, Lowe JE, Hernandez AR, Chambers JA, Fucasi F, Cragg PJ, et al. Linoleic acid and antioxidants protect against DNA damage and apoptosis induced by palmitic acid. *Mutat Res.* (2003) 530:27–33. doi: 10.1016/S0027-5107(03)00134-9
58. Clinical and Laboratory Standards Institute. *Performance Standards for Antimicrobial Disk Susceptibility Tests.* Wayne, PA: CLSI Standard M02 Clinical and Laboratory Standards Institute (2018).
59. Clinical and Laboratory Standards Institute. *Performance Standards for Dilution Antimicrobial Susceptibility Tests for Bacteria that Grow Aerobically.* Wayne, PA: CLSI Standard M07 Clinical and Laboratory Standards Institute (2018).

# Frontiers in Nutrition

Explores what and how we eat in the context of health, sustainability and 21st century food science

A multidisciplinary journal that integrates research on dietary behavior, agronomy and 21st century food science with a focus on human health.

## Discover the latest Research Topics

[See more →](#)

### Frontiers

Avenue du Tribunal-Fédéral 34  
1005 Lausanne, Switzerland  
[frontiersin.org](https://frontiersin.org)

### Contact us

+41 (0)21 510 17 00  
[frontiersin.org/about/contact](https://frontiersin.org/about/contact)

